

A Palaeoenvironmental Reconstruction of Galway Bay, Western Ireland, from the Last Glacial Maximum to Present Day

Denise McCullagh

Bachelor of Science: Geography, Archaeology and Palaeoecology, Queens University, Belfast, Northern Ireland, 2008

Master of Science: Dating and Chronology, Queens University, Belfast, Northern Ireland, 2013



Submitted for the degree of Doctor of Philosophy

Ulster University

Faculty of Life and Health Sciences

School of Geography and Environmental Sciences

August 2019

I confirm that the word count of this thesis is less than 100,000 words.

Declaration on access to contents and condition of use

I hereby declare that with effect from the date on which the thesis is deposited in Ulster University Doctoral College, I permit:

1. The Librarian of the University to allow the thesis to be copied in whole or in part without reference to me on the understanding that such authority applies to the provision of single copies made for study purposes or for inclusion within the stock of another library.

2. The thesis to be made available through the Ulster Institutional Repository and/or ETHOS under the terms of the Ulster eTheses Deposit Agreement which I have signed.

IT IS A CONDITION OF USE OF THIS THESIS THAT ANYONE WHO CONSULTS IT MUST
RECOGNISE THAT THE COPYRIGHT RESTS WITH THE AUTHOR AND THAT NO
QUOTATION FROM THE THESIS AND NO INFORMATION DERIVED FROM IT MAY BE
PUBLISHED UNLESS THE SOURCE IS PROPERLY ACKNOWLEDGED.

Acknowledgements

I would like to thank my supervisors Sara Benetti, Ruth Plets and Robin Edwards for their guidance, encouragement and support during my PhD, in particular to Sara and Ruth, without whom I would not have accomplished this.

Next, I would like to thank Ulster University and the Department of Education and Learning (DEL), whose scholarship funded this research and provided me with this opportunity. Further funding was provided by the Geological Survey of Ireland (Grant 2015_sc_073), the Marine Institute of Ireland, International Association of Sedimentology and Irish Quaternary Association (who provided radiocarbon dates). Without the use of the British Ocean Sediment Core Research Facility (BOSCORF), much of my analysis could not have been carried out, so my thanks for the use of this laboratory.

Sincere thanks to the crew and scientists on the R.V Celtic Voyager (cruise CV13031), who provided the sediment cores for my research and to the Marine Institute of Ireland for providing geophysical data. Without these resources I would not have had the opportunity to tackle this project.

Thanks go to my manuscript co-authors for their contribution of data and their valuable feedback.

Thanks to my colleagues and friends of the Quaternary research group, especially my office mates: Jared Peters, and in particular to Serena Tarlati and Kevin Schiele, for providing a sounding board for thoughts and ideas for the thesis. It has been a pleasure to work with you and to exchange ideas. I greatly appreciated your help and company.

Most of all, I want to thank my friends and family who kept me going over the period of this PhD. To Neal who graciously allowed me to stay in his home while I completed my research, to Sarah, Jane and Muldoon, who kept me sane and to my family for their continual support.

Finally, to all the people I met in Coleraine, in particular to Alex, Kevin and Serena who managed to make even the toughest times a great experience and who always provided beers at the end of a long day!

Without you I would not have come this far.

Table of Contents

Chapter 1: Introduction	1
1.1 Introduction and Rationale.....	1
1.2 Research Gap.....	5
1.3 Research aim and objectives	7
1.4 Thesis Structure.....	8
Chapter 2: Study area and Background	11
2.1 Study Area.....	11
2.2 Glacial history of the region.....	14
2.3 The Holocene.....	23
2.4 Sea-level history	33
Chapter 3: Data and methodologies	39
3.1 Topographic, bathymetric and backscatter data.....	39
3.2 Hydrodynamic data.....	43
3.3. Habitat Mapping	44
3.4 Core acquisition, storage and splitting	45
3.5 Sediment physical properties	47
3.6 Lithofacies identification.....	51
3.7 X-Ray Fluorescence analysis	52
3.8 Micropalaeontology	55
3.9 Geochronology.....	57
3.10 Sub-bottom profiling.....	60
Chapter 4: Coastline and inshore geomorphology of Galway Bay, Western Ireland	65
4.1. Introduction.....	66
4.1.1 Study Area.....	66
4.2 Materials and Methods.....	70
4.3 Results and Discussion	73
4.3.1 Hydrodynamic modelling.....	73
4.3.2 Coastline mapping	73
4.3.3 Substrate classification	74
4.3.4 Habitat mapping	76
4.3.5 Submarine bedforms and landforms.....	76
4.3.5.1 Channels.....	77
4.3.5.2 Subaqueous dunes	78

4.3.5.3 Sand waves	80
4.3.5.4 Ripples.....	81
4.3.5.5 Submerged marine terraces.....	82
4.3.5.6 Seafloor scouring	82
4.3.5.7 Pockmarks.....	83
4.3.5.8 Drumlins.....	84
4.4. Conclusion	85
Chapter 5: Results	87
5.1 Seismic Results.....	87
5.2 Geochronology Results	94
5.3 Lithofacies and geochemical results	96
5.4 Sequence stratigraphy and geographical distribution of lithofacies and seismic units	131
6.1 Seismic Interpretation.....	143
6.1.1 Acoustic unit 1	143
6.1.2 Acoustic unit 2	145
6.1.3 Acoustic sub-unit 3a.....	145
6.1.4 Acoustic sub-unit 3b	146
6.2 Lithostratigraphical Interpretation.....	147
6.3 Sedimentation Rates.....	163
6.4 Sequence stratigraphy interpretation	166
6.4.1 Inner bay stratigraphy.....	166
6.4.2 Mid-bay stratigraphy	167
6.4.3 Outer bay – South Sound stratigraphy	169
6.4.4 Outer central bay stratigraphy	170
6.4.5 Outer bay- North Sound stratigraphy.....	171
Chapter 7: Discussion	174
7.1 Glacial – Deglaciation period (>24.7 – ~15.5ka calBP)	174
7.2 Deglaciation – Early Holocene period (~15.5 – 11.7 ka cal BP).....	179
7.3 Early Holocene period – Greenlandian (11.7 – 8.3ka calBP)	184
7.4 Mid-Holocene period – Northgrippian (8.3- 4.2ka cal BP).....	188
7.5 Late Holocene period - Meghalayan (4.2 ka cal BP - Present).....	196
7.6 Sea-level changes in Galway Bay since the last deglaciation	201
Chapter 8: Conclusions	213
8.1 Main findings	213

8.2 Limitations	216
8.3 Future Research	217
References	219
Appendices	289

List of Figures

Figure 1.1: Extent of the BIIS across Ireland and offshore to the shelf edge, showing the flow lines of major ice streams and the position of the Donegal Barra Fan. Locations in the map include: OH-Outer Hebrides, KB-Kilda Basin, S-Skye, NC-North Channel, DBF-Donegal Barra Fan, DB- Donegal Bay, GB-Galway Bay, BB- Bantry Bay. The study area of Galway Bay is outlined in red (Adapted from Greenwood and Clark, 2009; Callard et al, 2018).

Figure 1.2: GIA model derived RSL predictions for Galway Bay (Brooks et al, 2008; Bradley et al, 2008; Kucker et al, 2012), based on mean sea-level. All SLIP points from the Irish database for Galway Bay have been plotted in black. These are all terrestrial limiting points.

Figure 2.1: Bathymetric map of Galway Bay, showing the modern-day rivers contributing to the freshwater input. The bay has been divided into 3 areas (inner, mid and outer) for ease in identification. The main inputs are shown in bold in the inner bay, from the Corrib, Clarinbridge and Dunkellin rivers. The general current direction in the bay is taken from the work of Booth (1975) and Ren et al (2015).

Figure 2.2: Map of Galway Bay showing the bedrock geology, divided by a, east-west fault line that runs through the bay, and some of the dominant features in the surrounding landscape (Adapted from Max et al, 1983; Williams et al, 1988; Clarke, 2013; GSI, 2013, 2016; INFOMAR, 2013).

Figure 2.3: Map showing the extent of the BIIS across Ireland. The dashed line represents the boundary of the earlier work that indicated the SIEM as the limit of the ice sheet (Bowen et al, 2002), while the solid black line represents the maximum extent of the ice sheet based on the most recent research (Clark et al., 2017).

Figure 2.4: Map of the glacial geomorphology of the BIIS. Compiled from a review of the published academic literature and Irish and British Geology survey mapping, at the University of Sheffield as part of the BRITICE-CHRONO project (Clark et al, 2017).

Figure 2.5: Image showing the global sea-level curve since the LGM and the occurrence of meltwater pulses (MWP). MWP 1A0: ~19.6 – 18.8 ka BP, MWP 1A: ~14.6-13.8 ka BP. MWP 1B: ~11-8.8 ka BP, MWP 1C: ~8.2-7.6 ka BP (Gornitz, 2012).

Figure 2.6: Image showing Bond events during the post-glacial, alongside ice core records from Greenland (Bond, 1997).

Figure 2.7: Relative sea-level curves from various regions in Ireland, adapted from Edwards and Craven (2017) and Brooks et al (2008). This demonstrates how SLIP's are mainly available for the Late-Holocene.

Figure 3.1: Image showing the ranges of various instrumentation for the acquisition of geophysical data in shallow water (courtesy of F. Sacchetti, Marine Institute of Ireland).

Figure 3.2: (A) Bathymetric and LiDAR and (B) backscatter map of Galway Bay, with the sediment cores represented in pink.

Figure 3.3: An example of the deck crew (A) bringing in a vibrocore after coring the Celtic shelf, on the GATEWAYS2 cruise, and (B) preparing for piston coring on the CE16010 cruise, on board the RV Celtic Explorer.

Figure 3.4: Image of pebbles visible in the x-ray (top) at the base of core 20VC but invisible to the naked eye (bottom).

Figure 3.5: Image of a shear vane measurement taken on core 18VC (CV13031) at Ulster University.

Figure 3.6: A map of Galway Bay showing the position of all viable seismic lines used in the construction of a seismic stratigraphy.

Figure 3.7: An example of the aforementioned reflector patterns used as the main criteria in stratigraphic analysis (Adapted from Mitchum et al, 1977). The overlying strata is coloured green and the underlying strata coloured blue.

Figure 3.8: Example of the internal reflection configuration patterns used as the main criteria in stratigraphic analysis (Adapted from Mitchum et al, 1977).

Figure 1: A geomorphology map of Galway Bay (main map), with smaller maps showing the LiDAR and bathymetry, backscatter, bottom currents and slope, from top to bottom on the right.

Figure 2: Bathymetric image of the study site showing the 0m contour line in black and sub-divided into 3 geographical areas: inner bay, mid bay and outer bay. Examples of features identified in the bay are outlined in red and will be discussed in further detail below.

Figure 3: (A) maximum residual depth-averaged current velocity with 200m gridline spacing, (B) mean orbital wave velocity with a 2800m gridline spacing and (C) maximum residual bottom current with a 200m gridline spacing.

Figure. 4: Cross section and bathymetric image of outcropping limestone bedrock, located in the outer central bay area.

Figure 5: Cross section and bathymetric image of (A) double lee dunes, (B) linear dune, (C) large transverse dune and (D) small transverse dunes. The black arrows indicate bottom current direction while the red arrows indicate depth-averaged current direction. The image shows both currents on a 200m grid using the most frequent direction. The pink line represents the 0m contour line.

Figure 6: (A) bathymetry and (B) backscatter data in the area of the sand-waves; (C) bathymetry and (D) backscatter of the ripples; all including cross sections. The black arrows indicate bottom current direction while the red arrows indicate depth-averaged current direction. The image shows both currents on a 200m grid using the most frequent direction.

Figure 7: Cross section and bathymetric image of scouring around bedrock in the mid-bay. The black arrows indicate bottom current direction while the red arrows indicate depth-averaged current direction. The image shows both currents on a 200m grid using the most frequent direction.

Figure 8: Cross section and bathymetric image of the largest pockmark visible in the bay. Artefacts are visible in the data to the south of the pockmarks.

Figure 9: (A) Drumlin field visible onshore (white box) and a zoomed out inset of image B (red box). The black line represents the 0m contour and present-day coastline. (B) Cross section and bathymetric image of drumlins visible in the bay. Artefacts are visible in the data to the north and west of the drumlins.

Figure 5.1: Map showing the 3 sections of the bay (Inner, Mid and Outer) outlined in purple, with sub sections (North Sound, South Sound and Central Bay) outlined in green. The cores from CV13031 are shown in pink and 3 of the highest quality seismic lines in the bay are shown in red.

Figure 5.2: Seismic line 1 extending northeast from Inishmor across the inner area of the North Sound showing all seismic units in the bay. Green reflector: represents the top of unit 1. Red Reflector: represents the top of unit 2. Yellow reflector represents the top of sub-unit 3a. Blue reflector: represents the seafloor.

Figure 5.3: Seismic line 2 through the inner bay showing the channel that extends westwards. Zoomed-in image clearly shows infilling in this channel. Green reflector: represents the top of unit 1. Red

Reflector: represents the top of unit 2. Yellow reflector represents the top of sub-unit 3a. Blue reflector: represents the seafloor.

Figure 5.4: Seismic line 3, extending from the inner bay south west to the South Sound, showing prograding clinoforms in the northeast. Green reflector: represents the top of unit 1. Red Reflector: represents the top of unit 2. Yellow reflector represents the top of sub-unit 3a. Blue reflector: represents the seafloor.

Figure 5.5: Grids showing the extent of the upper boundaries of all seismic units in Galway Bay. A) grid of the top of unit 1 topography, B) grid of the top of unit 2 topography, C) grid of the top unit 3a topography, D) grid of the top unit 3b topography. This data has been interpolated using a 500m gridding parameter and slight errors may exist.

Figure 5.6: Isopach map of (A) unit 2, (B) unit 3a and (C) unit 3b showing the extent and thickness of this unit in the bay.

Figure 5.7: A graph of core 03VC showing a core image, an x-ray image, a core log, MSCL measurements and shear strength values.

Figure 5.8: A graph showing the ITRAX analysis for core 03VC, with LF 1 at the base of the core. The data are presented at a resolution of 5mm and the large black arrows next to the chemical data represent general trends.

Figure 5.9: Examples of foraminifera species found in Galway Bay. A) *Quinqueloculina* sp., B) *Textularia* sp., C) *Elphidium excavatum*., D) *Rosalina globularis*, E) *Rosalina praegeri*, F) *Cibicides lobatulus*, G) *Planorbulina mediterraneensis*, and H) *Elphidium williamsoni*. These species were used for both qualitative analysis of marine environments and radiocarbon dating.

Figure 5.10: A graph of core 07VC showing a core image, an x-ray image, a core log, MSCL measurements and grain size values for LF2.

Figure 5.11: A graph showing the ITRAX analysis for core 07VC, showing LF 2 at the base of the core. The data are presented at a resolution of 5mm and the large black arrows next to the chemical data represent general trends.

Figure 5.12: Charts showing the overall grainsizes for each facies. This was done by combining all grainsize measurements taken within a particular facies to find the average composition. No grainsize samples were taken in LF1 or LF3, so no measurements are available for these lithofacies.

Figure 5.13: A graph of core 13VC showing a core image, an x-ray image, a core log, MSCL measurements and shear strength values.

Figure 5.14: A graph showing the ITRAX analysis for core 13VC, showing LF3 at the base of the core. The data are presented as a rolling average at a resolution of 5mm and the large black arrows next to the chemical data represent general trends.

Figure 5.15: A graph of core 22VC showing a core image, an x-ray image, a core log and MSCL measurements.

Figure 5.16: A graph of core 22VC showing a core image, an x-ray image, a core log, shear strength values and grain size measurements.

Figure 5.17: A graph showing the ITRAX analysis for core 22VC, showing LF 4 at the base of the core. The data are presented as a rolling average at a resolution of 5mm and the large black arrows next to the chemical data represent general trends.

Figure 5.18: A graph of core 06VC showing a core image, an x-ray image, a core log, MSCL measurements and grainsize measurements.

Figure: 5.19: A graph showing the ITRAX analysis for core 06VC, showing LF 5 at the base of the core. The data is presented at a resolution of 5mm and the large black arrows next to the chemical data represent general trends.

Figure 5.20: A graph of core 01VC showing a core image, an x-ray image, a core log, shear strength measurements, grain size values and percentages of sediment type for LF6 and LF7.

Figure 5.21: A graph showing the ITRAX analysis for core 01VC. LF6 is at the base of the core, while LF7 is in the middle of the core. The data is presented at a resolution of 5mm and the large black arrows next to the chemical data represent general trends.

Figure 5.22: A graph of core 02VC showing a core image, an x-ray image, a core log and MSCL measurements.

Figure 5.23: A graph showing the ITRAX analysis for core 02VC, showing LF8 at the top of the core. The data is presented as a rolling average at a resolution of 5mm and the large black arrows next to the chemical data represent general trends.

Figure 5.24: Map of Galway Bay showing the core positions and their associated lithofacies.

Figure 5.25: The cores in the inner bay, the mid bay, the latter 3 of which (12VC, 03VC & 02VC) are also part of the South Sound and cores in the outer bay central area.

Figure 5.26: Cores in the Outer Bay, both North and Central areas.

Figure 6.1: A summary of the stratigraphy in the bay, including the different seismic units, lithofacies, rates of sea-level rise and short descriptors of the environment. Reworked radiocarbon dates have been excluded, while the X represents facies where there are no radiocarbon dates available. The angle of the arrow indicates the likely rate of sea-level rise, based on the interpretation of the evidence from each facies/unit.

Figure 7.1: (A) BUIS extension off the west coast of Ireland (based on the works of Benetti et al, 2010; Dunlop et al, 2010; Ó Cofaigh et al, 2012; Sacchetti et al, 2012; Peters et al, 2015, 2016). (B) Retreat of ice through Galway Bay during deglaciation, between 16 – 15 ka cal BP (based on the References found in Table 2.1).

Figure 7.2: Summary of the post glacial terrestrial environmental conditions in (A) Europe (Booth et al, 2012a, 2012b; Mortensen et al, 2014; Seddon et al, 2015; Binney et al, 2017) and (B) Ireland (Harrison et al, 2010; Watson et al, 2010; Ballantyne and Ó Cofaigh, 2017). (C) Summary of the post glacial environment in Galway Bay between 15 and 13 ka cal BP, with the retreating shoreline positions based on GIA derived RSL predictions (Brooks et al, 2008; Bradley et al, 2011; Kuchar et al, 2012), data from this study (Table 5.3) and references found in Table 2.1.

Figure 7.3: Summary of the Younger Dryas terrestrial environmental conditions in (A) Europe, (B) Ireland and (C) Galway Bay, with retreat of shoreline positions between 12.9 – 11.7 ka cal BP, based on GIA derived RSL predictions (Brooks et al, 2008; Bradley et al, 2011; Kuchar et al, 2012), data from this study (Fig. 5.6 & Table 7.1), and references found in Table 2.1. ST: Surface Temperature. SST: sea surface temperature, based on foraminifera preferences (Murray, 1979, 2003, 2006; Appendix 3).

Figure 7.4: Summary of the early Holocene environmental conditions in (A) Europe, (B) Ireland and (C) Galway Bay, with the retreat of shoreline positions between 11.7 – 8.8 ka cal BP, based on GIA derived RSL predictions (Brooks et al, 2008; Bradley et al, 2011; Kuchar et al, 2012) and data from this study (Fig. 5.6 & Table 7.1). ST: Surface Temperature. SST: sea surface temperature, based on foraminifera preferences (Murray, 1979, 2003, 2006; Appendix 3).

Figure 7.5: Summary of the mid Holocene environmental conditions in (A) Europe, (B) Ireland and (C) Galway Bay, with the retreat of shoreline positions between 7.4 – 5.6 ka cal BP, based on GIA derived RSL predictions (Brooks et al, 2008; Bradley et al, 2011; Kuchar et al, 2012), data from this study (Fig. 5.6 & Table 7.1) and references found in Table 2.1. ST: Surface Temperature. SST: sea surface temperature, based on foraminifera preferences (Murray, 1979, 2003, 2006; Appendix 3).

Figure 7.6: Summary of the mid Holocene environmental conditions in (A) Europe, (B) Ireland and (C) Galway Bay, with the retreat of shoreline positions, between 5.6 – 4.1 ka cal BP, based on GIA derived RSL predictions (Brooks et al, 2008; Bradley et al, 2011; Kuchar et al, 2012), data from this study (Fig. 5.6 & Table 7.1) and references found in Table 2.1. ST: Surface Temperature. SST: sea surface temperature, based on foraminifera preferences (Murray, 1979, 2003, 2006; Appendix 3).

Figure 7.7: Summary of the late Holocene environmental conditions in (A) Europe, (B) Ireland and (C) Galway Bay, with shoreline positions based on GIA derived RSL predictions (Brooks et al, 2008; Bradley et al, 2011; Kuchar et al, 2012) and data from this study (Fig. 5.6 & Table 7.1). ST: Surface Temperature. SST: sea surface temperature, based on foraminifera preferences (Murray, 1979, 2003, 2006; Appendix 3).

Figure 7.8: Graph showing sea-level progression in Galway Bay from this research.

Figure 7.9: Graph showing sea-level progression in Galway Bay from this research, alongside all GIA derived RSL predictions and other sea-level work carried out in the bay. Significant global sea-level events are also included.

List of Tables

Table 2.1: Onshore dates after the LGM, from the Ox Mountains in Co. Sligo to the Shannon River in Co. Limerick, along the coastline of western Ireland. ¹⁰Be ages that have not used the Loch Lomond local production rate (LL LPR) have been recalibrated by Ballantyne and Ó Cofaigh (2017), while ¹⁴C ages have been recalibrated using the INTCAL13 calibration curve.

Table 3.1: Table showing information on the collected cores, including coordinates, water depth, coring method, length and number of sections in each core and the type of analysis carried out on each core. Water depth is corrected to lowest astronomical tide (LAT) while, MSCL represents analysis of physical properties, GSA is grain size analysis, XRF is chemical analysis, SS is shear strength, ¹⁴C is radiocarbon dating and Fossil analysis refers specifically to benthic foraminifera.

Table 3.2: Summary table of geochemical elements used in this study as proxies of environmental and sea-level change. An increase in the elements/ratios reported in the table indicate an increase in the parameter they refer to.

Table 3.3: A table showing the core, depth and lithofacies foraminifera samples were located in.

Table 3.4: Samples submitted for radiocarbon dating, showing the core number (from lowest to highest), depth of sample in each core, type of carbonate material used for analysis, weight of the sample material and the laboratory dating the samples. All foraminifera samples were composed of intact mixed benthic species; all shell samples were bivalves, while all *Turritella sp.* samples were intact.

Table 1: Summary statistics on the range of submarine bedforms and landforms in Galway Bay.

Table 5.1: Radiocarbon dates for each sample, with ages given as a mean value. Labs are indicated as BA: Beta Analytic and CC: Chrono Centre. 95% CA- refers to the calibrated age. PSCU Silt-Coarse Sand refers to Poorly sorted, coarsening upward silt to coarse sand, while CU Sandy mud refers to coarsening upwards sandy mud. All bivalve samples were composed of 1 valve with the exception of those marked *, which were fully intact.

Table 5.2: A lithofacies classification, with x-ray images, core photographs and descriptions. See Appendix 4 for raw data ranges of sediment cores.

Table 5.3: A foraminifera species table, with primarily marine species coloured in blue, estuarine species in green and brackish species in yellow. Species with more than one colour are found in different environments. The large red X represents a dominant species, estimated to have higher than 15% per sample, while the small black x represents a minor species, estimated to have less than 5% per sample (See Appendix 2 for details of numbers of foraminifera counted and references used for optima and tolerance ranges).

Table 6.1: A table showing the sedimentation rates in Galway Bay from deglaciation to present day. These rates all assume that there is no erosion of sediment occurring within the bay and have assumed that the core top/seabed represents present day. Rates in Blue have used the literature to obtain time ranges. Rates in Black are those where 2 radiocarbon dates are present within a sediment core. Rates in Red have a single radiocarbon date.

Table 7.1: Table showing all the data points used in RSL prediction based on data from this study. OB represents outer bay, while MB represents mid bay. All data points except point A are marine. Transitional water represents water levels between 8m and 36.45m above the sample.

Summary

Studies of past changes in the environment are essential to understand the speed and scale of modern-day climatic and environmental change. This research investigates the palaeoenvironmental changes throughout the last glacial and current interglacial period in Galway Bay, Western Ireland, using a multiproxy examination of geophysical data and twenty-two sediment cores. The methodologies used in this study include the interpretation of multibeam echo-sounder bathymetry and backscatter, altimetry, hydrological and seismic data, as well as the analysis and interpretation of the sediment cores' physical properties, X-radiographs, grain size analysis, microfossil content, geochemical signatures (micro-XRF) and radiocarbon dates. These data together allow for an interpretation of the driving forces behind the observed patterns in the distribution of sediments at the seafloor and sub-surface from the last glacial maximum until present day. Such data also provide field data, which can be used to constrain sea level in the bay after 19 ka cal BP. This is particularly valuable as the only available sea-level reconstructions for the area are derived from glacio-isostatic adjustment (GIA) models.

Seismic data cover the mid and outer bay and reveal three distinct seismic units, representing bedrock, glacial till and post-glacial marine sediments. The till unit, overlying the bedrock, shows evidence of a glaciofluvially cut channel along the northern portion of the bay, constraining the relative sea-level depth in the bay during deglaciation to 58m below modern-day levels. This lowstand is in broad agreement with a GIA predicted sea-level position at 15 ka cal BP. The overlying marine sediment unit, in which prograding clinoforms and infilling are visible, represents the sea-level transgression since 15 ka cal BP. Shoreline deposits (rounded pebbles in a silty sand matrix, found in four cores) were deposited in the mid and outer Bay between 12.6 ka cal BP and 8.8 ka cal BP. The identification of such submerged palaeo-shore line sediments in depths of 39-43m reveals a late glacial to early Holocene slowstand. This identified slowstand lasted 2500 years longer than predicted by GIA based predictions. Core data suggests that, due to this delayed subsequent transgression, GIA derived RSL level predictions were not reached until ~4000 years BP. As well as providing important information for RSL reconstructions, the sediments and foraminifera within

allow the identification of palaeoenvironmental conditions over time and space. In general, the pre- and early Holocene period is characterised by high sediment input in warm, productive, estuarine conditions with 2 separate inlets in the bay leading to two distinct environments: (1) a high energy beach environment transitioning to low energy, transitional waters in the north, and (2) a low energy, anoxic subtidal environment in the south. The mid Holocene period is characterised by the opening up of the bay and the presence of the gastropod *Turritella sp.* across the entire area. This represents a medium energy, warm, productive, environment in transitional waters. The late Holocene is typified by the disappearance of *Turritella sp.* and a transition to marine conditions. This represents a deepening, productive and high energy environment with warm and wet climatic conditions in the region. Interestingly though, global and regional climatic events such as the Younger Dryas, the 8.2 ka and 4.2 ka event have left no significant imprint on the sedimentary record. Overall, the data acquired from Galway Bay documents constant relative sea-level transgression, with a trend towards a wetter and marine- influenced environment after the initial deglaciation. The more recent Late Holocene sediments and current seabed topography record the influence of tidal currents, storm events and wave action, characteristic of the western Irish coastline.

Results from this research can help validate both climate and sea-level models for the region, which in turn provide predictions for future environmental developments.

Chapter 1: Introduction

1.1 Introduction and Rationale

The modern world is experiencing environmental changes that are occurring at a previously unseen rate (IPCC, Summary for Policymakers, 2013). These changes are polarising environmental processes across the globe, often leading to more extreme conditions. The marine environment is particularly affected, with changes in temperature, salinity, circulation, intensity and frequency of storm events and relative sea-level, as well as the knock-on effect on marine species, their ecosystems and biodiversity (Carter, 1982; Woolf et al., 2002; Hassol, 2004; Rignot et al, 2011; Emmerson and Lahn, 2012; IPCC, 2013; Marzeion et al, 2014; Radic et al, 2014). This is particularly significant for coastal regions, as they are affected by both marine and terrestrial processes. In order to understand and gauge the changes occurring in the climate and environment today, we need to investigate their effect over a prolonged period of time. This is where the study of palaeoenvironments, becomes crucial. The investigation of palaeoenvironmental archives, where environmental changes are recorded over large time periods, can provide analogues to many of the modern changing conditions, and help us predict likely future outcomes.

Numerical modelling of future climate in Ireland began with the creation of the Regional Climate Model C41 by Met Éireann (McGrath et al, 2005). However, the C41 model uses only historical data as far back as 1961 to validate its results (McGrath et al, 2005). In order to produce a more robust dataset and reduce uncertainties, palaeoenvironmental research can be used to elucidate patterns on longer timescales, something that cannot be observed over shorter modern instrumental records (Henderson et al, 2009). Relative sea-level (RSL) changes, which are a major concern in many low-lying areas can also be modelled to provide predictions on possible changes. In order to validate these models and implement relevant policies and management strategies (Mahony, 2015), records of past environments need to be studied in detail to provide ground-truth data.

Across Western Ireland, there is extensive variability in the data for both deglacial and postglacial, environmental and sea-level conditions (Edwards et al, 2017). This means that, in order to successfully reconstruct these conditions, local scale studies need to

be carried out. The study of Galway Bay, presented in this thesis, provides such a record of change in a marine environment.

The bay has been heavily influenced by both modern hydrological processes and by the glacial processes that occurred when Ireland was covered by the British-Irish Ice Sheet (BIIS) during the last glacial maximum, between 26 and 19 ka cal BP (Clark et al, 2009) (Fig. 1.1).

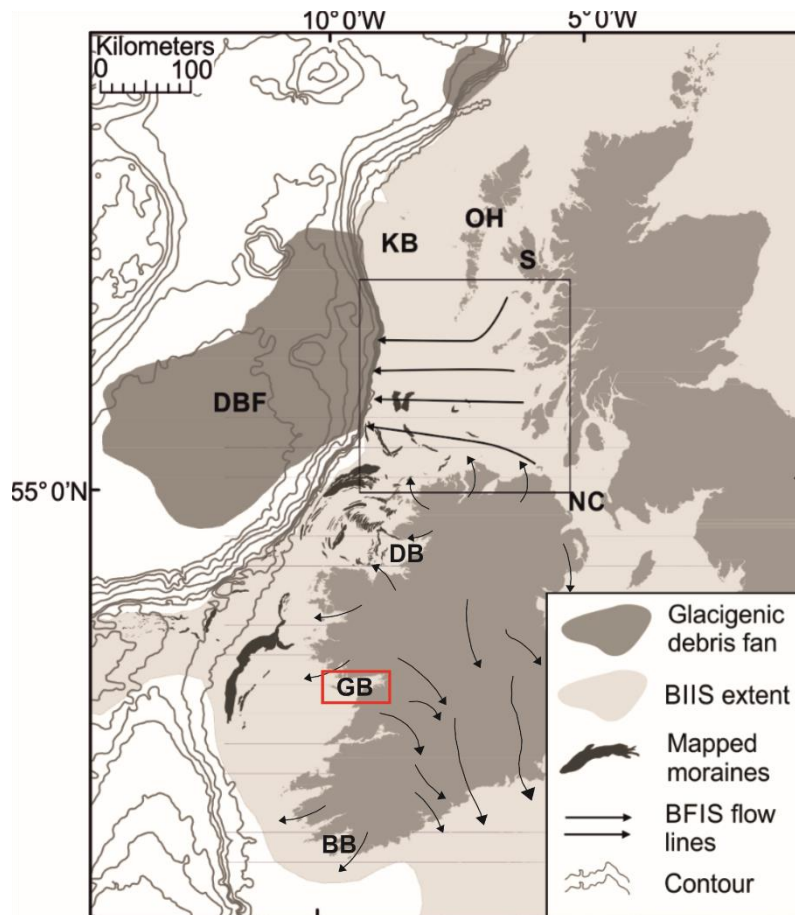


Figure 1.1: Extent of the BIIS across Ireland and offshore to the shelf edge, showing the flow lines of major ice streams and the position of the Donegal Barra Fan. Locations in the map include: OH-Outer Hebrides, KB-Kilda Basin, S-Skye, NC-North Channel, DBF-Donegal Barra Fan, DB- Donegal Bay, GB- Galway Bay, BB- Bantry Bay. The study area of Galway Bay is outlined in red (Adapted from Greenwood and Clark, 2009; Callard et al, 2018).

The deglaciation of this ice sheet was punctuated by shorter periods of readvance and relatively rapid retreat at its western margin over Ireland (Peters et al., 2016; Ballantyne and Ó Cofaigh, 2017; Barth et al., 2018; Callard et al, 2018). It exerted a

major influence on the environment with the transition from an ice margin grounded at the shelf edge (ca. 24 ka BP), retreating to a terrestrial position and finally with a localised presence as glacier cirques, before the final disappearance of all glacial ice in Ireland (ca. 15 ka BP) (Ballantyne and Ó Cofaigh, 2017). The signature of these glacial and deglacial processes have left a lasting impact on the landscape surrounding Galway bay, with evidence of meltwater channels, eskers, drumlins amongst other glacial landforms (Max et al, 1983; Williams et al, 1988; GSI, 2013). Global and local changes in ice sheet extent and ensuing isostatic changes also had a profound effect on relative sea level around Ireland.

Glacio-Isostatic Adjustment (GIA) models coupled with global sea-level change reconstruction curves provide RSL curves for the west of Ireland for the period after 20 ka cal BP (Brooks et al, 2008; Bradley et al, 2011; Kuchar et al, 2012). However, climate models have inherent uncertainties, due to the number of variables related to the initial environmental conditions and model parameters used (Semenov and Stratonovitch, 2010). By comparing model outputs against palaeo-data, the robustness of numerical models can be tested and validated. The palaeo-data used to validate the GIA models in Ireland have been sub-divided into four classes of data (Brooks and Edwards, 2006):

1. Primary index points - the best data for sea-level estimations providing information on location, age, altitude and indicative meaning. The sample and depositional environment is quantified and has age and altitude error estimates.
2. Secondary index points – similar to previous, but with variables unquantified or with significant uncertainty.
3. Limiting data type 1 – data where it is possible only to infer sea-level as above or below the sample.
4. Limiting data type 2 – data where it is possible only to infer sea-level as above or below the sample but whose source environment is unclear or contested.

As the palaeo-records in the west of Ireland are composed primarily of limiting data, with no data at all available for the period 9 – 13ka BP (Edwards et al, 2017), it is very difficult to validate such models. Therefore, in order to fill the gaps in our knowledge of paleo-environmental change in the region and to improve the shortcomings in the

current GIA and climatic models, further investigation of the post-glacial and Holocene environment in the west of Ireland is needed.

The three GIA model derived RSL curves for Galway Bay, which provide RSL estimates since the beginning of deglaciation at 20 ka cal BP (Brooks et al, 2008; Bradley et al, 2011; Kuchar et al, 2012), give significantly differing predictions for relative sea-level for much of the deglacial and early Holocene periods (Fig. 1.2), something which will be discussed in greater detail in Chapter 2. In order to help constrain sea-level in this area, this study will focus on providing information on the palaeoenvironment of Galway Bay.

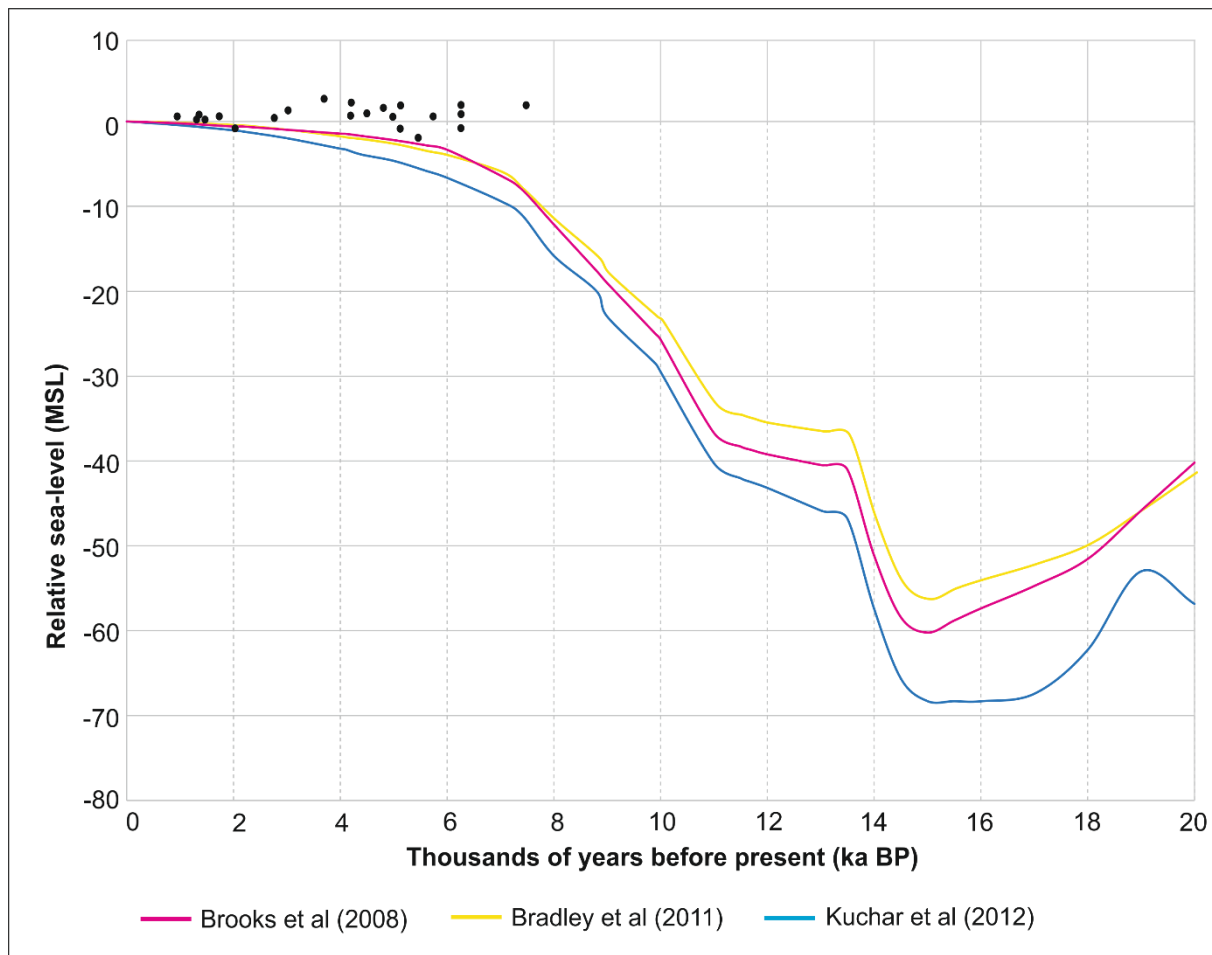


Figure 1.2: GIA model-derived RSL predictions for Galway Bay (Brooks et al, 2008; Bradley et al, 2008; Kucker et al, 2012), based on mean sea-level. All SLIP points from the Irish database for Galway Bay have been plotted in black. These are all terrestrial limiting points.

This coastal and shallow marine research is important, not only for Ireland, but also in a wider context. As coastal sites, particularly in the west of Ireland, are strongly influenced by changes in the marine as well as the terrestrial environment, changes in Galway Bay can be used to understand the wider forcing mechanisms of climate change and its impact on the North Atlantic Ocean.

1.2 Research Gap

While previous research has been carried out in Galway Bay, these studies have either been confined to a small area of the bay or have utilized only limited proxies for data analysis.

The most recent work of Novak (2017) used a wide range of analyses, including sedimentological, geochemical and microfossil data on sediment cores; however, only four cores were taken, all from the very inner bay and the mouth of the Corrib River (Fig. 1.3). In the early Holocene, Novak (2017) reports a marine intrusion into the modern-day Corrib estuary at 10.2 ka cal BP, evidence of a signature of the 8.2 ka climatic event and limiting data on the position of sea-level. However, this research covered only the early and very late Holocene, with a large hiatus in the data during the mid- and most of the late Holocene due to a lack of sediments of this age.

The work of Clarke (2013) used seismic data from across the bay, including sparker, chirp and pinger. Due to time and resource constraints, only a reduced number of seismic lines, mainly those from the inner bay and North Sound, were analysed in detail, and no ground-truthing was carried out. Clarke (2013) identifies 3 seismic units in the bay, corresponding to both the glacial and post glacial periods. A migrating, possible palaeo-Corrib, channel system was also identified in the inner bay.

Wood (2010) used sedimentological and microfossil analysis from 8 sediment cores in the bay (Fig. 1.3) and 1 core at 113m bsl, ~75km offshore of the Aran Islands. Many of the results, centred on the inner bay and North Sound, were found to have chronological inconsistencies and extensive reworking or coring disturbance are interpreted to have occurred in portions of the cores. Like Novak's cores, a hiatus during the mid and late-Holocene is apparent in the sediment record analysed from this study. The core taken from the offshore area, west of the Aran Islands, covers a

period of ~16ka years, but Wood et al (2017) note that either the past 9000 years are condensed into 55cm at the core top, or there is sediment missing altogether.

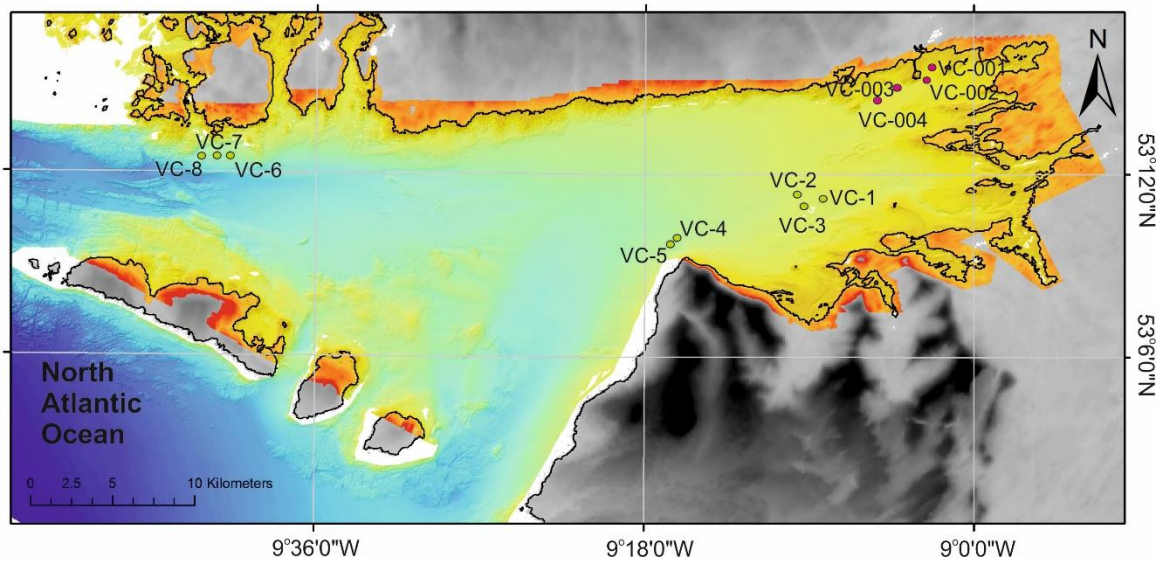


Figure 1.3: Map of Galway Bay, with Novak's (2017) sediment cores represented by the pink points and Woods' (2010) sediment cores represented by the green points.

Other studies around Galway Bay have found evidence of terrestrial material close to the present-day shoreline, thus providing information on past relative sea-level positions. Tree stumps of oak and pine, two species that prefer drier conditions and which were likely located above the high tide range, were found near An Spidéal, dated between 7435 and 5253 cal BP, and provide limiting data on the sea-level position (Williams and Doyle, 2014). Red deer antlers and horse remains were found in the intertidal zone near Rusheen Bay and may represent a midden deposit (O'Carra et al, 2014), which would be suggestive of a nearby settlement, around 1500 years ago, suggesting relative sea-level was below this point.

In the wider region of Ireland, palaeoenvironmental records from lacustrine, speleothem, peatland and marine sources are abundant, but only a limited number of these include the post glacial and early Holocene period (McDermott et al, 1999, 2001; Diefendorf et al, 2006; McKeown, 2013; Ghilardi and O'Connell, 2013; Schettler et al, 2006; Holmes et al, 2016). The Holocene records from Ireland suggest a high level of variability, with local factors as primary climatic drivers in many cases. Major climatic trends are nonetheless recognised. The Holocene Thermal Maximum (HTM) appears

to have occurred during the early Holocene in Ireland (10.8 – 9 ka cal BP), much earlier than in many other areas of Europe (Diefendorf et al, 2005, 2006; Holmes et al, 2007; Wanner et al, 2008; Bartlein et al, 2011; Renssen et al, 2012; Ghilardi and O’Connell, 2013; McKeown, 2013). A trend towards wetter conditions in the mid and late Holocene is also evident (Dodson, 1990; McDermott et al, 2001; Diefendorf et al, 2006; Holmes et al, 2010; Murnaghan et al, 2012; Ghilardi and O’Connell, 2013). Other major climatic events, such as the 8.2 ka event, the 5.2 ka event and the 4.2 ka event are not visible in many records, and in many cases where they do appear (Diefendorf et al, 2006; Williams and Doyle, 2014), there are chronological inconsistencies in different areas. Many of these events appear to have been prolonged climatic trends rather than the abrupt changes seen globally.

In Ireland, there is a lack of deglacial and early Holocene information and there is vast variability in the mid and late Holocene terrestrial records. In Galway Bay too, there is a lack of deglacial, mid and late Holocene information and, where it is available, there are chronological errors associated with the deposits. There is currently no coherent bay-wide reconstruction of past environments. In order to address these gaps, a multifaceted approach is needed together with a dataset spread more widely across the bay. Therefore, this research will use the entire geophysical dataset available for the bay collected by the INFOMAR programme (INtegrated mapping FOre the sustainable development of Ireland’s MARine Resources) which includes altimetry, multibeam-echosounder bathymetric and backscatter data, ground-truthing and pinger data, together with sediment cores recovered during R.V. Celtic Voyager cruise CE13031 (led by Ulster University) and hydrodynamic models developed for the bay by the Marine Institute of Ireland to provide such a reconstruction.

1.3 Research aim and objectives

The overall aim of this thesis is to reconstruct environmental and relative sea-level changes in Galway Bay from the last glacial period to present day by addressing the following research objectives:

- Mapping of present-day geomorphology of the coastline and seafloor of Galway Bay to determine which modern and/or glacial processes have shaped the submarine landscape of the bay.
- To build a seismic stratigraphy for Galway Bay through the identification of acoustic units using 3.5 kHz subsurface pinger geophysical data.
- To build a core stratigraphic chronology for Galway Bay through the identification and interpretation of the sedimentary processes, aided by multiple proxies such as x-radiographs, sedimentological, geochemical, microfossil analyses and radiocarbon dating.
- To reconstruct palaeoenvironmental conditions over the timespan covered by the abovementioned proxies and to examine the effects of global climate change in this region. In particular, abrupt climatic and oceanographic “events”, such as the Younger Dryas, the ‘8.2Ka’ event, and meltwater pulses 1A, 1B and 1C and how, or if, they affected Galway Bay.
- To produce a new relative sea-level reconstruction for the bay and compare it with the current Irish glacial isostatic adjustment (GIA) model reconstructions. This will help to refine post glacial sea-level reconstructions to be used for modelling of past and future coastal changes.

1.4 Thesis Structure

This PhD comprises 8 chapters, which address the PhD objectives. The outline of these chapters follows a traditional structure with the exception of chapter 4 which is a stand-alone research paper. Chapter 2 will discuss the study area and background. The geography of Galway Bay, its position in relation to the wider Irish shelf and its glacial and Holocene history, as well as the environmental history of relevant surrounding regions is presented. The drivers of climatic and sea-level changes and the wider global trends will be discussed, focusing in particular on studies that have used the various proxies that were used in this research. Chapter 3 contains a detailed description of the techniques used in this study, concentrating on geophysical data analysis, sedimentological, geochemical and microfossil analysis and their various benefits and drawbacks. Chapter 4 is a research paper titled: *Coastline and inshore geomorphology*

of Galway Bay, Western Ireland. It presents a present-day geomorphology map for Galway Bay, using satellite images, multibeam and altimetry data as well as ground truthed sediment samples. The results include a map detailing the submarine landforms, sediment substrate distribution and coastline classification. The map is used to explain the modern processes at work in the bay and better enables us to follow its evolution. It will be submitted for review in the Journal of Maps with co-authors. While the co-authors' support has been invaluable in editorial feedback and analytical work, all writing and geomorphological analysis for the completion of this thesis was carried out solely by the author. As this chapter is also a stand-alone paper there will be some overlap in the details of the study area and in the methods used (chapters 2 and 3 respectively). Chapter 5 presents the results, where all of the geophysical, sedimentological, geochemical and chronological data, including 18 radiocarbon dates, are brought together and the numerous datasets are presented and described. In Chapter 6 all the data available is interpreted to form a chronological reconstruction of the environmental changes within the bay, from the base of the seismic record, to the present-day geomorphology and sediment distribution. It evaluates how various processes denote particular environments, possible scenarios of how these environments were shaped and how they fit into the overall evolution of the bay. Chapter 7 discusses how the bay has evolved over time and how this fits into the wider, regional and global environmental changes occurring in the same period. In particular this chapter discusses relative sea-level changes and how the data from this research fit into sea-level reconstructions already available for the bay and the global trends of sea-level change. Chapter 8, the conclusion, provides a summary of the major findings of the research and makes suggestions for future work.

Chapter 2: Study area and Background

This chapter outlines the key characteristics of the study area. An overview of regional environmental change since the last glacial period is provided, with a focus on the global drivers of change and relative sea-level variations. Lastly, relevant proxies used for palaeoenvironmental reconstructions are presented.

2.1 Study Area

2.1.1 Geomorphology and hydrology

Galway Bay is a large (62km long, 32km wide), semi-enclosed marine embayment on the west coast of Ireland, between 53°02'N and 53°14'N and 09°00'W and 09°27'W. It is bordered by counties Galway and Clare to the north and south, respectively (Fig. 2.1). The bay has a gradually westward sloping bathymetric relief and water depths extend to ~70m below sea-level (bsl) in the north-west. It is a high energy, storm-dominated system with strong semi-diurnal tides and a mean spring tidal range of >4.5m (Booth, 1975; Marine Institute, 2017). Hydrodynamic models show current speeds between the Aran Islands above 45 cm/s in the ebbing spring tide, while wave models, based on wind speeds taken from the Mace Head atmospheric research station, show winter wave heights above 250 cm in the north and south sounds and mid-bay areas (Joshi et al., 2017). The primary inflow of Atlantic water into Galway Bay is through the South Sound, with tidal ranges reaching up to ~5m (Booth, 1975), and outflow through the North Sound, creating a counter clockwise gyre (Harte et al, 1982; Lei, 1995) (Fig. 2.1).

The primary freshwater source at the head of the bay is the river Corrib, a short but powerful river, with volumetric flow rates exceeding mean 311 m³/s almost every year since 1960 (OPW, 2012). Other freshwater inputs to the bay include submarine groundwater drainage streams along the northern shore at Spiddal, Barna and in the southeast at Kinvara Bay, the Oranmore, Clarinbridge and Dunkellin rivers to the east and Caher river to the south of the bay (Cave and Henry, 2011; Smith and Cave, 2012) (Fig. 2.1).

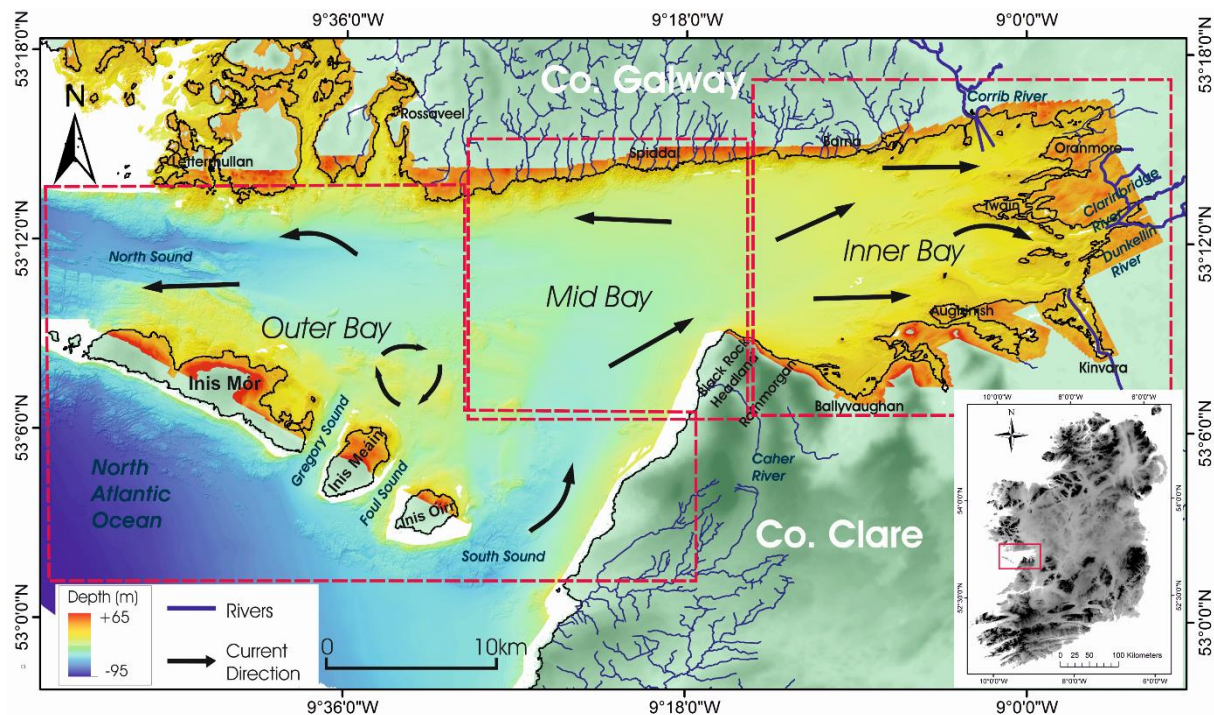


Figure 2.1: Bathymetric map of Galway Bay, showing the modern-day rivers contributing to the freshwater input. The bay has been divided into 3 areas (inner, mid and outer) for ease in identification. The main inputs are shown in bold in the inner bay, from the Corrib, Clarinbridge and Dunkellin rivers. The dominant current direction in the bay is taken from the work of Booth (1975) and Ren et al (2015).

The modern landscape of Galway Bay, as well as the surrounding region, was influenced by ice flow and retreat during Quaternary glaciations as it provided an important conduit for ice extension on to the shelf (Bowen et al, 2002; Sejrup et al, 2005; Stoker and Bradwell, 2005; Greenwood, 2008; Chiverrell and Thomas, 2010; Clark et al, 2012; Peters et al, 2015; Ballantyne and Ó Cofaigh, 2017; McCarron et al, 2018). Common glaciogenic landforms (Fig. 2.2) such as drumlins, meltwater channels, striae, streamlined bedrock and erratics (Kinahan, 1869; Kinahan et al, 1871; Cole et al, 1914; Greenwood and Clark, 2008; Fealy et al, 2009; GSI, 2013; Meehan, 2013), are present around the coastline of the bay and in the surrounding regions of counties Galway and Clare.

The combination of modern and past glacial, hydrological and sedimentological processes resulted in a variable littoral and submarine environment displaying a wide

range of habitats, including vegetated shingle, coastal lagoons, mud and sand flats, reefs and salt marsh, many of which are protected areas, with biological and ecological significance (Curtis and Sheehy Skeffington, 1998; NPWS, 2013).

Because of the importance of the regional glacial and postglacial history on the landscape of the bay, Section 2.2 will discuss this in more detail.

2.1.2 Geology

There are two predominant bedrock lithologies in this region (Fig. 2.2). Along the low lying, northern coastline of the bay, the bedrock is composed predominantly of granite, while the rest of the bay, including the Aran Islands, is composed of limestone.

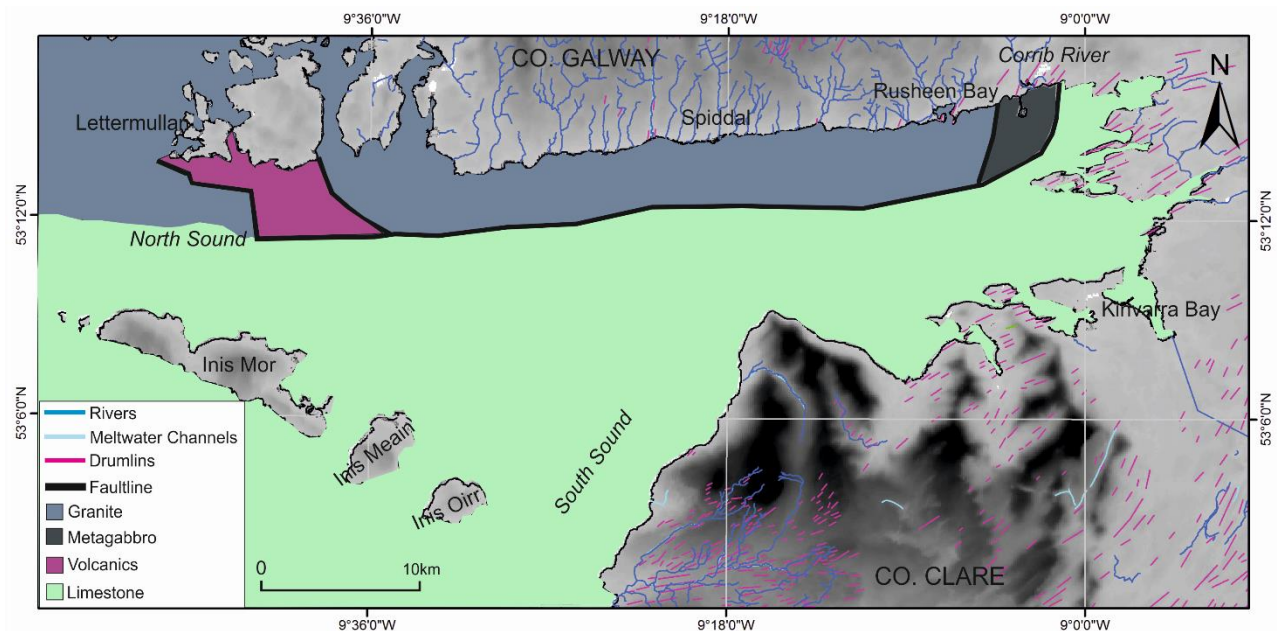


Figure 2.2: Map of Galway Bay showing the bedrock geology, divided by a, east-west fault line that runs through the bay, and some of the dominant features in the surrounding landscape (Adapted from Max et al, 1983; Williams et al, 1988; Clarke, 2013; GSI, 2013, 2016; INFOMAR, 2013).

The limestone was primarily formed during the Viséan stage of the Carboniferous age, ~345-326 million years ago (Pracht et al, 2004; Gallagher et al, 2006; McNamara and Hennessy, 2010), and provides a nearly continuous record of carbonate deposition over this period (Pracht et al, 2015). The granite in the north of the bay was formed during the Caledonian orogeny in the Devonian period, ~400 million years ago (Doyle,

1988; Leake, 1989, 2006; Feely et al, 2003; Pracht et al, 2004) and intruded into the pre-existing Metagabbro-Gneiss Suite of the region (Baxter et al, 2005). Small amounts of Ordovician metagabbro and orthogneiss intrusions define the geology around the area of Galway city while Ordovician volcanics are found near Lettermullan in the extreme northwest of the bay (Leake, 1989). The Galway Granite is cut by the Barna and Shannawona Faults (Fig. 2.2), which divide it from the Metagabbro to the east and the Volcanics to the west, respectively (Baxter et al, 2005; Callaghan, 2005). The rest of the bay is split by an east-west oriented fault line, known as the Galway Bay Fault, which runs through the entire northern region of the bay (Gatley et al, 2005; Philcox and Lees, 2006; Lees and Feely, 2016), and forms a clear divide between the northern granite, volcanics and metagabbro from the surrounding limestone. The Galway Bay Fault runs through the North Sound, the deepest region of the bay, and as it represents the limit of various types of geology, erosion in this area is likely to be more significant. The bedrock of the bay was then further shaped by denudation processes from Quaternary glaciations, which produced the current low elevation and subdued relief. This occurred before the last glacial period (Simms, 2005).

2.2 Glacial history of the region

The Quaternary period is characterised by multiple large-scale glaciations (i.e glacials), punctuated by climatic warm periods, (i.e interglacials). These periods are driven by orbital forcing, which controls levels of solar insolation on Earth, at different periodic occurrences, ranging from 100,000 to 23,000 years (Milankovitch, 1941; Berger and Loutre, 1991). Within the last glacial cycle shorter periodic occurrences, known as Dansgaard-Oeschger (D-O) events are also visible. These shorter cycles occur in 1,000-2,000-year intervals (Bond et al, 1999) leading to abrupt temperature increases, followed by prolonged cooling (Dansgaard et al, 1993). While their underlying cause is still poorly understood, it is believed that solar forcing and the dynamics of ocean-atmospheric systems play a part (Bond et al, 1999). A D-O event is recognised during the height of the Last Glacial Maximum (LGM) (~26 – 19 ka BP) (Clark et al, 2009), which refers to the global glacial maximum, where much of Eurasia was covered by massive ice sheets that coalesced to form the Eurasian ice sheet complex (EISC)

(Svendsen et al, 2004). The BIIS represents the maximum western extent, to the shelf edge off western Ireland, of the ice in Europe (Peters et al, 2015).

In Ireland, much of the older underlying sediments have been eroded during the last glacial period, with only a handful of pre-LGM deposits found on the island (McCabe, 1987; Coxon et al, 2017). The main intact sequences include the sites near Gort, Co. Galway; Baggotstown, Co. Limerick and Cork Harbour, Co. Cork (Dowling and Coxon, 2001; Jessen et al, 1959; Watts, 1964, 1985; Coxon et al, 1996; Dowling et al, 1998; Coxon and Dowling, 2015), where interglacial sediments have been found under till deposits.

In Galway Bay, the lack of any sedimentary units underlying the till deposits (Clarke, 2013), suggests that all pre-LGM sediment was removed through glacial action. As the current landscape of Galway Bay is inferred to have been mostly shaped during the last glacial cycle and ensuing interglacial period, the next sections summarise in more detail the Late Quaternary and Holocene history for this region.

2.2.1 The Last Glacial Maximum

During the late Midlandian (~25 – 11 ka cal BP) ice sheets covered much of Europe. The British-Irish ice sheet (BIIS), which covered most of UK and Ireland has been studied extensively (Hull, 1878; Lewis, 1877, 1894; Charlesworth, 1928; Wright, 1914; Synge and Stephens, 1960; McCabe, 1987; Bowen et al, 2002; Knight et al, 2004; Sejrup et al, 2005; Clark et al, 2009; Greenwood and Clark, 2009; Benetti et al, 2010; C. Clark et al. 2012; J. Clark et al, 2012; Ballantyne and Stone, 2015; Peters et al, 2015, 2016; Ballantyne and Ó Cofaigh, 2017; Callard et al, 2018). In recent years, research into the history of the BIIS has increased significantly due to the fact that it can provide an analogue for modern ice sheets as any data on the rate and style of retreat can feed into current glaciological models for the investigation of modern ice sheets under changing climate (Clark et al, 2012).

Some of the earliest work by Wright (1914) and Charlesworth (1928), who carried out a morphological and sedimentological analysis of the Irish landscape, suggested that the southernmost extent of a former ice sheet was at the 'Southern Ireland End Moraine' (SIEM), which stretches from the Shannon in the south-west to Wicklow in the south-east, with ice free areas in the west (Fig. 2.3). This reconstruction implied

that much of Southern Ireland was ice-free during the LGM (26 -19 ka BP). South of the SIEM, glaciogenic deposits were considered to have been deposited by an earlier glaciation (Bowen et al, 1986; McCabe, 1999). In the past 2 decades however, contradictory evidence regarding the SIEM as the limit of glacial ice in Ireland has come to light. Bowen (1973) and Warren (1979b) argue that Wright's (1914) separation of glaciogenic drift deposits into 'younger' and 'older' deposits is not stratigraphically conclusive, with no sedimentological basis for the distinction (Greenwood, 2008).

The current accepted view is that the whole of the island of Ireland was covered by ice during the LGM and that the SIEM represents a recessional standstill (McCabe and Ó Cofaigh, 1995; Ó Cofaigh et al, 2007). The model of LGM ice cover by Clark et al (2017), based on high resolution bathymetric and seismic data combined with the literature of groundtruthed sediments and onshore dates appears to best represent the limits of the ice margin during the LGM, which extend westwards as far as the shelf edge and southwards across the Celtic Sea (Fig. 2.3).

This model is now supported by numerous studies carried out both on land and offshore. In the Wicklow Mountains, evidence of glacial erosion up to 725m suggest that the ice extended to at least this altitude and erratic distribution patterns show that an ice dome existed during the LGM, feeding the paleo-ice stream moving southwards to the Celtic Sea (Ballantyne et al, 2006). In the north-west of Ireland, the mountains in counties Donegal and Mayo show evidence of glacial erosion at altitudes of 500-600m and on the Peninsula of Achill Island at up to 400m (Ballantyne et al, 2008) (Fig. 2.3). In western Ireland the minimum upper limit of glacial erosion in the mountains of county Mayo are at an altitude of 700m. Cosmogenic nuclide dates confirm that this glacial erosion occurred during the LGM (Ballantyne et al, 2008). The patterns of glacial features in these areas suggests that there were multiple independent ice domes feeding the ice sheet across Ireland (Ballantyne and Ó Cofaigh, 2017).

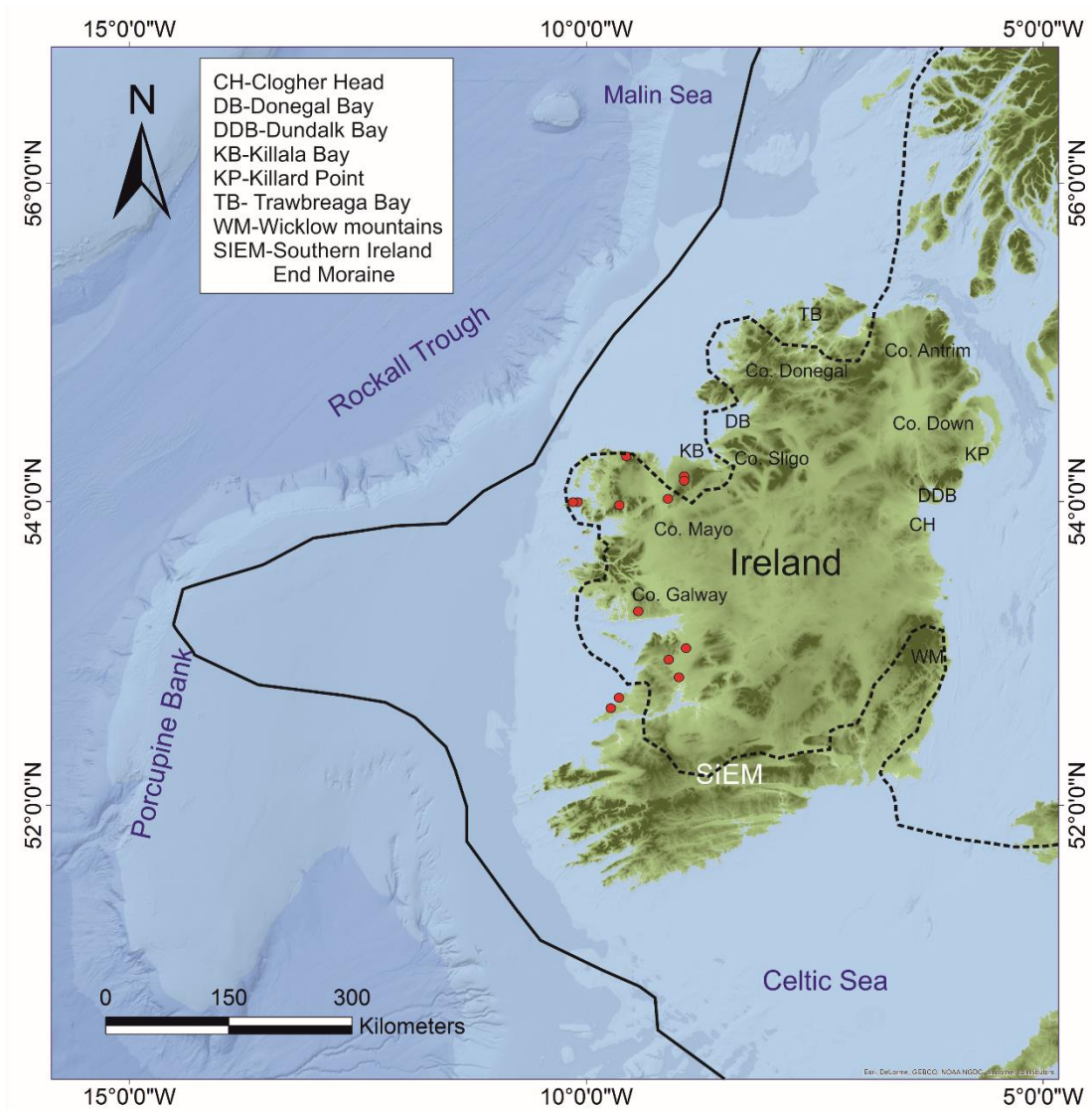


Figure 2.3: Map showing the extent of the BIIS across Ireland. The dashed line represents the boundary of the earlier work that indicated the SIEM as the limit of the ice sheet (Bowen et al, 2002), while the solid black line represents the maximum extent of the ice sheet based on the most recent research (Clark et al., 2017). The red points represent the sites in Table 2.1, where the movement of the ice sheet has been chronologically constrained, following the LGM.

The extent of the BIIS beyond the coastline has been less extensively studied than the terrestrial portion. However, with the terrestrial data suggesting an offshore extension onto the continental shelf, more research has been carried out in recent years in the marine environment. On the north-western and western Irish shelf, detailed mapping of the glacial landforms shows moraine complexes at to the shelf break (Benetti et al,

2010; Dunlop et al, 2010; Clark et al, 2012; Ó Cofaigh et al, 2012) (Fig. 2.4). Streamlined subglacial bedforms indicate a north-west and westerly ice flow from Donegal, while the NW-SE alignment of moraines and grounding-zone wedges on the Malin shelf suggest that the ice was flowing from western Scotland and merging with the ice sheet flowing from Ireland (Dunlop et al., 2010; Callard et al., 2018). Nested, arcuate moraines orientated in a NE-SW direction offshore of Donegal Bay, provide evidence of the ice extending from Counties Donegal and Sligo as far as the northern Porcupine Bank (Benetti et al., 2010; Fig. 2.4). More spatially constrained extensions of ice onto the shelf are indicated by the presence of morainic ridges in the inner continental shelf offshore Clew Bay and Killary Harbour (Peters et al., 2015). To the south west, the Galway Lobe Moraine represents a major still-stand for BIIS extension offshore of County Galway. However, the identification of ice-contact landforms on the northern Porcupine Bank and Slyne Trough pushes the maximum limit of the BIIS extension further westwards by 80km (Peters et al., 2015, 2016). In the south, sedimentological evidence shows that the BIIS extended southwards across the Celtic Sea, to the Irish/UK continental shelf edge (Praeg et al, 2015; Lockhart et al, 2018). The general agreement in the literature is that the maximum extent of the BIIS occurred before ~24 ka BP, after which ice sheet retreat occurred (Scourse et al, 2009; Chiverrell et al, 2013; Purcell, 2014; Peters et al, 2015).

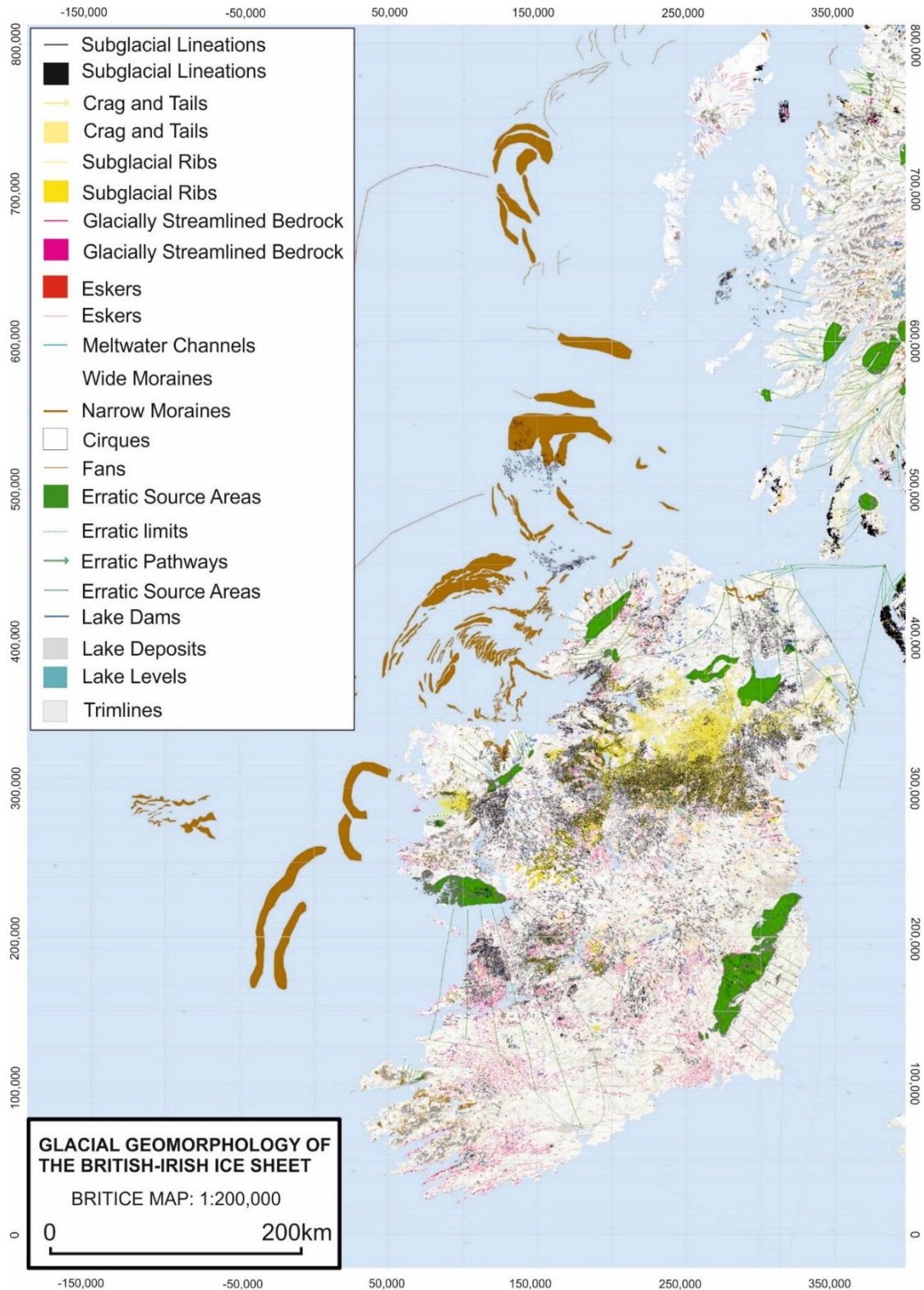


Figure 2.4: Map of the glacial geomorphology of the BIIS. Compiled from a review of the published academic literature and Irish and British Geology survey mapping, at the University of Sheffield as part of the BRITICE-CHRONO project (Clark et al, 2017).

2.2.2 Retreat of the BIIS

The timing of the initiation of ice sheet retreat from the shelf break is constrained to 27-24 ka cal BP (Peters et al., 2016; Callard et al., 2018; Lockart et al, 2018; Ó Cofaigh et al, 2019). However, due to the highly dynamic nature of the ice sheet, evidence of periods of stillstand and re-advance are abundant (Table 2.1). In the south, major and rapid deglaciation of the Celtic Sea was underway by 23 ka cal BP when the Irish Sea ice stream (ISIS), a fast-flowing stream of grounded ice in the Irish Sea basin, had started to recede. This coincided with a period of warming during Greenland Interstadial 2 (Johnson et al, 1992; Stokes and Clark, 2001; Scourse et al, 2009; Praeg et al, 2015; Ó Cofaigh et al, 2012; Chiverrell et al, 2013; Ballantyne and Ó Cofaigh, 2017). The rest of offshore Ireland experienced a slower, stepped glacial retreat that likely occurred over several millennia, as evidenced by the presence of recessional moraines (Benetti et al., 2010; Dunlop et al, 2010; Peters et al, 2015). In the north-west, the BIIS became lobate with separation in well-defined Scottish and Irish ice domes (Benetti et al., 2010; Dunlop et al, 2010). Ice had retreated to the coastline of Scotland by 20 ka cal BP (Small et al., 2017) and the north-western Irish coast by ~18 ka cal BP (Ó Cofaigh et al, 2019). In the west, Peters et al (2016) suggest that the first stage of retreat was <21.9 ka cal BP, caused by thinning and uncoupling of the ice sheet followed by the transformation into lobes. The central lobe then retreated to the Galway lobe grounding zone wedge (GLGZW), where a stillstand occurred for a period of ~3,300 years. By 19 ka cal BP, ice had retreated to the coastal fringes of Ireland and disappeared from some areas in the south of the island entirely (Hughes et al, 2011; Clark et al, 2012). This may have been accelerated by rising sea-levels and meltwater pulse 1A0. Meltwater pulses are caused by the catastrophic collapse of ice sheets that drain into the oceans causing rapid global eustatic sea-level rise (Fairbanks, 1989; Bard et al, 2010; Deschamps et al, 2012). At 19ka cal BP the influx of glacial meltwater in to the global oceans caused substantial sea-level increase (10-15m) (Clark et al, 2004; Carlson and Clark, 2012). The lobate behaviour of the ice sheet meant that smaller, regional re-advances occurred during deglaciation. In western Ireland, Peters et al (2016) found evidence of moraines representing a re-advance at <18.5ka BP and at ~15-14.5ka BP onto the shelf. In the north-west, a re-advance seemed to have occurred from the Ox mountains in Co. Sligo through Killala Bay and

Donegal Bay at <17.6ka BP (Greenwood and Clark, 2009; J. Clark et al, 2009; Schiele et al, 2017). In northern Ireland, in Co. Donegal, a re-advance into Trawbreaga Bay between 18-17ka cal BP (McCabe and Clark, 2003) is believed to be part of the same re-advance taking place at 17.5ka cal BP, further east in counties Derry and Antrim recorded by the Armoy moraine (Knight, 2004). In the north-east of Ireland, two significant re-advances into Dundalk Bay have been time constrained: the Clogher Head (Co. Louth) re-advance and the Killard Point (Co. Down) re-advance. At Clogher Head, the ice sheet re-advance has a maximum age between 18.3 and 17.3 ka cal BP while the Killard Point re-advance has a maximum age between 17.1 and 15.2 ka cal BP (McCabe and Haynes, 1996; Lowe and Walker, 1997; McCabe and Clark, 1998; McCabe et al, 1998; McCabe et al, 2007b). While it is accepted that a re-advance known as the east Antrim coastal re-advance (EACR) occurred, the timing of this re-advance is contested. McCabe and Williams (2012) correlate the EACR to other areas in both Scotland and Ireland, thus constraining the re-advance from 15.5-15 ka cal BP. Finlayson et al (2014), however, suggest that the EACR occurred due to rapid wasting of Irish terrestrial ice allowing the advance of Scottish ice at ~16.5 ka cal BP. Rapidly rising global temperatures c.15 ka cal BP (Watson et al, 2010), marked the beginning of the Woodgrange interstadial. At this time, or soon after, low lying areas across all of Ireland were likely to have been completely ice free. Although smaller glaciers may have survived in upland areas for a period of time after this, as in north-west Scotland (Bradwell et al, 2008), no conclusive evidence of this has been found in Ireland beyond the Woodgrange Interstadial. It has however been suggested that small mountain glaciers may have been present in Ireland during the Younger Dryas (Nahanagan Stadial) at ~12.6ka BP (Harrison et al, 2010; Barr et al, 2017; Clark et al, 2012, Hubbard et al, 2009). Overall, evidence on the collapse of the BIIS suggests a complex interaction of internal and external factors including the cycling of ice-streams, ocean temperatures and circulation, and land-surface albedo, was responsible for deglaciation (Alley and Clark, 1999).

Table 2.1: Onshore dates after the LGM, from the Ox Mountains in Co. Sligo to the Shannon River in Co. Limerick, along the coastline of western Ireland, represented spatially in Figure 2.3. ^{10}Be ages that have not used the Loch Lomond local production rate (LL LPR) have been recalibrated by Ballantyne and Ó Cofaigh (2017), while ^{14}C ages have been recalibrated using the INTCAL13 calibration curve.

Average Age (kaBP) recalibrated	Dating Technique	Location	Average Elevation (m)	Interpretation	Reference
17.88	CN ^{10}Be	Ox Mountains	233	Killard Point readvance age constraint	Clark et al., 2009
16.5	CN ^{10}Be	Ox Mountains	206	Exposure age from post LGM deglaciation	Schiele et al, 2017
16.2	CN ^{10}Be	Foxford	40	Deglaciation of Killala Bay ice lobe age constraint	Schiele et al, 2017
19.78	^{14}C AMS	Belderg Pier	-	Post LGM deglaciation	McCabe et al., 2005
13.6	CN ^{36}Cl	Acorrymore House	190	Erosion after deglaciation	Bowen et al., 2002
16.7	CN ^{36}Cl	Lough Acorrymore	195	Erosion after deglaciation	Bowen et al., 2002
13.7	CN ^{10}Be	Lough Acorrymore	225	Age constraint for retreat of corrie glaciers	Ballantyne et al., 2008
19.4	CN ^{10}Be	Anaffrin East Col	440	Post-LGM deglaciation	Ballantyne et al., 2008
17.7	CN ^{10}Be	Furnace Lough	36	Killard Point readvance age constraint	Clark et al., 2009b
19.2	CN ^{10}Be	Mweelrea	125	Post-LGM deglaciation	Ballantyne et al., 2008
16.1	CN ^{10}Be	Mweelrea	478	Post-LGM deglaciation age constraint	Ballantyne et al., 2008
20.9	CN ^{36}Cl	Cornarone	30	Exposure age from post LGM deglaciation	Bowen et al., 2002
11.6	^{14}C AMS	Fiddaun	-	Ice-free age constraint	van Asch et al., 2012
16.2	^{14}C AMS	Lough Inchiquin	25	Post-LGM deglaciation	Diefendorf et al., 2006
12.6	^{14}C AMS	Edenvale Cave Complex	-	Ice-free age constraint	Woodman et al., 1997
15.3	CN ^{36}Cl	Kilkeel	66	Erosion after deglaciation	Bowen et al., 2002
20.3	CN ^{36}Cl	Loop Head	120	Erosion after deglaciation	Bowen et al., 2002

2.3 The Holocene

After the Younger Dryas the period of warming known as the Holocene (<11.7ka BP) began. Records across the Northern hemisphere suggest that the Holocene is characterised by pronounced climate oscillations varying in length from 10's to 100's of years (O'Brien et al, 1995; Barber et al, 1999; Bianchi and McCave, 1999; Bond et al, 1999, 2001; Hu et al, 2003; Langdon et al, 2003; Mayewski et al, 2004; Charman, 2010; Swindles et al, 2013; Roland et al, 2014). As a result of an improved understanding of these oscillations, the Holocene has been sub-divided into 3 periods: the Greenlandian (11.7 – 8.2 ka BP); the Northgrippian (8.3 – 4.2 ka BP) and the Meghalayan (4.2 ka BP – present day) (Walker et al, 2018).

The Greenlandian period was marked by a drastic temperature increase following the Younger Dryas, (Birks and Ammann, 2000; Brooks and Birks, 2001; Schwark et al, 2002; Lang et al, 2010; van Asch et al, 2012).

This warmer period was punctuated by shorter, less pronounced, cold spells, beginning with the pre-boreal oscillation (PBO) at ~11.4 ka cal BP, which lasted between 150-250 years (Kapsner et al, 1995; Björck et al, 1998; Rasmussen et al, 2007; Jessen et al, 2008) and had an impact on the spread of woodlands across Europe (van der Plicht et al, 2004; Bohncke and Hoek, 2007; Bos et al, 2007). The pollen record in Ireland shows the earliest instances of Holocene vegetation immediately after the Younger Dryas, composed of *Juniperus* (Juniper) and *Betula* (Birch), which spread rapidly across the island (Mitchell, 1995, 2006). The PBO is possibly recorded as an increase in the $\delta^{18}\text{O}$ record of lacustrine marl (Diefendorf, 2006), but did not appear to have a significant impact upon the spreading vegetation. Some studies have speculated that a large meltwater flux from the draining of ice sheets into the North Atlantic was likely a contributing factor to the change in climate, coinciding with the PBO (Björck et al, 1998; Teller et al, 2002; Bos et al, 2007; Filoc et al, 2018). Several such meltwater pulses have been recognised in the coral record (Fairbanks, 1989; Edwards et al, 1993; Hanebuth et al, 2000; Weaver et al, 2003; Rasmussen, 2006; Bard et al, 2010;) (Fig. 2.5). MWP-1B has been linked to the PBO by several studies (Hughen et al, 1996; Björck et al, 1998; Hald and Hagen, 1998; Fisher et al, 2002).

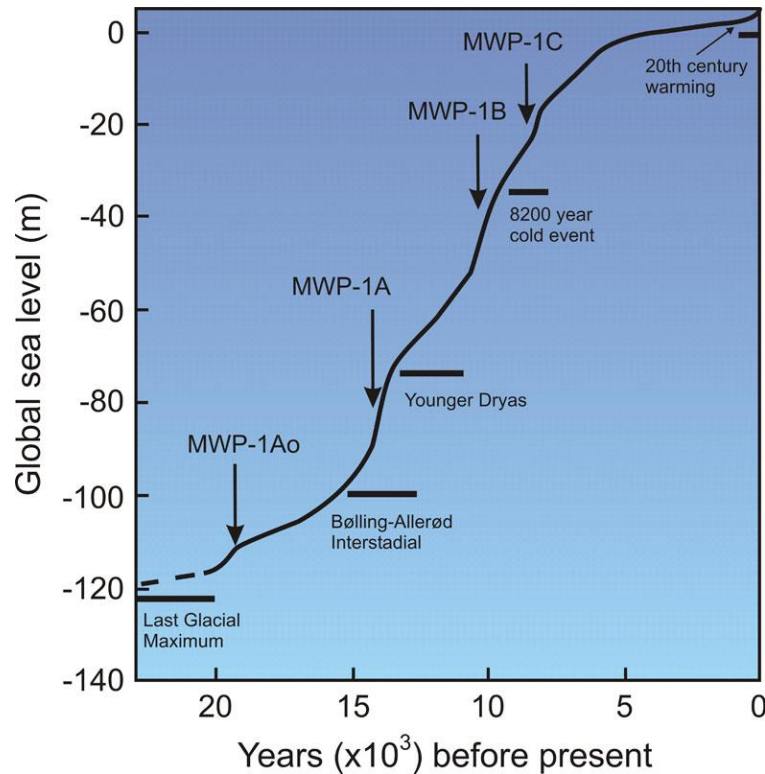


Figure 2.5: Image showing the global sea-level curve since the LGM and the occurrence of meltwater pulses (MWP). MWP 1A0: ~19.6 – 18.8 ka BP, MWP 1A: ~14.6-13.8 ka BP. MWP 1B: ~11-8.8 ka BP, MWP 1C: ~8.2-7.6 ka BP (Gornitz, 2012).

Following the PBO was a warm climatic phase that occurred globally between 11 and 5 ka cal BP. This climatic warming is known as the Holocene thermal maximum (HTM) and varied significantly in timing and magnitude (Kaufman et al, 2004; Jansen et al, 2007, 2008; Wanner et al, 2008; Bartlein et al, 2011; Renssen et al, 2012). The HTM is considered to have occurred in Ireland, for a shorter period, between 10.8 and 9 ka cal BP (Diefendorf et al, 2005, 2006; Holmes et al, 2007; Ghilardi and O’Connell, 2013; McKeown et al, 2013). The Irish climate became warmer again and there was an increase in the spread of vegetation, when trees, especially hazel, began to rapidly colonise former grassland areas (Smith and Goddard, 1991; Hall, 1997; Mitchell, 2006; Holmes et al, 2007). The next significant cooling event, within the Greenlandian period, occurred at ~9.3ka BP (Yu et al, 2010). This cold period is seen from ice core records in Greenland (Vinther et al, 2006) to speleothem records in China (Shao et al, 2006) and tree-ring records in Germany (Spurk et al, 2002). In British records, it is

expressed as an increase in snow cover, recorded in an increase in animal remains and different cosmogenic ^{10}Be surface exposure dates from gritstone outcrops (Wilson et al, 2013; Lord et al, 2015). In Irish pollen records, there is a decline in vegetation sensitive to frost and an increase in trees tolerant of colder climates (Ghilardi and O'Connell, 2013). However, in the Irish records the timing of this cooler period is less clearly defined, with an age range between 9.4 and 8.8 ka BP in speleothem and lake records from south western Ireland (Diefendorf, 2005; McDermott et al, 2001). This lack of chronologically constrained evidence may indicate that the 9.3ka event was not as significant in Ireland as elsewhere and was characterized instead by a longer period of cooler weather rather than a sharp climatic oscillation.

The beginning of the Northgrippian period is defined by the catastrophic drainage of melting ice from glaciers into the Atlantic Ocean, culminating in the 8.2 ka event (Hammer et al, 1986; Klitgaard-Kristensen et al, 1998; Johnsen et al, 2001). This event was characterised by an influx of cold, fresh water that disrupted the Atlantic Meridional Overturning Circulation (AMOC) and caused a climatic cooling that lasted ~160 years. It affected climate on a global scale (Thomas et al, 2007; Morrill et al, 2013a; Rasmussen et al, 2014; Matero et al, 2017). Although there is some evidence for this melting occurring in 2 phases (Clark et al, 2004; Hillaire-Marcel et al, 2007), or even as an abrupt increase within a larger cooling period (Rohling and Palike, 2005), all evidence suggests that a significant volume of freshwater was introduced into the Atlantic Ocean between 8.5 and 8 ka cal BP (Ellison et al, 2006; Törnqvist and Hijma, 2012; Matero et al, 2017). This climatic event is the most prominent climatic change in the Northgrippian and is seen globally, across a range of records including ice cores, marine and lake sediments, peat deposits and speleothems (Street-Perrott and Perrott, 1990; Dansgaard et al, 1993; Hughen et al, 1996; Bond et al, 1997; Rousseau et al, 1998; Hu et al, 1999; McFadden et al, 2004). In western Ireland, the 8.2 ka event is seen in the terrestrial record in speleothem trace element records in Co. Kerry (Baldini et al, 2002), $\delta^{18}\text{O}$ ostracod calcite records in Lough Monreagh, Co. Clare (McKenzie, 2010), $\delta^{18}\text{O}$, ostracod assemblage and pollen records from Cooney Lough, Co. Sligo, Lochs Avolla, and Gealain, Co. Clare, Loch Corrib, Co. Galway (Holmes et al, 2016) and An Loch Mor, Co. Galway (Holmes et al, 2007; Ghilardi and O'Connell, 2013; Molloy and O'Connell, 2004, 2014). These all suggest a cooler, drier climate with a

decrease in plant coverage. Shallow water marine studies in the area show signatures that may relate to a cooling phase at this time. Wood et al (2017) note an increase in the $\delta^{18}\text{O}$ record after 9.26 ka cal BP while Novak (2017) notes a freshwater pulse and a decrease in organic content between 8.8 - 8.4 and 8.1 - 7.8 ka cal BP. In deeper water records, there is also a recognisable decrease in sea surface temperatures based on dinoflagellate cyst assemblages and planktonic foraminifera (Hillaire-Marcel et al, 2001, 2007; de Vernal and Hillaire-Marcel, 2006)

Following the 8.2 ka event, temperatures recovered, and a warming trend began at ~ 8 ka BP, leading to the prolonged HTM in many places across Europe between 8 and 6 ka cal BP (Caseldine et al, 2006; Renssen et al, 2009). While the climate in Ireland also underwent a warming, evidence from pollen and lake (chironmid) records shows that it did not reach the temperatures of the early Holocene. Hence, the shorter HTM period in Ireland (Diefendorf et al, 2005, 2006; Holmes et al, 2007; Ghilardi and O'Connell, 2013; McKeown et al, 2013).

This warming is evident across Europe in the spread of vegetation; especially thermophilous trees such as hazel, elm and oak, which thrive in warmer conditions (Molloy and O'Connell, 2014; Mitchell, 2006). The fern population in western Ireland also has very high pollen percentages at this time, suggesting that this increasing tree population formed open woodland (Fossitt, 1994; O'Connell et al, 1999). The climate in Ireland appears to have become wetter during this period, with the first signs of Alder (*Alnus*) populations, a tree that prefers wet soils, in Co. Sligo after 8ka BP (Ghilardi and O'Connell, 2013), and thriving populations across the landscape by ~ 7 ka cal BP (Smith and Goddard, 1991). However, within this warm period a shorter cooling trend is evident between ~ 7.3 and 6.7 ka cal BP in the $\delta^{18}\text{O}$ speleothem and lake records. However, this appears to be regionally restricted to western Ireland (Diefendorf et al, 2005, 2006; McDermott et al, 2001).

Within the global warming trend of the Northgrippian, the mid-Holocene period was punctuated by short lived cold events, in particular at 6.4, 5.3 and at 4.2 ka cal BP, the latter a significant climatic change which ended the Northgrippian (Wanner et al, 2011, 2015; Bassetti et al, 2016). In western Ireland, a further regional climatic event is evident from 7.3 to 7 ka cal BP in lake records and speleothem records (McDermott et al, 2001; Diefendorf et al, 2006). This is a wetter phase that, in $\delta^{18}\text{O}$ lake records from

Inis Mór, appears even more prominent than the 8.2 ka event (Diedendorf et al, 2006). This increase in winter precipitation, based on the negative excursion in the $\delta^{18}\text{O}$ and relatively unaffected total organic matter, is also seen in other European records with higher lake levels between 7.5 and 7.25 ka cal BP (Magny and Bégeot, 2004), while in cave records from Italy, the wettest phase occurs between 8.2 – 7.3 ka cal BP (Spotl et al, 2010). Following this, the climate across Europe experienced an enhanced number of dry events between 7.2 and 5.7 ka BP, corresponding with the HTM in many areas (Andrews and Giraudeau, 2003; Davis et al, 2003; Bjune et al, 2005; Caseldine, 2006; Wanner et al, 2008, 2011, 2015; Stivrins et al, 2017). Between 6.5 and 5.9 ka cal BP, reduced solar activity was the most likely driver of a worldwide climatic cooling with the expansion of glaciers and lower sea temperatures in the northern hemisphere (Grove, 2004; Berner et al, 2008; Steinhilber et al, 2009; Wanner et al, 2011; Solomina et al, 2015; Khan et al, 2017), drier conditions with abrupt changes causing weakened monsoon systems (Bonfils et al., 2001; Braconnot et al., 2000; Brooks, 2006; Damnati, 2000; Saraswat et al, 2013; Xiao et al, 2014; Yu et al, 2006) and an increase in aridity in Africa and Asia (Sirocko et al, 1993; Gasse and Van Campo, 1994; Damnati, 2000; Guo et al, 2000; Brooks, 2006). This colder drier period corresponds to a Bond event at ~5.9 ka cal BP (Bond et al, 1997). Bond events are caused by increased ice-rafting, causing a weakening of the thermohaline circulation, changes in the North Atlantic oscillation (NAO) and a southward shift of the Atlantic westerlies. They have a cyclicity of ~1000 years and by altering the distribution of precipitation, they can have a knock-on effect on regional climatic conditions across Europe (Fig. 2.6).

This colder and drier climatic trend at 5.9 ka cal BP is not, however, seen that clearly across Europe. Here the records primarily show warmer and wetter conditions (Lamb et al, 1977; Davis et al, 2003; Brewer et al, 2007; Constantin et al, 2007; Cvetkoska et al, 2014). This is the case in western Ireland too, where the records show a warm, wet climate with well-established woodlands (Dodson, 1990; McDermott et al, 2001; Diefendorf et al, 2006; Holmes et al, 2010; Murnaghan et al, 2012; Ghilardi and O'Connell, 2013). Where it does leave a signature, such as in chironomid assemblages In Lough Nakeeroge in Co. Mayo, the climatic cooling appears later, between 6 and 5.65 ka cal BP, although McKeown et al (2013) attributes this variation in age due to dating errors.

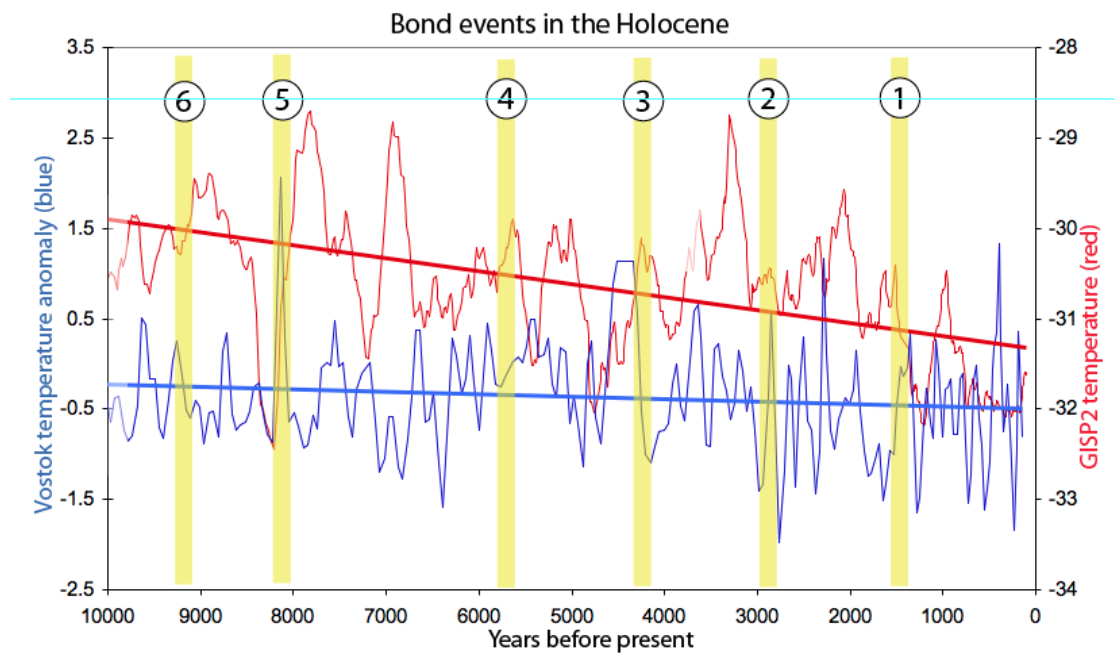


Figure 2.6: Image showing Bond events during the post-glacial, alongside ice core records from Greenland (Bond, 1997).

The only significant indicator of a climatic downturn across Europe at this time is related to the decline in the elm population. This decline has been dated both earlier and later, but the majority of dates are clustered around 6 – 5.9 ka cal BP, (Whittington et al, 1991; Innes et al, 2006; Albert and Innes, 2015), corresponding with the aforementioned Bond event. In the British Isles, this decline is seen over a wider time range from 6.3 – 5.3ka cal BP (Parker et al, 2002). The cause of the mid-Holocene elm decline is believed to be due to a number of factors including the spread of pathogens, human influence during the transition from the Mesolithic to the Neolithic and climate change (Skog and Regnell, 1995; Parker et al, 2002; Batchelor et al, 2014; Grosvenor et al, 2017). However, in Ireland the elm decline is not affected by the 5.9 ka cal BP climatic event, as elm populations in Ireland remain stable until 5.5 ka cal BP, when there is a 5-10% decrease in pollen records (Lamb and Thompson, 2005). In Ireland, especially western Ireland, the advent of extensive pastoral farming and the decline of tree populations is considered to have begun at 5.8 ka cal BP (Hall, 1997; O’Connell and Molloy, 2001; McLaughlin et al, 2016), suggesting that while the climate

may be becoming wetter and cooler, it had not deteriorated drastically enough to slow the expansion of Neolithic farming. This phase of pastoral expansion, after 6 ka cal BP, is known as the Landnam phase and is seen throughout much of north-western Europe (Inverson, 1941; Pilcher et al, 1971; Brown, 2008; Shennan et al, 2013). In Ireland, it appears to last longer than in other areas, continuing up to 5.45 ka cal BP (Smith et al, 1981; Stolze et al, 2012). This expansion of farming was possible due to a temperate, moderate climate, evidence of which can also be seen in Galway Bay, where oak and pine trees, species that do not thrive in waterlogged conditions, grew along the northern shoreline until 5.2 ka cal BP (Williams and Doyle, 2014).

During the mid-Holocene, a reversal in the climatic conditions of the HTM is observed globally, believed to have been caused by decreases in solar activity (Magny et al, 2006 and references therein). Most of these climate changes across the world occurred in short multi-centennial events between 5.6 and 5 ka cal BP, collectively known as the 5.2 ka event (Magny et al, 2006). This period coincides with the creation of the first large, organised, urbanised civilisations, likely driven by the changing climate and the loss of land suitable for farming (Sandweiss et al, 2001; Berglund, 2003; Staubwasser and Weiss, 2006; Brooks, 2006, 2012). In Ireland, increased storminess, higher lake levels and wetter conditions are evident in lake, bog and cave records from 5.5 – 5.1ka cal BP, coinciding with the sharp decline in Neolithic farming practises, the abandonment of agricultural land and the beginning of a clear change in bog hydrology and blanket bog expansion across the landscape (Molloy and O’Connell, 1995; McDermott et al, 2001; O’Connell and Molloy, 2001; Baille and Brown, 2002; Huang, 2002; Caseldine et al, 2005; Schettler et al, 2006; Tibert et al, 2007; Verrill and Tipping, 2010; Langdon et al, 2012; Ghilardi and O’Connell, 2013; Roland et al, 2015; Gallego-Sala et al, 2016; McLaughlin et al, 2016).

Worldwide, a significant climatic change occurred between 4.4 – 3.8 ka cal BP, known as the 4.2 ka event, which marked the end of the Northgrippian and beginning of the Meghalayan period (Walker et al, 2012; Walker et al, 2018), and is reflected in proxies in both the northern and southern hemispheres. The 4.2 ka event is known, in particular, for the aridification of lower latitude areas in Africa and Asia (Magri and Parra, 2002; Davis and Thompson, 2006; Parker et al, 2006; Roberts et al, 2011), as well as shift towards a cooler, drier, climate in North America and Southern Europe

(Magny, 2004; Booth et al, 2005; Larsen et al, 2012). This climatic shift had a huge impact on human populations and has been linked to the collapse of major civilisations (Weiss et al, 1993; Cullen et al, 2000; DeMenocal, 2001; Stanley et al, 2003; Staubwasser et al, 2003; Welc and Marks, 2014). Bond et al (2001) argue that this event was triggered by changes in solar irradiance, corresponding to Bond event 3 (Fig. 2.6). This does not however, explain the variation in timing of the onset of these changes, nor does it explain why some areas show major climatic shifts, while other higher, latitude regions, such as Great Britain and Ireland have no such uniform changes (Roland et al, 2014).

In Ireland there is a shift to slightly wetter conditions in some bog records (Barber et al, 2003). In speleothem records, McDermott et al (2001) note that a drop in $\delta^{18}\text{O}$, indicates a cooler period, coinciding (within dating uncertainties) with the 4.2 ka event and may represent a weaker North Atlantic thermohaline circulation. This, however, conflicts with chironomid and pollen records from a lake in the north-west of Ireland, which show a warm, dry phase that continues until 3.8 ka cal BP, with evidence of a decrease in bog pollen and an increase in chironomid species that prefer higher temperatures (Taylor et al, 2018). This drier phase is also seen in various bog records in Ireland which show decreased water table levels (Swindles et al, 2010). On the other hand, a wetter climate is indicated by O'Connell and Molloy (2001), who note an abrupt end to the colonisation of dried out peat regions by pine trees at 4.2 ka cal BP, corresponding to increased yew populations, which prefer mild, humid, maritime conditions (Gegechkori, 2018) and a decrease in farming (Molloy and O'Connell, 2004). In the marine record just offshore of the Aran Islands, Wood et al (2017) note no change in the isotopic record suggesting stable climatic conditions, at least locally. Overall, there appears to be no synchronous Irish record of the ~4.2 ka BP event. The rest of the Meghalayan period shows a general trend of increasing temperature with shorter periods of climatic deterioration. There is a shift to wetter/colder conditions globally at ~2.8 ka cal BP. In Ireland, there appears to have been a delay in the response, with the climate only becoming much wetter between ~2.7 and 2.4 ka cal BP (Wanner et al, 2011), as indicated by terrestrial records including peatland water table records (Langdon et al, 2012; Swindles et al, 2007, 2010, 2013), as well as a pronounced decrease in woodland clearance, archaeological sites and a population

downturn (Plunkett, 2009; Bevan et al, 2017). This wet/cold phase is seen across Europe in bog records in Britain (Charman et al, 2006), Germany (Barber et al, 2004), the Netherlands (van Geel, 1978), the Czech Republic (Speranza et al, 2002) and in Siberia (vanGeel et al, 1996), as well as in lake and pollen records from the Alps region (Magny et al, 2009). This wetter climate is also recorded for the southern hemisphere, with the Andean region of South America experiencing increased precipitation (Chambers et al, 2007). Other areas also experienced climatic changes; however, these conditions show a trend towards a drier climate. Speleothem and sand dune records in China (Dykoski et al, 2005; Wang et al, 2005; Duan et al, 2014; Zhou et al, 2008) and lake records from north Africa (Armitage et al, 2015) show that drought, caused by a weakening of the monsoon systems, was prevalent. These global climatic changes coincide with Bond event 2 (Fig. 2.6) (Bond et al, 1997; Bond et al, 1999) and were likely influenced by solar forcing (van Geel et al, 1996, 2000; Blaauw et al, 2004; Mauquoy et al, 2004).

After 2.4 ka cal BP, the Irish climate began to improve, with an increase in temperature, inferred from chironomid records (Taylor et al, 2018), and drier conditions, inferred from peat and lake records across Ireland (Swindles et al, 2013; Langdon et al, 2012). This warmer period is considered to have lasted for a millennium, until 1.4 ka cal BP. The peak point of this warmer/drier environment coincides with the Roman Warm Period (RWP) (2.25 – 1.6 ka cal BP) seen across most of the northern hemisphere, including Europe and North America. Pollen records over Europe show both lower modelled winter and summer precipitation 2000 years ago (Mauri et al, 2015), while in North America, tree-ring (Stahle and Cleaveland, 1994), lacustrine diatom and ostracod (Fritz et al., 2000; Laird et al., 1996a; 1996b) records and altered forest compositions (Willard et al, 2003) indicate periods of severe drought. After the RWP, records across Ireland show a drop in temperature and a return to a wetter climate. These events once again coincide with a Bond event (1) (Fig. 2.6) (Bond et al, 1997; Bond et al, 1999) and are seen on a larger scale, suggesting that it is part of a much larger climatic phenomena. Changing conditions are seen across the northern hemisphere, with a drop in the solar activity (Wanner et al, 2008) and an increase in glacier activity (Reyes and Clague, 2004; Matthews et al, 2005; Koch and Clague, 2006; Nesje et al, 2008). This climatic downturn is known as the Dark Ages

Cold Period (DACP), lasting from 500 to 900 AD (Helama et al, 2017). Lamb (1982, 1995), using documentary evidence, identified a period of colder, disturbed conditions, particularly in Europe, which correspond to the decline of the Roman Empire and the migration of large numbers of people. In Ireland, speleothem records from Crag cave (McDermott et al, 1999) also indicate a colder period, preceding and following warmer periods, associated with the DACP. Volcanic eruptions dated between 535AD and 540AD, identified in the Greenland and Antarctic ice core (Larsen et al, 2008) as well as Irish tree ring records, showing a significant reduction in growth rings during these years (Baillie, 1991, 1995), also occurred within the DACP and possibly exacerbated this climatic deterioration. Following the DACP there is once again a period of worldwide warming, known as the Medieval Climatic Anomaly (MCA), which occurs between 900 and 1350 AD depending on location (Lamb, 1965; Graham et al, 2011; Mann et al, 2009; Diaz et al, 2011). It is documented in historical records across Western Europe (Lamb, 1965) and tree ring records in California, USA (LaMarche, 1974) as a climatic amelioration, with warmer, drier weather. However, in other regions, this anomaly caused a range of temperatures and varying levels of precipitation (Folland et al, 1992; Hughes and Diaz, 1994; Bradley et al, 2003; Graham et al, 2011; Kaniewski et al, 2011). In Ireland, $\delta^{18}\text{O}$ speleothem records from Crag Cave (McDermott et al, 2001), and lake records from Inis Oírr, on the Aran Islands (Diefendorf et al, 2005), show strong evidence of a warm period, while the presence of oak trees located on bogs at this time suggests that the climate was drier (Turney et al, 2006). This climatic anomaly is succeeded by the Little Ice Age (LIA) at 1300 – 1900AD, the most recent significant cold event in climatic records, a period similar to the DACP. The drop in temperatures at this time coincides with a bond event (0) (Fig. 2.7), and is associated with climate forcing (Broecker, 2000; Mauquoy et al, 2002). This climatic downturn occurred across the world, causing severe winters, detailed in historical records (Manley, 1957; Lamb, 1967, 1977) and evident in glacier advances (Grove, 2004; Rabatel et al, 2005; Ledru et al, 2013), ice records (Fischer et al, 1998), pollen records (Kaniewski et al, 2011), tree ring records (Wiles et al, 2008) and many other terrestrial and marine records. This LIA displayed various climatic conditions in differing locations, with drought in some areas and a wetter climate in others. The temperature, though generally colder, varied in severity throughout the world

(Thompson et al, 1986; Briffa, 2000; Jacobeit et al, 2001; Jones et al, 2001; Luterbacher et al, 2004; Meyers and Pagani, 2006; Pollack et al, 2006; Osborn and Briffa, 2006; Araneda et al, 2007; Kuhlemann et al, 2008; Richter et al, 2009). In Europe, the LIA is also associated with increased storminess (Fagan, 2000; Dawson et al, 2004; Sorrel et al, 2012) with large storm events recorded along the Atlantic seaboard (Lamb, 1991; Bryant, 2005; Douglas et al, 2009). In Ireland, this event is represented as a colder period in the speleothem (McDermott et al, 1999, 2001) and historical records (Kinealy, 2006; Kelly and Ó Gráda, 2013), while in the bog, testate amoebae, plant macrofossil and humidification records suggest a variable climate, with both wetter and drier spells throughout the LIA (Caseldine and Gearey, 2005; Swindles et al, 2010, 2013; Stastney et al, 2018).

This record of Holocene environmental history indicates that, while the Holocene is known as a time of climatic warming, there is a notable variability within this period and this is bound to be recorded in marine sediments around Ireland too.

2.4 Sea-level history

Changes in sea-level have the ability to profoundly change the geomorphology and environment of an area (Mastronuzzi et al, 2005). In order to understand what drives the timing and scale of these variations in sea-level, research over prolonged time periods is crucial. The end of the LGM caused substantial sea-level changes across the globe, ultimately shaping the modern coastline of the Holocene.

Glacio-isostatic adjustment (GIA) that was occurring during the down-wasting of the BIIS and following deglaciation in Ireland, resulted in an acceleration in uplift when the total weight of the ice sheet covering the island was removed at ~15 ka cal BP (Brooks et al, 2008; Bradley et al, 2011; Kuchar et al, 2012). This was contemporaneous with a global sea-level rise due to the melting of not only the BIIS, but ice sheets across the world (Lambeck, 1995). This is something that has led to significant variation in RSL across different parts of Ireland.

In the past, the main method for determining sea-level changes was the detection of raised and submerged shorelines (Stephens, 1957; Mitchell, 1960; Stephens and Syngé, 1965). In Ireland, a RSL record for the post glacial period has been established

using this method over several decades (Synge, 1977; Carter, 1982; Carter et al, 1989; Devoy et al, 1996). However, uncertainty in the dating of coastal deposits, the previous lack of knowledge about the exact extent and thickness of the BIIS and the difficulty in determining the significance of specific coastal processes have contributed to fragmented research that is open to errors (Carter, 1982; Gallagher and Thorp, 1997; Duffy and Devoy, 1999). International research carried out during the International Geoscience Programme (IGCP) projects established the use of sea-level index points (SLIPs) as a methodology for producing records of RSL change on sedimentary coasts, at a specific time and place (Tooley, 1978; Preuss, 1979; Shennan, 1982; van de Plassche, 1986). A SLIP provides information on location, altitude, age and vertical relationship to contemporaneous tide level and can be used to provide high resolution information on past RSL positions. Even if a SLIP does not provide information on the relationship between the sample and a known tide level, it can still be used as a limit of possible RSL (limiting point – see Chapter 1) (Edwards and Brooks, 2008).

In Ireland, observational data from SLIPs have been incorporated into GIA models that generate sea-level curves showing RSL (Shennan et al, 2006; Edwards and Craven, 2017). A sea-level database for Ireland containing all of these SLIPs has been created (Brooks and Edwards, 2006). SLIPs are also used to validate GIA models and associated RSL curves. This becomes more effective when there are numerous local data points for comparison in each area. In Ireland, due to the complex and spatially variable RSL history in the region, related to the isostatic depression caused by the advance and retreat of the BIIS (Edwards and Craven, 2017), a wide range of data points are necessary in order to accurately reconstruct RSL changes. However, SLIP data are sparse here, with only 200 data points in the Irish sea-level database. Less than a third of these data are composed of index points, with the majority composed of the lesser quality limiting points. Data from the west coast of Ireland, in particular, are composed primarily of limiting points, while index points are located mainly in the south and northwest (Fig. 1.2). Almost all of the data of late-glacial to early Holocene age are from limiting data, making it much less precise and more prone to inaccuracies when compared with data from primary and secondary index points (Brooks and Edwards, 2006).

Using the sea-level database alongside ice coverage and earth's crustal rebound GIA models, RSL curves have been created to explain regional changes (Brooks et al, 2008; Bradley et al, 2011; Kuchar et al, 2012). These curves can then be tested against known dates to see how closely they resemble the geological and geomorphological data (Fig. 1.2). Although the models and geological and geomorphological data rarely produce a perfect fit due to the inherent errors involved in both modelling and radiocarbon dating, modelled curves of late Holocene sea-level change fit well with the data available in Ireland (Fig. 1.2 & 2.7). The 3 GIA models that cover Ireland are Brooks et al (2008), Bradley et al (2011) and Kuchar et al (2012), hereafter referred to as Brooks', Bradley's and Kuchar's models. These models use slightly different parameters. Brooks et al (2008) and Bradley et al (2011), are more similar to each other, having used similar ice thickness and extent parameters. Kuchar et al (2012) used a considerably thicker ice sheet and less laterally extensive cover than the other versions, leading to differences in output (Fig. 1.2 and 2.7).

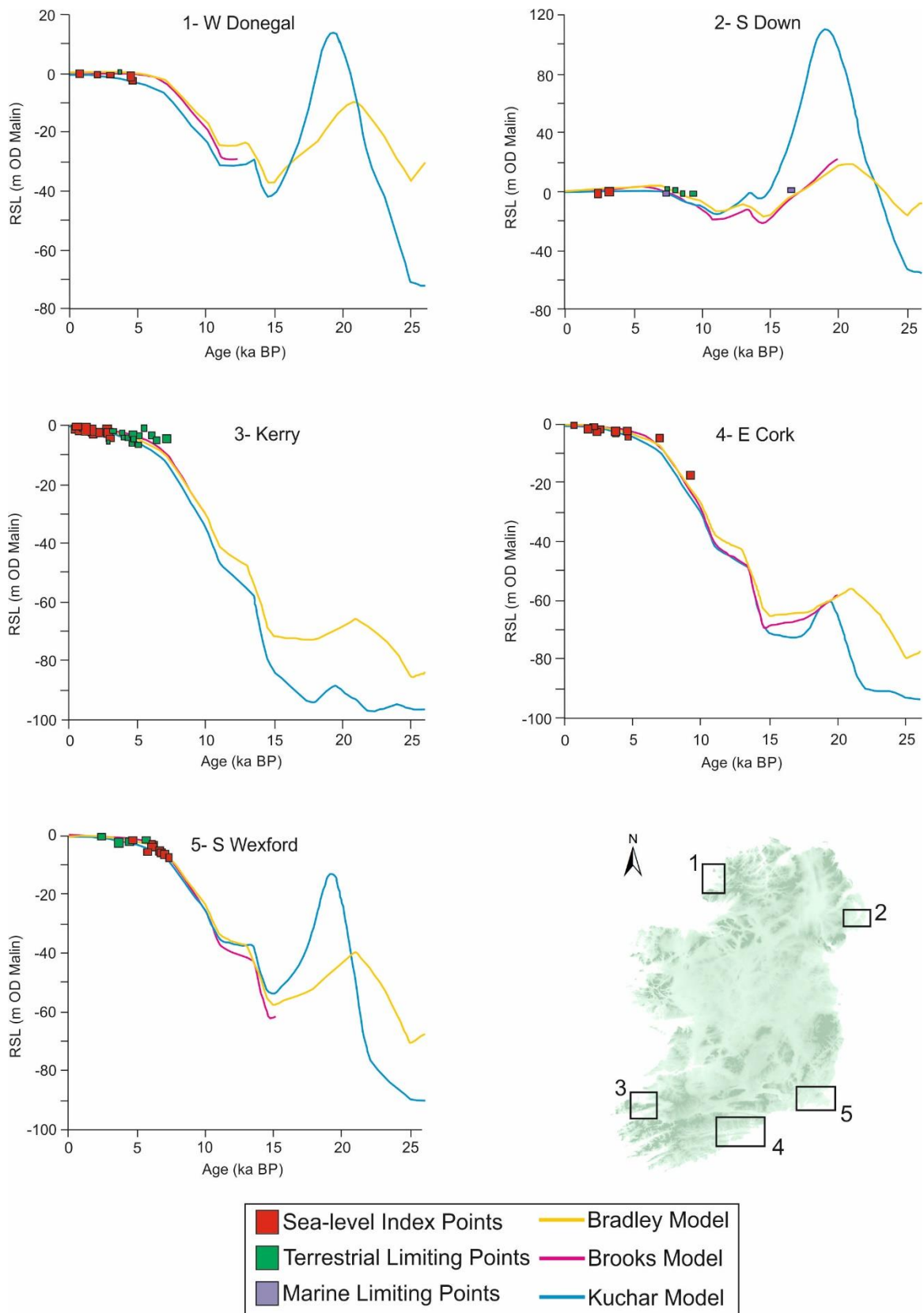


Figure 2.7: Relative sea-level curves from various regions in Ireland, adapted from Edwards and Craven (2017) and Brooks et al (2008). This demonstrates how SLIP's are mainly available for the Late-Holocene.

During the deglacial period, all models show a rapid RSL rise across most of Ireland at ~15-14 ka cal BP, coinciding with global meltwater pulse 1A related to the final downwasting of ice sheets (Fairbanks, 1989; Weaver et al, 2003; Peltier, 2005). During the Holocene, when ice coverage is non-existent, the models yield similar results, in that RSL predictions are generally within 5m of each other. However, prior to 14 ka cal BP, substantial variations are visible in the RSL models, in particular in the northeast of Ireland where Kuchar's model predicts sea levels ~120m above present levels from ~18 and 20 ka cal BP (Fig. 2.7), while Brooks and Bradley's models shows sea-levels comparable to modern day. As more data is compiled into the sea-level database for Ireland, the more refined these GIA models can be made with new time constraints from new SLIPs (Fig. 1.2). This would definitely require a larger number of early Holocene and late Pleistocene data points.

In the late Holocene, where a larger number of data points are available, patterns of RSL have been inferred for certain sites around Ireland from the GIA models. In the south, in counties Wexford and Cork, rising sea levels during the Holocene are evident in the GIA models, with RSL reaching 4m bsl by 6 ka cal BP. In the east, in Co. Dublin, RSL appears to have reached 5m bsl by 8 ka BP. In the southwest and northwest in counties Kerry and Donegal, the same trend is evident with RSL reaching 3m bsl by 3 ka cal BP and 3m bsl by 5 ka cal BP respectively. In Co. Donegal a mid-Holocene high is visible with sea-levels above present day around 6 ka BP (Figure 2.7). A similar oscillation is inferred for the northeast in Co. Down, where RSL was equal to or (in the Bradley Model) above present day levels by 4 ka BP (Carter, 1982) and higher than present during the late glacial to early Holocene (Roe and Swindles et al, 2008), presenting a more complex pattern of sea-level change than in other areas of Ireland (Fig. 2.7). Many of these modelled sea-level curves are validated by the available SLIP data across Ireland.

In Galway Bay (Fig. 1.2), the modelled sea-level curves indicate a sea-level drop at 19 ka cal BP to a lowstand between 16 and 15 ka cal BP, followed by a sharp rise until 6 ka cal BP. This is interrupted only by a slowstand between 13.5 and 11 ka cal BP, before levelling off towards present day sea-levels (Fig. 1.2). There are clear differences between the 3 models, with Kuchar et al (2012), suggesting a much lower RSL during

the lowstand than Brooks et al (2008) or Bradley et al (2011). This trend continues throughout the Holocene, with Kucher et al's (2012) consistently predicting lower RSL, while Bradley et al (2011) consistently predict higher RSL (Fig. 1.2). As Galway Bay has only 23 limiting points in the Irish sea-level database, all of which are younger than 7.5 ka cal BP, there is not yet enough detail to provide validation for these GIA model derived RSL predictions (Fig. 1.2), something this study hopes to address.

Chapter 3: Data and methodologies

In order to investigate palaeoenvironmental changes, meaningful proxies are commonly used in Quaternary science. This chapter provides an overview of all the analytical and data collection techniques used in this project. This research involved a multiproxy approach including geophysical, sedimentological, geomorphological, micropalaeontological and geochronological analyses, as our understanding of post-glacial environmental change has largely been derived from paleoenvironmental studies of key physical, chemical and biological components of both terrestrial and marine sediments. The more environmental proxies available in a region, the more accurate and complete the reconstruction of past environmental changes will be. The rationale for the use of each methodology is discussed in detail in this chapter. These methods collectively allowed the reconstruction of the environmental history of Galway bay from the Late Quaternary to present day.

3.1 Topographic, bathymetric and backscatter data

Different kinds of altimetry and imagery data (including multibeam bathymetry and backscatter, LiDAR altimetry, satellite and aerial imagery) were used in this research to map the modern-day topography and coastline of Galway Bay. These data were all acquired at high resolution and in optimal conditions and are of excellent quality. Multibeam bathymetric and backscatter data are acquired when a multibeam echosounder (MBES) transmits an array of ‘pings’ in a fan beneath the vessel; this energy is then bounced back off the seabed to the vessel, and depending on the depth of the water, will arrive back at the vessel at slightly different times, allowing the seabed depth to be computed (Fig. 3.1). Acoustic backscatter data are also collected during this process and can be used to interpret variations in seabed hardness and, therefore, grain size (Lamarche et al, 2011).

MBES data were acquired by the INFOMAR programme between 2006 and 2014 on board the RV *Celtic Voyager* using a Kongsberg Simrad EM3002 multibeam echosounder (300kHz) and the RV *Keary* using a Kongsberg Simrad EM2040 multibeam echosounder (300kHz). The 300kHz frequency is ideal for shallow water applications as the high frequency ensures narrow beams with small physical dimensions, allowing for

a much higher resolution and a cleaner signal when mapping (Lurton, 2010). These data were processed and tidally corrected by INFOMAR, using CARIS Hydrographic information Processing Systems (HIPS) and Sonar Image Processing Software (SIPS) and gridded at 5m resolution. This was done in order to compensate for artefacts in the data, caused by variations in seafloor topography, water column properties and multibeam system configuration parameters (Hellequin et al., 1997). The collection and processing of the multibeam echosounder (MBES) data was carried out by INFOMAR. Bathymetric and backscatter data are available for most of the bay and the areas surrounding the Aran Islands (Fig. 3.2A). All areas between -18m and -95m have MBES data available and, although there are some data available in the shallower areas of the bay, it is sparse and generally confined to the Corrib estuary.

As well as MBES bathymetric data, LiDAR (Light detection and ranging) altimetry data were also collected for INFOMAR between 2006 and 2010 by Tenix LADS Corporation. LiDAR is a near-shore surveying technique that uses air-borne lasers (Fig. 3.1), in much the same way as the aforementioned acoustic methods, to survey areas that are difficult to reach by boat, particularly shallow water less than 15m (Kotilainen and Kaskela, 2017). LiDAR is very useful and has, in recent years, become a cost effective and time saving alternative to mapping techniques using multibeam echosounders. However, as with all technologies, it has limitations. In particular, LiDAR data are affected by the turbidity of the water and the extent to which the water column reflects or absorbs the light (Yang et al, 2007). These limitations are particularly problematic in water less than 2m in depth (Pe'eri and Philpot, 2007).

Like the MBES data, the LiDAR data was gridded at 5m resolution and combined with the available bathymetry data to form a more complete picture of the seabed and coastal topography by INFOMAR (Fig. 3.2). The LiDAR data provide additional bathymetric data from above 18m water depth to the coastline and merges with terrestrial altimetry data up to 5km from the coastline, though it generally extends less than 2km.

The combination of these datasets, taken from lowest astronomical tide (LAT), allow for the depth and hardness of the seafloor to be computed, providing valuable information of the lithology and geomorphology of the seabed.

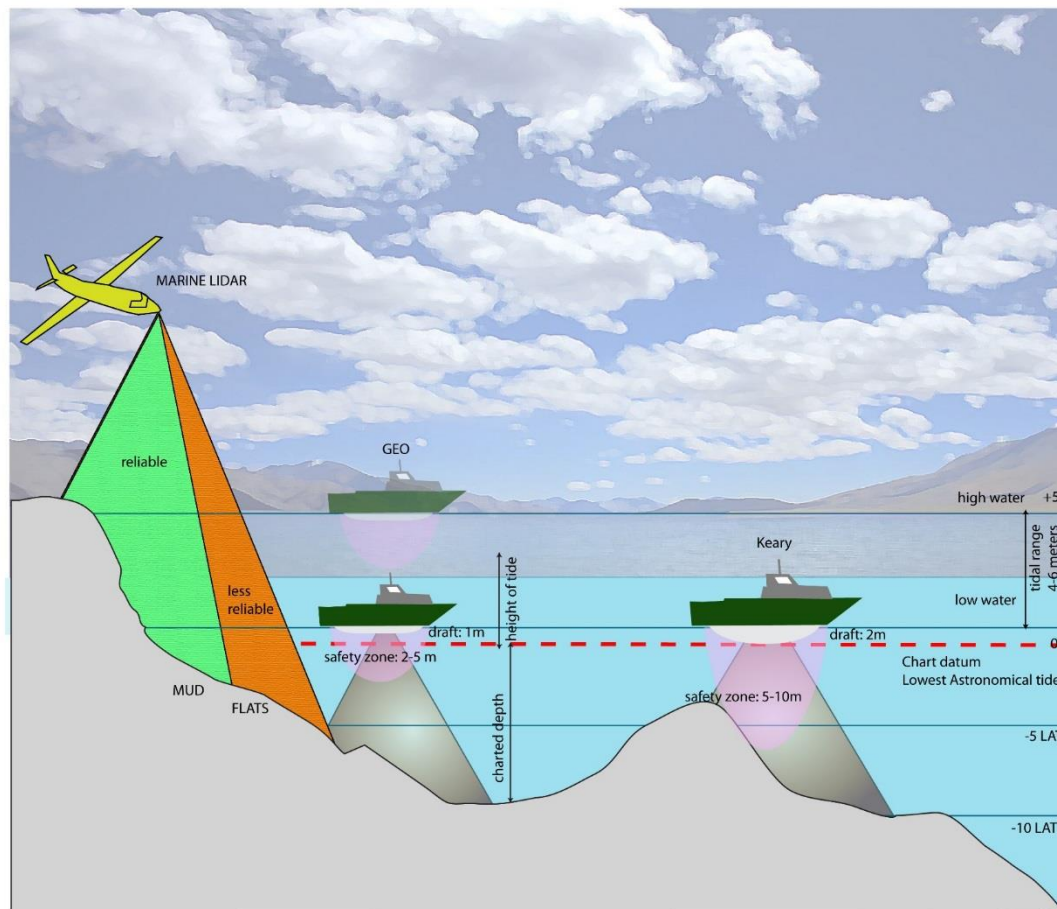


Figure 3.1: Image showing the ranges of various instrumentation for the acquisition of geophysical data in shallow water (courtesy of F. Sacchetti, Marine Institute of Ireland).

Shaded relief with vertical exaggeration (x10) and different illuminations were generated in ESRI ArcGIS 10.1 to aid the interpretation of landforms for both MBES and LiDAR data. In order to avoid azimuth biasing, features were considered with numerous illuminations ($30^{\circ} - 70^{\circ}$ and $120^{\circ} - 160^{\circ}$) as well as without azimuth (Smith and Clark, 2005; Hillier and Smith, 2008). Contour lines (10m spacing), slope angle and aspect were derived using the spatial analyst extension tool to aid geomorphological interpretation. The profiling tool was used to derive information on geometric properties including wavelength, amplitude, symmetry and slope for the mapped landforms (cf. Ashley, 1990; Van Landeghem et al., 2009).

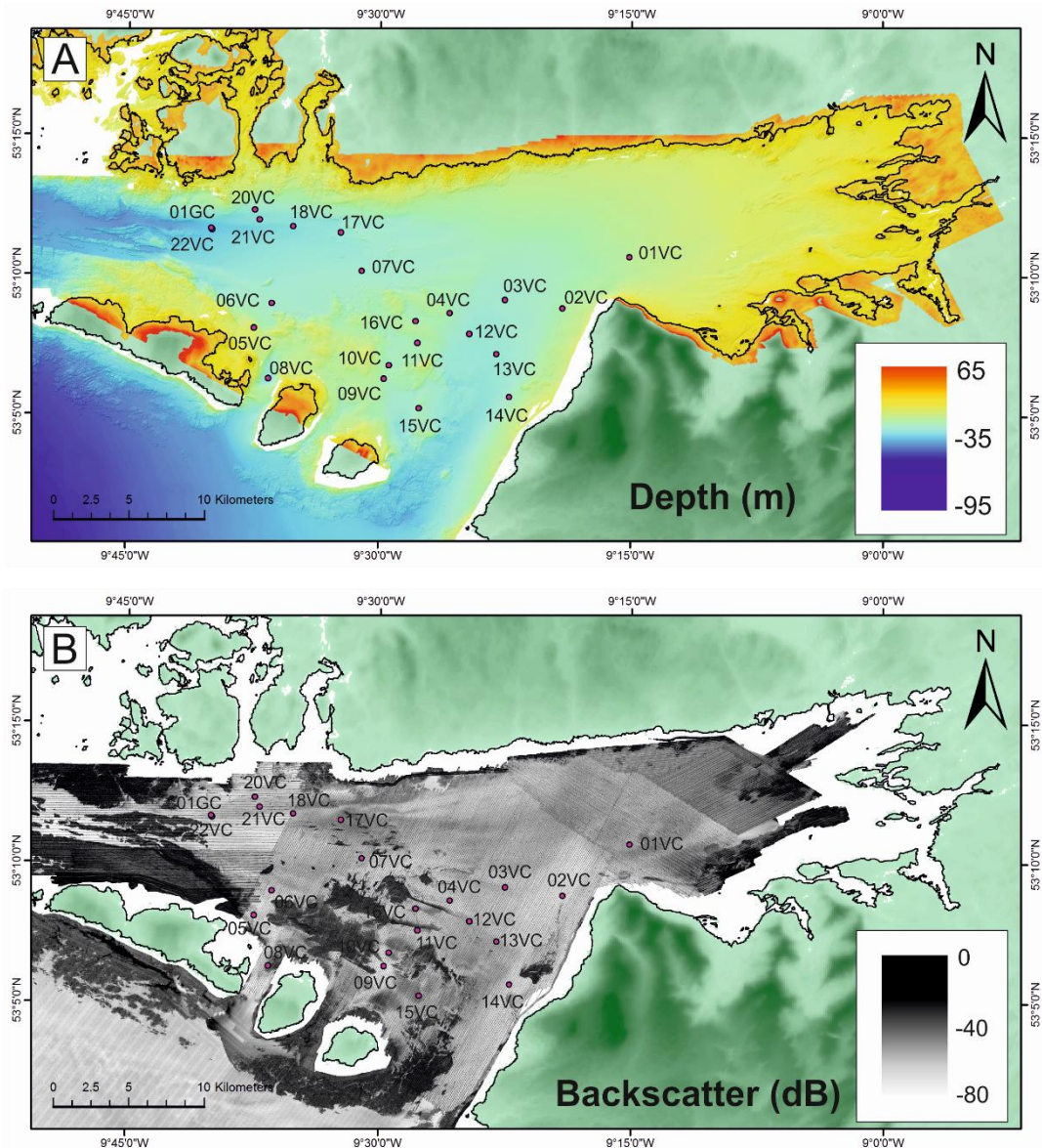


Figure 3.2: (A) Bathymetric and LiDAR and (B) backscatter map of Galway Bay, with the sediment cores represented in pink.

In addition to the interpretation of the landforms, a seabed classification map for Galway Bay produced by the Marine Institute of Ireland (2017) was used to support the interpretation of the numerous features visible in the MBES data, especially in terms of their sediment composition. The map (shown in Chapter 4 and included as part of a paper to be submitted for peer-review), comprises the data from the different INFOMAR seabed surveys mentioned above and merged together into one composite map showing key habitats. The majority of the data (subtidal depths >20m) have been interpreted from MBES bathymetric and backscatter data. The shallower

subtidal data and intertidal data have been interpolated from biological samples and traced from orthoimagery and LiDAR. The samples were collected as part of detailed surveys of Natura 2000 sites between the years 2009 and 2012. These surveys resulted in maps of marine community types, which were translated to a modified Folk class and combined to result in a single habitat map layer (NPWS, 2013).

Additionally, for this study, a classification of coastline types was carried out from a combination of satellite images and LiDAR data. Satellite images at 20m resolution were obtained from TerraMetrics and Google Earth and consist of a mixture of mid- and high-resolution satellite and aerial imagery from multiple providers including the U.S Navy, SIO (Scripps Institution of Oceanography) and NOAA National Oceanic and Atmospheric Administration (Google Earth, 2018). The coastline was divided into 3 categories: coastal cliffs, sandy beaches and rocky beaches, according to Woodroffe (2002). The criteria for the classification of a coastal cliff relied heavily on slope angle, with near vertical slopes of consolidated material necessary for an area of coastline to be defined as a cliff (Sunamura, 1992). Sandy beaches were defined through a more or less smooth profile with a low slope angle (Russell, 1958). Rocky beaches were defined similarly to sandy beaches, with lower slopes than cliffs but composed of larger grain sizes such as gravel, encompassing both a shingle and boulder beach habitat. These categories were decided based on other coastline studies (Hansom and Moore, 1981; May and Hansom, 2003; Fairbridge, 2004; Biolchi et al, 2014; Kaliraj et al, 2017) and the resolution of the available data for the bay.

3.2 Hydrodynamic data

Hydrodynamic data were used as part of this project in order to assess the strength and direction of currents and waves in the bay and how they have influenced sediment mobility and helped shaped the modern-day topography of Galway Bay. Modelled current data for the Greater Galway Bay area were provided by the Marine Institute of Ireland (MI) as vector data. The model used is an implementation of the Regional Ocean Modelling System (ROMS), as described by Shehpetkin and McWilliams (2005). The model has a horizontal resolution of 200 metres and 20 vertical levels and provides depth-averaged and three-dimensional velocity fields at a

temporal resolution of three hours. The model includes atmospheric and tidal forcing, and climatological river input. One year of data, from 2016-2017, were used to calculate mean and maximum depth-averaged and bottom velocities for Galway Bay. In this study, the modelled data were then used to produce different grids. Grid sizes of 200m and 1000m, which were applied to the bottom and depth-averaged current data, were found to be the best to represent the respective datasets. A 1000m grid resolution was interpolated for current velocity data for the entire bay, while a 200m grid resolution was used to closely investigate the relationship between hydrodynamic forces and specific seabed landforms.

Wave orbital velocities, modelled by the Marine Institute of Ireland, were taken from a regional wave model (SWAN), as described by Rusu (2011). The domain of this model covers all of Irish waters in the northeast Atlantic at a resolution of 0.025 degrees and is available at three-hourly intervals. For this study, one year of data, from 2016-2017, was used to calculate mean orbital velocities. In this study, the model outputs were then displayed as 2800m grids, the highest resolution available from the modelled data. This was all done in order to provide an overview of the general trend of the bottom, and depth-averaged currents and the mean speed of the orbital wave velocity. The arrows in all grids indicate the most frequent flow direction, while the speed is represented on a colour scale from slow (green) to fast (red) (relevant figures are provided in Chapter 4). Both models used to obtain hydrodynamic data from Galway Bay have undergone quality control through comparison with data from weather buoys, ARGO floats, tide gauges and satellite radiometers.

3.3. Habitat Mapping

The habitat mapping in the bay was carried out by the Marine Institute of Ireland. QTC Impact software undertakes principal component analysis to pick features which account for variation in the multibeam data from the bay. These data are then grouped based on the highest statistical significance. The criteria for habitat classification are defined by location, acoustic characteristics, biological communities and geomorphology (Dalkin, 2008; Walker et al, 2008).

3.4 Core acquisition, storage and splitting

Twenty-two sediment cores were used in this study. They were collected by the RV *Celtic Voyager* during cruise CV13031 in September 2013 (Table 3.1) and core sites (Fig. 3.1) were based on the available geophysical data for the area, including MBES bathymetry and backscatter and sub-bottom pinger data (3.5kHz) and Chirp and Sparker data previously obtained by Clarke (2013). In particular, areas with possible till layers or thick unconsolidated sediments visible on the seismic data were targeted (Peters et al, 2015). For succinctness in the rest of the thesis, the cores are referred to with a short name (for example, CV13031_01vc will be 01VC).

The cores were collected using a Geo Marine Survey System Geo-Corer 3000 with a 3m barrel. Cores were cut into 1m sections (Fig. 3.3) and stored vertically, prior to splitting. The cores were split using a circular saw blade until only a thin sliver of plastic remained and then finished with a knife to avoid contamination. A wire was then used to split the sediment cores in half, creating a working half for analysis and an archive half. These halves were photographed and wrapped in plastic to prevent degradation when stored. This was done in the sediment lab at Ulster University, Coleraine, between December 2014 and September 2015. Cores were and are stored at a constant temperature of 4°C to preserve physical and chemical properties as much as possible.

Table 3.1: Table showing information on the collected cores, including coordinates, water depth, coring method, length and number of sections in each core and the type of analysis carried out on each core. Water depth is corrected to lowest astronomical tide (LAT) while, MSCL represents analysis of physical properties, GSA is grain size analysis, XRF is chemical analysis, SS is shear strength, 14C is radiocarbon dating and Fossil analysis refers specifically to benthic foraminifera.

Core	Latitude °N.	Longitude °W	Depth (m)	Core type	Sections	Length (m)	X-rays	MSCL	GSA	XRF	SS	14C	Fossils
CV13031_01vc	53°10'42.002	9°15'7.518	29.5	vibro	3	2.2	x	x	x	x	x		x
CV13031_02vc	53°8'51.194	9°19'5.417	32.4	vibro	3	2.97	x	x	x	x		x	
CV13031_03vc	53°9'9.863	9°22'30.305	39	vibro	3	2.35	x	x		x	x	x	x
CV13031_04vc	53°8'41.368	9°25'47.649	33	vibro	2	1.84	x		x	x			
CV13031_05vc	53°8'8.306	9°37'26.755	19.1	vibro	1	0.63	x						
CV13031_06vc	53°9'1.096	9°36'19.867	39	vibro	3	2.57	x	x	x	x		x	
CV13031_07vc	53°10'11.085	9°31'3.808	42	vibro	3	2.13	x	x	x	x		x	x
CV13031_08vc	53°6'17.252	9°36'37.129	43.9	vibro	1	0.32	x						
CV13031_09vc	53°6'19.176	9°29'42.768	32.9	vibro	3	2.38	x	x		x			
CV13031_10vc	53°6'46.014	9°29'23.51	35.3	vibro	3	2.25	x	x		x		x	
CV13031_11vc	53°7'35.65	9°27'42.651	33.1	vibro	1	0.69	x						
CV13031_12vc	53°7'56.663	9°24'37.798	40.3	vibro	2	1.71	x		x	x		x	
CV13031_13vc	53°7'12.044	9°22'57.745	41.4	vibro	3	2.41	x	x		x	x	x	x
CV13031_14vc	53°5'41.218	9°22'10.709	35.2	vibro	3	2.88	x	x		x	x		x
CV13031_15vc	53°5'16.524	9°27'39.383	31.5	vibro	1	0.75	x			x			
CV13031_16vc	53°8'24.847	9°27'52.078	28.6	vibro	1	0.57	x						
CV13031_17vc	53°11'35.318	9°32'16.107	39.9	vibro	2	1.42	x			x	x	x	x
CV13031_18vc	53°11'45.187	9°35'12.672	44.9	vibro	3	2.79	x	x		x	x		
CV13031_20vc	53°12'20.876	9°37'30.423	38.7	vibro	2	1.3	x		x	x		x	
CV13031_21vc	53°11'57.434	9°37'10.476	25.6	vibro	2	0.74	x						
CV13031_22vc	53°11'38.337	9°39'57.724	57	vibro	3	2.88	x	x	x	x	x	x	x
CV13031_01gc	53°11'41.427	9°40'2.634	57	gravity	1	1.0	x			x	x		x



Figure 3.3: An example of the deck crew (A) bringing in a vibrocore after coring the Celtic shelf, on the GATEWAYS2 cruise, and (B) preparing for piston coring on the CE16010 cruise, on board the RV Celtic Explorer.

3.5 Sediment physical properties

3.5.1 X-radiographs

X-radiography has become common practice in the analysis of sediment cores as it allows for the identification of structures within the core that may not be apparent to the naked eye, including bioturbation, laminae and denser material as well as smaller pebbles and shells (Jennings and Weiner, 1996; Andrews et al, 1997; Principato, 2004). X-radiographs of all the sediment cores in this study were acquired using a CARESTREAM DRX Evolution system at Ulster University, Jordanstown, in December 2014. This was carried out on unsplit cores, so that deformation due to splitting is not present in the x-radiographs. These x-radiographs were then used to identify features not visible on the surface of the core (Fig 3.4).

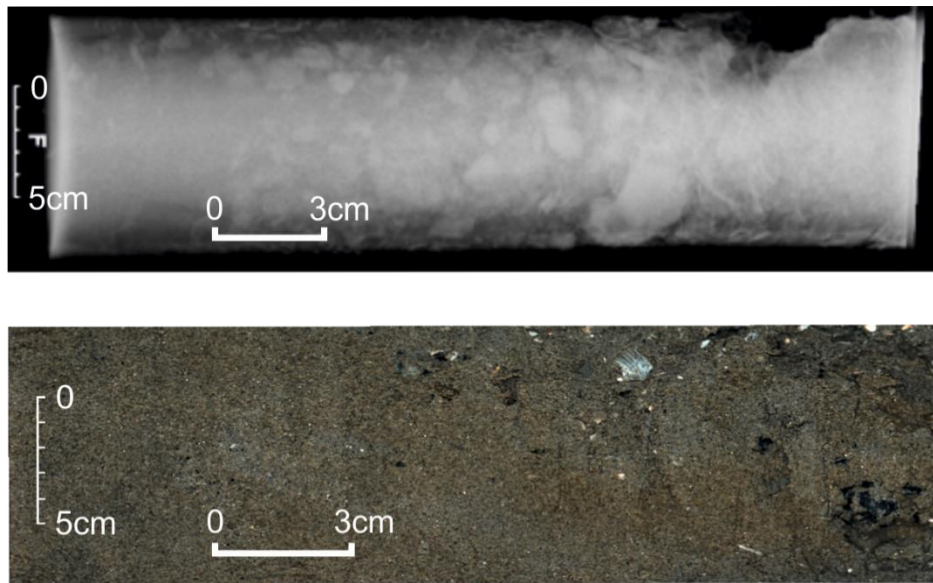


Figure 3.4: Image of pebbles visible in the x-ray (top) at the base of core 20VC but invisible to the naked eye (bottom).

3.5.2 Multi-sensor Core Logger

A selection of ten cores were scanned using a Geotek Standard Multi-Sensor Core Logger (MSCL-S) prior to splitting, at the British Ocean Sediment Core Research Facility (BOSCORF) in Southampton in August 2015. As there were time constraints on the use of the MSCL, all cores chosen were more than 2m in length in order to maximise the chance of obtaining the longest and most detailed environmental record for the bay. The cost of this analysis was covered under the NERC remit in the area of marine science.

MSCL provides a non-destructive, high resolution (1cm intervals), measurement of P-wave velocity, gamma ray attenuation, magnetic susceptibility and electrical resistivity (Schultheiss and McPhail, 1989; Best and Gunn, 1999). This involves placing the cores on the MSCL track, where they are automatically pushed past the sensors, which collect data at each 1cm increment, chosen to provide a high-resolution record of the physical properties of the cores. The next section is placed on the track as the first one finishes, allowing for continuous measurements. The stepper motor controlling the track is controlled by the computer, which also controls the sensors, allowing for the data to be automatically correlated (Geotek, 2016). P-wave velocity is used to calculate acoustic

impedance, with higher values indicating more cohesive material. This is done by producing a short P-wave pulse from a transmitter which propagates through the core and is intercepted by a receiver. The travel time of this pulse is measured using pulse timing software (Geotek, 2016). Gamma ray attenuation measures sediment bulk density, with higher values indicating lower porosity. A gamma ray source, in this case Caesium-137, and a detector are placed on sensors that are aligned on either side of the core centre. A beam of gamma rays is emitted from the source and picked up by the detector. By measuring the amount of transmitted gamma photons that pass unattenuated through the core, the density of the sediment can be determined (Geotek, 2016). Magnetic susceptibility measures the degree to which a material can be magnetised (Gunn and Best, 1998), with higher values representing sediment containing more ferromagnetic elements. It is measured by producing a low intensity magnetic field, which shows a change in its oscillator frequency every time a material with magnetic susceptibility is near it (Geotek, 2016). Electrical resistivity is measured by creating a high frequency magnetic field from a transmitter coil, which in turn induces electrical currents inversely proportional to the sediment's resistivity. The magnetic fields generated by the electrical currents are then measured by a receiver coil (Geotek, 2016). Higher electrical resistivity values indicate more porous material or a decrease in salt content (Munoz-Castelblanco et al, 2012; Satriani et al, 2012).

MSCL measurements are valuable in determining boundaries between lithofacies, as well as interpretation of different lithofacies. However, although MSCL analysis is extremely useful in providing information on the sediment characteristics and variability within the cores, there are drawbacks in this type of analysis. Under-filled core liners, varying levels of saturation and absence of a flat scanning surface can adversely affected MSCL measurements, causing gaps in the data and anomalous results (Insua, 2013). This was addressed through the removal of data from areas where these issues were clearly evident in the cores.

The MSCL data were imported into a Grapher 8™ program to create graphs that allowed for a single overview of all of the available data for each core. The plots were exported into a CorelDRAW X6 to be displayed alongside the core logs. This was done in order to support the identification of lithofacies boundaries and of significant trends or changes within each unit, as well as to correlate the characteristics of each lithofacies.

3.5.3 Shear strength

Shear strength is a measure of the sediment's resistance to shear stress. In this study, it is measured using a shear vane and recorded in kPa. This is done in order to determine the level of compaction, as the rapid deposition of finer material can lead to under-consolidation, with low shear strength values (Whelan et al, 1977), while higher shear strength values can be suggestive of an erosive or glacial environment (Grabowski, 2014). In particular, values above 50kPa are considered to represent lodgement till (Peters et al, 2016; Hillenbrand et al, 2005; Dowdeswell et al, 2004). Shear strength analysis is carried out only on consolidated sediment, as in unconsolidated sediments the required tension cannot be built up. Shear strength was measured on 8 sediment cores in this study that contained consolidated sediment (Table 3.1), by inserting the impact shear vane into the sediment at 20cm intervals and slowly rotating the torque head until the sediment failed (Fig. 3.5). This was done in order to get representative measurements throughout the cores and to obtain a response to the various forces that have been applied to the sediment in the bay over time.

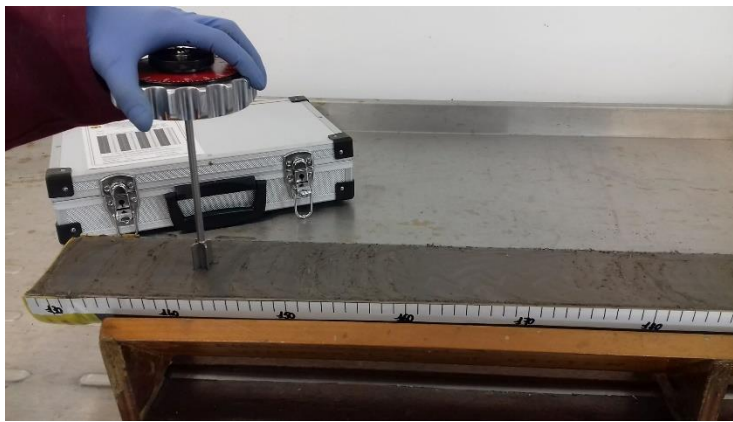


Figure 3.5: Image of a shear vane measurement taken on core 18VC (CV13031) at Ulster University.

3.5.4 Grain size analysis

Grain Size Analysis (GSA) is a tool for revealing information on the relative percentages of gravel, sand, silt and clay and level of sorting in the samples. From the grainsize, vital information on the depositional processes, provenance and hydrology of an area can be inferred. Sediments that have large percentages of fine material such as clay and silt tend

to represent lower energy environments, while sediment with coarser material such as sand and pebbles represent higher energy environments (Switzer and Pile, 2015). GSA was performed on 8 sediment cores (Table 3.1) at approximately 20cm intervals, with the exception of intervals rich in larger biogenic material, which would have been difficult to process for analysis and would not have provided a representative sample. Samples were chosen from cores where clear differences in grain size were difficult to see with the naked eye. Samples were pre-treated through soaking in a 5% calgon solution for 12 hours, followed by placement on a rotating table for 12 hours (following the methodology outlined in Sperazza et al., 2004). Grain-size analysis was then carried out through laser granulometry using a MALVERN Mastersizer 3000 at the School of Geography and Environmental Science at Ulster University. The Malvern Mastersizer 3000 is capable of measuring grain sizes up to 2mm and therefore, in order to avoid damage to the system, the sediment dispersion was put through a 1.8mm sieve before being poured into the sample dispersion unit. The only drawback with using the Malvern Mastersizer is when grains larger than 2mm, as in the case of coarse sand and gravel. To obtain representative results in the case of these samples, the fraction >2mm was also weighed, calculated as a percentage of the entire sample and used in the final analysis. The results of the grain size analysis of these samples were calculated and plotted using GRADISTAT (Blott and Pye, 2001) in order to determine mean grain size. While it is possible to identify grain size using the Udden-Wentworth scale (Udden, 1914; Wentworth, 1922), this is a laborious, time consuming process, whereas the GRADISTAT programme can rapidly calculate size, determine sorting, skewness and kurtosis and allows for flexibility in the input and output parameters (Blott and Pye, 2001).

3.6 Lithofacies identification

All 22 sediment cores were examined visually and classified into units using sediment colour, type, structures, contacts and biogenic content. The visual examination involved creating a core log for each core, detailing grain size, lithology, sorting, biogenic content, contacts, or any other identifying features in the core (including the archive half). The colour of the sediment was determined using a Munsell colour chart. This analysis was carried out following the methods of Kemp et al, (2001), Last (2001), and Benetti (2007).

Lithofacies were ultimately defined using a combination of the visual analysis, X-radiographs, shear strength measurements, MSCL physical properties and grain size analysis. These lithofacies were then displayed as sediment log images using CoreIDRAW X6 and are reported in Chapter 5 and Appendix 1.

3.7 X-Ray Fluorescence analysis

X-Ray fluorescence (XRF) is used to acquire detailed geochemical data from sediment cores through which environmental and sedimentological changes can be inferred (Croudace et al, 2006). Traditionally XRF data were acquired from sediment cores by sampling the material and processing it, something which resulted in the destruction of the samples. Micro x-ray fluorescence (μ -XRF) is a relatively new technique, developed in the past 20 years that allows for geochemical analysis of sediment cores in a non-destructive way. Studies that have utilized this new technique include lacustrine, coastal and deep-sea marine sediment cores (Calvert and Pederson, 2007; Romero et al 2008; Hunt et al, 2014; Rothwell and Croudace, 2015).

This technique is extremely useful for a relatively rapid, high resolution chemical analysis of both lighter and heavier elements to determine environmental and sedimentological trends recorded in the sediment (Croudace et al., 2006). The ITRAX scanner collects element profiles ranging from Silicon-Uranium simultaneously throughout a sediment core at a count rate of 100,000 cps (counts per second). The more intense the element concentration the higher the number of total counts. Sections were scanned with an energy dispersive fluorescence radiation to measure chemical composition at 1mm, 2mm or 5mm resolutions. Due to time constraints, only some cores were able to be scanned at higher resolutions. As cores composed of finer material, with a smoother surface generally produce the most reliable results, cores 01GC, 02VC, 12VC, 18VC and 22VC were chosen for 1mm scanning resolution, while cores 13VC and 15VC were scanned at 2mm resolution and all other cores were scanned at 5mm resolution.

Seventeen split sediment cores were scanned using an ITRAX micro-XRF core scanner at BOSCORF in Southampton, in May 2016. As time constraints once again applied to the use of this analysis, only cores over 0.75m in length were selected. This was done in order to obtain the most information possible across the longest timeframe. The cores were first

processed by scraping to remove a fine layer of sediment and smooth the surface, and then by covering the surface with ultralene film in order to avoid contamination. The ITRAX scanner successfully detected a range of element, even in the cores composed of fine sand. As the data generated by the ITRAX scanner is semi-quantitative (Rothwell and Rack, 2006) all element counts below 10,000 were discarded and elements were displayed as ratios following the practices outlined in the relevant literature (Rollinson, 1993; Weijden, 2002; Weltje and Tjallingii, 2008; Croudace et al, 2015), in order to provide the best representation of the trends in the data.

Like MSCL, μ -XRF analysis can display anomalous results or gaps in the data when the core liner is unfilled, or the sediment surface is uneven. As this analysis was carried out to obtain trends in the data rather than quantifiable ranges, and to ensure the highest level of quality control, all anomalous extremes in the data, that were not part of an overall trend, were discarded.

The elements and elemental ratios used in this study are shown in Table 3.2, and varying trends in each element or elemental ratio represent variations in the environmental conditions to which they refer to. The selected elements and ratios were chosen due to their use as proxies for environmental conditions, in particular for sea-level change. They include: Ca, S, Si, Sr/Ba, Ba/Ca and Br/Cl. All single elements were normalized to elemental ratios using Ti. Titanium was chosen because it is analytically reliable, and because it is a conservative element (weather resistant) and does not play a role in biological processes (Koinig et al., 2003; Croudace et al., 2006; Kylander et al., 2013b; Shala et al., 2014; Stuut et al., 2014).

Table 3.2: Summary table of geochemical elements used in this study as proxies of environmental and sea-level change. An increase in the elements/ratios reported in the table indicate an increase in the parameter they refer to.

Element or Ratio	Interpretation/Use/Indicator	References
Ca	- Core correlation - Marine Transgression - Calcium carbonate content	Bahr et al., 2008; Kwiecien et al., 2008; Soulet et al., 2011; Wolters et al., 2010; Piva et al., 2008
S	- Identification of redox transitions - Precipitation of pyrite and reducing seafloor conditions/bottom water anoxia	Richter et al., 2006; Harff et al., 2011; Sluijs et al., 2009
Si	- Terrigenous or productivity indicator - Variation in terrigenous sediment delivery	Rothwell et al., 2006; Blanchet et al., 2007; Kleiven et al., 2007; Marsh et al., 2007; Agnihotri et al., 2008; Frings et al., 2016; Sospedra et al., 2018
Ba/Ca	- Proxy for shallow water aragonite - Precipitation and runoff	Grove et al., 2010; Weldeab et al., 2007; Saraswat et al., 2013; He and Xu, 2015
Br/Cl	- Presence of organic rich layers - Increased porosity	Rothwell et al., 2006; Thomson et al., 2006
Sr	- Marker of biogenic origin - Higher salinity	Zaragosi et al., 2006; Arz et al., 2001b, 2003
Sr/Ba	- Higher salinity	Deng and Qian, 1993; McCulloch et al., 2005; Jia et al., 2013; Cao et al., 2016
Sr/Ca	- Presence of high Sr aragonite which requires a shallow water source - Mixing of marine and freshwater sources	Grove et al., 2010; Rothwell et al., 2006; Thomson et al., 2006; Ziegler et al., 2008
Fe	- Variations in terrigenous sediment delivery - Increased input from terrestrial sources/Runoff proxy	Arz et al., 1999, 2001b, 2003; Carlson et al., 2008; Harff et al., 2011; Haug et al., 2001; Heinrich et al., 2010; Itambi et al., 2010; Kissel et al., 2010

Ca, S and Si are useful proxies of an oscillating coastline and transgressive surfaces (Wolters et al, 2010; Croudace et al, 2015). High Ca/Ti ratios are indicative of increased marine carbonate content, while high S/Ti represents high levels of organic matter and high Si/Ti ratios suggest high levels of silica, likely from terrestrial runoff (Sospedra et al, 2018). High Sr/Ba ratios represent high salinity levels, as Ba enters marine environments primarily through riverine input (Cao et al, 2016; Setiawan et al, 2017), while high Br/Cl ratios represent high levels of marine organic carbon, as terrestrial organic matter contains low Br (Croudace et al, 2015). High Ba/Ca ratios are representative of an increased freshwater influence (Weldeab et al, 2007; Saraswat et al, 2013) and shallower water, as are high Sr/Ca ratios, which may indicate the presence of high Sr aragonite, requiring a shallow water source (Croudace et al, 2006; Grove et al., 2010). High Fe/Ti ratios generally relate to the terrigenous fraction of the sediment and are good indicators of increases in terrestrial runoff and changes in hinterland climatic conditions, with higher ratios indicating more terrestrial runoff and lower ratios indicating less terrestrial runoff (Westerhold et al., 2007).

Funding to carry out XRF analyses was obtained through the award of a GSI (Geological Survey of Ireland) research programme short call grant (2015-sc-073) and under the NERC (Natural Environment Research Council) remit for marine science.

3.8 Micropalaeontology

Microfossils are found in most environments and make exceptionally good indicators of palaeoenvironmental conditions as they provide a continuous record of change in an ecosystem over time. One of the main microfossils used in palaeoenvironmental reconstruction are foraminifera; testate, unicellular organisms, that are either planktonic (free-floating) or benthic (bottom dwelling) and are found throughout the marine environment (Corliss, 1985; Koutsoukos and Hart, 1990; Nagy et al, 1995, 1997; Murray and Alve, 1999; Scott et al, 2001; Beavington-Penney and Racey, 2004; Kamininski and Gradstein, 2005; Reolid et al, 2008, 2010; Setoyama et al, 2011; Hayward et al, 2013). Foraminifera have a close connection to the habitat they live in and have been extensively used as indicators of environmental change through comparisons to modern analogues.

Table 3.3: A table showing the core, depth and lithofacies foraminifera samples were located in.

Core	Sample depth (cm)	Lithofacies
01GC	1-2	Poorly sorted (Silty) fine to coarse sand coarsening upward
	30-31	Shell hash
	99-100	Sandy mud coarsening upward
01VC	1-2	Poorly sorted (Silty) fine to coarse sand coarsening upward
	60-61	Silty sand
	100-101	Interbedded sandy silt and silty sand
	187-188	Interbedded sandy silt and silty sand
03VC	227 – 228	Laminated mud
07VC	78-79	Poorly sorted (Silty) fine to coarse sand coarsening upward
	160-161	Shell hash
	201-204	Gravelly fine sand and silt
13VC	116-117	Silty sand/Sandy silt
	234-235	Silty sand/Sandy silt
14VC	45-46	Poorly sorted (Silty) fine to coarse sand coarsening upward
	110-111	Shell hash
	197-198	Shell hash
	278-279	Silty sand/Sandy silt
17VC	15-16	Poorly sorted (Silty) fine to coarse sand coarsening upward
	82-83	Gravelly fine sand and silt
	117-118	Gravelly fine sand and silt
	139-140	Gravelly fine sand and silt
22VC	150-151	Sandy mud coarsening upward
	269-270	Sandy mud coarsening upward

Micropalaeontological analysis of foraminifera tests was carried out on a selection of 8 sediment cores selected in order to provide maximum geographical coverage of the bay. One cm thick sediment slabs were taken at various depths across all identified lithofacies

(Table 3.3). The slabs were collected from the centre of the core, avoiding the core liner in order to ensure that sediments that may have been disturbed during acquisition were avoided. Slabs (~100g) were soaked for 24 hours, then wet sieved through a 63µm sieve and rinsed in distilled water, in order to remove the finer mud fraction. The samples were then dried under infra-red lamps until completely dehydrated. Larger samples were split into aliquots, using a Green geological microsplits, in order to obtain a smaller sample size. This prevents bias towards larger heavier specimens when examining and allows a fair representation of the foraminiferal population (Boltovskoy and Wright, 1976). Intact benthic foraminifera from the entire aliquot were examined using an Olympus SZX16 low-power binocular microscope, and species were identified as either present or absent and an estimate of their abundance within each lithofacies was made. The classifications used for identification of foraminifera species followed Haynes (1973; 1981), Loeblich and Tappan (1988) and Murray (2006). As foraminifera are strongly influenced by the habitat they live in they have been used in many studies as indicators of palaeoenvironmental conditions (Horton et al., 1999; Murray, 2000; Sejrup et al., 2004; Horton and Edwards, 2006; Leorri and Cearreta, 2009; Leorri et al., 2010; Milker et al., 2011; Lopez-Belzunce et al., 2014; Benito et al., 2016).

While microfossil analysis is exceptionally beneficial to the analysis and determination of environmental conditions, the small number of samples across the bay and the lack of statistically analysis carried out due to the time constraints of the project, has meant that this analysis will be used to reinforce the multiple other methodologies, rather than as a fully stand-alone investigation.

3.9 Geochronology

The chronology of many environmental changes, particularly in the marine environment are constrained through Accelerator Mass Spectrometer (AMS) radiocarbon dating. AMS can be used to measure the amount of ^{14}C in organic material. All living organisms contain ^{14}C which starts to decay from the time of death, at a measurable rate, known as the ^{14}C half-life (Taylor, 1987). By determining the level of ^{14}C in a fossil the age of the material it was deposited in can be derived. Accelerated mass spectrometry (AMS) radiocarbon dating is one of the most widely used (Taylor, 1987; Hajdas et al, 1993) and reputable methods

by which to determine the age of an object and can be completed with small sample sizes, which becomes advantageous when there is minimal organic material available to be dated.

Radiocarbon dating has been used to chronologically constraint the sediment record in this research. Calcareous material, that can be used in radiocarbon dating, such as foraminifera, ostracod, gastropods and bivalves, have been found in all of the sampled cores. As AMS radiocarbon dating can be completed with small sample sizes, it is advantageous when there is minimal organic material available in a core to be dated. By choosing to date organic material, at least 6mg in weight, that appears to be *in situ* and shows little sign of bioturbation, the likelihood of error in the dating process is reduced and the chronology established for significant core horizons, is much more reliable. When picking foraminifera, benthic species only were chosen, and whenever possible the number of species were limited to <3. The intention was to date samples which showed clear changes in the sediment core, either above or below the sampling point, in order to define the chronology of changes within the bay. Samples were also picked in sediments that appeared sedimentologically similar, to determine if the same processes showed a chronological correlation in different geographical areas of the bay. When dating the samples, the marine reservoir effect was taken into account and the appropriate calculations made according to Reimer et al. (2002). In total, 18 samples were dated; 15 at Beta Analytic private laboratory in Miami (USA) and 3 at Queen's University Chrono Centre in Belfast (Table 3.4). Dating was funded by the Geological Survey of Ireland (GSI) and Irish Quaternary Association (IQUA) grants respectively. All dates were calibrated using Calib 7.1 with the Marine13 calibration curve (Reimer et al., 2013) which takes into account the global reservoir correction. The delta R used was 40+/-47 years, which was taken from an average of 10 sites around the Irish coast. All radiocarbon ages are quoted as the average value of the range of uncertainty.

Samples were taken throughout the cores in the bay, (Table 3.4), in order to provide an age constraint. Samples were chosen from specimens that were intact or were known to have been broken during core splitting or sampling, in order to reduce the possibility that the samples were transported or reworked.

Table 3.4: Samples submitted for radiocarbon dating, showing the core number (from lowest to highest), depth of sample in each core, type of carbonate material used for analysis, weight of the sample material and the laboratory dating the samples. All foraminifera samples were composed of intact mixed benthic species; all shell samples were bivalves, while all *Turritella sp.* samples were intact.

Core	Depth (cm)	Material	Weight (mg)	Lab
CV13031-02VC	279-280	Shell	2000	Beta Analytic
CV13031-03VC	71	Shell	2485	Beta Analytic
CV13031-03VC	72	Turritella	558	Beta Analytic
CV13031-06VC	144-145	Shell	2001	Beta Analytic
CV13031-07VC	120-121	Turritella	335	Beta Analytic
CV13031-10VC	105	Shell	824	Chrono Centre
CV13031-10VC	126-127	Turritella	1248	Beta Analytic
CV13031-10VC	200-201	Turritella	217	Beta Analytic
CV13031-12VC	148-152	Shell	3000	Beta Analytic
CV13031-13VC	100-101	Turritella	1992	Beta Analytic
CV13031-13VC	177-179	Shell	2117	Beta Analytic
CV13031-13VC	235-236	Foram	7	Beta Analytic
CV13031-17VC	130	Shell	710	Chrono Centre
CV13031-20VC	81-82	Turritella	320	Beta Analytic
CV13031-20VC	117-118	Foram	6	Beta Analytic
CV13031-20VC	124	Shell	765	Chrono Centre
CV13031-22VC	38-39	Turritella	265	Beta Analytic
CV13031-22VC	269-270	Foram	4	Beta Analytic

3.10 Sub-bottom profiling

The sub-bottom data were obtained by the INFOMAR seabed mapping programme between 2007 and 2014 on board the RV *Celtic Voyager*, at the same time as the multibeam acquisition. These data were obtained using a SES 5000 3.5 kHz hull mounted pinger system. This system has a vertical resolution of 0.3-0.5m and a penetration range of 10-50m. Unfortunately, a portion of this data was lost by INFOMAR and therefore in this study the sub-bottom data is comprised of the remaining ~20,000km of high resolution pinger lines (Fig. 3.6). The data were converted from CODA to SEGY, processed and tidally corrected to lowest astronomical tide (LAT) within IHS kingdom 8.8 software. Of the 916 available lines, 728 were found to be viable in the seismic analysis of Galway Bay, as the others contained too much noise.

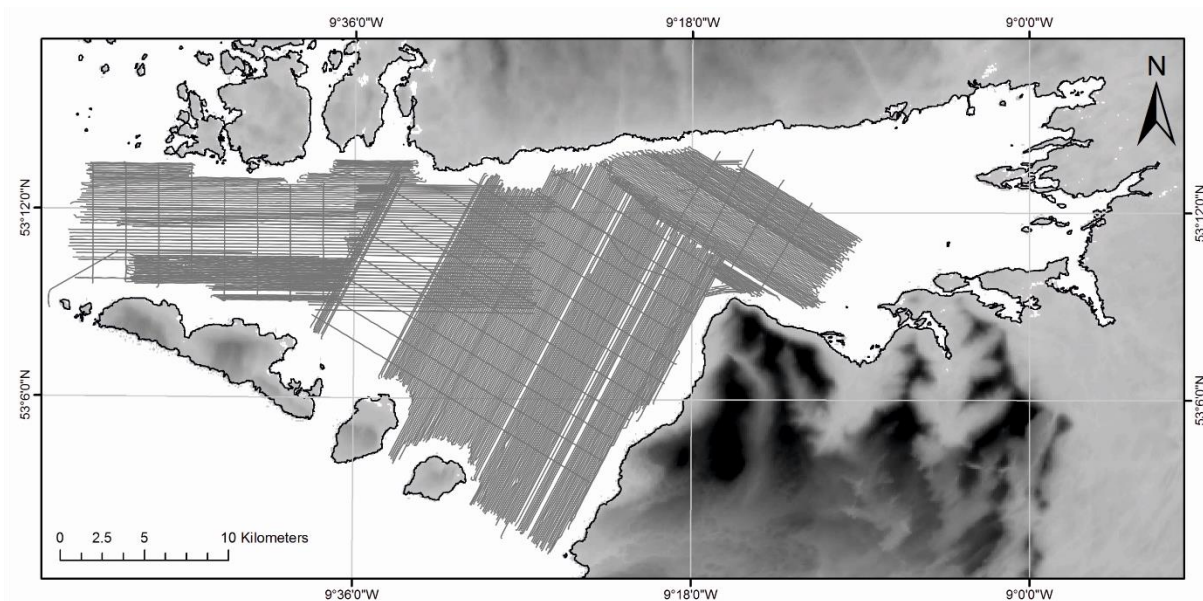


Figure 3.6: A map of Galway Bay showing the position of all viable seismic lines used in the construction of a seismic stratigraphy.

3.10.1 Data processing and horizon identification

Trapezoid band pass filtering (0.8-1.2 – 6.0-6.2kHz), automatic gain control (10 and 20ms) and wavelet envelope calculation were applied to the raw data, in order to improve the signal to noise ratio and remove artefacts, allowing a more easily interpreted image. The principles used to interpret the key seismic facies are those described by Mitchum and

Vail (1977) and Mitchum et al, (1977). Reflectors separating acoustic facies and bounded by their unconformities and correlative conformities were mapped throughout the bay and used to identify the stratigraphic boundaries.

The acoustic facies were defined visually using key characteristics in their geometry and internal configuration; this can be used to identify the sedimentary and environmental conditions that created them (Vail and Mitchum, 1977).

The characteristic geometries of the reflectors found in the sub-bottom data followed the scheme by Mitchum et al. (1977) and are outlined below (Fig. 3.7):

- Erosional truncation: the lateral termination of reflectors through erosion. Evident near the upper boundary of a sequence and generally the result of erosion.
- Toplap: the termination of reflectors at the top of a sequence against the upper boundary. Generally, occurs due to non-deposition.
- Concordance: occurs at both the upper and lower boundaries of a sequence and occurs when the reflectors do not terminate against, but instead follow the under or overlying strata. This indicates a non-erosional boundary.
- Onlap: occurs at the lower boundary when horizontal or inclined reflectors terminate against an underlying strata that is more inclined. Generally, an indicator of a non-depositional hiatus.
- Downlap: occurs at the lower boundary when reflectors terminate downwards against a horizontal or inclined underlying facies. This generally occurs in the opposite direction of the sediment supply and is an indicator of a non-depositional hiatus.

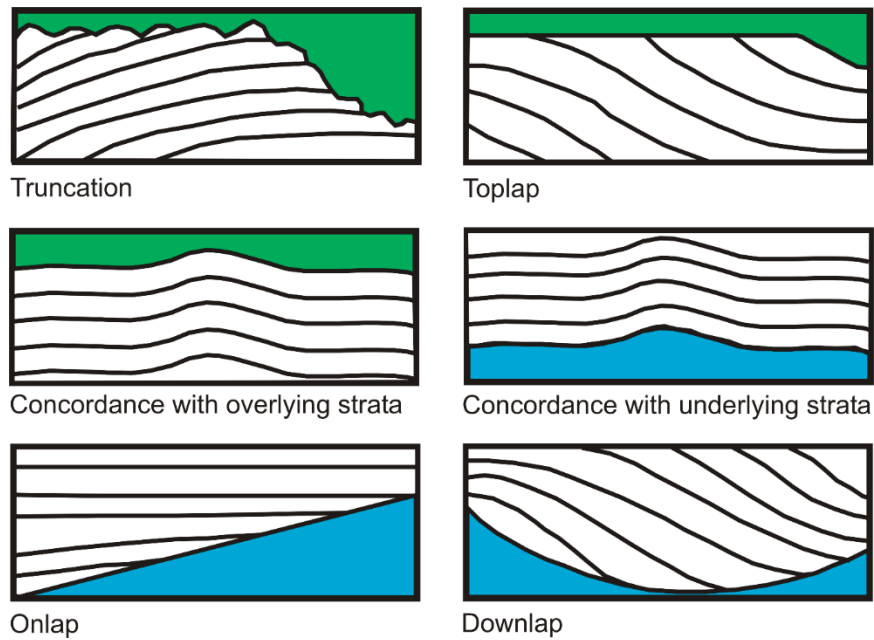


Figure 3.7: An example of the aforementioned reflector patterns used as the main criteria in stratigraphic analysis (Adapted from Mitchum et al, 1977). The overlying strata is coloured green and the underlying strata coloured blue.

The common internal configurations of the seismic facies found in the sub-bottom data are divided into 3 types of reflection patterns (Mitchum et al, 1997) and are outlined below (Fig. 3.8):

- Parallel reflector patterns: These include parallel, subparallel and wavy patterns, which commonly indicate uniform depositional rates on a stable basin or a constant subsiding shelf, and divergent patterns which usually indicate that the rate of deposition varies laterally.
- Discontinuous reflector patterns: These include hummocky, lenticular, disrupted, chaotic, contorted and reflection free. Hummocky, lenticular and disrupted patterns generally indicate interlocking clinoform lobes building into shallow water. Chaotic and contorted reflectors generally represent strata deposited in a variable high energy environment, such as cut and fill channels and faulted zones. Reflection free patterns commonly indicate homogenous or non-stratified units.
- Prograding reflector patterns: These include Sigmoid, oblique (tangential and parallel), complex sigmoid-oblique and shingled, all of which are prograding patterns. Sigmoid patterns suggest a low sediment supply and/or rapid sea-level

rise in a low energy environment. Oblique patterns indicate a high sediment supply and a sea-level stillstand in a high energy environment. A complex sigmoid-oblique pattern, as the name suggests, represents an environment with a combination of sigmoid and oblique patterns. A shingled pattern generally indicates progradation into shallow water.

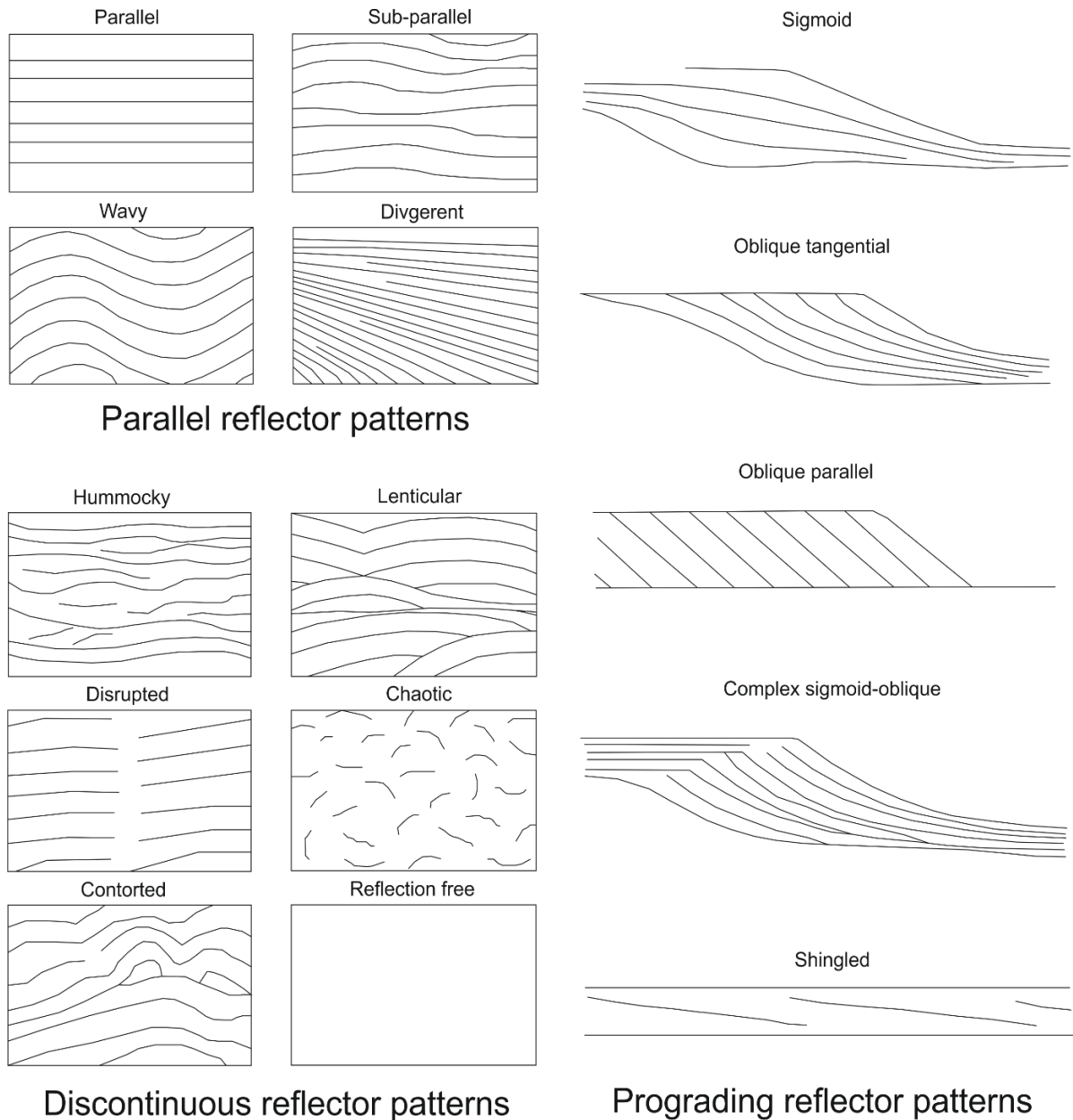


Figure 3.8: Example of the internal reflection configuration patterns used as the main criteria in stratigraphic analysis (Adapted from Mitchum et al, 1977).

3.10.2 Isopach maps

Isopach maps measure the thickness of a seismic facies by measuring the distance in two-way time between the horizons and converting this to metres using an average of the p-wave velocity data, obtained from the MSCL measurements. They allow the visualisation of the spatial distribution of each unit, its variations in thickness, as well as the comparison of spatial patterns. In order to create these maps, the spatial occurrence of mapped horizons stretching over large portions of the bay was necessary. Seismic horizons mapped using the pinger data were subsequently gridded before being used to identify the thickness of seismic units in IHS Kingdom 8.8. These gridded horizons were produced using a 500 x500 m cell size and the flex gridding algorithm, in order to best represent the maximum amount of data available in the bay.

Seismic profile depths were measured in Two-Way Travel Time (TWTT) and displayed in milliseconds (ms). For the conversion to depth the average acoustic velocity of the sediment cores was used. The average p-wave velocity for the 10 cores with MSCL measurements, was 1700m/s. In the water column, an average acoustic velocity of 1500m/s was used to calculate the depth conversion. This is based on the speed of sound in seawater offshore of Ireland, as calculated by Shillington et al (2007). When gridding the top of each unit, with the exception of the seabed, the average velocity of sound in both the water column and sub-surface, which is 1600m/s, was used. An average was applied, as in order to reach the top of these horizons sound had to travel through both the water column and sub-surface. When gridding the seabed horizon, the average sound velocity through the water column, 1500m/s, was applied, while 1700m/s, the average velocity of the sediment cores in the bay, was used when converting the thickness of each acoustic unit from milliseconds to depth in metres.

While all efforts possible were made to ensure the isopach maps were as accurate as possible, there are inherent errors associated with the creation of these maps. When either the upper or lower boundary of the unit is missing from the data, an average depth is assumed based on the overall grid. This can cause an averaging effect and may not be representative of the actual thickness of the seismic facies.

Chapter 4: Coastline and inshore geomorphology of Galway Bay, Western Ireland

This chapter follows a different layout compared to the other chapters as it is intended for publication in Journal of Maps. It has been presented following the recommended style and word count indicated by the journal. Within the thesis, geomorphological mapping is used to understand modern day processes in the bay. This offers a baseline against which change since the last glacial period can be mapped.

¹Denise McCullagh, ¹Sara Benetti, ¹Ruth Plets, ²Fabio Sacchetti, ²Eimear O’Keeffe and ²Kieran Lyons

¹*School of Geography and Environmental Sciences, Ulster University, Coleraine, Northern Ireland*

²*Marine Institute of Ireland, Oranmore, Galway*

Abstract

A combination of multibeam bathymetry and backscatter, LiDAR, and modelled hydrodynamic data, alongside online satellite images, were used to map the seafloor and coastline features in Galway Bay (Western Ireland). This is the first time these multiple datasets have been integrated into a single geomorphological map, something which is then used to make inferences on how the features in the bay are affected by the modern oceanographic regime. The modelled current and wave maps show high current velocities in the inner-bay, between the Aran Islands, located at the mouth of the bay and along the northern shoreline, and lower velocities in the mid-bay area. The current and wave maps correlate well with the seabed features in the bay. The main depositional features include dunes and ripples, while the main erosional features include scouring and outcropping bedrock. The substrate of the bay is predominantly mud and sand with extensive outcropping bedrock around the coastline. Galway Bay has been shaped glacially through the extension and retreat of the British-Irish Ice sheet across the bay and the deposition of glacially derived and later marine sediment. Many of the geomorphological features mapped at the seafloor are however modern and current-induced, as shown by the relationship between the direction and intensity of the prevailing currents in the bay, and the location and shape of the depositional and erosional features.

4.1. Introduction

Extensive seabed mapping has been carried out as part of the Irish government-funded initiatives to map Ireland's Exclusive Economic Zone, beginning with the Irish National Seabed Survey (INSS, 1999-2005) and continuing as the Integrated Mapping for the Sustainable Development of Ireland's Marine Resource project (INFOMAR, 2005-2019). To date, marine geophysical data (including opensource multibeam echo-sounder bathymetry and backscatter) have been collected in a large portion of Ireland's territorial waters, including Galway Bay. The ability to map the seabed at high-resolution continues to improve our understanding of coastal and marine environments and processes. This is necessary for the development of marine infrastructure, such as submarine cables and equipment for renewable energy, as well as the management of marine resources (Poppe et al., 2006; Li and King, 2007; Barnard et al, 2013). Geomorphological maps have the potential to provide baseline data from which human and environmental changes over varying timescales can be monitored. They can also act as a tool for environmental management, risk assessment of various geomorphological hazards, and to improve our understanding of the overall terrain of an area. They are essential in order to implement practical landscape management at government levels and to promote sustainable development.

In this paper, geophysical datasets are combined with satellite images, sea-floor samples and hydrological data and integrated into a single geomorphology map for the first time, providing a coherent picture of the coastline and seabed features in Galway Bay, located on the western Irish seaboard.

4.1.1 Study Area

Galway Bay is a large (62km long, 32km wide) marine embayment on the west coast of Ireland, between 53°02'N and 53°14'N and 09°00'W and 09°27'W. It is a high energy, storm-dominated system protected from the full force of the Atlantic Ocean by the Aran Islands (Inis Mór, Inis Meáin and Inis Óírr) at its western edge (Fig. 2) The bay encounters strong semi-diurnal tides, with a mean spring tidal range of >4.5m (Booth, 1975; Marine Institute, 2017). Hydrodynamic models show current speeds between the Aran Islands above 45cm/s in the ebbing spring tide, while wave models, based on wind speeds taken

from the Mace Head atmospheric research station, show winter wave heights above 250cm in the North and South Sounds and mid-bay areas (Joshi et al., 2017).

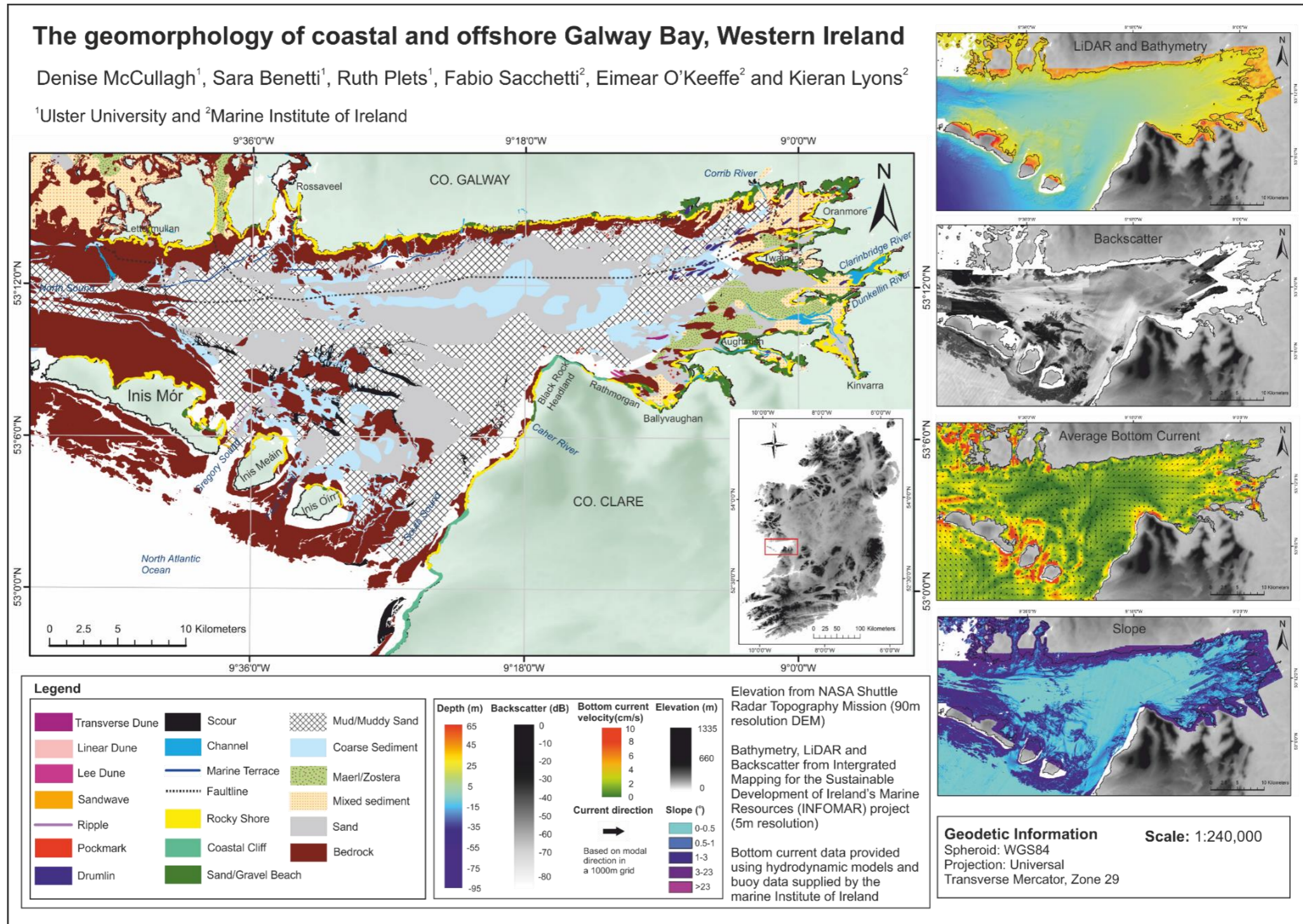
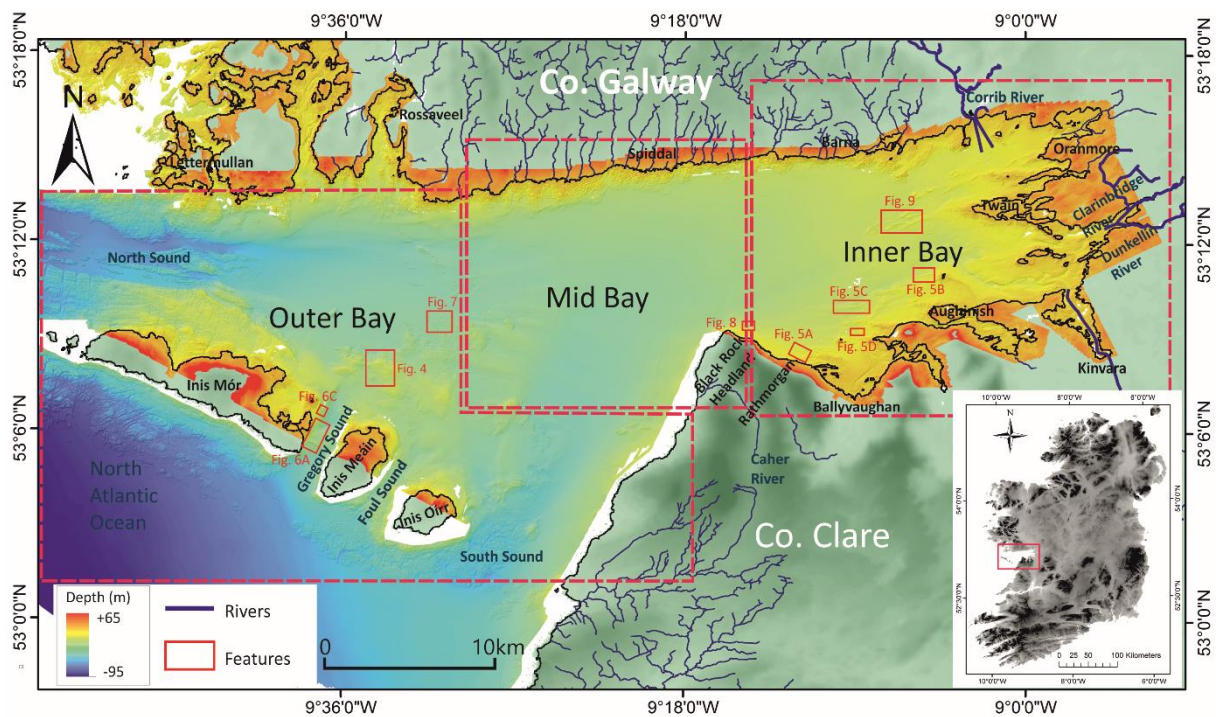


Figure 1: A geomorphology map of Galway Bay (main map), with smaller maps showing the LiDAR and bathymetry, backscatter, bottom currents and slope, from top to bottom on the right.

The primary inflow of Atlantic water into Galway Bay is through the South Sound, with outflow through the North Sound, creating a counter clockwise gyre (Harte et al., 1982; Lei, 1995). The main freshwater source at the head of the bay is the river Corrib, with volumetric flow rates usually exceeding 311 m³/s per year (OPW, 2012). Other freshwater inputs to the bay include submarine groundwater drainage streams along the northern shore at Spiddal and Barna and the Oranmore, Clarinbridge and Dunkellin rivers to the east and Caher to the south of the bay (Cave and Henry, 2011; Smith and Cave, 2012) (Fig.



2).

Figure 2: Bathymetric image of the study site showing the 0m contour line in black and sub-divided into 3 geographical areas: inner bay, mid bay and outer bay. Examples of features identified in the bay are outlined in red and will be discussed in further detail below.

The geology of the northern side of the bay is dominated by granite of the Caledonian Orogeny age, with the rest of the area (including the Aran Islands) made of Carboniferous Viséan limestone (Pracht et al, 2004). The landscape to the north and east of the bay is flat and low lying, with the majority of areas within 5km of the coastline generally below 30m. In contrast, to the south, the landscape is hillier with peaks above 100m, allowing for a steeper coastline. A submarine fault runs across the northern side of the Bay (mapped by Clarke, 2013) (Fig. 1).

During the last glaciation Ireland was covered by the British-Irish Ice Sheet (BIIS) (Clark et al., 2017). This ice sheet extended as far as the shelf edge west of Ireland and resulted in a wide range of glacial landforms across the landscape. Near Galway city and along the north and south coast, drumlins are found onshore (GSI, 2013). Offshore, ~150km west of the study area, a large morainic complex has been mapped at mid-shelf (Peters et al, 2015). Dating of this feature indicates that ice rapidly retreated onshore after 18.5ka BP, with all low-lying areas ice-free by 15ka BP (Ballantyne and Ó Cofaigh, 2017; Peters et al., 2016).

4.2 Materials and Methods

Multibeam bathymetric and backscatter data were acquired by the INFOMAR programme between 2006 and 2014 on board the RV Celtic Voyager using a Kongsberg Simrad EM3002D multibeam echosounder (300kHz). These data were processed and tidally corrected using CARIS HIPS & SIPS and gridded at 5m resolution by INFOMAR. LiDAR (Light detection and ranging) altimetry data were collected for INFOMAR between 2006 and 2010 by Tenix LADS Corporation. These datasets were combined to create a detailed altimetric/bathymetric map of Galway Bay that was used, together with backscatter classification (INFOMAR, 2011), satellite images and lithological data (Google Earth, 2017; INFOMAR, 2011), to identify and map submarine landforms and coastline types. Shaded relief with vertical exaggeration (x10) and different illuminations were generated in ESRI ArcGIS 10.1 to aid the interpretation of landforms. In order to avoid azimuth biasing, features were considered with multiple illuminations as well as without azimuth (Smith and Clark, 2005; Hillier and Smith, 2008). Contour lines (10m spacing), slope angle and aspect were derived using the spatial analyst extension tool to aid geomorphological interpretation. The profiling tool was used to derive information on geometric properties including wavelength, amplitude, symmetry and slope (cf. Ashley, 1990; Van Landeghem et al., 2009).

The substrate classification included in the map (Fig. 1) is derived from the interpretation of multibeam echosounder (MBES) bathymetric and backscatter data for subtidal depths >20m and the interpolation of biological samples and subtidal and intertidal data traced from orthoimagery and LiDAR datasets. Rock outcrops have been traced from orthoimagery, LiDAR data and MBES bathymetric shaded relief data. An automated

classification of the MBES data using QTC Multiview resulted in acoustic classes corresponding to different sediment types. These sediment types were then groundtruthed with subtidal grab samples (carried out by the Marine Institute) to produce a sediment map of the subtidal area. The traced rock outcrops, subtidal sediment map and the results of the point interpolation were then merged. All maps were translated to a modified Folk class and protected habitats were also attributed. Once standardised, the datasets could be displayed together as a single habitat map layer.

Modelled current data for the Greater Galway Bay area were provided by the Marine Institute. The model used is an implementation of the Regional Ocean Modelling System (ROMS), as described by Jackson et al. (2012). The model bathymetry is based on the INFOMAR dataset. It has a horizontal resolution of 200 metres and 20 vertical levels. It provides depth-averaged and three-dimensional velocity fields at a temporal resolution of three hours. The model includes atmospheric and tidal forcing, and climatological river input. For this study, one year of data were used to calculate mean and maximum depth-averaged and bottom velocities for Galway Bay. Two different grids were applied to the bottom and depth-averaged current data. A 1000m grid resolution was interpolated for current velocity data for the entire bay, while a 200m grid resolution was used to closely investigate the relationship between hydrodynamic forces and specific seabed landforms (Fig. 4 to 8). Modelled wave orbital velocities were taken from the regional wave model (SWAN) supplied by the Marine Institute. The domain covers all of Irish waters in the northeast Atlantic at a resolution of 0.025 degrees and is available at three-hourly intervals. For this study, one year of data was used to calculate mean orbital velocities. The model outputs provide an overview of the general trend of the bottom and depth-averaged currents, and the mean speed of the orbital wave velocity at a 2800m grid spacing (Fig. 3). The arrows in all grids indicate the most frequent flow direction, while the speed is represented on a colour scale from slow (green) to fast (red). The geomorphology map (Fig. 1) shows the average current velocity, while the current maps (Fig. 3) show the maximum velocities, as both are important in the process of forming and maintaining depositional/geomorphological features.

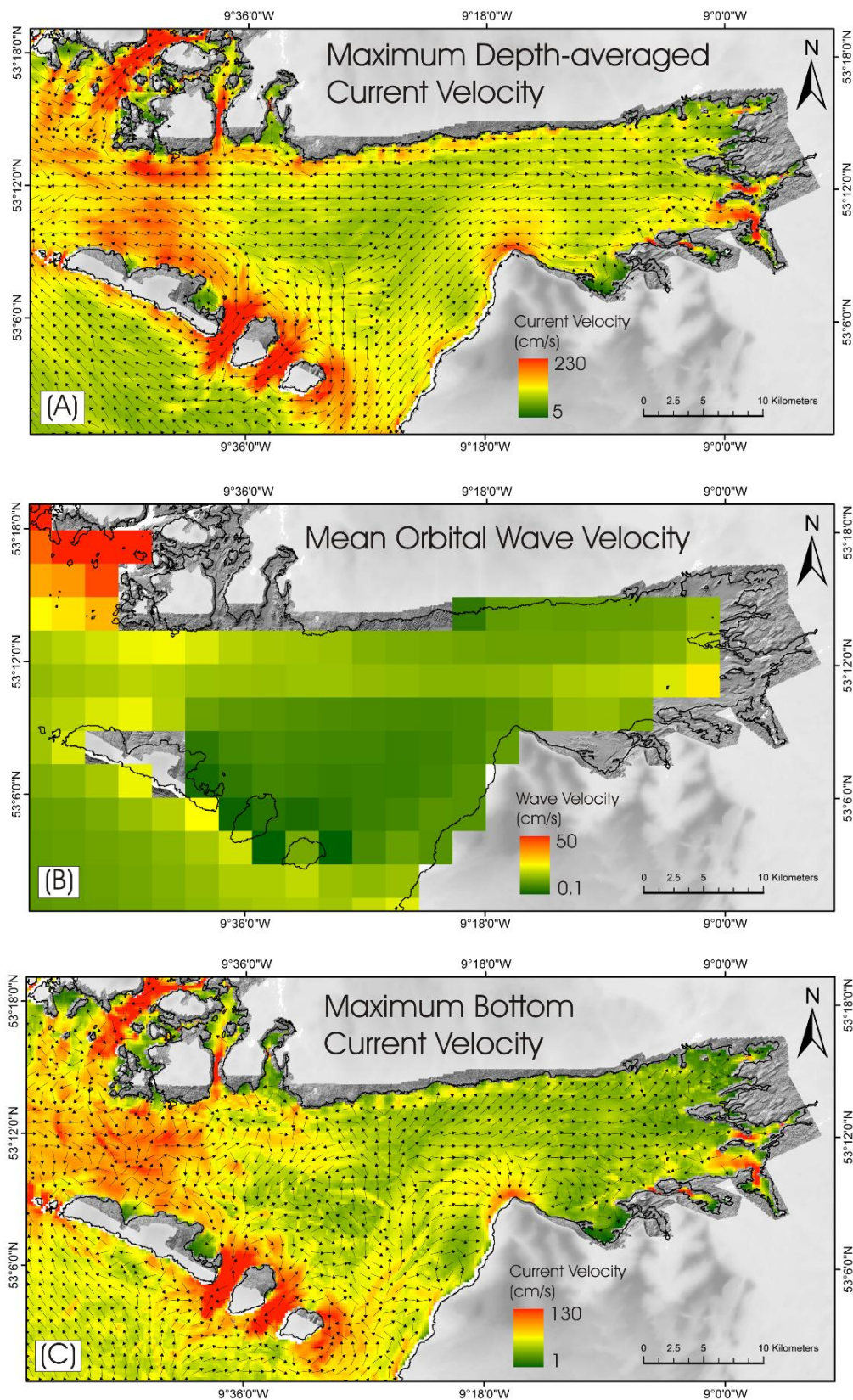


Figure 3: (A) maximum residual depth-averaged current velocity with 200m gridline spacing, (B) mean orbital wave velocity with a 2800m gridline spacing and (C) maximum residual bottom current with a 200m gridline spacing.

4.3 Results and Discussion

4.3.1 Hydrodynamic modelling

Across Galway Bay, the mean bottom current ranges from 0.01cm/s to 10cm/s (Fig. 1) with the highest velocities occurring around the Aran Islands, near the headland of Black Rock, in the inlets of the inner-bay and along the north shore. The average mean velocity is \sim 1cm/s, while the maximum bottom current can reach up to 130cm/s (Fig. 3A). The mean depth-averaged currents range between 0.01cm – 17cm/s, while the maximum depth-averaged current reaches up to 230cm/s (Fig. 3B). The highest average velocities follow the same overall pattern as the bottom currents, with the area around the Aran Islands, the inner-bay inlets and Black Rock headland showing the highest speeds. However, the influence of the various streams and rivers, particularly the river Corrib, can be seen in the inner-bay, with higher speeds in these areas evident in the depth-averaged current (Fig. 3A) and with the velocity through the North Sound reaching a maximum of 230cm/s. The orbital wave velocity is highest in the inner-bay area, near Kinvarra Bay, in the North Sound and along the northern shoreline, reaching an average velocity of 20cm/s (Fig. 3C). The lowest wave velocities occur behind the Aran Islands and towards the mid-bay area (Fig. 3C). This is likely due to the islands forming a barrier from the ocean force. There is a general movement of water towards the east and north east (Fig. 3B). Gyres are present in the bottom current model in the mid- and inner-bay areas as well as along the northern shoreline (Fig. 3A). This circulation pattern correlates with the presence of outcropping bedrock and coastal inlets, as the water flows fastest around these features. The contrast between the directions of the bottom- and depth-averaged currents suggests that the bedrock outcrops are influencing the circulation of bottom water in the bay, by forcing it in a different direction compared with other areas along the Irish Coast, Galway Bay encounters relatively low current speeds (O'Rourke et al., 2010).

4.3.2 Coastline mapping

Rocky shores, defined as areas composed mainly of boulders and cobbles, are present along large stretches (up to 75%) of the coastline around the bay. They are the dominant coastline feature, particularly in the outer-bay and around the Aran Islands, where the maximum depth averaged current velocities are strongest, up to 230cm/s. Sandy beaches are found mainly in the inner-bay, especially around the river Corrib, and other smaller

rivers and streams. The input of sediment from rivers, as well as the strong tidal and medium wave energy constantly acting upon the inner bay, are interpreted as the reason for the formation of the beaches. Coastal rock cliffs are found only along the southern side of the bay, beginning just east of Rathmorgan and continuing intermittently as far as the outer bay. They are located where the current velocities are highest (140-170cm/s) and wave velocities are of medium (7-10cm/s) strength (Fig. 3) and appear only in the higher elevation limestone areas. This correlates with previous studies which suggest that the geology, wave and current action and ground and surface water runoff are the major drivers in the formation of cliffs (Sunamura, 1992; Benumof and Griggs, 1999; Pierre and Lahousse, 2005).

4.3.3 Substrate classification

Bedrock outcropping at the seafloor is clearly visible on both the bathymetry and backscatter (Fig. 1), particularly in the North and South Sounds, eastwards of the Aran Islands, in the inner-bay areas near Twain Island and in particular along the northern coastline. In total, ~20% of the seafloor of Galway Bay consists of exposed bedrock. These outcrops are dominated by very high backscatter levels and tend to protrude 10-15m above the immediate surrounding areas, with slope angles $>23^\circ$ on most of the outcrops (Fig. 4). North of the fault line, the outcrops are expected to be granite and south of the fault line of limestone. Medium orbital wave velocity (16cm/s) and high current velocities for both bottom (~100cm/s) and depth-averaged (~170cm/s) currents, correspond with the outcropping bedrock in the North and South Sounds as well as the inner-bay areas. In the mid-bay area there are only a small number of examples of outcropping bedrock (Fig. 4), and the bottom current velocities tend to be much lower (~40cm/s). This suggests that the bedrock is influencing currents in the bay, resulting in sediment erosion or transport from the bedrock areas.

Coarse sediment, defined as material consisting of cobbles, pebbles and coarse sand, is predominantly found in the mid-bay and to the north east of Inis Meáin and Inis Óírr, covering ~10% of the bay. The coarse sediments are found around areas of outcropping bedrock and scouring where there is medium average bottom current velocity (~1.5cm/s) (Fig. 1), suggesting a link. Along the north coast, the coarse sediments frequently occur near the mouth of the rivers originating from Connemara, and it is possible that the coarser material has been transported from this area into the bay via fluvial processes. In

the mid bay area, there are patches of coarse sediment that do not appear to be connected to any landform in the bay and lie in areas of low current and wave velocities. It is likely these coarse sediments are related to the recorded occurrence of severe storms that can mobilize coarse sediment to depths beyond the effect of fair-weather waves and currents (Williams and Hall, 2004). There have also been studies on the connection of gravel patches and palaeo-channels (Browder and McNinch, 2006). As there is a palaeo-channel running along the northern coastline of the bay (See Chapter 5), this may be influencing the position of the coarser sediment in this area.

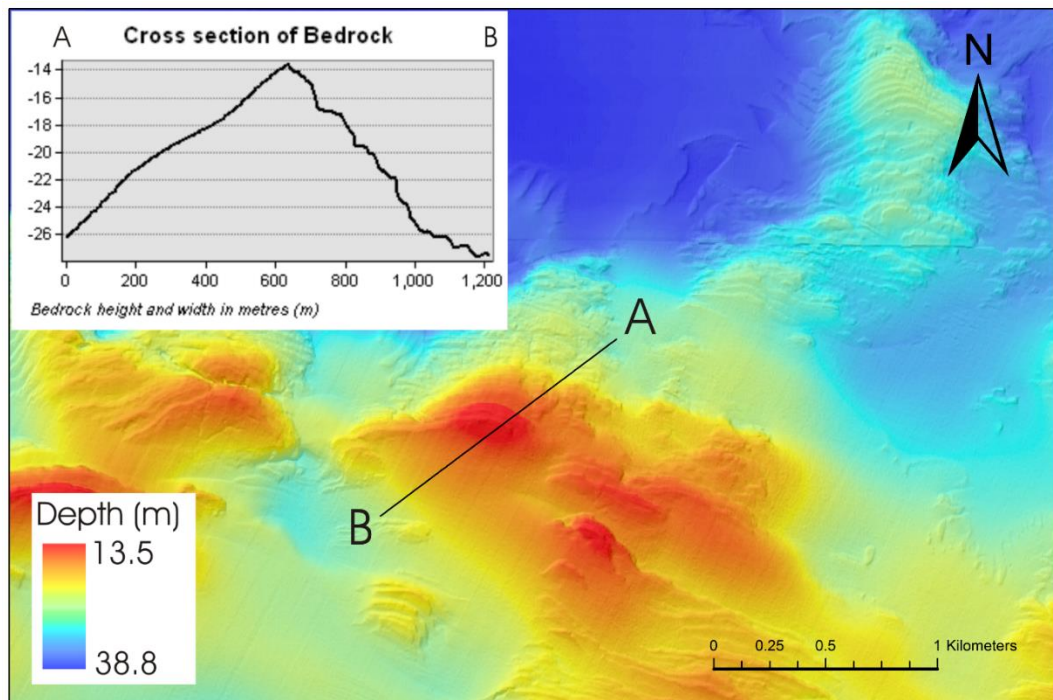


Figure. 4: Cross section and bathymetric image of outcropping limestone bedrock, located in the outer central bay area.

Sand in the bay makes up ~25% of the surficial sediment and tends to surround areas of coarser material (Fig. 1). The mid-bay appears to have the highest concentration of sand, which extends toward the outer bay in an elongated pattern along the northern coastline. It is found across a range of current velocities, from high to low, in both the bottom and depth averaged currents. One possibility for an abundance of material of this grainsize is that it is being introduced from the Corrib River and transported and deposited outwards along this area.

Mixed sediment covers only a small area in the inner bay (~5%), coinciding closely with the distribution of terrestrial streams in the same area (Fig. 1). It is probable this material is the result of fluvial deposition from these active channels, as there does not appear to be any obvious relationship within the current velocity data.

Mud/Muddy sand is the dominant sediment in the bay, covering ~35% of the total bay area. It is present across the entire area, but much less dominant in the inner bay. It is found only in areas where the average current and wave velocities are low (0.1-0.9cm/s) and never in areas where the average bottom current velocity exceeds 1.5cm/s (Fig. 1). This suggests that the muddy sediment is relatively cohesive, and the current speeds are not strong enough to transport or erode it (cf. Wu et al., 2011).

4.3.4 Habitat mapping

Maerl is a calcareous, free-living, red algae (rhodolith) that provides a niche habitat for an abundance of shallow water marine life. Zostera is a type of seagrass found in shallow marine environments across the world. Like Maerl, Zostera plays an important role in maintaining biodiversity (Dale et al., 2007) and both are protected under annex V of the EC Habitats Directive (EC Council Directive 92/43/EEC). Both these benthic species thrive in the euphotic zone and on heterogeneous sediment types (De Grave, 1999). Collectively they compose ~5% of the substrate in Galway Bay and are found <20m in depth and only in the very inner bay areas and in some of the Connemara inlets. The average bottom current in these areas is of medium velocity ranging from 1.4 to 3cm/s (Fig. 1), while the maximum wave velocity is also of medium strength at 16cm/s (Fig. 3B). This moderate velocity appears to provide an environment where the Maerl and Zostera communities are protected from the destructive force of waves and currents, yet fine sediment does not get a chance to settle on and smother them (Wilson et al., 2004). Maerl and Zostera can be found on a range of sediments, however, in Galway Bay they are predominantly found on a sandy substrate.

4.3.5 Submarine bedforms and landforms

The individual morphological features recognised in Galway Bay are discussed in the following sections. Most submarine landforms occur in the inner- and outer-bay areas and are defined by their shape and dimensions (Table 1). In the centre mid-bay area, no

distinct bedforms are present. This may be due to constant mobilisation by waves and currents, as there is sediment in this area.

Table 1: Summary statistics on dimensions and other characteristics of submarine bedforms and landforms in Galway Bay.

Feature	Length (m)	Width (m)	Depth/Height (m)	Lee Slope (°)	Stoss Slope (°)	Sediment type	Symmetry / shape
Channels (meso scale)	Variable-extending inland	2 - 460	0.5 - 14	Variable - generally > 39	Variable - generally > 39	-	Slightly sinuous
Lee Dunes	950 - 1370	133 - 175	1 - 3	4.3 - 5	1.1 - 5	Sand	Asymmetrical with rounded crest
Linear Dunes	924	130	1.5	5	2.5	Mixed	Slightly asymmetrical with rounded crest
Transverse Dunes	60 - 80	250	1.8 – 2.5	6.6 (large) 7.5 (small)	1.8 (large) 5 (small)	Coarse/sand (large) Sand/mixed (small)	Crescentic (large) Sinuous/symmetrical (small) Both with rounded crest
Sand waves	403 - 822	58 - 120	1.5 - 8	3.75 – 26.5	7.15 - 30.5	Sand	Symmetrical with sharp crests
Ripples	70 - 390	6 - 25	0.1 – 0.5	Variable	Variable	Sand	Linear
Marine Terraces	Up to 55,000	Variable	Variable	Variable	Variable	Sand	Slightly sinuous
Scouring	Variable	Variable	0.3 – 0.6	Variable - generally >45	Variable - generally >45	-	Variable
Pockmarks	<16 - 80	<16 - 80	0.5 - 8	<13 - >23	<13 - >23	-	Circular/Oval
Drumlins	185 - 1500	60 - 300	2 - 6	Variable	Variable	Mixed	Elongate

4.3.5.1 Channels

There are meso- and macro-scale channels in the bay. The meso-scale channels are smaller channels and are confined to the inner-bay and to some areas along the northern coastline (Fig. 1), where runoff, flowing southwards from Connemara, has exploited existing cracks through the bedrock in the outer-bay. These channels are up to 14m deep, 460m in width and are clearly visible in the bathymetry and LiDAR data in intertidal areas. All channels have sides with slopes >10° and in most cases >39°. Many of these are either active channels or they are an indication of former active channels during periods of lower than present sea-levels in the bay.

The macro-scale channels are much larger, over 15m in depth and 1km in width (the Sounds, Fig. 1 (represented only by name-not in blue)), that exist between the Aran Islands and the mainland. The North and South Sounds, as well as, to a lesser extent, the Gregory's and Foul Sounds provide the inlet for oceanic water into the bay and control the current circulation in the bay. The North Sound is the deepest channel in the bay, reaching a depth of 77m, and extending as far east as the mid-bay at Spiddal, more than 30km in length. This channel is located along a fault line, where the contact point between the granite and limestone could make it prone to erosion by current oceanographic processes and the past advance and retreat of the BIIS across the region.

4.3.5.2 Subaqueous dunes

Subaqueous dunes are defined by Ashley (1990) as large flow transverse bedforms with heights $>0.075\text{m}$ and spacing $>0.6\text{m}$. These bedforms are good indicators of the hydrology of an area, as they are controlled by flow depth, grain size, current velocity and direction (Mazumder, 2003; Rubin and McCulloch, 1980). Dunes are present only in the inner-bay areas and are located near the bedrock outcrops. They can be classified as transverse, lee and linear dunes.

Lee dunes are commonly formed on the leeward side of an obstacle, with double lee dunes forming as an elongate pair on the lee side of an obstacle (Huggett, 2011). One example of a double lee dune is found in Galway Bay north of Rathmorgan along the coastline of Co. Clare (Fig. 5A). It ranges in height from 1 to 3m and in width from 133 to 175m. The obstacle in this case is topographic, in the form of bedrock. The double lee dune is straight, elongated (up to 921m in length) and slightly asymmetrical with rounded crests, with stoss slopes between 1.1° and 1.5° and lee slopes between 4.3° and 5° . While there is no backscatter data for the lee dunes, the area beside them has a medium backscatter return and based on the classification of substrate in the bay, is composed of sand (Fig. 1). It is inferred that the dunes are therefore likely composed of sand. The bottom and depth-averaged currents are flowing in different directions over them. Based on the dune morphology, relatively shallow depth and the higher current velocity, the depth-averaged currents flowing parallel to the dunes appear to be more significant than the bottom currents in their formation.

Linear dunes form parallel to the flow direction and the only example here is an isolated dune located between outcropping bedrock (Fig. 5B), north of Aughinish Island. It is 1.5m in height and 924m in length. This dune is slightly asymmetrical with a rounded crest. The stoss slope is 2.5° while the lee slope is 5° . There is a slight change of direction in the currents towards the eastern end of the dune indicating a more northerly flow direction and possibly causing the observed sinuosity in the dune (cf. Bristow et al., 2000). While there is no backscatter available for the dune, the nearest area shows a high backscatter return and the substratum is composed of mixed sediment, maerl and seagrass (Fig. 1), suggesting a mixed sediment composition for this dune. Both the depth-averaged and bottom currents flow parallel to this dune, typical of the flow over any linear dune.

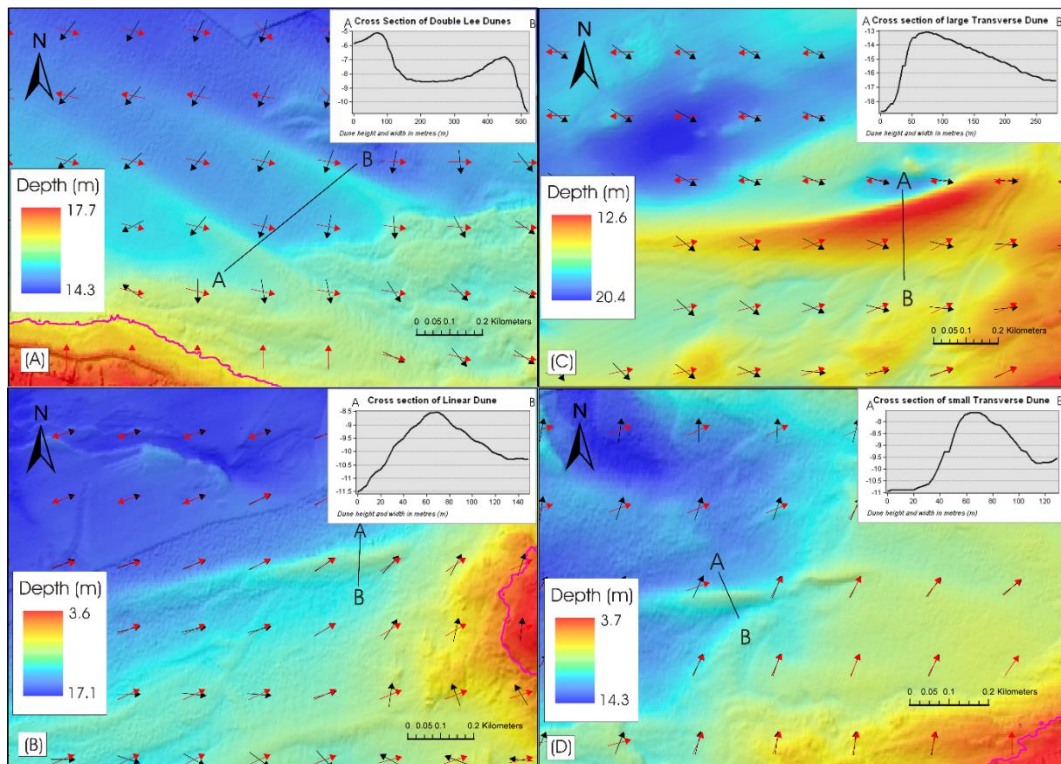


Figure 5: Cross section and bathymetric image of (A) double lee dunes, (B) linear dune, (C) large transverse dune and (D) small transverse dunes. The black arrows indicate bottom current direction while the red arrows indicate depth-averaged current direction. The image shows both currents on a 200m grid using the most frequent direction. The pink line represents the 0m contour line.

Transverse dunes form transverse to the flow direction and have an asymmetrical ridge. There are two transverse dunes visible in the inner bay directly north of Ballyvaughan,

which range from 1.8 to 2.5m in height and from 60 to 180m in length. The larger dune (Fig. 5C) is crescentic in shape with a rounded crest. The stoss slope is 1.8° while the lee slope is 6.6° . Backscatter data that partially covers this dune and the surrounding area shows a high backscatter return. The large dune is thus predominantly composed of coarser material, however, based on the classification map, there is sand on its northern side (Fig. 1). The smaller dune (Fig. 5D) is sinuous in shape, more symmetrical and rounded at the crest, with a stoss slope of 5° and a lee slope of 7.5° . The dune is composed of sand and mixed sediment based on the backscatter and classification maps (Fig. 1). The smaller transverse dune has bottom and depth-averaged currents flowing in similar directions, while the larger dune shows bottom and depth-averaged currents flowing in opposite directions. As both features show the typical morphology of a transverse dune and appear to be orientated transverse to the bottom current, the bottom currents rather than the depth-averaged currents must contribute to the shaping of these features.

4.3.5.3 Sand waves

Sand waves differ from subaqueous dunes in that they are formed under reversing flows with an average velocity of 30-75cm/s (Allen, 1980; Stow et al., 2009). They are the most common feature in shallow shelf environments with an average wavelength of 5 to 500m (Stow et al., 2009) and average height of 2-5m, although larger sand waves are also found (Ashley, 1990; Terwindt, 1971). Sand waves in Galway Bay are confined to the area between Inis Meáin and Inis Mór, with four examples identified in the data (Fig. 6A). These measure up to 8m in height and 120m in width. They are all symmetrical with sharp crests, transverse to the flow direction. Three of the sand waves are straight and one has a more crescent shape. They all have slopes between 3.75° and 30.5° , with the slip faces $>55^{\circ}$. They are located in areas of low backscatter intensity (Figure 4.6B) and are most likely composed of sand (Fig. 1). The strong semi-diurnal tide and accelerated flow between the islands in the bay provides a perfect environment for their formation (cf. Van Landeghem et al., 2009).

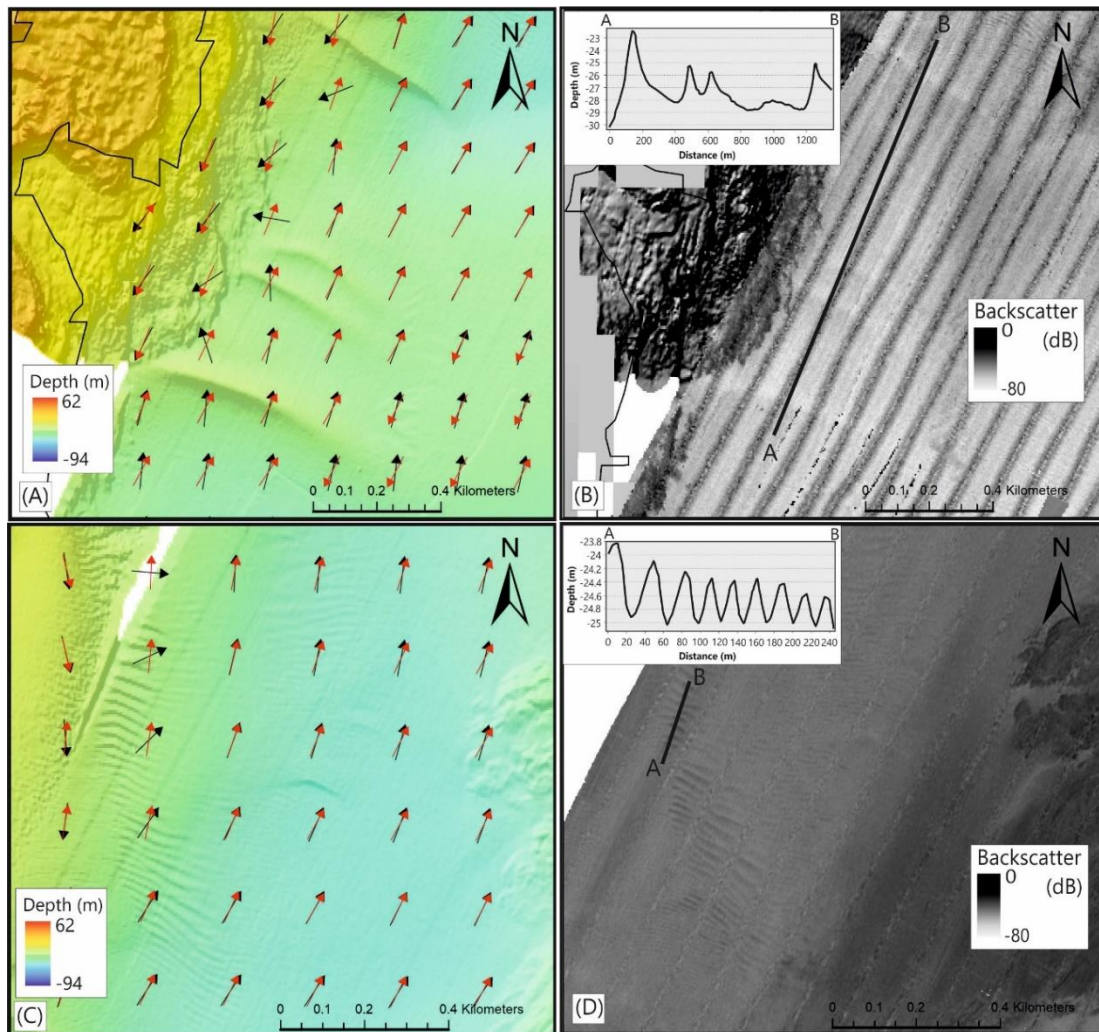


Figure 6: (A) bathymetry and (B) backscatter data in the area of the sand-waves; (C) bathymetry and (D) backscatter of the ripples; all including cross sections. The black arrows indicate bottom current direction while the red arrows indicate depth-averaged current direction. The image shows both currents on a 200m grid using the most frequent direction.

4.3.5.4 Ripples

Generally, based on their dimensions, ripples can be distinguished as 'ordinary' ripples or mega-ripples. Ordinary ripples are defined as depositional features with wavelengths between 0.1-0.6m and heights between 0.02-0.1m (Stow et al., 2009), and develop in sediments finer than 0.7mm (Mazumder, 2003). Mega-ripples are larger, with wavelengths of 1 - 25m and heights of 0.1 - 1.5m (Ashley 1990; Gallagher, 2003). All ripples identified in Galway Bay are classified as mega-ripples based on their dimensions (Fig. 6C).

Found on the landward side of the Aran Islands, in front of the strait between Inis Meáin and Inis Mór, transverse to the flow direction, the ripples extend over an area of 2.5km by 3km. These bedforms are up to 0.5m in height and 20m in wavelength. The steepest slip face angle is up to 10°. They are generally linguoid in form and asymmetrical with sharp crests, fitting the morphology of ripples formed by currents rather than waves (cf. Selley, 2000; Stow et al., 2009) and the faster restricted currents between the Aran Islands are believed to account for the linguoid shape. All ripples show a very low backscatter return but are surrounded by higher backscatter levels (Fig. 6D), suggesting the ripples are composed of mud and sand and surrounded by gravel and bedrock (Fig. 1).

4.3.5.5 Submerged marine terraces

Along the northern edge of the bay from Spiddal to Lettermullan several ridges, up to 55km in length are observed (Fig. 1). They show a seaward drop of ~5m from a relatively flat platform on the landward side. The ridges from Spiddal to Rossaveel have medium to low backscatter values suggesting they are composed of mud and sand. The ridges further eastwards have higher backscatter values and therefore are composed of sand. They occur where wave velocity is of medium strength (9-17cm/s) and average current velocities low (0.08-0.6 cm/s). Using sea-level reconstructions for the region (Bradley et al., 2011), the depth of the marine terraces at ~20m and ~27m matches well with sea-level positions between 11 - 14ka BP, a time of lower sea-level that was experiencing a stable period of sea-level rise. Due to their shape, depth and parallel position to the shoreline, it is believed that these ridges are therefore marine terraces (Reis et al., 2013; Martinez-Martos et al., 2016), submerged by rising sea levels and that they represent palaeo-shorelines.

4.3.5.6 Seafloor scouring

Scour marks are defined as local depressions as a result of local-non-uniform flow over the seabed, around a topographic obstacle (Whitehouse, 1998; Maity and Mazumder 2014). Scouring is visible on both the bathymetric and backscatter data around the bedrock outcrops west of Black Rock Headland and to a lesser extent in the North and South Sounds. The scour marks are all <1m deep, ranging between 0.3 - 0.6m (Fig. 7) and are composed of coarser sediment, suggesting that the finer sediment has been

winnowed away. The clear association with the bedrock outcrops in the area suggests that this is an influential factor in the scouring, possibly due to increased current velocities forced between these outcrops.

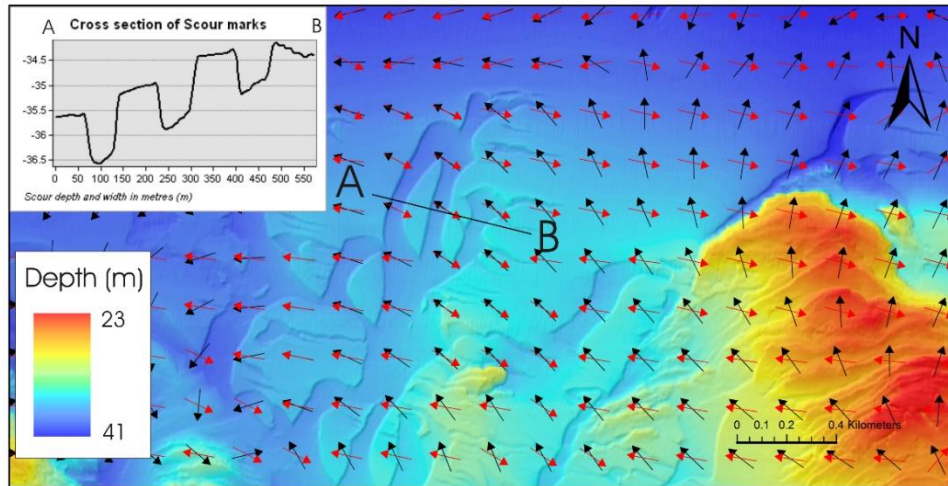


Figure 7: Cross section and bathymetric image of scouring around bedrock in the mid-bay. The black arrows indicate bottom current direction while the red arrows indicate depth-averaged current direction. The image shows both currents on a 200m grid using the most frequent direction.

4.3.5.7 Pockmarks

Pockmarks are concave, conical depressions commonly found along continental margins, shallow waters and deep-water basins worldwide (Sumida et al., 2004; Rogers et al., 2006; Wenau et al., 2017). In Galway Bay they are found exclusively near Rathmorgan along the southern coastline and west of Barna along the northern coastline. In the north, only five small (<16m in diameter) pockmarks are visible in the bathymetric data, while in the south there is a slightly higher concentration, ranging from 20-80m in diameter and 0.5-8m in depth (Fig. 8). The larger pockmarks have steep side angles >23°, while the smaller pockmarks' sides are <13°, and all are circular. Pockmarks are generally formed by fluid or gas discharge (Ussler et al., 2003). Most reported cases of pockmarks are caused by methane gas (Hovland et al., 2010). This is a possibility for Galway Bay, as gas pockmarks have been discovered in numerous locations on the Irish shelf, including Dunmanus Bay in the southwest and on the Malin Shelf in the northwest (Monteys, 2008; Szpak et al., 2012). The dimensions and association with finer-grained sediments correlate well with those in Dunmanus Bay, which may suggest a similar formation mechanism of

hydrocarbon expulsion through the sediment (Szpak et al., 2015). The pockmarks in the bay do not appear to correlate to wave or current velocities in either location or shape, occurring as both circular and elongated under both fast and slow flow conditions.

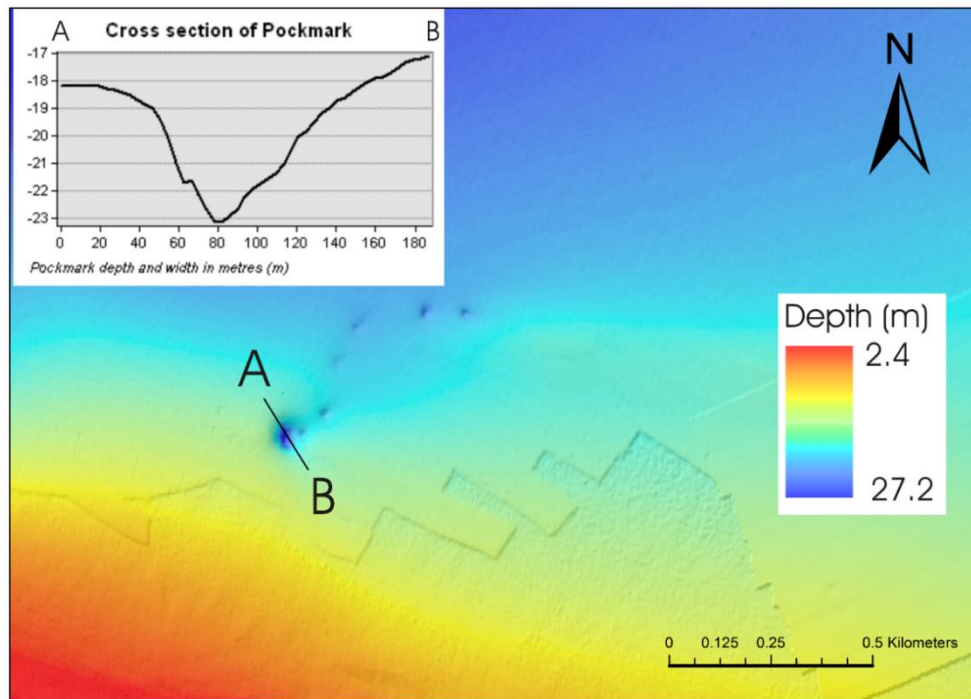


Figure 8: Cross section and bathymetric image of the largest pockmark visible in the bay. Artefacts are visible in the data to the south of the pockmarks.

4.3.5.8 Drumlins

Drumlins are elongate oval mounds, generally composed of mixed sediments, formed beneath an ice sheet and streamlined in the direction of the ice-flow (Clark et al., 2009; Ó Cofaigh et al., 2016). Onshore drumlins (Fig. 9A) are found in the inner area of the bay (Fig. 9B) and range from ~60-300m in width and ~185-1600m in length. The submerged drumlins (Fig. 9B) follow the same morphology and orientation as those on land at the head of the bay. Their dimensions range from 140-250m in width and 450-1500m in length. Reworking and flattening of their tops is visible, likely due to their position in the surf zone. The vast majority of the drumlins in the offshore region of Galway Bay are NE-SW aligned and are characterised by high backscatter intensity and are composed of coarse or mixed sediments (Fig. 1).

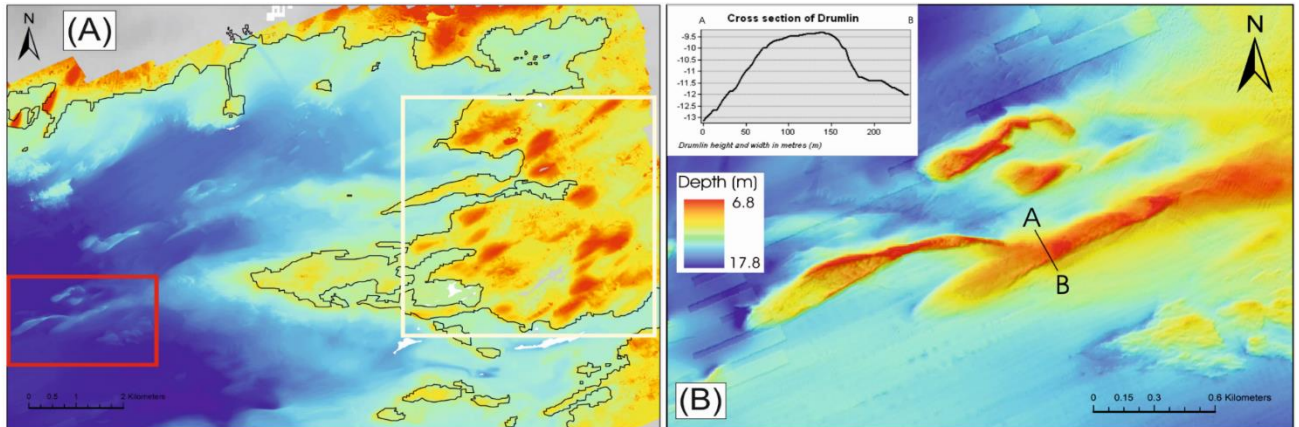


Figure 9: (A) Drumlin field visible onshore (white box) and a zoomed out inset of image B (red box). The black line represents the 0m contour and present day coastline. (B) Cross section and bathymetric image of drumlins visible in the bay. Artefacts are visible in the data to the north and west of the drumlins.

These features display the same morphology of drumlins found in both the Irish and UK terrestrial and marine landscapes (Benetti et al., 2010; Clark et al., 2009; McCabe and Dunlop, 2006; Ó Cofaigh et al., 2002). The drumlins visible in the bay are an extension of those mapped on land in Co. Galway and Co. Clare (McCabe, 1989) and their orientation suggests ice flowing in an offshore direction.

4.4. Conclusion

The first geomorphological map of Galway Bay, based on bathymetric, backscatter, altimetry data and sediment samples, shows that the majority of depositional features, including ripples and sandwaves, are located near the Aran Islands, with a few lone dunes in the inner bay. Erosional features, such as scouring and outcropping bedrock, are located mainly in the outer bay. Bottom and surface currents as well as wave action all play an important part in the hydrology of the bay, with the depth-averaged currents being more influential on the geomorphology in the shallower inner-bay and bottom currents more influential in the deeper mid- and outer-bay. The bottom currents show a circulation pattern from the south to the north, entering through the South Sound and exiting through the North Sound (Fig. 1 & 2). Between the Aran Islands, current velocity is at its highest as water from the Atlantic Ocean is pushed through the narrow channels causing acceleration. The areas that show higher velocity currents are those that have the highest concentration of erosional features, suggesting active transport and erosion. A

clear build-up of muddy sediment, behind the bedrock outcrops in the mid-bay in an eastward direction and in the inner bay in a westward direction, may represent tidal movement in the bay. The drumlins and marine terraces of Galway Bay were created many thousands of years ago, whilst the majority of the other submerged landforms visible in the bay appear to be due to present-day hydrological influences or geomorphologic controls.

This geomorphological map provides a complete picture of the landforms in the bay and an indication of their formation mechanisms, thanks to the connection with hydrological models. However, it is important to note that some of the data used were collected over 10 years ago. Based on our interpretation of the landforms, it is possible for these features to undergo evolution or migration under current hydrodynamic conditions. This research therefore provides a base map for future assessment of sediment mobility in the bay through, for example, repeat surveys and the ensuing analysis of time-series data. It also provides a practical resource in order to promote sustainable development in the bay, in particular with regards to the planned extension of Galway harbour and for the proposed establishment of renewable energy sources (wind turbines) within the bay.

Chapter 5: Results

This chapter outlines the results from the analysis of the seismic data and sediment cores. The results of a detailed analysis of the available seismic data are presented first. This is followed by the chronological analysis from 18 radiocarbon dates taken at various points across a number of sediment cores. Following the presentation of the radiocarbon dates is the sedimentological analyses; ordered by lithological, biological and then chemical analysis. Only the most representative cores are shown here, however, logs and data for all cores are available in the appendix (Appendix 1). Finally, a sequence stratigraphy based on geographical position in the bay is presented.

5.1 Seismic Results

The seismic lines used in this study were of variable quality. Of the ~800 lines available for the bay, only a third were of sufficient quality to allow detailed analysis. The lines southwest across the North Sound and the lines extending southwest from the inner bay through the South Sound were of the highest quality and are the ones primarily used in the analysis of seismic units and reflectors (Fig. 5.1, 5.2, 5.3 & 5.4).

The seismic lines in the rest of the bay were used to determine main seismic horizons and to produce grids and isopach maps of the units (Fig. 3.5). It is important to note that these grids and maps were produced using polygons across 500m grids and as such data that were missing from some of these areas have been interpolated, which may have caused slight errors. Acoustic penetration ranges from 20 to 100ms and the deepest penetration occurs in the North Sound. There are 3 distinct seismic units found in Galway bay with different acoustic characters and distribution. These are discussed in the next sections.

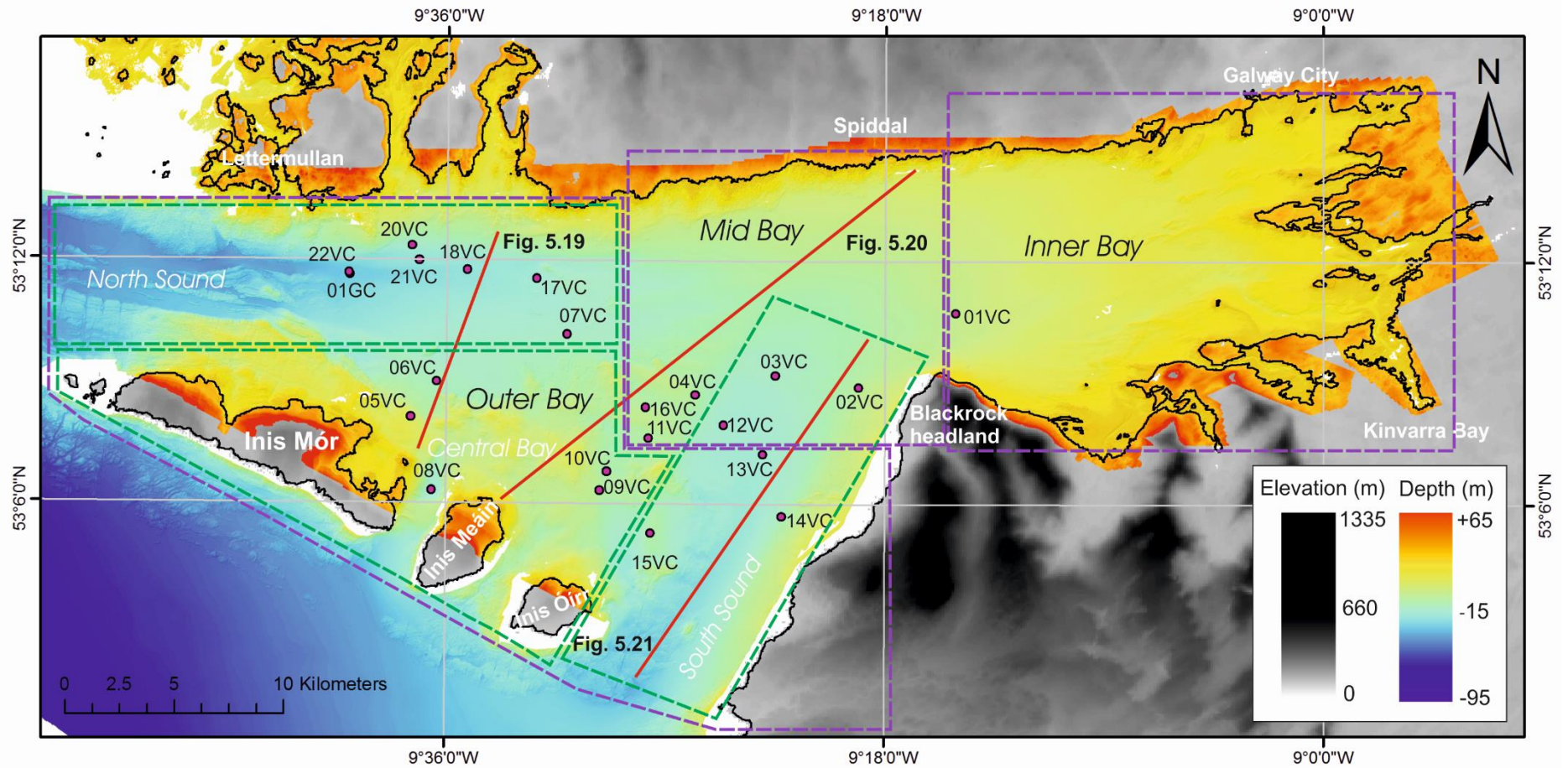


Figure 5.1: Map showing the 3 sections of the bay (Inner, Mid and Outer) outlined in purple, with sub sections (North Sound, South Sound and Central Bay) outlined in green. The cores from CV13031 are shown in pink and 3 of the highest quality seismic lines in the bay are shown in red.

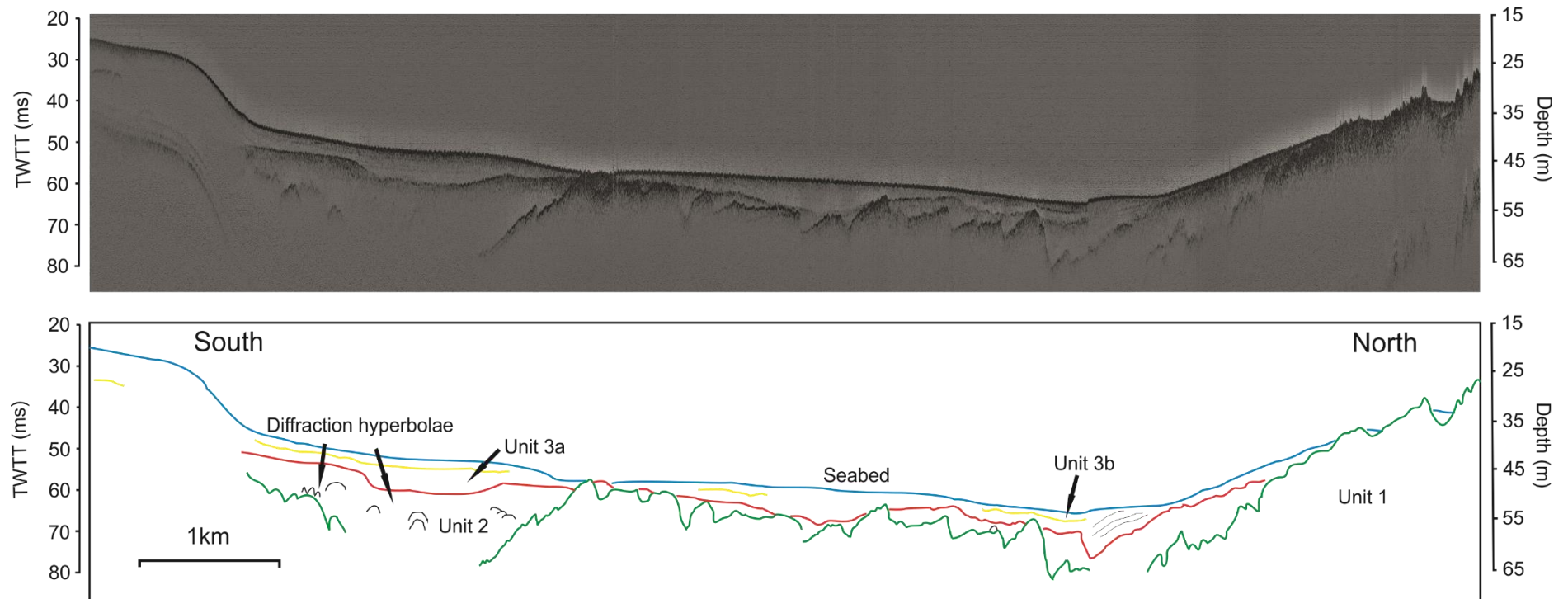


Figure 5.2: Seismic line 1 extending northeast from Inishmor across the inner area of the North Sound showing all seismic units in the bay. Green reflector: represents the top of unit 1. Red Reflector: represents the top of unit 2. Yellow reflector represents the top of sub-unit 3a. Blue reflector: represents the seafloor.

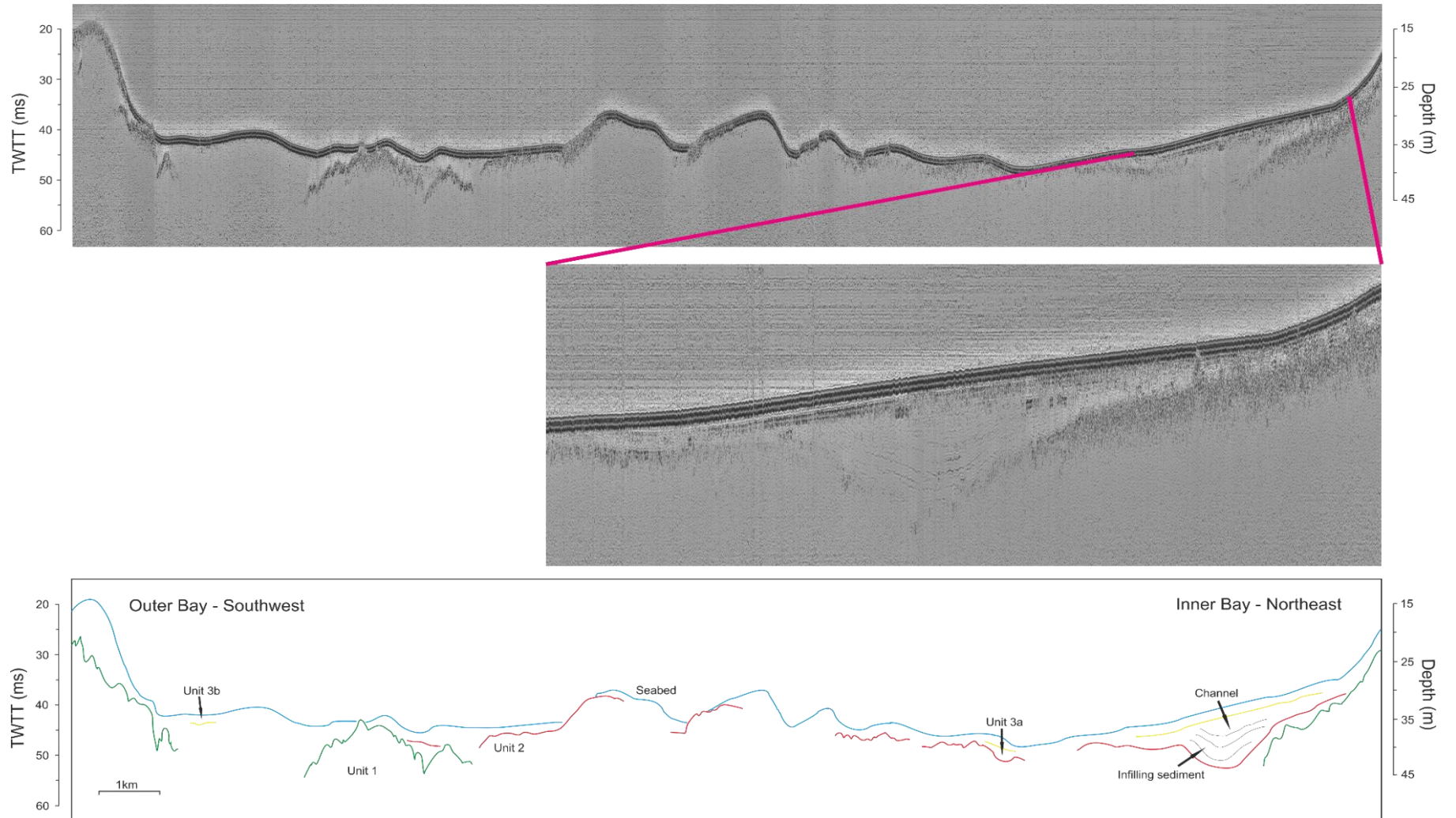


Figure 5.3: Seismic line 2 through the inner bay showing the channel that extends westwards. Zoomed-in image clearly shows infilling in this channel. Green reflector: represents the top of unit 1. Red Reflector: represents the top of unit 2. Yellow reflector represents the top of sub-unit 3a. Blue reflector: represents the seafloor.

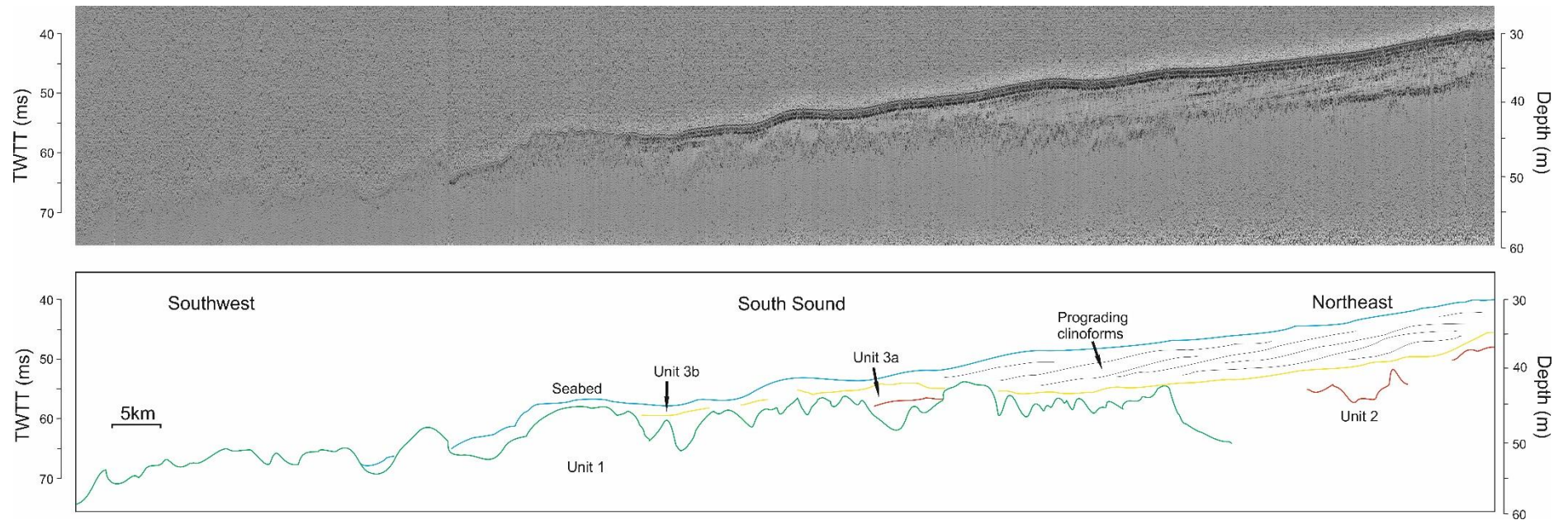


Figure 5.4: Seismic line 3, extending from the inner bay south west to the South Sound, showing prograding clinoforms in the northeast. Green reflector: represents the top of unit 1. Red Reflector: represents the top of unit 2. Yellow reflector represents the top of sub-unit 3a. Blue reflector: represents the seafloor.

5.1.1 Unit 1

This unit is the deepest and represents the acoustic basement in much of the bay. The upper boundary of unit 1 is an unconformity and is the strongest acoustic reflector after the seabed. Its upper surface is marked by a high amplitude, continuous reflector (Fig. 5.2, 5.3 & 5.4). The unit itself is represented by chaotic internal bedding structures. The top of this unit extends from 14m to 70m below the sea surface (Fig. 5.5A). It is visible throughout nearly the entire bay with the exception of the central mid and inner bay areas. To the north of the fault line, the unit appears much more transparent, although structures that are visible are still chaotic in character. The overlying strata onlap onto this unit. Throughout much of the North and South Sounds, this unit either represents the seabed or lies immediately underneath it. The outer central bay also has numerous outcrops and areas where the basement lies directly underneath the seafloor (Fig. 5.4). None of the cores penetrated this acoustic unit. The topographical profile of this unit is similar to the modern-day topography in the outer North and South Sounds and the outer central bay (Fig. 5.5), as it is outcropping and forms the seafloor in these areas. However, it is clearly located much deeper than the current seabed in the mid bay region and in the inner Sounds, forming a depositional basin. It is not visible on the seismic data inland of Blackrock headland, suggesting it must be positioned below the limit of acoustic penetration in this area.

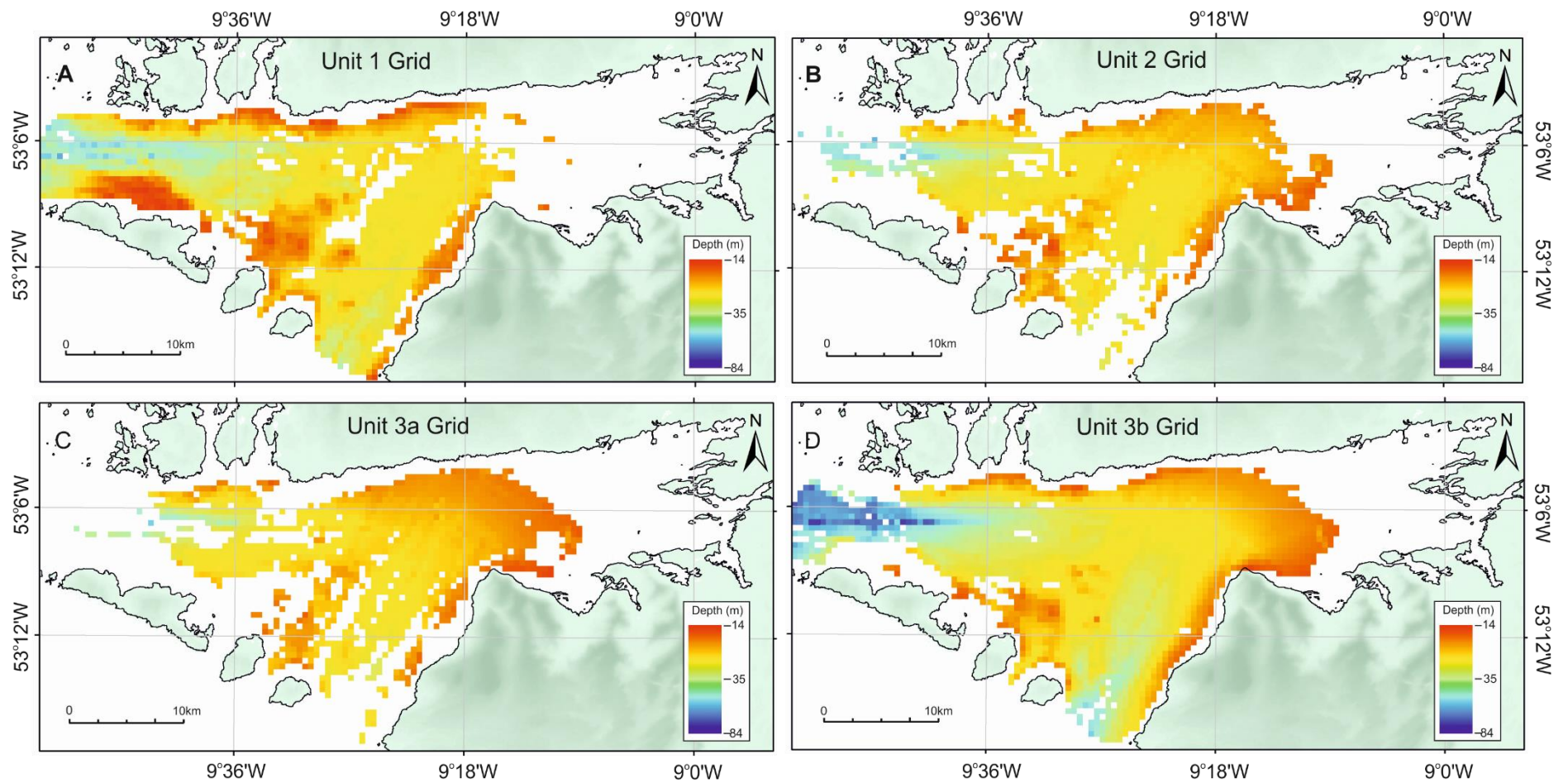


Figure 5.5: Grids showing the extent of the upper boundaries of all seismic units in Galway Bay. A) grid of the top of unit 1 topography, B) grid of the top of unit 2 topography, C) grid of the top unit 3a topography, D) grid of the top unit 3b topography. This data has been interpolated using a 500m gridding parameter and slight errors may exist.

5.1.2 Unit 2

This unit infills the depressions found in Unit 1, smoothing its topography (Fig. 5.3 & 5.4). The upper boundary of unit 2 is an unconformity, found between 17 and 66m below sea-level (Fig. 5.5B) and is represented by a strong, high amplitude reflector. It is present in much of the inner and mid bay but tapers out near the west of the North Sound and is almost entirely missing from the outermost South Sound, where unit 1 is predominant. This unit is characterised by hummocky and chaotic/contorted discontinuous reflectors. This unit ranges from 0.5 to 16m in thickness (Fig. 5.6A), in areas where both the upper and lower boundaries have been identified. The isopach maps of this unit show that deposition is thickest along the southern edge of the North Sound, where the underlying unit is characterised by depressions, while it appears to be a much thinner in the South Sound (Figure 5.5A). It is absent from the acoustic basement highs in the central bay and North and South Sounds.

This unit onlaps the underlying unit 1, while the unit above (unit 3) drapes and infills it. There is also evidence of both diffraction hyperbolae and a channel along the northern coastline (Fig. 5.3). None of the sediment cores in this study penetrate this unit.

5.1.3 Unit 3

Unit 3 is directly below the seabed surface and is the youngest seismic facies. It has much lower amplitude reflectors than the other units and is divided into 2 sub-units, Unit 3a and Unit 3b. Both consist of sediment draped over the underlying unit. Overall unit 3 is up to 14 m thick and it is found across all of the bay, with the exception of the areas in the North Sound where unit 1 is outcropping (Fig. 5.5C & 5.5D).

Sub-unit 3a overlies unit 2 and is the thicker of the sub-units, measuring up to 12.5m in thickness (Fig. 5.6B). It is comprised of low frequency, medium amplitude reflectors. The upper boundary of this unit is found between 18 and 58m below the sea-level (Fig. 5.5C) and is a medium amplitude, continuous reflector in concordance with the overlying strata. The internal structure of this unit is characterised by continuous, wavy, parallel/ sub-parallel to lenticular reflectors (Fig. 5.2, 5.3 & 5.4).

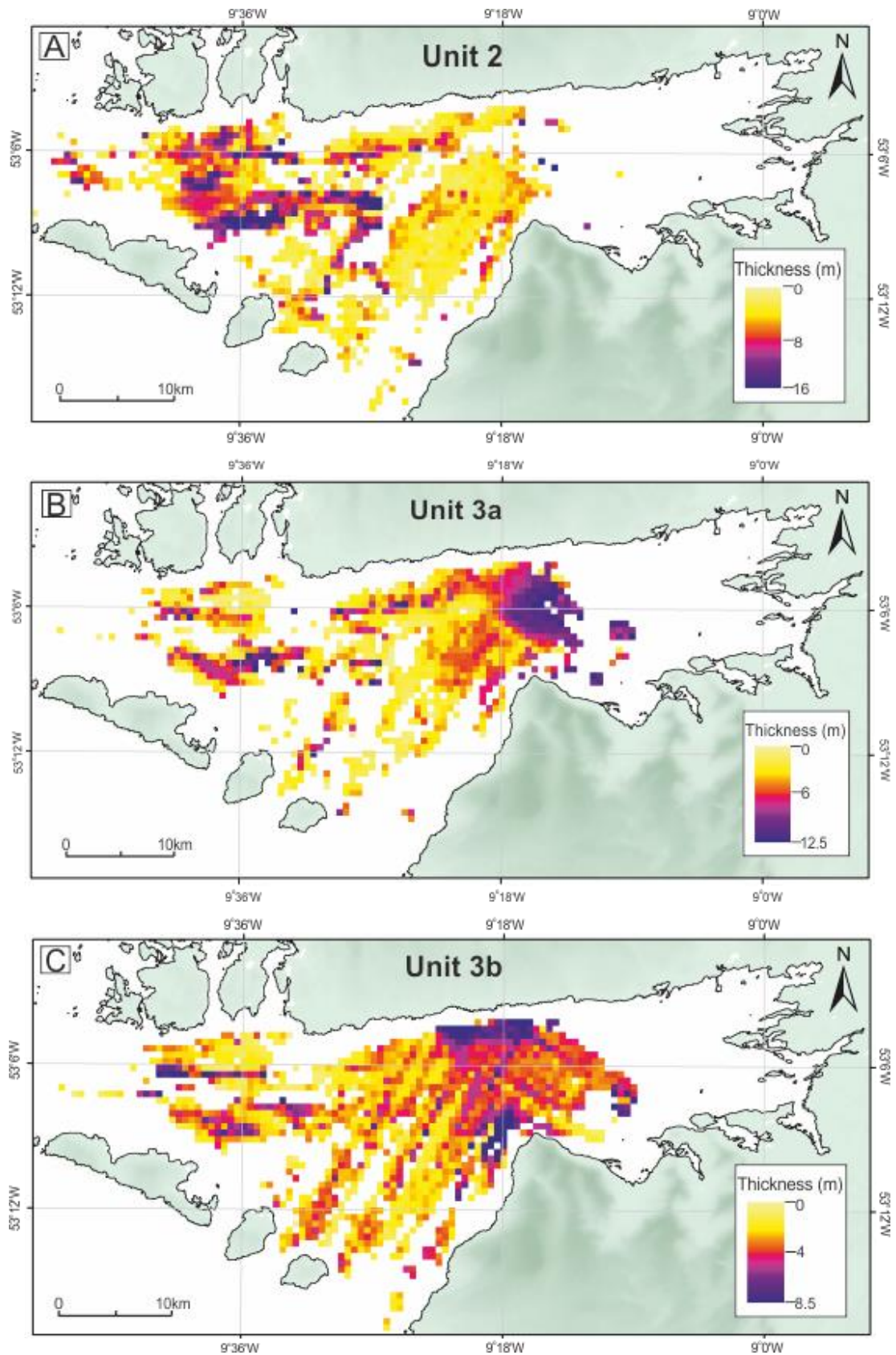


Figure 5.6: Isopach map of (A) unit 2, (B) unit 3a and (C) unit 3b showing the extent and thickness of this unit in the bay.

Based on the isopach map (Fig. 5.6B) this sub-unit is found predominantly in the inner bay area and is absent almost entirely from the South Sound and the outermost North Sound, as well as much of the central bay around the Aran Islands. Sub-unit 3a onlaps the unit below with westward dipping reflectors visible in the inner and mid bay. Sub-unit 3a is infilling the channel cut in unit 2 (Fig. 5.2 & 5.3) and is thickest in this channel, the inner bay and on the southern edge of the North Sound. The thinnest deposition of this unit is in the mid-bay area which is generally <6m. This unit does not cover any of the highs of the basement unit in the bay. None of the sediment cores in this study penetrate sub-unit 3a.

Sub-unit 3b is the thinnest unit in the bay, with a maximum thickness of 8.5m based on the isopach map (Fig. 5.6C). Its upper boundary is between 17 and 77m below sea-level (Fig. 5.5D) and forms the current seafloor in most of the bay, with the exception of some areas in the North and South Sounds where it is not visible in the data (Fig. 5.4 & 5.5), due to outcropping of unit 1. It is characterised by internal reflectors that are mostly continuous, wavy, and parallel to sub-parallel. Sub-unit 3b is composed of lower amplitude and higher frequency reflectors than sub-unit 3a and onlaps onto the unit below. In the mid-bay and into the South Sound, southwest oriented lines show that clinoforms are present. These are prograding in a sigmoid configuration (Fig. 5.4). Sub-unit 3b is found predominantly in the mid and inner bay area and is absent almost entirely from parts of the South Sound and the westernmost North Sound, as well as much of the central bay around the Aran Islands. It drapes the underlying sub-unit 3a and is thickest in the inner and mid bay areas where sub-unit 3a is also present (Fig. 5.6B & 5.6C). All the sediment cores from this study are found within sub-unit 3b.

5.2 Geochronology Results

Radiocarbon dates were obtained from 18 samples across 10 cores, providing dates across 5 of the subsequently identified lithofacies (Table 5.1). As radiocarbon dates, alongside the other analyses, were used to help construct the final lithofacies identification, they were not available across each lithofacies, despite the fact that every attempt was made to date areas with visible changes in the sediment cores. The samples consisted of bivalves, gastropods and mixed benthic foraminifera, particularly

Quinqueloculina spp. Dates are displayed as the mean value of the 95% calibrated age (Table 5.3).

Table 5.1: Radiocarbon dates for each sample, with ages given as a mean value. Labs are indicated as BA: Beta Analytic and CC: Chrono Centre. 95% CA- refers to the calibrated age. PCSU Silt-Coarse Sand refers to Poorly sorted, coarsening upward silt to coarse sand, while CU Sandy mud refers to coarsening upwards sandy mud. All bivalve samples were composed of 1 valve with the exception of those marked *, which were fully intact.

Core	Depth (cm)	Material	Weight (mg)	Lithofacies	Conventional age (years BP)	95% cal (years BP)	Lab
02VC	279-280	Bivalve*	2000	Shell Hash	5270 +/- 30	5588 +/-30	BA
03VC	71	Bivalve	2485	Shell Hash	1400 +/- 30	905 +/-30	BA
03VC	72	Turritella	558	Shell Hash	4070 +/- 30	4054 +/-30	BA
06VC	144-145	Bivalve*	2001	Shell Hash	3890 +/- 30	4304 +/-30	BA
07VC	120-121	Turritella	335	Shell Hash	5850 +/- 30	6230 +/-30	BA
10VC	105	Bivalve	824	PCSU Silt-Coarse Sand	2611 +/-24	2226 +/-24	CC
10VC	126-127	Turritella	1248	Shell Hash	4340 +/- 30	4410 +/-30	BA
10VC	200-201	Turritella	217	Shell Hash	6930 +/- 30	7396 +/-30	BA
12VC	148-152	Bivalve*	3000	Gravelly Sand and Silt	10,300 +/- 40	11,301 +/-40	BA
13VC	100-101	Turritella	1992	Shell Hash	6040 +/- 30	6419 +/-30	BA
13VC	177-179	Bivalve	2117	Silty sand/Sandy silt	9180 +/- 30	9908 +/-30	BA
13VC	235-236	Foram	7	Silty sand/Sandy silt	11,660 +/- 50	13,092 +/-50	BA
17VC	130	Bivalve	710	Gravelly Sand and Silt	8275 +/-45	8772 +/-45	CC
20VC	81-82	Turritella	320	Shell Hash	6760 +/- 30	7264 +/-30	BA
20VC	117-118	Foram	6	Gravelly Sand and Silt	11,140 +/- 80	12,624 +/-80	BA
20VC	124	Bivalve	765	Gravelly Sand and Silt	10587 +/-49	11,720 +/-49	CC
22VC	38-39	Turritella	265	Shell Hash	6390 +/-30	6814 +/-30	BA
22VC	269-270	Foram	4	CU Sandy Mud	9220 +/- 30	9960 +/-30	BA

The results of the radiocarbon dates showed an age range between 13.1 ± 0.05 ka cal BP and 0.9 ± 0.03 ka cal BP. These dates are used to establish a chronology for sediment deposition in the bay. The oldest dates come from a silty sand / sandy silt facies, and

range from 13.1 ± 0.05 ka to 9.9 ± 0.03 ka cal BP. A gravelly sand and silt facies is dated within the range of 12.6 ± 0.08 ka to 8.8 ± 0.045 ka cal BP. A facies of coarsening upward sandy mud, which overlies the previously mentioned gravelly sand and silt facies, has a single foraminifera date of 10 ± 0.03 ka cal BP. A shell hash facies is found across the bay and has a large age range between 7.4 ± 30 ka and 0.9 ± 0.03 ka cal BP. However, with the exception of the single very young age, all dates fall within the age range of 7.4 ± 0.03 ka to 4.1 ± 0.03 ka cal BP. A poorly sorted, coarsening upwards silt to coarse sand facies, which is found in all cores across the bay, has a single date in core 10VC of 2.2 ± 0.024 ka cal BP. In core 20VC, shell and foraminifera samples, both taken in gravelly sand and silt, only 6cm apart, returned results of a 900-year difference and were out of sequence. The youngest shell date (11.7 ± 0.049 ka cal BP) fell lower in the sample than the older foraminifera date (12.6 ± 0.08 ka cal BP). Caution was used with this latter date.



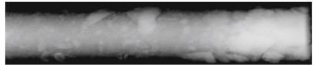













5.3 Lithofacies and geochemical results

On the basis of radiocarbon dates, grain size, lithology, colour, sedimentary structures physical properties, shear strength, biological content and geochemistry, 8 distinct lithofacies were identified in the sediment cores (Table 5.2, Appendix 1&2). These lithofacies include:

- LF1: Mud with occasional laminations;
- LF2: Gravelly sand and silt;
- LF3: Silty sand / sandy silt;
- LF4: Coarsening upwards sandy mud;
- LF5: Shell hash;
- LF 6: Interbedded sandy silt and silty sand;
- LF7: Silty sand;
- LF8: Poorly sorted, coarsening upwards silt to coarse sand.

A more detailed description of each lithofacies is given in the following sections. For each lithofacies, the sedimentology, microfossil content and geochemical signal (with a focus on the elements and ratios Ca, S, Si/Ti, Ba/Ca, Br/Cl, Sr/Ba, Sr/Ti, Sr/Ca, and Fe/Ti) are outlined.

Table 5.2: A lithofacies classification, with x-ray images, core photographs and descriptions. See Appendix 4 for raw data ranges of sediment core

Lithofacies	X-Ray Image	Photograph	Sediment Description	Foraminifera Description	Geochemical Description
1 - Mud with occasional laminations	 4cm	 4cm	Laminated mud with very sparse shell fragments	Dominated by <i>Quinqueloculina</i> spp, <i>Lagena</i> spp, <i>Milliolinella subrotunda</i> and <i>Spirillina vivipara</i>	Low Ca/Ti, S/Ti and Si/Ti, increasing upcore. High Ba/Ca and Sr/Ca, decreasing upcore
2 - Gravelly silt and sand	 4cm	 4cm	Gravel of various clast sizes, most commonly granules and pebbles in a sand or silt matrix	Dominated by <i>Textularia</i> spp, <i>Quinqueloculina</i> spp, <i>Sahulina conica</i> and <i>Milliolinella subrotunda</i>	Low Br/Cl and Sr/Ba. High Si/Ti and Ba/Ca
3 - Silty sand / Sandy silt	 4cm	 4cm	Sandy silt and silty sand with shell fragments	Dominated by <i>Quinqueloculina</i> spp, <i>Ammonia beccarii</i> and <i>Haynesina germanica</i>	Low Ca/Ti, Sr/Ba and Br/Cl. High Ba/Ca
4 - Coarsening upward sandy mud	 4cm	 4cm	Sandy, silty mud coarsening upwards, with sparse shell fragments	Dominated by <i>Lagena</i> spp, <i>Stainforthia fusiformis</i> , <i>Nonionella turgida</i> and <i>Bolivina</i> spp	Low Ca/Ti, S/Ti, Br/Cl, Sr/Ba and Si/Ti. High Ba/Ca
5 - Shell hash	 4cm	 4cm	Intact gastropods and bivalve shells in a compact layer	Dominated by <i>Quinqueloculina</i> spp and <i>Haynesina germanica</i>	Low S/Ti. High peaks of Ca/Ti. Decreasing trends of Ba/Ca. Increasing trends of Br/Cl and Sr/Ba
6 - Interbedded sandy silt and silty sand	 4cm	 4cm	Laminated sandy silt and silty sand with extensive bioturbation and abundant shell fragments shell	Dominated by <i>Rosalina praegeri</i> , <i>Quinqueloculina</i> spp, <i>Ammonia beccarii</i> , <i>Spirillina vivipara</i> and <i>Elphidium excavatum</i>	Low Ca/Ti and Fe/Ti. High Si/Ti and S/Ti. Increasing Br/Cl and Sr/Ba upcore. Decreasing Ba/Ca upcore
7 - Silty sand	 4cm	 4cm	Silty sand with shell fragments	Dominated by <i>Ammonia beccarii</i> , <i>Quinqueloculina</i> spp, and <i>Haynesina germanica</i> .	Low Sr/Ba. High Si/Ti and Ba/Ca. Increasing Ca/Ti. Decreasing Fe/Ti.
8 - Poorly sorted, coarsening upwards silt to coarse sand	 4cm	 4cm	Silty fine to coarse sand coarsening upwards with abundant shell fragments	Dominated by <i>Quinqueloculina</i> spp, <i>Lagena</i> spp, <i>Cibicides lobatulus</i> , <i>Ammonia beccarii</i> and <i>Planorbulina mediterraneensis</i>	Low Ba/Ca. High Br/Cl. Increasing Sr/Ba, Sr/Ca. Variable Ca/Ti, S/Ti Fe/Ti and Si/Ti.

5.3.1 Lithofacies 1 – Mud with occasional laminations

a) Sedimentology

This lithofacies is a silty mud, dark grey in colour and has almost no visible biogenic content, with only a few shell small fragments near the base of the facies (Fig. 5.7). This facies is only found at the base of core 03VC, located in the South Sound area of the mid bay (Fig. 5.24). This facies is 60cm thick and at the bottom of the core, parallel laminations and layers are visible in the x-rays (Table 5.2). P-wave velocity, wet bulk density, magnetic susceptibility and electrical resistivity range from 1650 to 1730m/s, 1.9 to 2.3g/cm³, 3.6 to 3.7 SI*10⁻⁸m³/kg and 2.7 to 3.2Ω.m respectively and show increasing trends upcore. Shear strength measurements in this facies are 24 and 49kPa, with the highest value of 49kPa at 200cm downcore and the lowest value of 24kPa at 220cm downcore (Fig. 5.7). The facies forms the base of the core and has a gradual boundary with the overlying facies 3.

b) Foraminifera analysis

Lithofacies 1 was sampled in core 03VC at 227-228cm. It is dominated by *Quinqueloculina spp.*, *Lagena spp.*, *Miliolinella subrotunda*, and *Spirillina vivipara*. In lesser numbers *Haynesina germanica*, *Bulimina marginata* and *Stainforthia fusiformis* are also present (Table 5.3). These species are quite large, especially specimens of *Quinqueloculina spp.*, and are intact, however they are much sparser than in the overlying facies (Appendix 2).

c) Chemical analysis

Ca/Ti, S/Ti and Si/Ti content in this facies is the lowest in the core, and all have an increasing trend upcore (Fig. 5.8). Ba/Ca and Sr/Ca levels are highest in this facies of the core and have a decreasing trend upcore, with small peaks and dips evident throughout the facies. Br/Cl, Sr/Ba and Fe/Ti ratios all show a relatively constant or slightly decreasing trend up facies, with small peaks and dips throughout (Fig. 5.8). The upper boundary shows a gradual transition in most elements with a minor drop in Ca/Ti, S/Ti and Si/Ti near the boundary

Table 5.3: A foraminifera species table, with primarily marine species coloured in blue, estuarine species in green and brackish species in yellow. Species with more than one colour are found in different environments. The large red X represents a dominant species, estimated to have higher than 15% per sample, while the small black x represents a minor species, estimated to have less than 5% per sample (See Appendix 2 for details of numbers of foraminifera counted and references used for optima and tolerance ranges).

	<i>Lagena</i> spp	<i>Textularia</i> spp	<i>Sahulia conica</i>	<i>Bulimina marginata</i>	<i>Nonionella turgida</i>	<i>Fissurina elliptica</i>	<i>Oolina Williamsoni</i>	<i>Planorbulina mediterraneensis</i>	<i>Stainforthia fusiformis</i>	<i>Spirillina vivipara</i>	<i>Cibicides lobatulus</i>	<i>Bolivina</i> spp	<i>Quinqueloculina</i> spp	<i>Planorbulina distoma</i>	<i>Miliolinella subrotunda</i>	<i>Rosalina globularis</i>	<i>Rosalina praegeri</i>	<i>Elphidium excavatum</i>	<i>Ammonia beccarii</i>	<i>Haynesina germanica</i>	<i>Jadammina macrescens</i>	
LF 1	X			x					x	X			X		X						x	
LF 2		X	X					x			x		X		X	x					x	
LF 3		x		x	x		x	x			x		X		x	x	x	x	X	X	x	
LF 4	X				X				X			X	x				x					
LF 5	x	x		x			x			x	x		X				x	x			X	
LF 6										X			X	x			X	X	X	X	x	
LF 7													X				x	x	X	X		
LF 8	X	x		x	x	x	x	X			X	x	X				x		X	x		

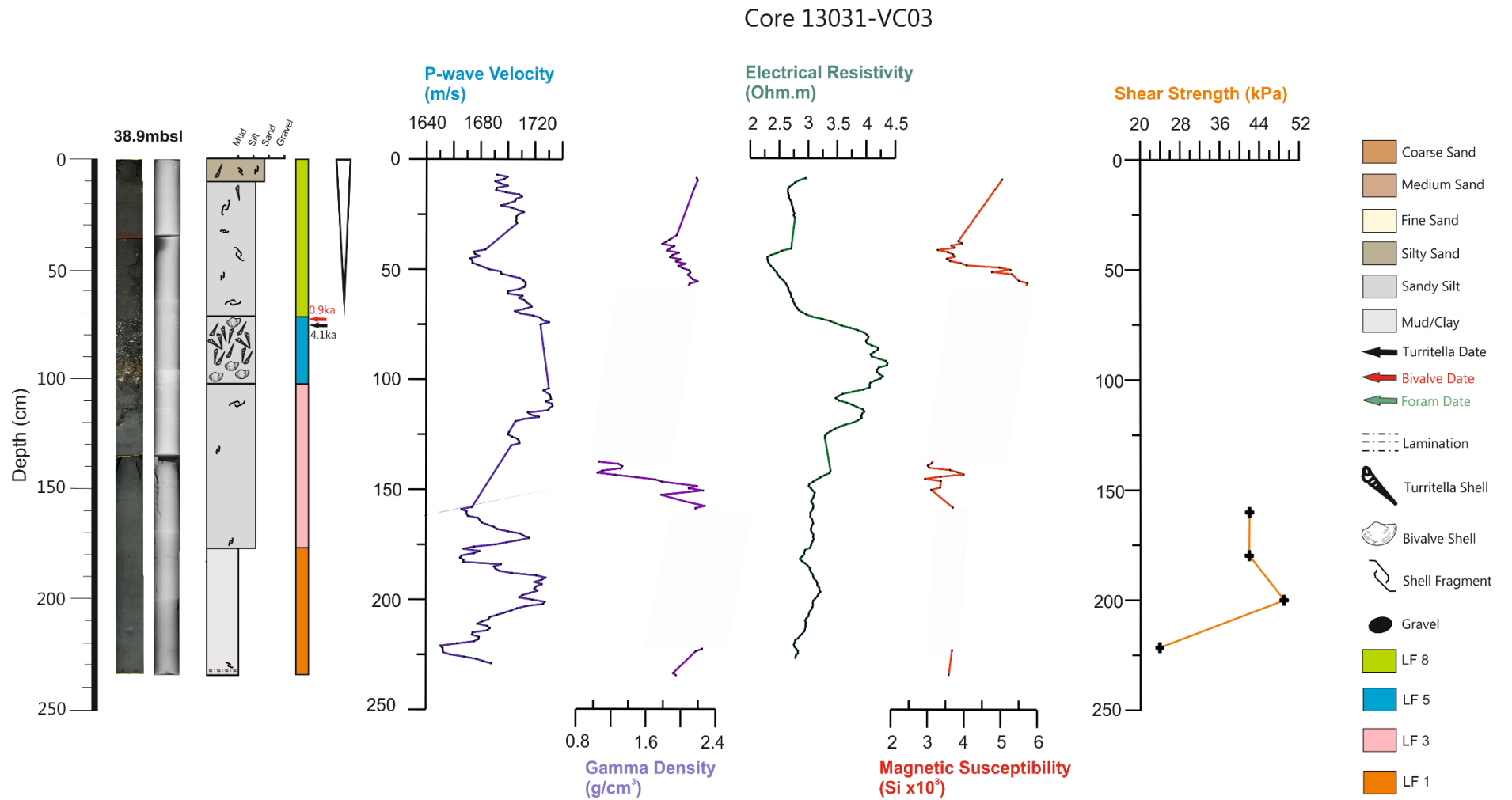


Figure 5.7: A graph of core 03VC showing a core image, an x-ray image, a core log, MSCL measurements and shear strength values.

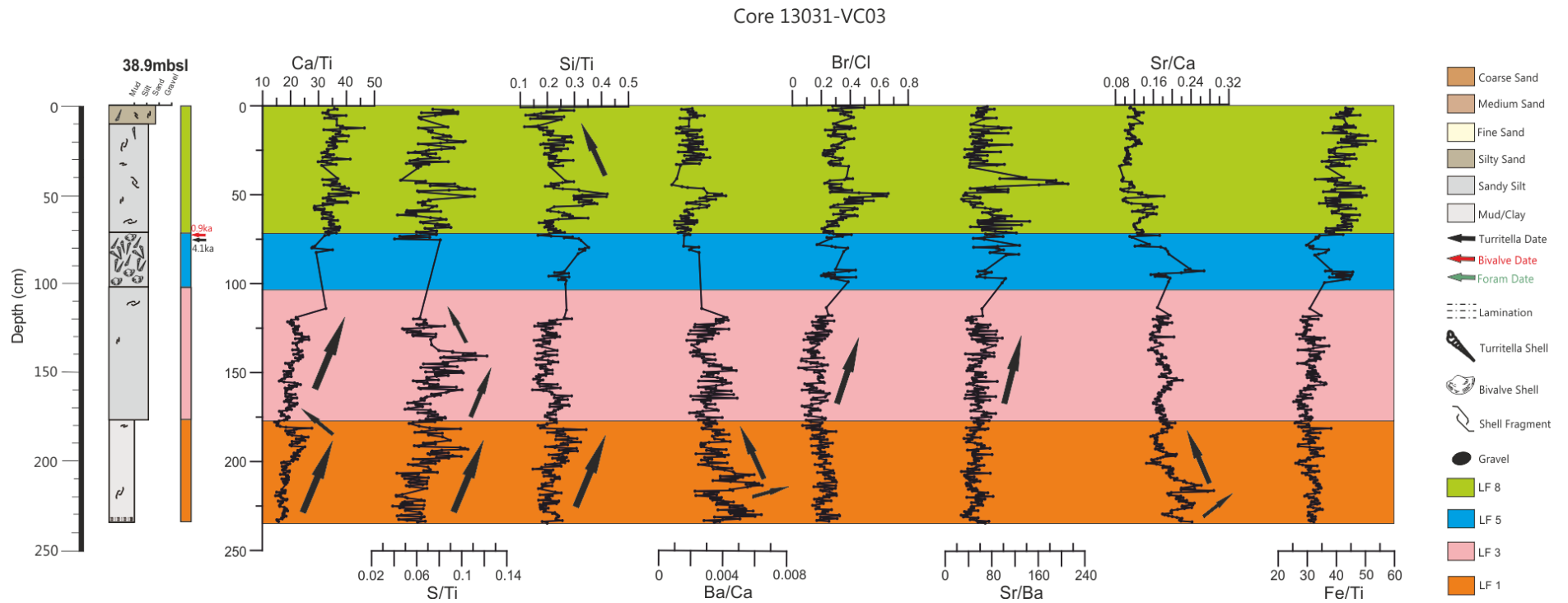


Figure 5.8: A graph showing the ITRAX analysis for core 03VC, with LF 1 at the base of the core. The data are presented at a resolution of 5mm and the large black arrows next to the chemical data represent general trends.

5.3.2 Lithofacies 2 – Gravelly sand and silt

a) Sedimentology

This lithofacies is characterised by gravel of various clast sizes (granules, pebbles and cobbles) in a matrix of medium sand and silt with no visible grading (Fig. 5.12). The gravel is generally <6cm in diameter, however in core 12VC the cobbles reach up to 11cm. These pebbles and cobbles are composed of granite and limestone respectively. This lithofacies is dark grey-dark greenish grey in colour and is found at the base of cores 07VC, 12VC, 17VC and 20VC, in the outer bay areas in both the north and south of the bay (Fig. 5.24). Shell fragments and intact shells, generally bivalves, are found throughout this facies. P-wave velocity and electrical resistivity were obtained for core 07VC as this was the only core over 2m in length (Fig. 5.10). P-wave velocity ranges from 1800 to 1880m/s, while electrical resistivity ranges from 4 to 5.3 Ω .m, with both showing a decreasing trend upcore. Shear strength measurements were taken from one core (17VC) at 126cm and 136cm downcore, where the matrix was less sandy, with measurements of 10 and 25kPa respectively. This lithofacies is between 20 and 67cm thick and typically has an erosional upper contact with the overlying lithofacies 5, with the exception of 17VC, where the upper contact is more gradual transitioning into lithofacies 4.

b) Foraminifera analysis

In Lithofacies 2, cores 17VC and 07VC were selected to investigate the foraminifera assemblages. Samples were collected at 139-140cm, 117-118cm and at 82-83cm in core 17VC and at 201-204cm in core 07VC. *Textularia spp.*, *Quinqueloculina spp.*, *Sahulia conica*, and *Miliolinella subrotunda* (Fig. 5.9) were found to be by far the most dominant species in this interval, although smaller numbers of *Rosalina globularis*, *Planorbulina mediterraneensis*, *Haynesina germanica* and *Cibicides lobatulus* were also present (Table 5.3). This facies appears to have the highest number of broken foraminifera tests overall, with the majority of these being *Quinqueloculina spp.*, located near the base of the facies (Appendix 2).

c) Chemical analysis

Chemical analysis was carried out on all cores that contained Lithofacies 2. Ca/Ti content in this facies is quite low in all cores. There is a constant to slightly increasing trend

upcore in this facies, and peaks are visible throughout. S/Ti content is generally low, however there is variability in the trends between cores. Core 07VC shows a steady increase upcore (Fig. 5.11), core 12VC shows a constant upcore trend, while cores 17VC and 20VC have a decreasing trend upcore with large dips evident at the base and mid-facies point, something which is more pronounced in core 20VC. The Si/Ti counts are the highest in this facies in all cores, with a decreasing trend upcore and several large peaks throughout. The Ba/Ca ratio in this facies is the highest in all 4 cores and shows a decreasing trend upcore. In all cores, peaks and dips are visible within this facies, in particular, cores 07VC and 12VC show sharp decreases, followed by an increase in content upcore (Fig. 5.11). The Br/Cl and Sr/Ba ratios in these cores show this facies to have the lowest counts and all cores show an increasing trend upcore. The Sr/Ca ratios in this facies show a variable trend upcore, while the Fe/Ti content shows a more constant to increasing trend overall with smaller peaks and dips visible.

The upper boundary with both LF4 and LF5 is gradual with only minor changes in some elements.

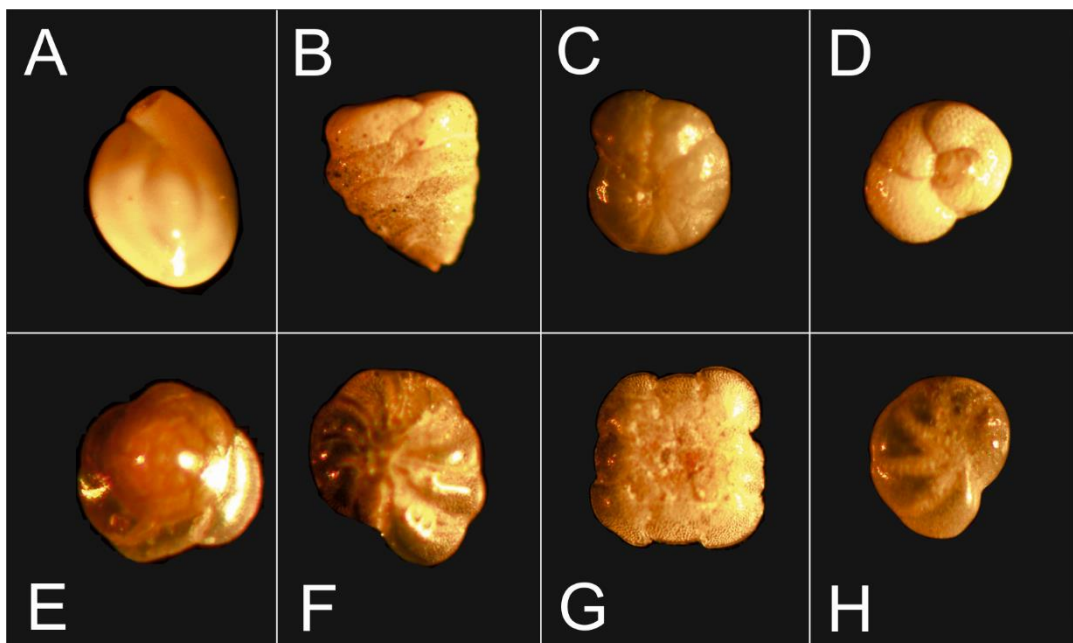


Figure 5.9: Examples of foraminifera species found in Galway Bay. A) *Quinqueloculina* sp., B) *Textularia* sp., C) *Elphidium excavatum*., D) *Rosalina globularis*, E) *Rosalina praegeri*, F) *Cibicides lobatulus*, G) *Planorbulina mediterraneensis*, and H) *Elphidium williamsoni*. These species were used for both qualitative analysis of marine environments and radiocarbon dating

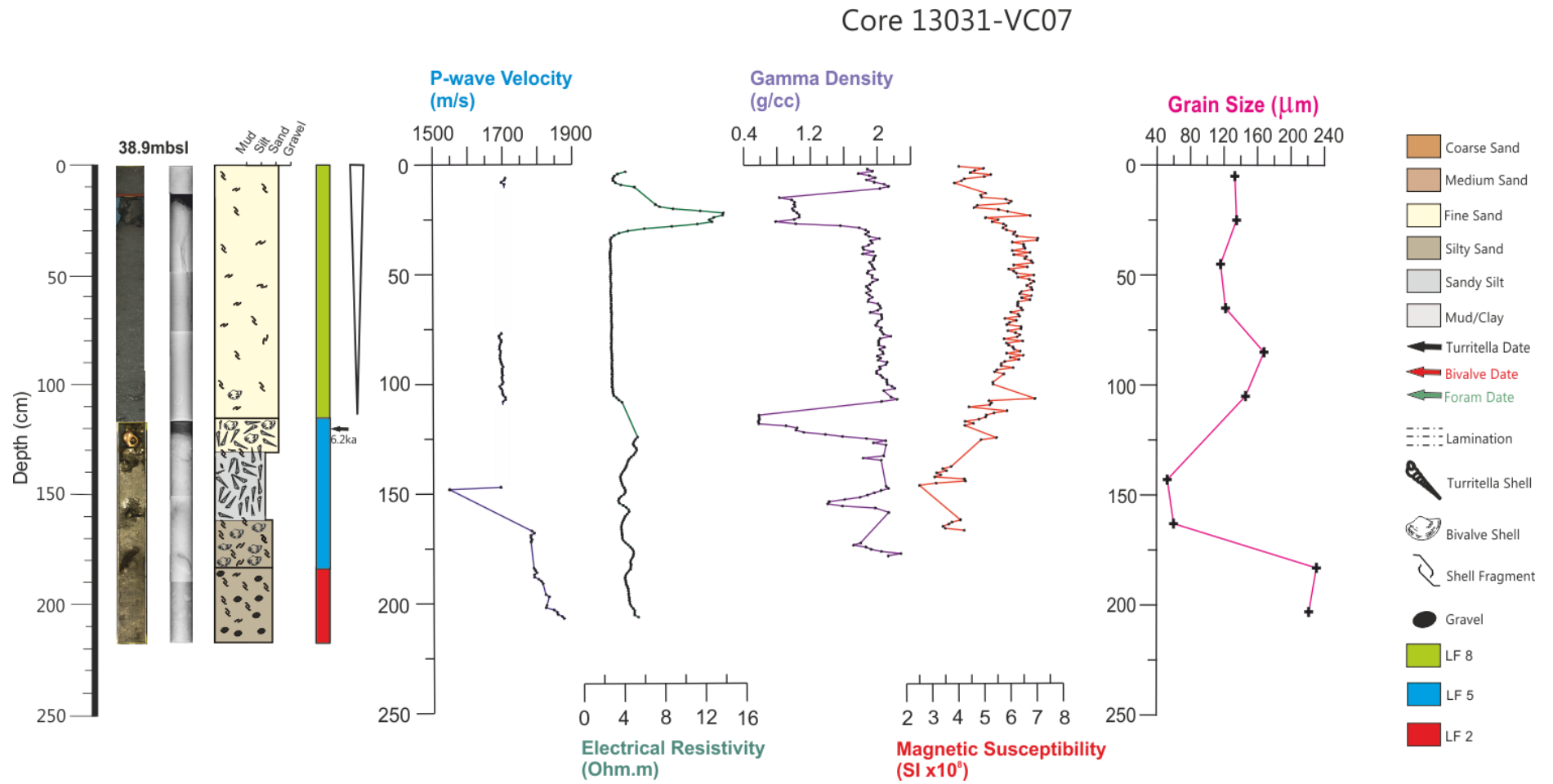


Figure 5.10: A graph of core 07VC showing a core image, an x-ray image, a core log, MSCL measurements and grain size values for LF2.

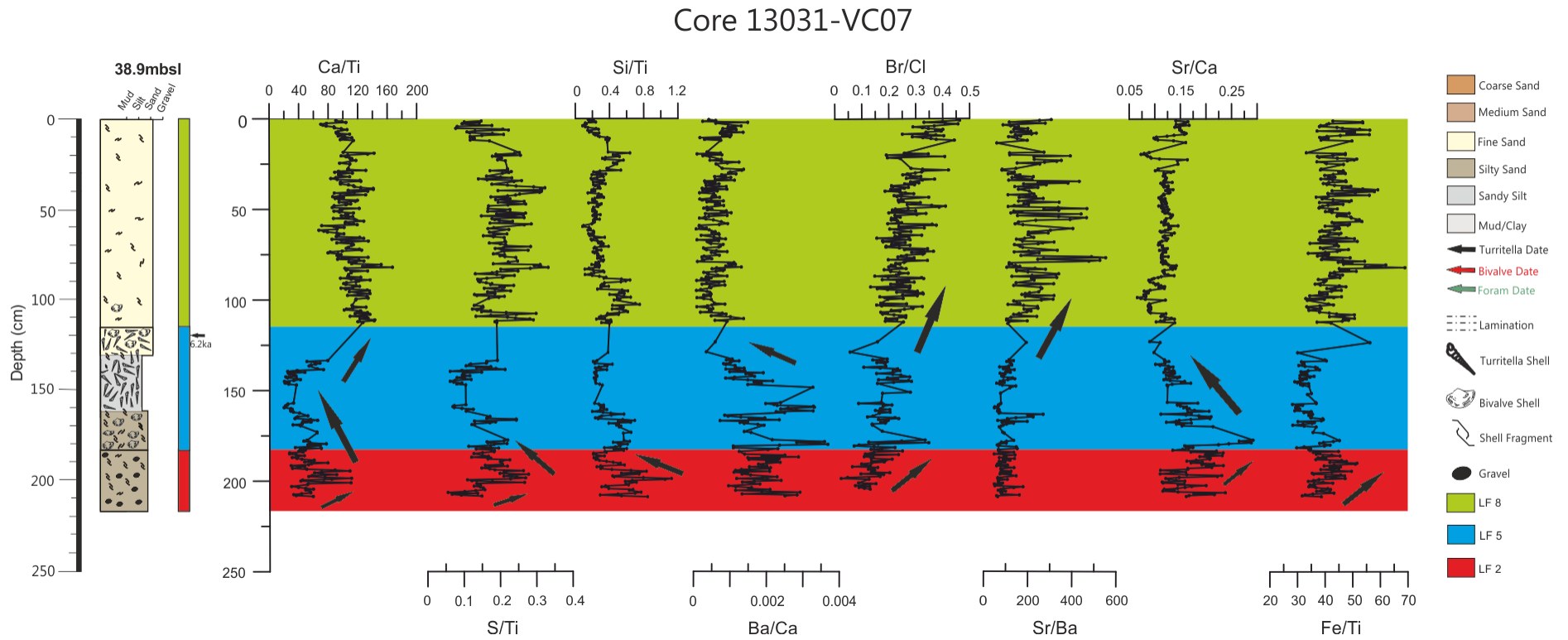


Figure 5.11: A graph showing the ITRAX analysis for core 07VC, showing LF 2 at the base of the core. The data are presented at a resolution of 5mm and the large black arrows next to the chemical data represent general trends.

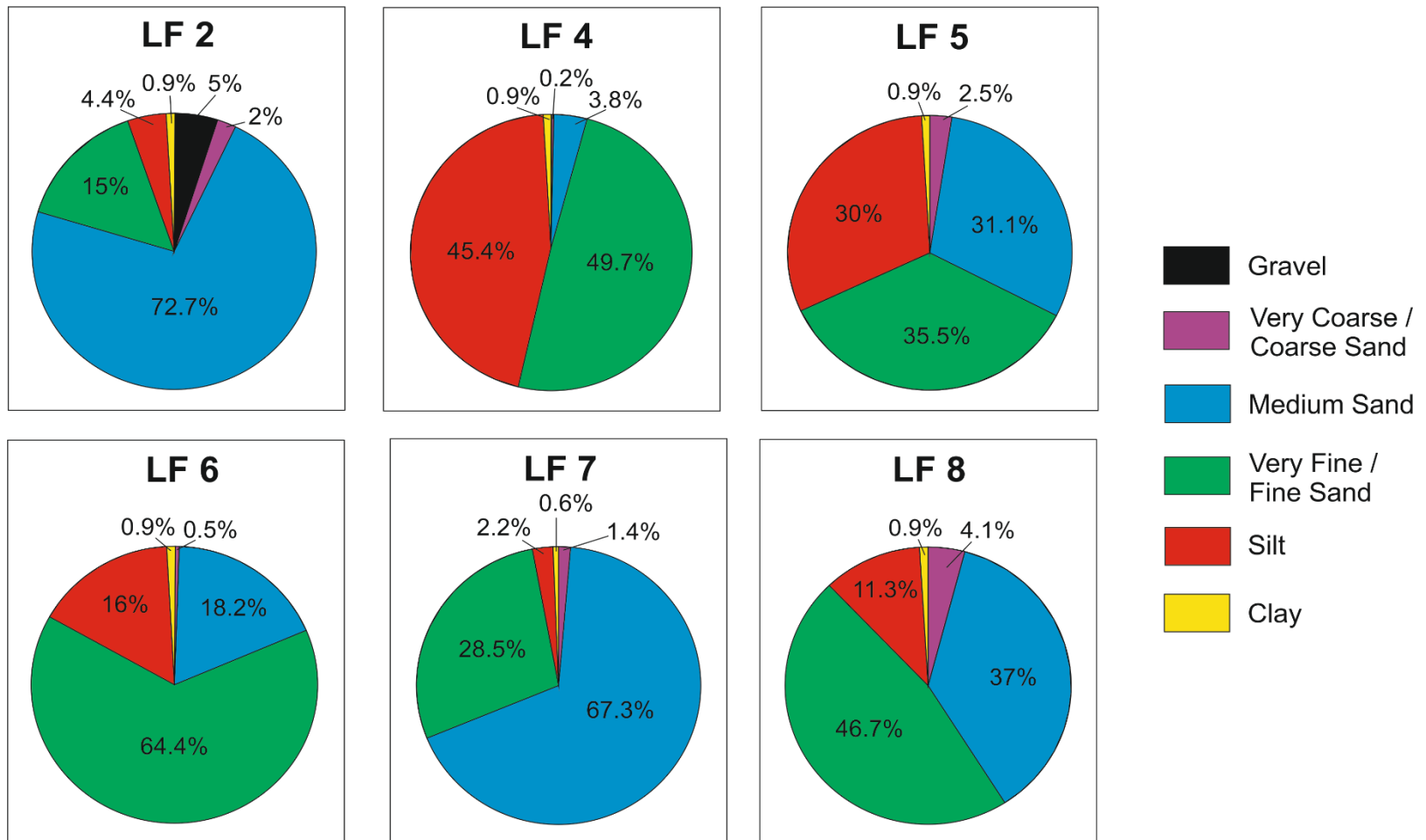


Figure 5.12: Charts showing the overall grainsizes for each facies. This was done by combining all grainsize measurements taken within a particular facies to find the average composition. No grainsize samples were taken in LF1 or LF3, so no measurements are available for these lithofacies.

5.3.3 Lithofacies 3 – Silty sand / sandy silt

a) Sedimentology

This lithofacies is silty sand and sandy silt, dark grey in colour and its biogenic content includes both intact shells, particularly bivalves such as cockles, shell fragments and microfossils such as foraminifera and ostracods. It is found in cores, 03VC, 10VC, 13VC and 14VC (Fig. 5.24) and the thickness of this facies ranges from 22cm in core 10VC to 127cm in core 13VC (Fig. 5.13). P-wave velocity generally ranges from 1645 to 1790m/s, with a sharp peak reaching 1975m/s in core 13VC (Fig. 5.12). Electrical resistivity, magnetic susceptibility and wet bulk density range from 2.75 to 4.4Ω.m, 2.6 to 5 SI*10⁻⁸m³/kg and 0.75 to 2.3g/cm³ respectively. Shear strength measurements in this lithofacies range from 23 to 42kPa. This facies has a sharp upper contact in all cores, with LF5, except 14VC, where a more gradual contact is evident. When it does not form the base of the core, as in core 03VC, a gradual lower contact is also visible with lithofacies 1 (Fig. 5.7).

b) Foraminifera analysis

For Lithofacies 3, cores 13VC and 14VC were selected for foraminifera sampling at 234-235cm, 116-117cm and 278-279cm respectively. The dominant species are *Quinqueloculina spp.*, *Ammonia beccarii* and *Haynesina germanica*. Also present in smaller numbers are *Oolina williamsoni*, *Elphidium excavatum*, *Textularia spp.*, *Rosalina globularis*, *Bulimina marginata*, *Planorbulina mediterraneensis*, *Rosalina praegeri*, *Miliolinella subrotunda*, *Cibicides lobatulus*, *Jadammina macrescens* and *Nonionella turgida* (Table 5.3 & Fig. 5.9). There is an increase in the size and abundance of *Quinqueloculina spp.*, *Haynesina germanica* and *Ammonia beccarii* up core. *Lagena spp.* are absent from the bottom of this lithofacies but increase in abundance up core, while *Elphidium excavatum* and *Nonionella turgida* are present at the bottom of this lithofacies but decrease upcore. Overall there is a trend of increasing diversity in foraminifera up core in this lithofacies, and specimens are relatively intact (Appendix 2).

c) Chemical analysis

Chemical analysis for this lithofacies was carried out on 4 cores (03VC, 10VC, 13VC and 14VC). However, data were not recovered from this lithofacies in core 10VC due to the

presence of extensive biogenic content at the core surface, making the surface extremely uneven and very difficult for the ITRAX core scanner to scan it.

Ca/Ti content is the lowest in this facies in all cores. In cores 03VC and 14VC there is an increasing trend in the Ca/Ti content upcore, however in core 13VC a decreasing trend is evident until 175cm and then the Ca/Ti content shows a slight increasing trend from 175cm to the top of the facies. S/Ti content in this facies shows an overall decreasing trend, with large peaks in cores 03VC and 13VC. Si/Ti content shows a stepped trend with a lower content at the base of the cores and a sharp increase in content upcore. The Ba/Ca ratios are high in all cores, with only lithofacies 1 in core 03VC showing higher counts, compared to this facies (Fig. 5.8). An overall decreasing trend is evident upcore, however in core 14VC there is a decrease to the middle of the facies before a steady rise towards the facies top. Smaller peaks and dips are visible in all cores throughout this facies. The Br/Cl ratios in this facies are the lowest of all lithofacies in these cores, with a steadily increasing trend upcore. The Sr/Ba ratios in this facies have low counts in all cores, an overall slightly increasing trend upcore and small peaks and dips visible throughout. The Sr/Ca ratios in this facies shows an overall slightly decreasing trend upcore, with large peaks visible in all cores. The Fe/Ti content in this facies shows a relatively constant trend upcore however, peaks are evident throughout (Fig. 5.14). Overall the lower boundary between lithofacies 3 and underlying lithofacies 1 is gradual with only small changes visible in the Ca/Ti, S/Ti and Si/Ti contents (Fig. 5.8). The upper boundary of this unit with overlying lithofacies 5 is gradual, with no clear elemental changes.

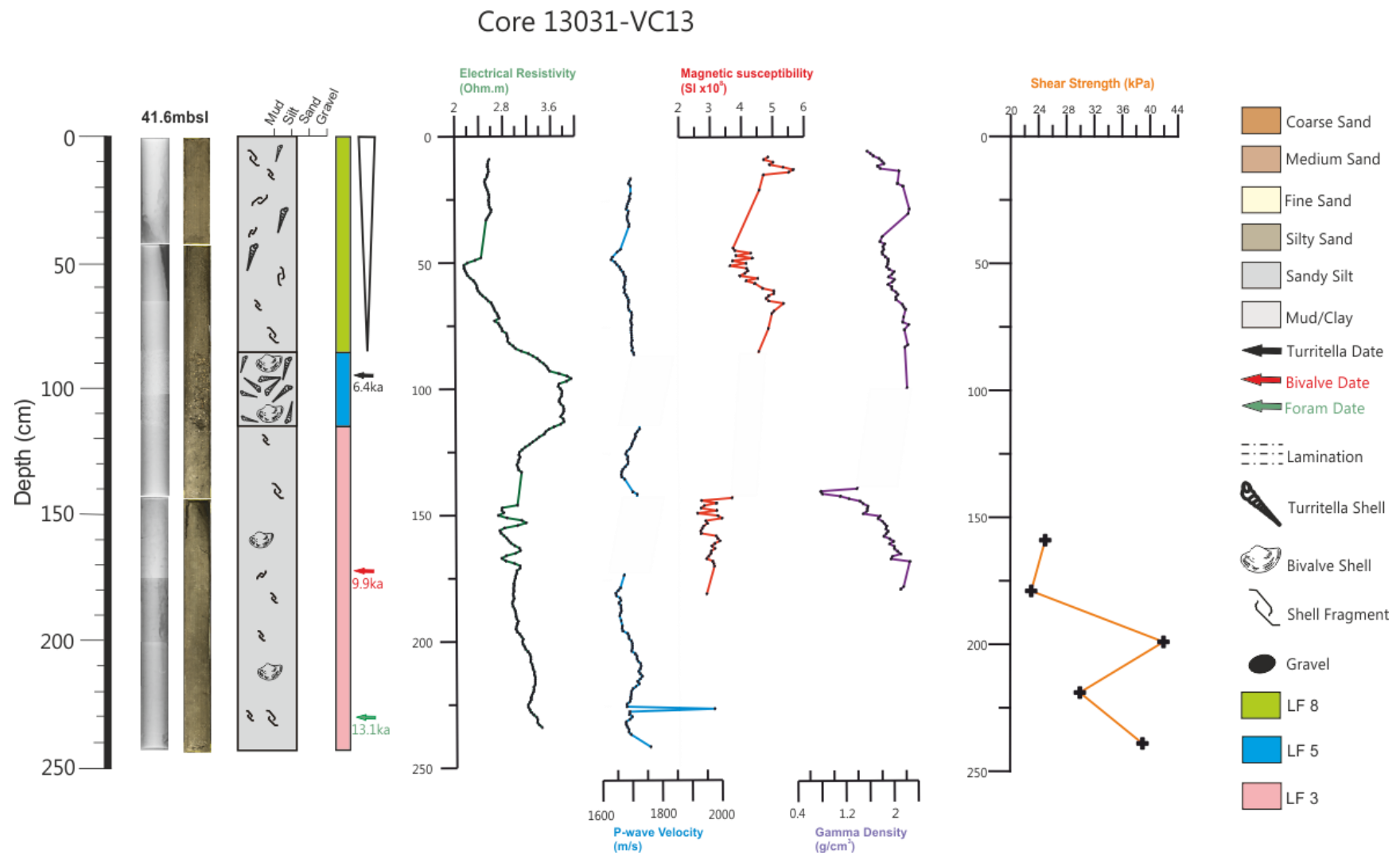


Figure 5.13: A graph of core 13VC showing a core image, an x-ray image, a core log, MSCL measurements and shear strength values.

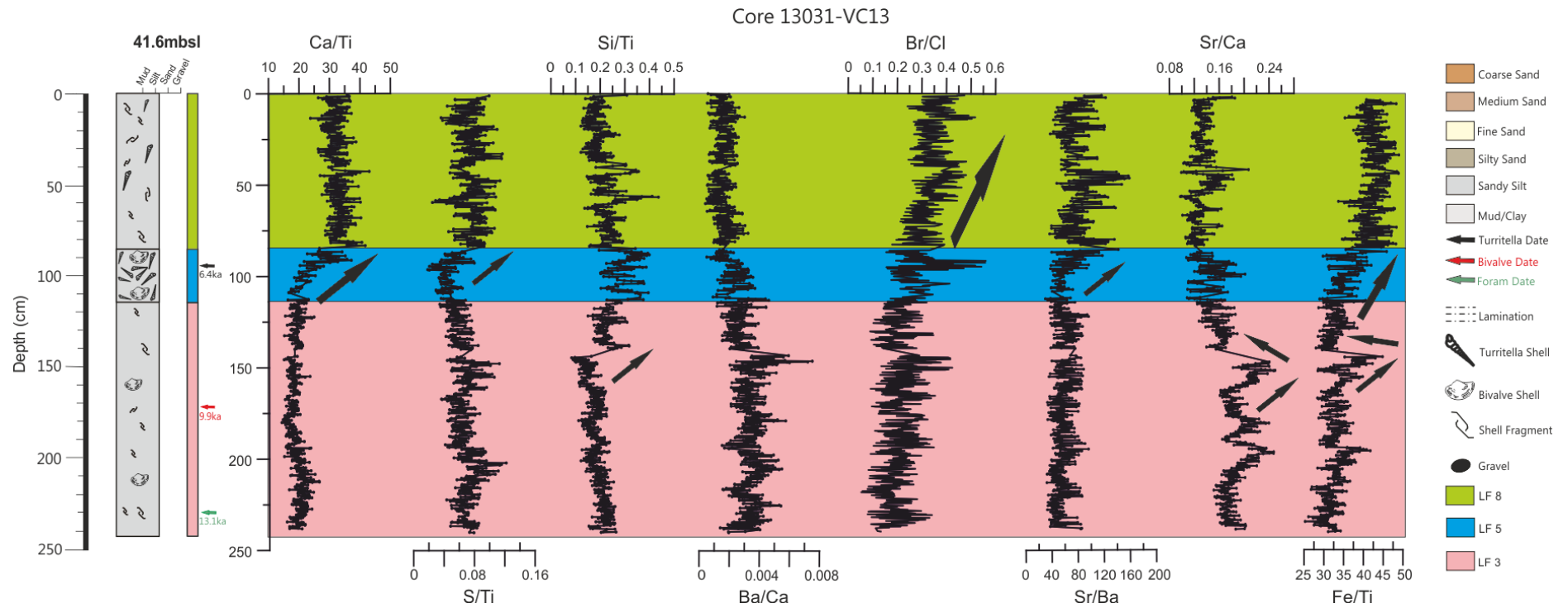


Figure 5.14: A graph showing the ITRAX analysis for core 13VC, showing LF3 at the base of the core. The data are presented as a rolling average at a resolution of 5mm and the large black arrows next to the chemical data represent general trends.

5.3.4 Lithofacies 4 – Coarsening upwards sandy mud

a) Sedimentology

This lithofacies is found in 4 cores, 01GC, 17VC, 18VC and 22VC (Fig. 5.25), and is characterised by coarsening upwards sandy mud (Fig. 5.12). It is very dark grey to dark greenish grey in colour, has sparse biogenic content, with some small intact shells. The only sedimentary structures in this lithofacies are thin parallel laminations (~0.1cm thick), found near the core bottom in 01GC and visible only on the x-rays. This facies is found only in the North Sound area and is missing entirely from the central bay and South Sound area (Fig. 5.24). P-wave velocity, electrical resistivity, magnetic susceptibility and wet bulk density range from 1570 to 1645m/s, 2.2 to 3.2Ω.m, 1 to 4 SI*10⁻⁸m³/kg, and 1.58 to 2.3g/cm³ respectively, across all cores (Fig. 5.15). P-wave velocity, electrical resistivity and wet bulk density show a decreasing trend upcore, while magnetic susceptibility shows an increasing trend upcore. Shear strength measurements in this lithofacies range from 4 to 25kPa, with a generally decreasing trend upcore, with the exception of core 22VC (Fig. 5.16), which is more variable. The lowest shear strength is found in core 18VC, where a sharp decrease to 4kPa is visible mid-facies (Appendix 1). This facies forms the base of all the cores it is found in, with the exception of core 17VC. In core 17VC it overlies lithofacies 2 with a gradual lower contact. This facies is highly variable in thickness, ranging from 28cm in core 17VC to 235cm in core 18VC and has a sharp erosional upper contact in all cores (Fig. 5.15).

b) Foraminifera analysis

Lithofacies 4 was sampled in core 01GC at 99-100cm, in core 22VC at 269-270cm and 150-151cm in sandy mud. The dominant species are *Lagena spp.*, *Stainforthia fusiformis*, *Nonionella turgida* and *Bolivina spp.* Other species, such as *Rosalina praegeri* and *Quinqueloculina spp.* were present in smaller numbers (Table 5.3). *Lagena spp.* shows a decreasing trend downcore. Specimens in this facies were intact (Appendix 2).

c) Chemical analysis

Chemical analysis was carried out on 4 cores that contained Lithofacies 4 (01GC, 17VC, 18VC and 22VC).

Ca/Ti, S/Ti and Si/Ti content in this facies is low in all 4 cores and shows a constant or increasing trend upcore, with small peaks and dips throughout. Ba/Ca ratios are high, with a constant or decreasing trend upcore and some small peaks and dips throughout. Br/Cl and Sr/Ba ratios are low, generally showing a constant to increasing trend upcore, with small peaks and dips evident throughout the facies. Sr/Ca content in this facies shows an overall decreasing trend upcore with large peaks throughout. However, in cores 01GC and 17VC, there is only a decreasing trend to the mid-facies point before the content begins to show an increasing trend. Fe/Ti shows a constant to slightly increasing trend upcore in this facies.

Overall, the lower boundary between lithofacies 4 and underlying lithofacies 2 is relatively gradual with only minor changes in elemental ratios. The upper boundary with overlying lithofacies 5, however, is sharp, with significant changes in the chemistry across a number of elements.

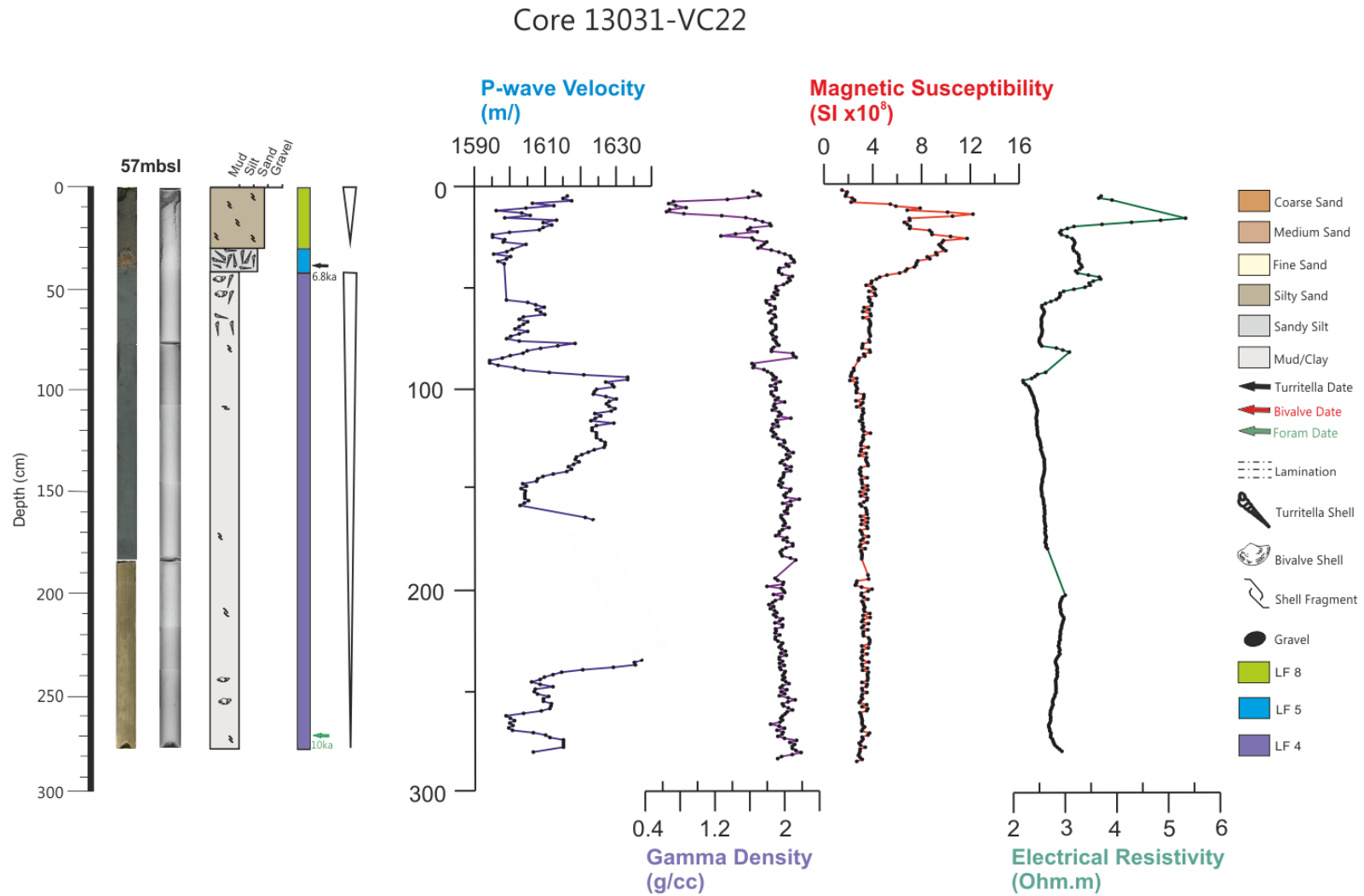


Figure 5.15: A graph of core 22VC showing a core image, an x-ray image, a core log and MSCL measurements.

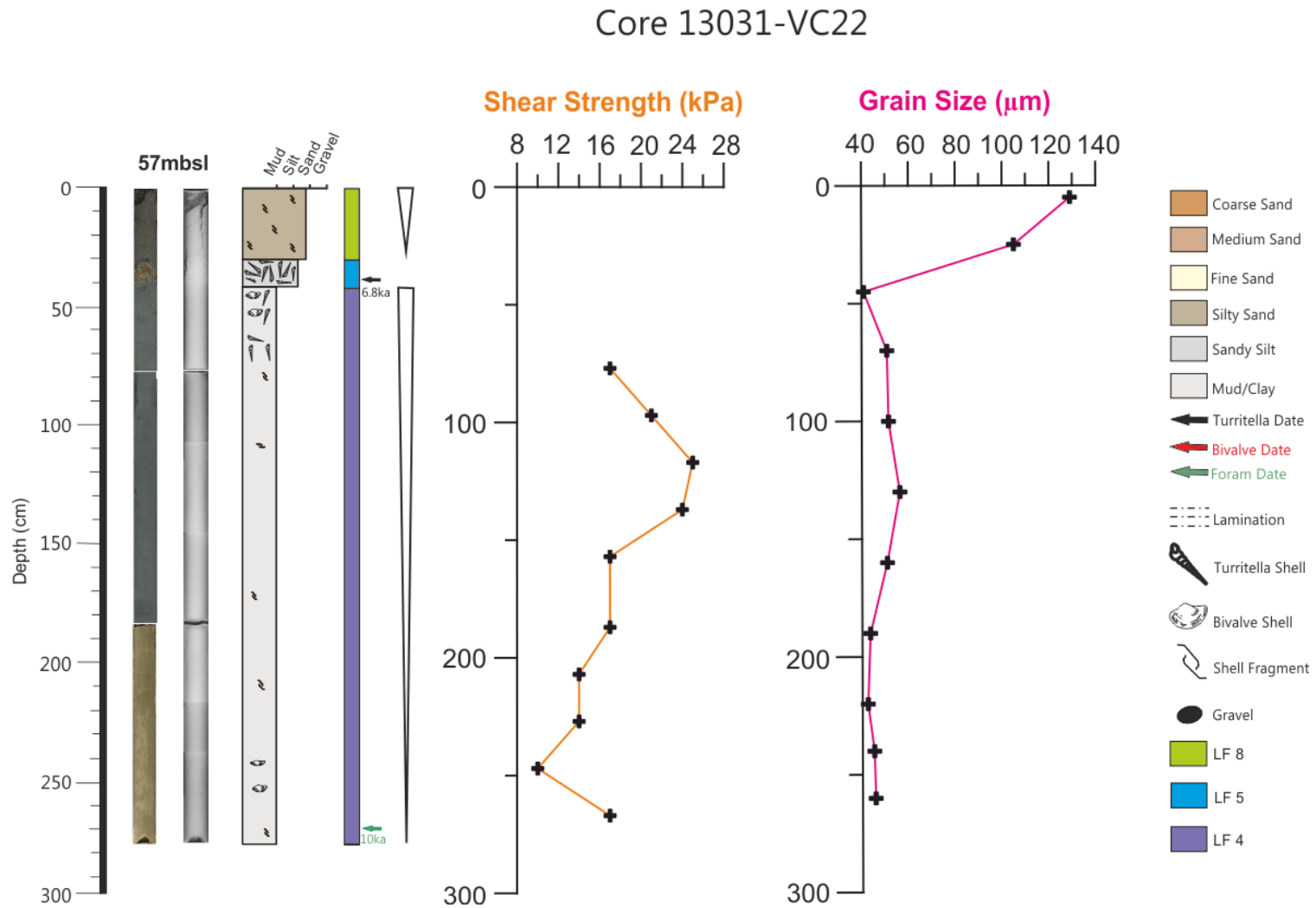


Figure 5.16: A graph of core 22VC showing a core image, an x-ray image, a core log, shear strength values and grain size measurements.

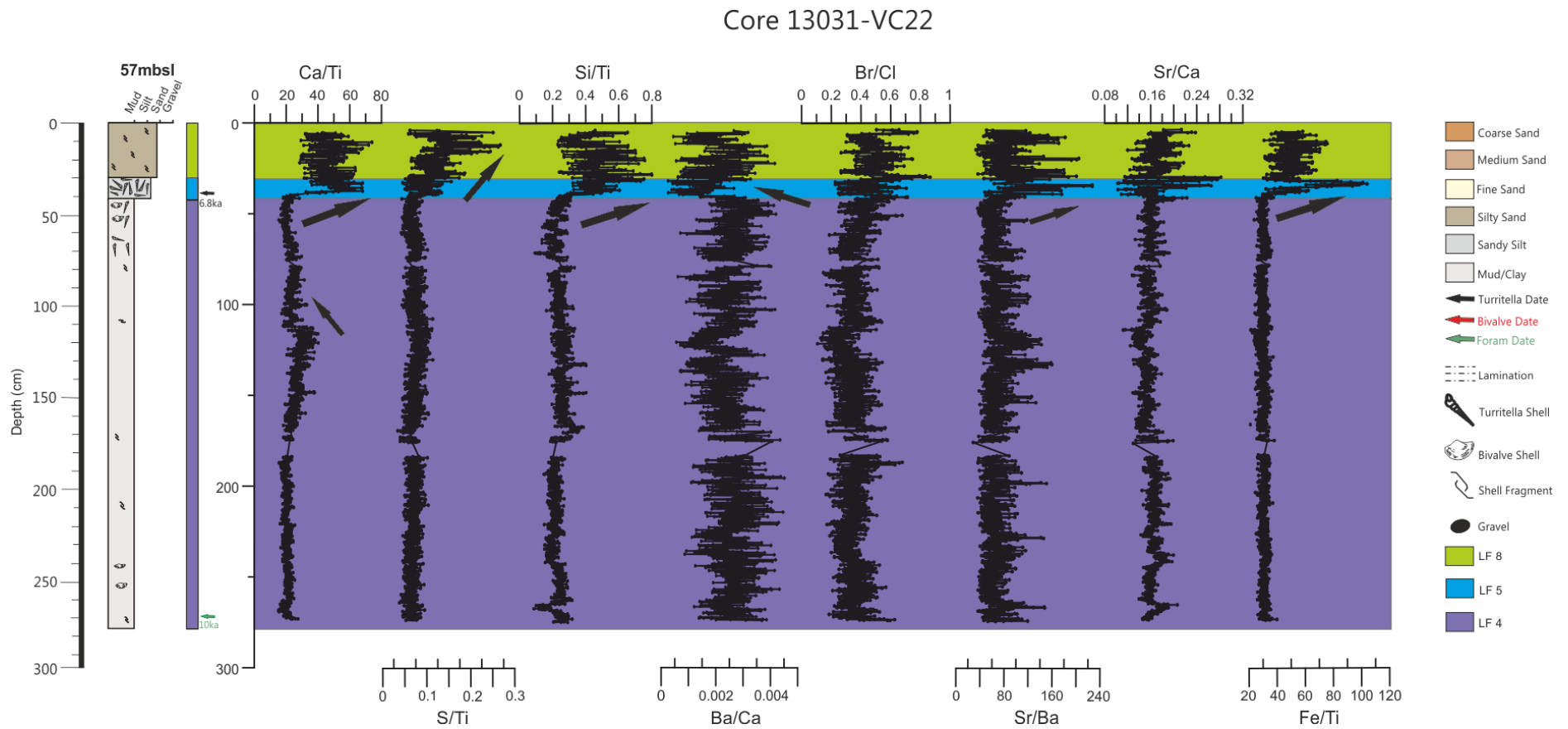


Figure 5.17: A graph showing the ITRAX analysis for core 22VC, showing LF 4 at the base of the core. The data are presented as a rolling average at a resolution of 5mm and the large black arrows next to the chemical data represent general trends.

5.3.5 Lithofacies 5 –Shell-hash

a) Sedimentology

This lithofacies is found in 13 cores across the bay (Fig. 5.24) and is composed of generally intact molluscs (gastropods and bivalves) in a sand and silt matrix (Fig. 5.12). The most common gastropod found is *Turritella communis* with an average length of ~3cm. A range of bivalves including scallops, oysters, cockles, mussels and nut shells, up to 11cm in diameter, are found throughout this facies. This facies is dark greenish grey to dark olive grey in colour and the thickness ranges from 20–107 cm. P-wave velocity, magnetic susceptibility, electrical resistivity and wet bulk density range from 1550 to 1764m/s, 1.8 to 10 SI*10⁻⁸m³/kg, 1.25 to 5Ω.m and 0.6 to 3.12g/cm³ respectively (Fig. 5.18). While the magnetic susceptibility and electrical resistivity show general increasing and decreasing trends upcore, respectively, the p-wave velocity and wet bulk density show no obvious trends. The p-wave velocity, in particular, covers a larger range than in most other facies. However, due to the very uneven scanning surface in this lithofacies, many cores had no data available, a factor which is likely influential in the lack of a visible trend. Shear strength measurements were not carried out on this lithofacies due to the high shell content. Both the upper and lower contacts of this facies are generally sharp and erosional, except in cores 14VC, 06VC and 02VC, where they are gradual (Fig. 5.18).

b) Foraminifera analysis

Lithofacies 5 was sampled in core 07VC at 160-161cm, core 01GC at 30-31cm and core 14VC at 110-111cm and 197-198cm. *Quinqueloculina spp.*, and *Haynesina germanica* are still the most prominent forams in this facies (Table 5.3). In lesser numbers *Textularia spp.*, *Lagena spp.*, *Oolina williamsoni*, *Cibicides lobatulus*, and *Rosalina praegeri* are present and remain constant up core. *Bulimina marginata* increases up core and *Spirillina vivipara* is re-introduced in this facies (it is absent in LF2, LF3 and LF4), while *Elphidium spp.*, which is not present in the bottom of the facies, appears in small numbers upcore. Overall, in this facies there is a decrease in foraminifera size and abundance (Appendix 2).

c) Chemical analysis

Chemical analysis was carried out on 13 cores that contained Lithofacies 5. This included cores from all areas of the mid and outer bay. Core 10VC is missing large portions of data from the bottom of this facies due to extensive shelly material, causing an uneven scanning surface and issues with the XRF scanning.

Ca/Ti content is highly variable, however large peaks in Ca/Ti are evident in all cores. The overall trend for Ca/Ti shows increasing values upcore (Fig. 5.19). The S/Ti content is low but variable in all cores, with peaks and dips throughout. Like the Ca/Ti content, it shows an overall increasing trend upcore throughout lithofacies 5. The Si/Ti content in this facies generally represents values that fall between the underlying and overlying facies, across a number of cores (Appendix 1). There is generally a constant or decreasing trend upcore, with the exception of cores 02VC, 03VC, 06VC and 22VC, which show a slight increasing trend upcore throughout lithofacies 5. Ba/Ca ratios show a decreasing trend upcore, with the exception of cores 17VC and 22VC which show a slight increase in content. There are peaks and dips in Ba/Ca levels evident throughout all cores. Br/Cl ratios show an increasing trend upcore and are on average lower than the overlying lithofacies. Sr/Ba and Sr/Ti content show an overall increasing trend up facies in all cores, with small peaks and troughs throughout. Sr/Ca content shows an overall decreasing trend upcore in this facies in all cores, with the exception of 17VC and 20VC, which show increases in the Sr/Ca content upcore (Appendix 1). Fe/Ti content is overall variable upcore, with large peaks and troughs throughout this facies. An exception to this are cores 03VC and 06VC which show a slight decreasing trend upcore (Fig. 5.19).

Overall, lithofacies 5 has a lower boundary with 3 other lithofacies. Its boundary with the underlying lithofacies 4 is sharp with changes across several elemental ratios, including Ca/Ti, and Fe/Ti. The boundary between lithofacies 5 and underlying lithofacies 3 shows gradual changes in all cores, as does the boundary between lithofacies 5 and underlying lithofacies 2 which also has only minor changes in some elements. The boundary between the overlying lithofacies 8 is gradual with only minor changes. However, lithofacies 5 is missing significant amounts of data due to its uneven scanning surface and this may have distorted how the boundaries between these lithofacies are represented in the data.

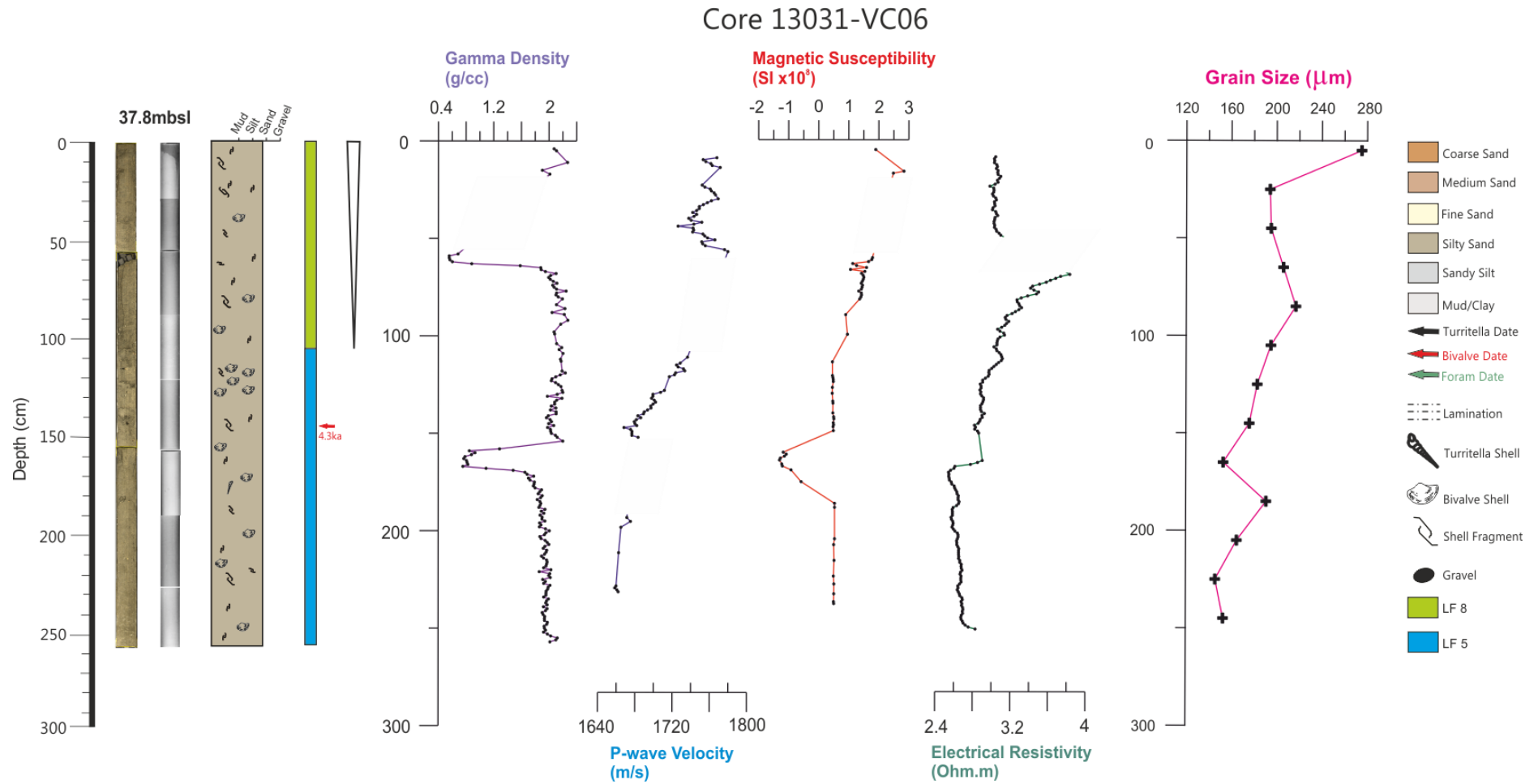


Figure 5.18: A graph of core 06VC showing a core image, an x-ray image, a core log, MSCL measurements and grainsize measurements.

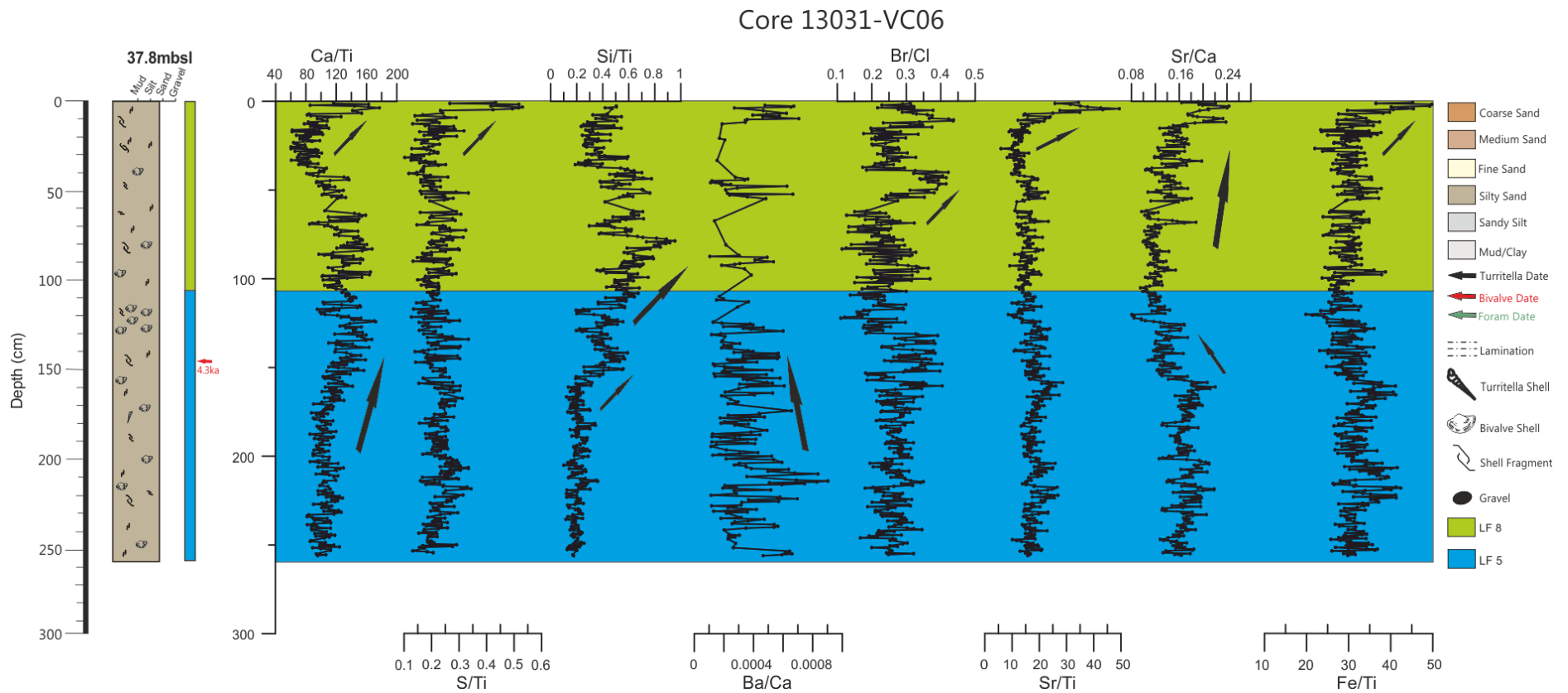


Figure: 5.19: A graph showing the ITRAX analysis for core 06VC, showing LF 5 at the base of the core. The data is presented at a resolution of 5mm and the large black arrows next to the chemical data represent general trends.

5.3.6 Lithofacies 6 –Interbedded silty sand and sandy silt

a) Sedimentology

This lithofacies is found in only one core (01VC) in the inner bay and is 128cm thick (Fig. 5.20 & 5.24). It is characterised by dark brown to dark grey interbedded sandy silt and silty sand (Fig. 5.12) layers with shell fragments throughout. Layers of sandy silt, visible to the naked eye through colour changes, as well as parallel laminations/layers up to 0.5cm thick (Table. 5.2) and extending for ~20cm, visible only on x-radiographs, are present near the top of this facies (Fig. 5.20). Downcore there are no further layers/laminations visible in the x-rays. However, banded layers of sandy silt and silty sand are still visible to the naked eye in the bottom half of the facies. The grainsize in this facies ranges from 54.4 to 88.8 μm (Fig. 5.20) and is variable throughout. Burrowing is visible under x-ray, below the laminations and extending downwards for 20cm from 140 to 160cm downcore. No MSCL measurements were obtained for this core, as only cores over 2m were selected for analysis. Shear strength measurements ranged from 13 to 31kPa in this facies and are lower near the facies top and bottom and higher mid-facies. The upper boundary of this unit is sharp, with a significant increase in sediment size between this facies and the overlying lithofacies 7, as well as a significant change in the density as seen on the x-ray imagery.

b) Foraminifera analysis

Samples at 187-188cm and 100-101cm from core 01VC show *Ammonia beccarii*, *Rosalina praegeri*, *Quinqueloculina spp.*, *Spirillina vivipara*, and *Elphidium excavatum* to be the dominant species, while smaller amounts of *Haynesina germanica* and *Planorbulina distoma* are present (Table 5.3). There is a large decrease in species abundance upcore in this facies and the foraminifera samples contain a mixture of broken and intact tests (Appendix 2).

c) Chemical analysis

The Ca/Ti represents the lowest ratio in the core and shows an increasing trend upcore, with larger peaks throughout. In particular a sharp increase is evident at 120cm near the facies top. The S/Ti content is highest at the base of the core, with a gradually decreasing

trend upcore. The average Si/Ti content is highest in this facies compared to LF7 and LF8 and has 2 distinct phases. The first phase has a small peak near the base of the facies at ~210cm, but otherwise is constant from the base of the core to 120cm. The second phase shows an increase in content at 120cm-115cm, coinciding with the increase in Ca/Ti, which remains constant to the top of the facies. This stepped trend shows an overall increase in Si/Ti up facies. The Ba/Ca ratio shows a steadily decreasing trend upcore, while both the Br/Cl and Sr/Ba ratios show an overall increasing trend upcore, with smaller peaks and dips. The Sr/Ca ratio, like the Si/Ti ratio has 2 phases. From the base of the core to ~120cm, a relatively constant trend is evident. However, at ~120cm there is a sharp decrease, which corresponds to the peaks in Ca/Ti and Si/Ti, this lower ratio of Sr/Ca remains constant to the facies top. The Fe/Ti content in this facies is the lowest in the core and shows a slight decreasing trend upcore.

Lithofacies 6 has no lower boundary with another facies, however the upper boundary with lithofacies 7 shows sharp changes in Si/Ti, S/Ti, Sr/Ba and Ba/Ca (Fig. 5.21).

5.3.7 Lithofacies 7 – Silty Sand

a) Sedimentology

This lithofacies is characterised by well sorted, brown, silty medium sand with large shell fragments throughout (Fig. 5.12). Like lithofacies 6, it is found only in core 01VC in the inner bay (Fig. 5.24) and is 45cm thick. No physical property measurements were obtained for this core and shear strength measurements could not be carried out due to the sandy nature of this facies. While similar to lithofacies 3, its sediment is coarser (more medium than fine sand) (Fig. 5.12), the colour is brown rather than grey and there are no intact shells visible in this facies. This facies has a sharp upper boundary with the overlying lithofacies 8. The lower boundary with lithofacies 6, while not evident to the naked eye, shows up as a distinct change in the density on the x-ray imagery (Fig. 5.20).

b) Foraminifera analysis

A foraminifera sample at 60-61cm from core 01VC, shows the dominant species in this facies to be *Ammonia beccarii*, *Quinqueloculina spp.*, and *Haynesina germanica*, while

smaller amounts of *Elphidium excavatum*, and *Rosalina praegeri*, are present (Table 5.3). There is a high number of broken tests in this facies (Appendix 2).

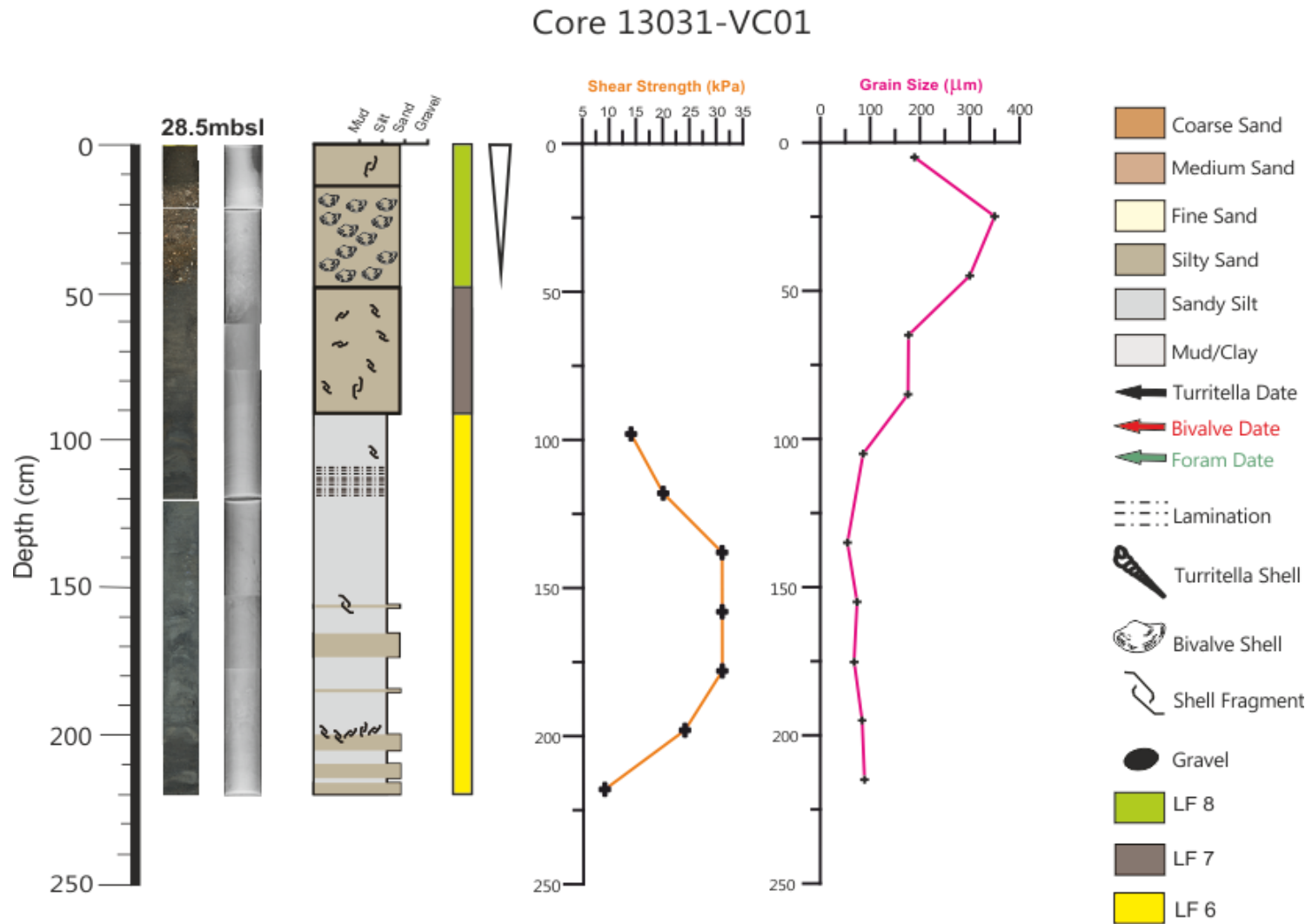


Figure 5.20: A graph of core 01VC showing a core image, an x-ray image, a core log, shear strength measurements, grain size values and percentages of sediment type for LF6 and LF7.

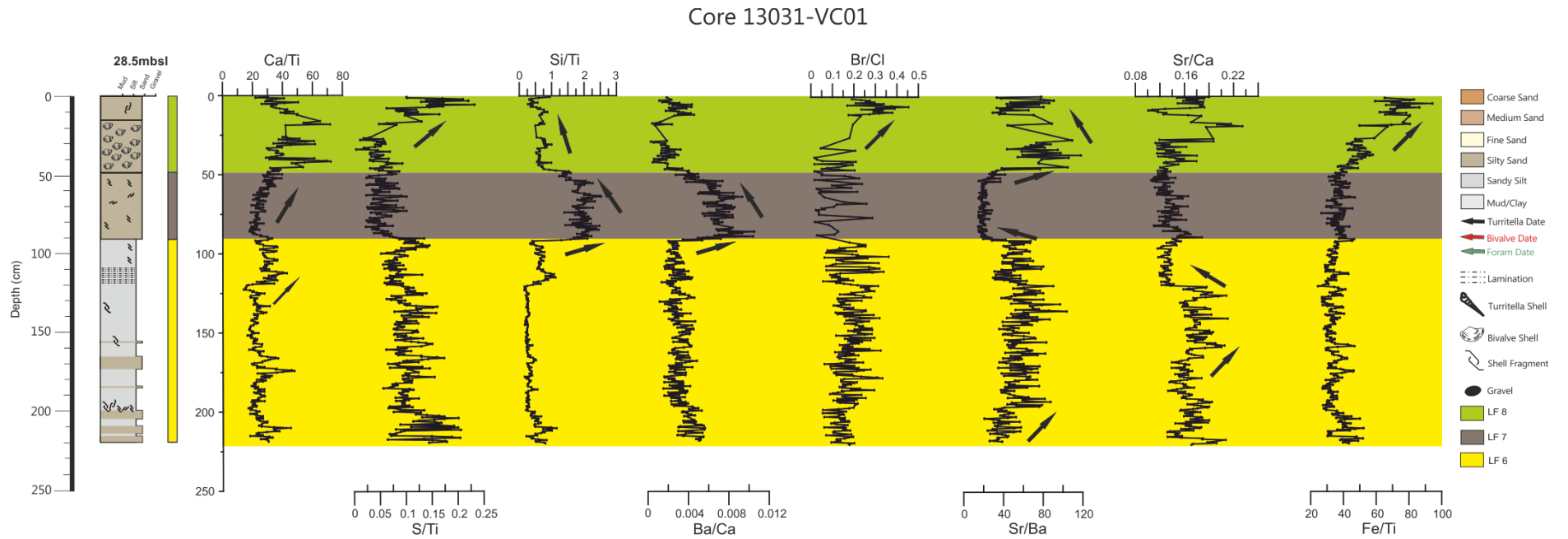


Figure 5.21: A graph showing the ITRAX analysis for core 01VC. LF6 is at the base of the core, while LF7 is in the middle of the core. The data is presented at a resolution of 5mm and the large black arrows next to the chemical data represent general trends.

c) Chemical analysis

The Ca/Ti content in this facies shows a steadily increasing trend upcore. The S/Ti content has more variability, however, the trend is overall constant upcore. The Si/Ti content in this facies is the highest. There is a huge increase in Si/Ti from the underlying facies before a steadily declining trend upcore (Fig. 5.21), with smaller peaks and dips throughout this facies. The Ba/Ca content shows a very similar trend to the Si/Ti levels, with the Ba/Ca levels in this facies the highest in the core. There is also a significant increase between the underlying facies and the base of this facies and a decreasing trend upcore. There are peaks and dips throughout, with the largest peak at the base of the facies. The Br/Cl levels in this facies appear to show a relatively constant trend upcore with large peaks throughout. However, this elemental ratio is clearly missing data in this facies and the Br/Cl trend may be incomplete. The Sr/Ba trend in this facies is constant upcore until ~55cm where it begins to gradually increase to the top of the facies. The Sr/Ba content in this facies is the lowest in the core and there is a substantial change in Sr/Ba levels between both the overlying and underlying facies. There is a large decrease between the underlying facies and LF6 while a significant increase is visible between this facies and LF8. The Sr/Ca content in this facies shows a decreasing trend upcore, with a peak at the base of the facies, coinciding with the peaks in Ba/Ca. The Fe/Ti levels show a steadily decreasing trend upcore in this facies with some smaller peaks and dips throughout (Fig. 5.21). Overall, the boundary between this unit and the underlying lithofacies 6 shows extremely sharp changes in elemental ratios, in particular changes in S/Ti, Si/Ti, Ba/Ca and Sr/Ba are substantial. The upper boundary with this unit and the overlying lithofacies 8 also shows clear changes in most of the elements and a sharp increase in Sr/Ba (Fig. 5.21).

5.3.8 Lithofacies 8 – Poorly sorted, coarsening upwards silt to coarse sand**a) Sedimentology**

This lithofacies is found across the bay in all cores (Fig. 5.24 & 5.25) and is characterised by fine to coarse sand, with a minor silt component, coarsening upwards (Fig. 5.12), with abundant shell fragments and bivalves. Core 08VC has pebbles near

the core top, however, it is the only one. It ranges in colour from light yellowish brown to black and is the thickest unit, up to 257cm. P-wave velocity, electrical resistivity, wet bulk density and magnetic susceptibility range from 1595 to 1780m/s, 0.7 to 19 Ω .m, 0.5 to 3.32g/cm³, and 1.8 to 10 SI*10⁻⁸m³/kg respectively (Fig. 5.22). This facies has the highest range of values in all MSCL measurements (Appendix 1). Overall the p-wave velocity and wet bulk density show a decreasing trend upcore while the magnetic susceptibility shows an increasing upcore trend and there is no discernible trend in the electrical resistivity values. Shear strength measurements could not be carried out on this lithofacies due to the high sand content. This facies is always found at the core top and overlies lithofacies 5, with the exception of 01VC where it overlies facies 6. It has a sharp erosional lower contact in all cores (Fig. 5.16), except in cores 14VC and 02VC where the contact is more gradual (Fig. 5.22).

b) Foraminifera analysis

Lithofacies 8 was sampled at 1-2cm in core 01VC, 78-79cm in core 07VC, in core 14VC at 45-46cm, in core 17VC at 15-16cm and in core 01GC at 1-2cm. *Quinqueloculina spp.*, *Lagena spp.*, *Cibicides lobatulus*, *Planorbulina mediterraneensis* and *Ammonia beccarii* are the dominant species in this facies, although *Quinqueloculina* less so than in other facies. *Fissurina elliptica* and *Bolivina spp.* are common in this facies, while *Textularia spp.*, *Oolina williamsoni*, *Bulimina marginata*, *Haynesina germanica*, *Nonionella turgida* and *Rosalina praegeri* also appear, but in relatively smaller quantities (Table 5.3). There appears to be a trend toward smaller species in this facies, although it is more diverse and relatively intact (Appendix 2).

c) Chemical analysis

Chemical analysis was carried out on 17 cores that contained Lithofacies 8 (Fig. 5.8, 5.11, 5.14, 5.17, 5.19, 5.21, & 5.23). The Ca/Ti levels show a variable content with peaks and dips throughout lithofacies 8, however, there is a decreasing trend up facies in all cores. S/Ti content is variable throughout all cores, again with peaks and dips throughout the facies. However, there is a general trend of decreasing S/Ti levels up facies in all cores, except 01VC, 02VC, 04VC and 22VC, which show an increasing trend

upcore. Cores 01VC and 06VC in particular shows a sharp increase in S/Ti levels towards the core top (Fig. 5.14 & 5.21). The Si/Ti content is variable in this facies with peaks throughout, however it shows a decreasing trend up facies overall. Only in cores 01GC and 14VC is there an increase in content, although core 06VC displays an increasing trend from the base of the facies to ~80cm before decreasing to the core top. Ba/Ca generally shows a constant or decreasing trend upcore, however some cores show an increasing trend upcore. These include cores 01GC, 04VC and 06VC (Fig. 5.19), while cores 15VC and 22VC (Fig. 5.17) show an increase to mid-facies then a decreasing trend to the core top. There are peaks and dips throughout this facies, however the cores which show an increasing trend up core appear to have more distinct peaks in this facies. Br/Cl shows an increasing trend upcore in all cores except 04VC. Overall, this facies has the highest content of Br/Cl of all facies throughout the cores. Core 04VC appears to have a stepped decreasing trend up core with higher levels from the base of the core to ~95cm, before a sharp peak and then a decrease to slightly lower levels than before and a constant trend to the core top. Sr/Ba and Sr/Ti content is variable with large peaks throughout lithofacies 8, however there is an overall increasing trend up facies, with the exception of cores 01GC and 14VC which show a decreasing trend upcore. Sr/Ca content shows a similar trend to Sr/Ba and Sr/Ti, with an increasing trend up facies in all cores except 01GC, 03VC and 14VC, which show a decreasing trend. Fe/Ti content is variable with large peaks and dips throughout this facies. It shows an increasing trend up facies in all cores except for 01GC, 09VC and 14VC which show a slight decreasing trend. Core 14VC appears to differ from the general trend in this facies across many elemental ratios. However, it is important to note that it is missing a large amount of data in the middle of this facies and this may have distorted the trends visible in the geochemical results.

Overall, the lower boundary between lithofacies 8 and the underlying lithofacies 5 appears to be rather gradual (Fig. 5.8, 5.14 & 5.17) throughout the cores with only minor differences visible in some of the elements, with the exception of cores 01GC, 18VC and 22VC (Fig. 5.17). These show significant changes in a number of elemental ratios including Ca/Ti, Si/Ti, Sr/Ca and Fe/Ti. The lower boundary between lithofacies 8

and underlying lithofacies 7 however is much sharper with major changes in many of the elements, in particular Sr/Ba, which shows a significant decrease in content.

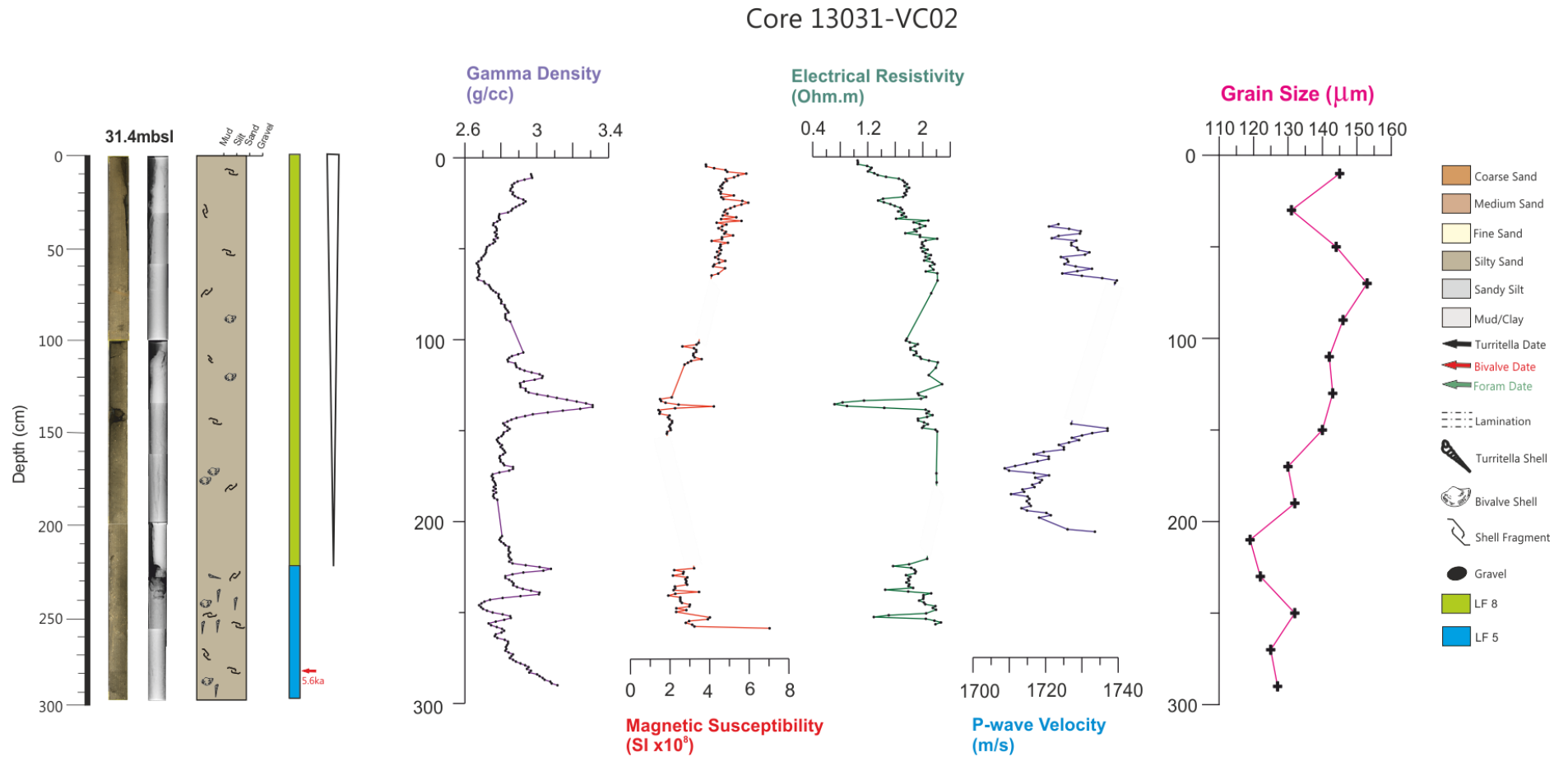


Figure 5.22: A graph of core 02VC showing a core image, an x-ray image, a core log and MSCL measurements.

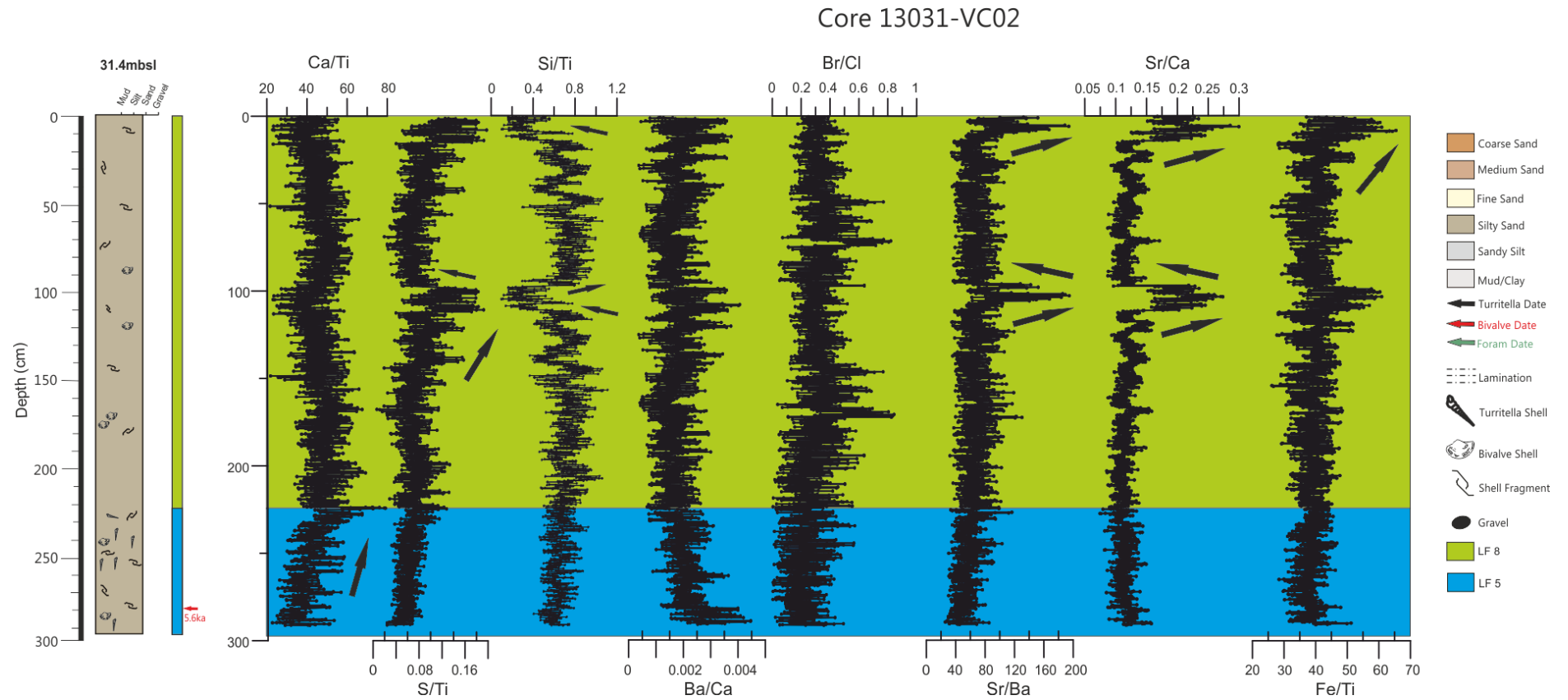


Figure 5.23: A graph showing the ITRAX analysis for core O2VC, showing LF8 at the top of the core. The data is presented as a rolling average at a resolution of 5mm and the large black arrows next to the chemical data represent general trends.

5.4 Sequence stratigraphy and geographical distribution of lithofacies and seismic units

The bay was divided into 3 geographical areas (Fig. 5.24) to best present the overall results. These are, a) the inner bay, b) the mid bay and c) the outer bay. Within these areas sub divisions have been made in the mid and outer bay. The mid bay sub-division includes part of the South Sound, while the outer bay has been sub-divided into the South Sound, North Sound and central bay. The distribution of the acoustic lithofacies in each of these areas is discussed in detail below.

5.4.1 Inner Bay

The predominant acoustic units found in the inner bay are sub-units 3a and 3b, with units 1 and 2 generally only visible at the northern and southern edges of the inner bay (Fig. 5.5). Acoustic sub-unit 3a is generally between 10 and 12.5m thick, which largely represents the limit of penetration in this area, indicating that the unit may be thicker than this, whilst sub-unit 3b drapes sub-unit 3a and is generally 3 – 5m thick (Fig. 5.6B & 5.6C). The depositional centres appear to shift with sub-unit 3a concentrated near the mid-bay boundary (Fig. 5.6B), whilst sub-unit 3b is mostly found offshore Spiddal (Fig. 5.6C).

The only core in this area (01VC) penetrated sub-unit 3b. It is located at a depth of 29m bsl and consists of multiple lithofacies, LF6, LF7 and LF8, two of which (LF6 and LF7), were not identified in any other area (Fig. 5.24). While no radiocarbon dates were taken directly from core 01VC, LF8 was dated in the middle of the facies, in the outer central area of the bay at 2.2 ka cal BP (Fig. 5.26). LF6 is the deepest facies in this core (Fig. 5.24 & 5.25) and is characterized by interbedded brownish grey, sandy silt and silty sand with shell fragments throughout (Table 5.1). There is extensive bioturbation mid facies, followed by parallel laminations. The dominant foraminifera species are *Ammonia beccarii*, *Rosalina praegeri*, *Quinqueloculina spp.*, *Spirillina vivipara*, and *Elphidium excavatum* (Fig. 5.8). There is a decrease in abundance up facies and a mixture of broken and intact tests throughout (Appendix 2). The shear strength measurements show an increase from the base of the core to mid-facies, before decreasing towards the facies top (Fig 5.20).

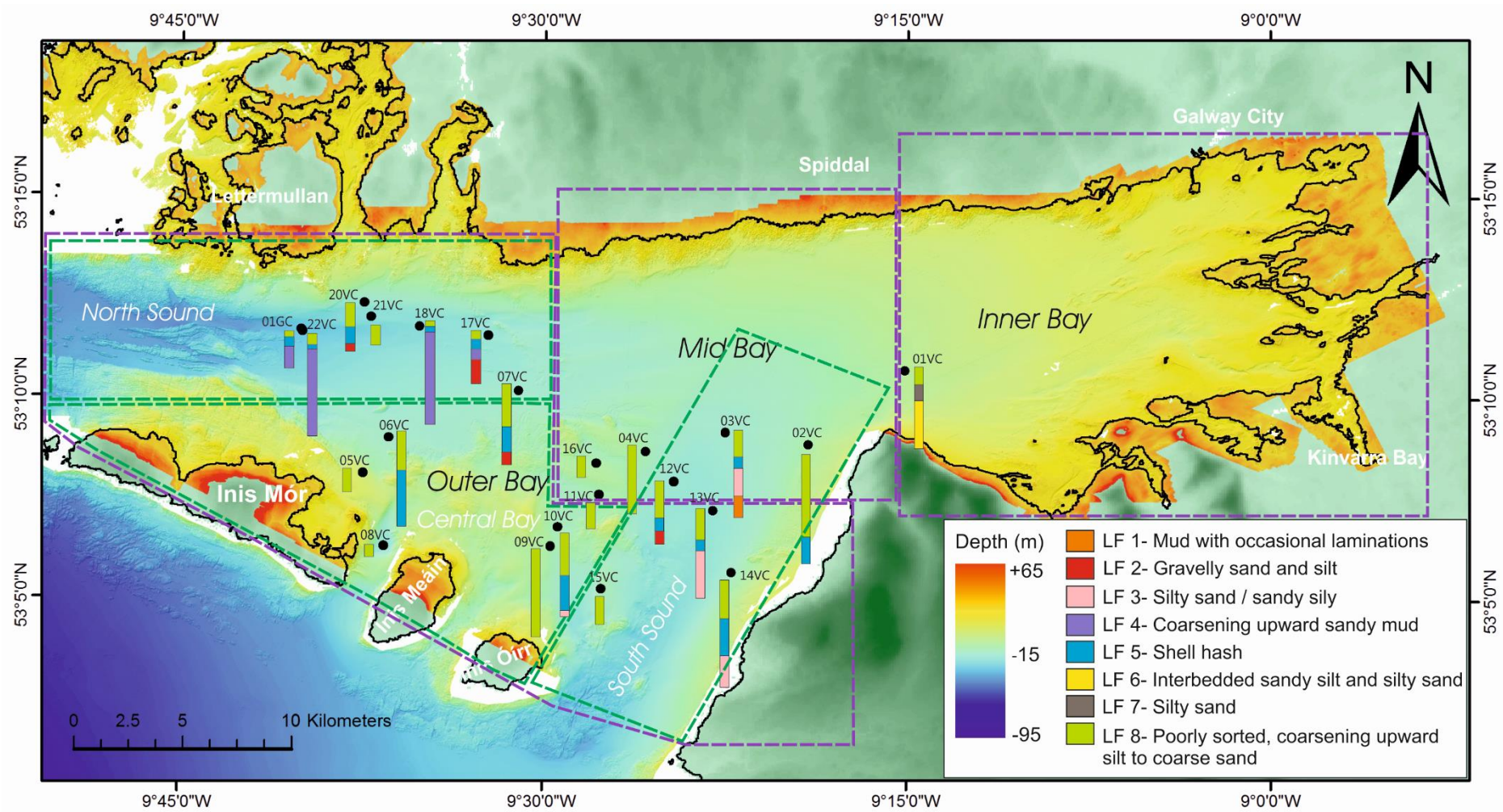


Figure 5.24: Map of Galway Bay showing the core positions and their associated lithofacies.

Near the top of LF6, the XRF results show a jump in Ca/Ti, Si/Ti and a decrease in Sr/Ca content. The upper boundary of LF6 is not visible on the core section, however there is a clear change in density on the x-rays, a sharp change in the sediment size (Fig. 5.20) and in the 3 chemical element ratios; Si/Ti, Ba/Ca and Sr/Ba (Fig. 5.21).

The dominant foraminifera species in this facies are *Ammonia beccarii*, *Quinqueloculina spp.*, and *Haynesina germanica* (Fig. 5.8) and there is a decrease in the abundance and preservation of foraminifera from the underlying facies (Appendix 2). This facies has very high Ba/Ca and Si/Ti content which decreases drastically up facies and very low Sr/Ba content (Fig. 5.21). The upper boundary of this facies is sharp, with a visible change to a shell layer in both the core and x-rays (Fig. 5.20). This boundary is also marked by a jump in grain size and a significant sharp increase in the Sr/Ba content.

Above LF7 is LF8, a brown silty sand facies coarsening upcore with abundant shell, both intact and fragmented (Appendix 2). There are shell layers at the base of this facies with abundant smaller bivalves. The dominant foraminifera species in this facies are *Quinqueloculina spp.*, *Lagena spp.*, *Cibicides lobatulus*, *Planorbulina mediterranensis* and *Ammonia beccarii* (Fig. 5.8). There are abundant and diverse species in this facies, although they tend to be smaller than the underlying facies. The facies has the highest Br/Cl and lowest Ba/Ca contents in core 01VC, which show an increasing and decreasing trend upcore respectively. The Ca/Ti content is high but it has a decreasing trend upcore in this facies (Fig. 5.21). This facies forms the modern seafloor and the sequence terminates at its top (Fig. 5.25).

5.4.2 Mid Bay

Like the inner bay, the predominant seismic units in the mid-bay are 3a and 3b. Unlike the inner bay, both seismic units 1 and 2 are also present throughout much of the mid-bay (Fig. 5.5). Overall, sub-unit 3b has the most extensive coverage and is the thickest seismic unit in the mid-bay, between 4 and 7m, with deposition up to 8.5m thick along the northern coastline and in the south-east around Blackrock headland, where it is part of the South Sound (Fig. 5.6B). Sub-unit 3a reaches a similar thickness, generally

between 4 and 6m, with a small area along the eastern boundary up to 11m in thickness (Fig. 5.6C), while unit 2 is generally less than 4m in thickness (Fig. 5.6A). There are 6 sediment cores within the mid-bay; 04VC, 16VC, 11VC, 12VC, 03VC and 02VC, the latter 3 of which are located in the South Sound (Fig. 5.24). These cores penetrated acoustic sub-unit 3b and are located in water depths from 31 to 42m. While cores 04VC, 11VC and 16VC only contain 1 lithofacies (LF8), the cores in the South Sound mid-bay area (02VC, 03VC and 12VC) contain multiple lithofacies, including LF1, LF2, LF3, LF5 and LF8 (Fig. 5.25). Cores 04VC, 16VC and 11VC are the shallowest in the mid-bay (31.17 – 33.5m). They are composed of silty and fine sand and contain both abundant shell fragments and foraminiferal content. Core 12VC is the oldest in the mid-bay, with LF2 in core 12VC, dated to 11.5 ka cal BP (Table 5.3 & Fig. 5.25).

LF1 is present only in core 03VC and underlies LF3, which in another core (13VC) contains the oldest date for the bay. LF1 is composed of dark grey mud with occasional laminations (Table 5.1), very sparse shell content and has the highest shear strength values in the bay which increase up facies to 49kPa (Fig. 5.7). The common foraminifera species are *Quinqueloculina spp.*, *Lagena spp.*, *Miliolinella subrotunda*, and *Spirillina vivipara*, and they are large in comparison to other facies (Table 5.2). The geochemistry of LF1 shows an increasing trend upcore in Ca/Ti, S/Ti and Si/Ti and a decreasing trend upcore in Ba/Ca, Br/Cl and Sr/Ca, while Sr/Ba and Fe/Ti remain constant upcore (Fig. 5.8). A gradual transition is evident in both sedimentology and geochemistry with the overlying LF3.

As for LF1, LF3 is also present in the mid-bay in core 03VC. In this core LF3 is composed of dark grey sandy silt with sparse shell content and abundant foraminiferal content, primarily composed of *Quinqueloculina spp.*, *Ammonia beccarii* and *Haynesina germanica*. The geochemistry of LF3 in the mid-bay shows an increasing trend upcore in Ca/Ti, Si/Ti, Br/Cl, Sr/Ba, and Fe/Ti and a decreasing trend upcore in S/Ti, Ba/Ca, and Sr/Ca (Fig. 5.14).

Core 12VC is the only core located outside the North Sound to contain LF2 (Fig. 5.25 & 5.26). LF2 in the mid bay is composed of brown fine-medium sandy silt with gravel (Fig. 5.8) with abundant shell fragments. The foraminiferal content is composed primarily

of *Textularia spp.*, *Quinqueloculina sp.*, *Sahulia conica*, and *Miliolinella subrotunda* (Fig. 5.8) and test breakage is high. The geochemistry of LF2 in the mid-bay shows an increasing upcore trend in Ca/Ti, Br/Cl, Sr/Ba and Sr/Ca, a decreasing trend upcore in Si/Ti and Ba/Ca and a constant upcore trend in S/Ti and Fe/Ti (Fig. 5.11).

LF4 is not seen in the mid bay region.

LF5 is found only in cores in the South Sound area of the mid-bay and has been dated near the base of core 02VC to 5.6 ka cal BP and in core 03VC to 4.1 and 0.9 ka cal BP (Table 5.3, Fig. 5.24 & 5.25). The youngest date may be reworked from the facies above (LF8) as no other dates from LF5 throughout the bay suggest such a young age (Table 5.3). In the mid-bay area, LF5 is composed of shell hash in a brown-grey sandy silt and silty sand matrix (Fig. 5.12) and the dominant foraminifera species are *Quinqueloculina spp.*, and *Haynesina germanica* (Table 5.2). The geochemistry in LF5 shows an increasing trend in Ca/Ti, S/Ti, Br/Cl and Sr/Ba upcore, a decreasing trend in Ba/Ca, a constant upcore trend in Si/Ti and Sr/Ca and variable trends in Fe/Ti (Fig. 5.8, 5.11 & 5.14).

LF8 in the mid-bay is generally composed of a grey-brown sandy silt with abundant shell fragments and abundant foraminiferal content, with *Quinqueloculina spp.*, *Lagena spp.*, *Cibicides lobatulus*, *Planorbulina mediterraneensis* and *Ammonia beccarii* as the primary species (Table 5.2).

The geochemistry of LF8 in the mid bay area shows a decreasing trend upcore in Ca/Ti and Si/Ti, an increasing trend upcore in S/Ti, Sr/Ca, and Fe/Ti, while there is variability between the cores in Ba/Ca and Br/Cl (Fig 5.8).

5.4.3 Outer Bay - South Sound

The outer bay South Sound sub-bottom data (Fig. 5.1) are dominated by unit 1 with extensive outcropping at the western edge of the Sound, where it forms the present seafloor (Fig. 5.5). Other units are rarely visible in this area (Fig. 5.5) and are generally less than 4m in thickness (Fig. 5.6). Sediments that are deposited above unit 1 are most concentrated in the inner Sound near the mid-bay boundary and along the edges of the South Sound. Deposition is generally between 2 and 4m, in unit 2 and sub-units 3a and 3b, however deposition in sub-unit 3b covers a more extensive area (Fig. 5.6).

The 3 cores (13VC, 14VC and 15VC) found in the outer bay South Sound area, all recovered acoustic sub-unit 3b, in water depths ranging from 34 to 42m. The sediment is between 0.75 and 2.88m thick and dated to be younger than 13.1 ka cal BP based on a foram date from the bottom of core 13VC (Table 5.3).

The lithofacies sequence in the outer bay South Sound consists of LF3, LF5 & LF8 in cores 13VC and 14VC and LF8 in core 15VC (Fig. 5.24 & 5.25).

LF3 is the oldest facies, with dates of 9.9 and 13.1 ka cal BP, dated in core 13VC. It is composed of a dark grey silty sand and sandy silt with both broken and intact shells. The p-wave velocity in this facies is the highest in the bay, up to 1975m/s, while shear strength measurements are also relatively high, up to 42kPa (Fig. 5.13). The dominant foraminifera species are *Quinqueloculina spp.*, *Ammonia beccarii* and *Haynesina germanica* (Table 5.2). There is a large species diversity and abundance, increasing upcore in this facies. In the geochemistry there is an increase in Si/Ti, Br/Cl and Sr/Ba content up facies, a decrease in S/Ti and Ba/Ca, a constant upcore trend in Ca/Ti and variability in the Sr/Ca and Fe/Ti content (Fig. 5.14). The boundary between this facies and the overlying LF5 is sharp, with a distinctive increase in shell content at the upper boundary of LF3. Overlying LF3 is LF5, a shell layer, with both gastropod and bivalves that have been dated at 6.4 ka cal BP in core 13VC (Fig. 5.25). The dominant foraminiferal species are *Quinqueloculina spp.* and *Haynesina germanica*, and there is a decrease in size and abundance in all species up facies (Table 5.3). The chemical elements show increasing trends of Ca/Ti, Br/Cl, Sr/Ba and Fe/Ti, decreasing Ba/Ca and Sr/Ca, constant Si/Ti and variable S/Ti content upcore in LF5 in the outer bay, South Sound (Fig. 5.18). There is a sharp boundary between this shell layer and the overlying LF8, with a significant decrease in shell content. The youngest facies, LF8, is a brownish grey silty sand and sandy silt, coarsening upwards, with shell, both intact and fragmented. *Quinqueloculina spp.*, *Lagena spp.*, *Cibicides lobatulus*, *Planorbulina mediterraneensis* and *Ammonia beccarii* are the dominant foraminifera species in this facies (Table 5.2), with small intact tests common. This lithofacies generally shows a decreasing S/Ti and Si/Ti, an increasing Br/Cl, Sr/Ba and Fe/Ti a constant Ba/Ca and Ca/Ti content and a variable Sr/Ca content up facies which terminates at the core top (Fig. 5.22).

5.4.4 Outer Bay - Central

Unit 1 is the most extensive seismic unit in the outer bay central area and outcrops widely at the seafloor (Fig. 5.5A). Unit 2 is present in the south and north east part of the central bay but is missing around Inis Mór Island and from the middle of the central outer bay (Fig. 5.5B). Where unit 2 is present it is thickest along the north-eastern border with the North Sound, reaching up to 16m (Fig. 5.6A). Sub-unit 3a is rarely found in the central outer bay area, only present in the north-east, along the border with the north sound, where it is ~9m thick, and in the south, in a strip extending north-eastwards from Inis Óirr (Fig. 5.5C & 5.6B). While seismic sub-unit 3b is thin (generally <4m in thickness), it covers much of the outer central bay, with the exception of the area around Inis Mór Island. The isopach maps suggest that there is a sediment depocentre along the north-eastern edge of the central outer bay, with all sedimentary units (Unit 2 and Sub-units 3a and 3b) having their thickest occurrence here (Fig. 5.6). All of the cores, 05VC, 06VC, 08VC, 09VC and 10VC, penetrated only seismic sub-unit 3b. These cores were collected in water depths ranging from 19 to 44m and contain multiple lithofacies (LF3, LF5 and LF8) (Fig. 5.24 & 5.26).

The lithofacies sequence in core 10VC, the only core which contains all 3 lithofacies, begins with LF3, followed by LF5 and finally LF8. Cores 09VC and 06VC both contain LF5 and LF8, while cores 05VC and 08VC contain only LF8 (Fig. 5.26). LF3, considered to be the oldest facies reached in the outer central bay, is composed of brown/grey silty sand with shell fragments. The dominant foraminifera species found in LF3 are *Quinqueloculina spp.*, *Ammonia beccarii* and *Haynesina germanica*, although there are many more species as this is one of the most diverse lithofacies with regard to foraminifera species (Table 5.2). No geochemical data for LF3 in the outer central bay is available. There is a distinctive sharp boundary between this facies and the overlying one and an increase in shell content. LF3 is overlain by LF5, the shell hash layer of gastropods and bivalves, dated between 7.4 and 4.4 ka cal BP in core 10VC. This shell layer is up to 1.5m thick and has distinctive low magnetic susceptibility values, down to $-1.3 \text{ SI} \cdot 10^{-8} \text{ m}^3/\text{kg}$ in core 06VC (Fig. 5.17). The dominant foraminifera in this facies are *Quinqueloculina spp.*, and *Haynesina germanica*, although other species are present in lesser numbers. All foraminifera species decrease in size and relative

abundance upcore in this facies (Appendix 2). There are geochemical results for LF5 in core 06VC only, in the outer bay. There is an increase upcore in Ca/Ti, Si/Ti and Br/Cl content, a decrease in Ba/Ca, Sr/Ca and Fe/Ti content and a constant trend in Sr/Ti and S/Ti (Fig. 5.18). There is a sharp boundary between the shell layer and the overlying LF8, the youngest facies and the one found at the modern-day seafloor, which has been radiocarbon dated to < 2.2 ka cal BP, in core 10VC (Table 5.3 & Fig. 5.25). This facies is between 0.32 to 2.57m thick in the outer central bay and is composed of brownish grey silty to coarse sand, with abundant intact shells and shell fragments. The foraminifera species in this facies are abundant in both number and species type and relatively intact. The dominant foraminifera species in LF8 include; *Quinqueloculina spp.*, *Lagena spp.*, *Cibicides lobatulus*, *Planorbulina mediterraneensis* and *Ammonia beccarii* (Table 5.2). The facies has high Br/Cl content and low Ba/Ca and Si/Ti contents which show increasing and decreasing trends upcore, respectively. The Ca/Ti is high however, it has a decreasing trend upcore in this facies, corresponding to the shell layers at the base of this facies.

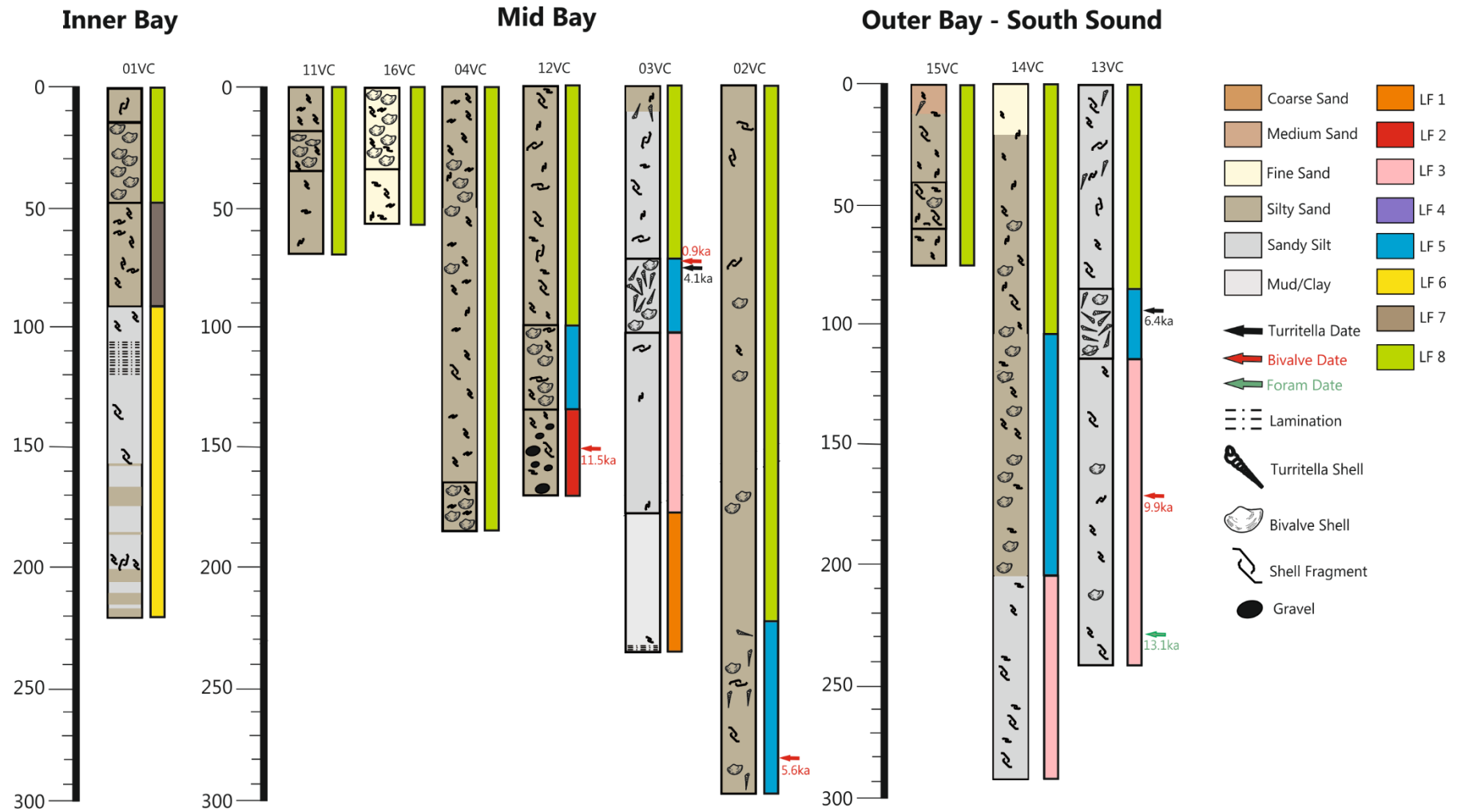


Figure 5.25: The cores in the inner bay, the mid bay, the latter 3 of which (12VC, 03VC & 02VC) are also part of the South Sound and cores in the outer bay central area.

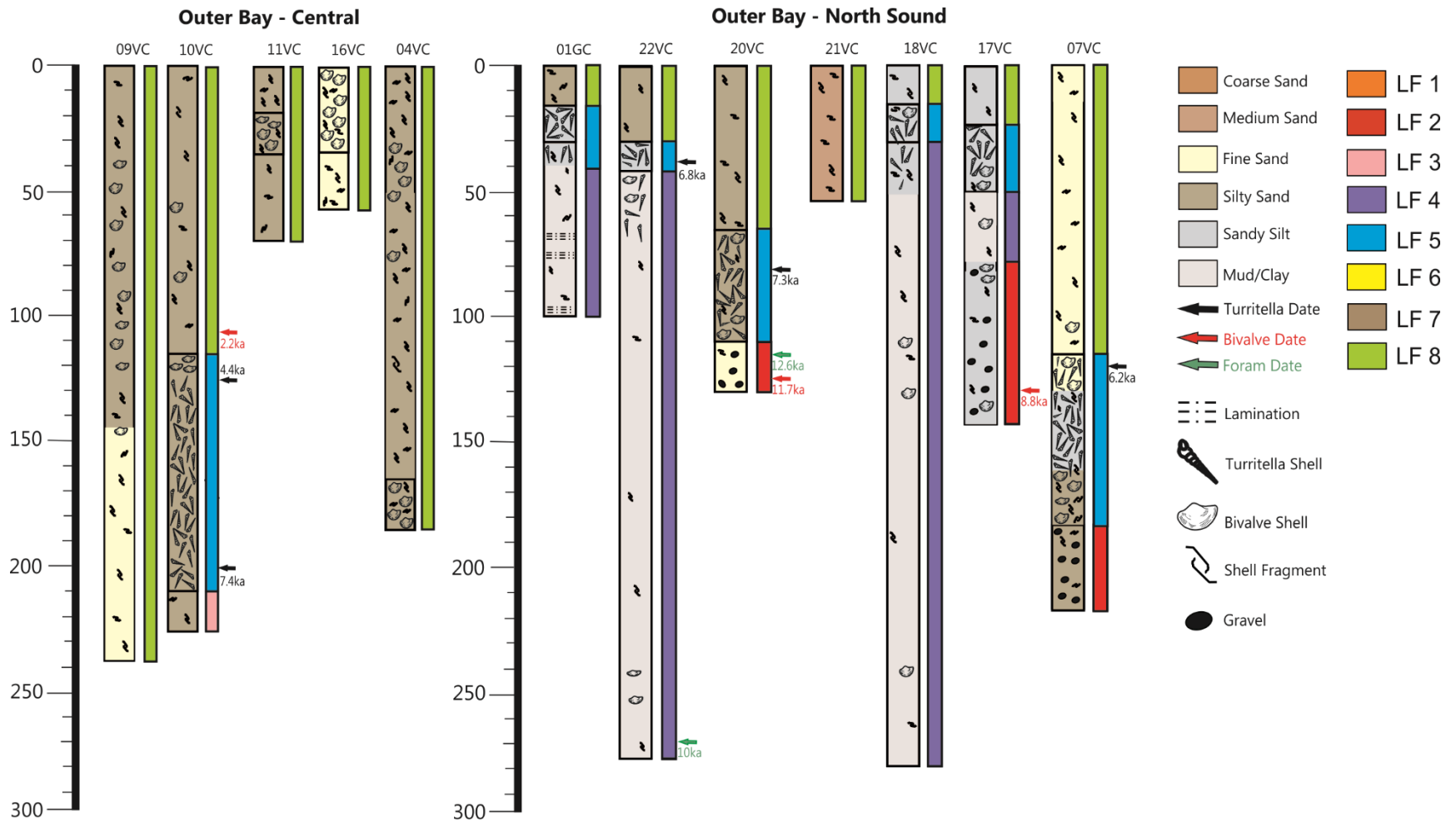


Figure 5.26: Cores in the Outer Bay, both North and Central areas.

5.5.5 Outer Bay - North Sound

The basement reflector (unit 1) is by far the most extensive seismic horizon in the North Sound with outcropping bedrock forming much of the seafloor along the northern, southern and western edges of this area (Fig. 5.2). Acoustic Unit 2 tends to be predominantly found towards the middle of the North Sound area, between Lettermullan and Rossaveel and is absent along the northern and southern edges of the North Sound in the west (Fig. 5.5B). Where it is present in the outer bay North/Sound area, it is between 4 and 16m in thickness (Fig. 5.6A) and infills the topographical lows in acoustic unit 1 (Fig. 5.2). Sub-unit 3a is patchy and only present across a small area northwards of the channel in the North Sound (Fig. 5.2), along the northern coastline, from Lettermullan to Rossaveel (Fig. 5.5C). Sub-unit 3a is the thinnest in the North Sound, generally less than 4m thick (Fig. 5.6B) and where present, generally drapes unit 2. The exception to this is through the North Sound channel, where sub-unit 3a is infilling unit 1 (Fig. 5.2) and is up to 11m thick (Fig. 5.6B). Sub-unit 3b is the most extensive in the North Sound after unit 1. It is found throughout most of the North Sound, with the exception of the northern and southern edges in the west, where unit 1 forms the seafloor (Fig. 5.5). Sub-unit 3b is generally between 1.5 and 6.5m thick (Fig. 5.6C), and all sediment cores in the North Sound are found within the upper 3m of sub-unit 3b.

The cores in the North Sound are the deepest in the bay, ranging from 40 to 57m in depth and have multiple lithofacies; LF2, LF4, LF5 and LF8 (Fig. 5.26). The oldest lithofacies in the North Sound is LF2, which is found in cores, 07VC, 17VC and 20VC, and has 3 radiocarbon dates, 12.6 and 11.7 ka cal BP (in core 20VC) (Fig. 5.26) and 8.8 ka cal BP (in core 17VC) and forms the base of the sequence in all 3 cores. LF2 is composed of dark grey gravelly sand and silt (Fig. 5.12) with abundant shell fragments. P-wave velocity in this facies is high, up to 1888m/s while shear is medium, reaching 25kPa in the North Sound (Fig. 5.10). The dominant foraminifera species are *Textularia spp.*, *Quinqueloculina sp.*, *Sahulia conica*, and *Miliolinella subrotunda*. There is an abundance of foraminifera in this facies, however, there is also a high number of damaged and broken foraminifera. There is a clear decreasing trend in the Si/Ti and Ba/Ca content upcore in this facies, while the Br/Cl and Sr/Ba content shows a clear

increasing trend upcore. There is a sharp boundary between LF2 and the overlying facies LF 5, with a significant increase in intact shell content, while there is a more gradual boundary between LF2 and LF4.

LF4 forms the base of cores 01GC, 18VC and 22VC, and overlies LF2 in core 17VC (Fig. 5.26). This lithofacies is not found in any of the other regions and is dated at 10 ka cal BP at the base of core 22VC, making it contemporary with LF3 in the South Sound (13VC), which is dated at 9.9 ka cal BP (Table 5.3). LF4 is composed of dark grey to dark greenish grey, silty mud, coarsening upwards (Fig. 5.12 & 5.16) with very sparse shell content. P-wave velocity and shear strength are the lowest in the bay, from 1570 to 1645 m/s and 4 to 25 kPa, respectively (Fig. 5.15 & 5.16). The dominant foraminifera species are *Lagena spp.*, *Stainforthia fusiformis*, *Nonionella turgida* and *Bolivina spp.* (Table 5.2). This facies does not have a high species diversity and there were very few broken foraminifera tests in LF4. The Br/Cl content in this facies shows a slight increasing trend upcore, however many of the elements have constant up facies trends (Fig. 5.17). The boundary between LF4 and the overlying facies is sharp, with a clear change in biogenic content.

Overlying LF4 is LF5, a shell hash layer, which is dated between 7.3 and 6.2 ka cal BP, from 3 radiocarbon dates in cores 20VC (7.3 ka cal BP), 22VC (6.8 ka cal BP) and 07VC (6.2 ka cal BP) in the North Sound (Table 5.3). LF5 is a condensed shell hash layer with almost no sediment and formed almost completely of the gastropod *Turritella*. The chemical elements in this facies show significant changes from LF4, with large peaks evident in Ca/Ti and Fe/Ti content (Fig. 5.17). The boundary between LF5 and the overlying LF8 is sharp, with a clear decrease in the abundance of shell content. LF8 is composed of a dark grey/brown silt and sand (Fig. 5.12), coarsening upwards.

Magnetic susceptibility in this facies is higher than in any other area of the bay, reaching up to $8 \text{ SI} \cdot 10^{-8} \text{ m}^3/\text{kg}$. *Quinqueloculina spp.*, *Lagena spp.*, *Cibicides lobatulus*, *Planorbulina mediterraneanensis* and *Ammonia beccarii* are the dominant foraminifera species. There is a high relative and species abundance of intact specimens in LF8, although they are smaller than in all underlying facies. The geochemistry shows a clear trend of increasing Br/Cl content upcore in this facies. While it is the uppermost lithofacies, LF8 is not dated in this area (Fig. 5.26).

Chapter 6: Interpretation

The seismic stratigraphy will be interpreted first, working through each unit in detail. This is followed by a stratigraphical interpretation using the lithology, micropalaeontology (foraminifera), XRF results and radiocarbon dates for each individual lithofacies found in the sediment cores. This is then followed by sedimentation rates across different time periods following deglaciation, before building the regional stratigraphy of the different areas of the bay (Fig. 6.1).

6.1 Seismic Interpretation

6.1.1 Acoustic unit 1

This unit is the deepest in the bay and is interpreted as the acoustic basement. It is lacking in internal structure and outcrops are visible throughout the bay (Fig. 5.24), but particularly in the North and South Sounds (Fig. 5.23), this interpretation of unit 1 as bedrock is confirmed by the multibeam data (Fig. 3.2). In the north of the bay, this unit is part of the Galway granite complex, while the acoustic basement to the south is composed of limestone, split by a fault line running across the bay (Lees and Feely, 2016). The erosional boundary that exists between Units 1 and 2 is interpreted to have been created by glacial action during the last glacial maximum, in particular the advance and retreat of the ice sheet through the bay. None of the sediment cores reached this unit, however, the base of cores 07VC and 12VC come very close to the top of this seismic unit. It is possible that the pebbles and cobbles found in these cores are eroded from the bedrock surface, as they generally represent the same lithology as the underlying surface; granite in the North (Feely et al, 2003; Selby et al, 2004) and limestone in the south (Pracht et al, 2004). The overall topography of the bedrock in the bay appears to be defined by the structural geology of the area, rather than the erosive force of the ice which was present during the last glacial maximum, in that they tend to follow the trend of faults. There is no evidence of U-shaped valleys scoured out by ice, or any other features commonly created by glacial erosion (Fig. 5.24).

Seismic Unit	Lithofacies					RSL					C ¹⁴ Dates (ka cal BP)					Environment				
	Inner Bay	Mid Bay	Outer South Sound	Outer Central Bay	Outer North Sound	Inner Bay	Mid Bay	South Sound	Central Bay	North Sound	Inner Bay	Mid Bay	South Sound	Central Bay	North Sound	Inner Bay	Mid Bay	Outer-South Sound	Outer-Central Bay	Outer-North Sound
U3b	LF 8	LF 8	LF 8	LF 8	LF 8	←								2.2-0		Variable terrestrial input Temperate Marine Oxidic High energy				
	LF 7	LF 5	LF 5	LF 5	LF 5	←	←				X	4.1-7.4				Nearby river High Transgression energy	Estuarine/Marine	Nutrient rich	Variable energy	Transgression
	LF 6					←	←				X					Variable energy Subtidal High sediment supply	Low sediment supply	Oxidic	Nearby river	
		LF 2/ LF 3	LF 3	LF 3	LF 4/ LF 2		↖	↖	↖	↖		11.5	9.9-13.1	10		Transgression High energy Beach	Marsh-Estuarine	Nutrient rich	Transgression	
	LF 1					↖					X					Transgression	Anoxic Transgression	Low energy Oxidic High energy Beach Transgression		
U3a						←										High sediment supply Glacio-fluvial/Marine Deposition Transgression Variable energy				
U2	Glacial Advance and Retreat																			
U1	Bedrock																			

Figure 6.1: A summary of the stratigraphy in the bay, including the different seismic units, lithofacies, rates of sea-level rise and short descriptors of the environment. Reworked radiocarbon dates have been excluded, while the X represents facies where there are no radiocarbon dates available (0 represents present day). The angle of the arrow indicates the likely rate of sea-level rise, based on the interpretation of the evidence from each facies/unit.

6.1.2 Acoustic unit 2

This is the oldest identifiable sedimentary unit in the bay. Unit 2's chaotic/contorted reflectors, which are bounded by a high amplitude upper boundary, are indicative of ice contact deposits (Gilbert, 1985). Specifically, diffraction hyperbolae in this unit also suggests coarser grained material such as boulders, an indicator of glacial deposits. These features mean that unit 2 can be interpreted as diamict and based on the glacial history of the region (Coxon et al, 2017), is likely to be glacial till, related to the last glacial advance on the shelf. Further offshore of Galway other diamict has been cored and considered to be lodgement till laid down during the extension of the BIIS (Peters et al, 2015, 2016). In Wood's (2011) study, one core, VC07, comes close to the upper boundary of this unit. According to Wood's description, the base of this core is dominated by large pebbles. This corresponds with the evidence from this study, as core 20VC lies near the boundary of this acoustic unit and also contains pebbles at its base that may have been reworked from this unit. However, none of the cores in this study penetrated this unit so we cannot comment further on its sedimentary nature, other than to note that it must be older than 13.1 ka cal BP, the oldest radiocarbon date taken from the sediment cores in the bay.

This unit shows evidence of the formation of a channel/valley feature on its surface, running along the north coast, following the existing Galway fault line which narrows and deepens westward, from the north inner bay to the North Sound (Fig. 5.22). Based on the position of the ice sheet (Refs. in Table 2.1) and sea-level at the time, which was much further offshore (Brooks et al, 2008; Bradley et al, 2011; Kuchar et al, 2012), the channel appears to have been cut by glaciofluvial action during the retreat of the ice sheet. There is no other evidence of glacial landforms in this unit and it is therefore interpreted as a till sheet. The upper boundary of this unit shows erosional truncation and has likely been reworked by marine processes in the bay and may represent a transgressive surface.

6.1.3 Acoustic sub-unit 3a

Sub-unit 3a drapes and infills unit 2. Lenticular reflectors at the base of this sub-unit in the westernmost areas, suggest deposition in a shallow, variable energy, environment

which means the sea-level was much lower in Galway bay, as this unit is up to 70m below current sea-level in the outer bay. This is supported by the prograding infilling of depressions and valley features present at the base of this unit, as well as the glaciofluvially cut channel in the North Sound (Fig. 5.21 & 5.22). Further evidence for meltwater deposits are visible at Leenaum in Connemara, just to the south of Galway Bay. Here the glacial meltwater formed a delta (Thomas and Chiverell, 2006). Towards the top of this sub-unit, parallel-sub-parallel reflectors are more prominent suggesting a lower energy depositional environment (Fig. 5.21). Although it is thicker in the rest of the bay reaching up to 12.5m in the inner bay area, it is almost non-existent towards the westernmost areas of the North and South Sounds. This is likely because the fast movement of water through these channels has caused erosion or non-deposition. As no sediment cores penetrate this sub-unit it is impossible to determine its age. However, based on radiocarbon dates from LF3 in acoustic sub-unit 3b, this acoustic facies must be older than 13.1 ka BP. The upper boundary of this sub-unit has a clear medium amplitude reflector and the unit is conformable with the overlying unit, suggesting a period of changing deposition, without erosion. Ice extent projections for the region show that ice retreated from the bay between 16 – 15 ka cal BP and that Galway Bay was completely ice free by 15 ka cal BP (Clark et al, 2009; Schiele, 2017). This subunit may therefore represent this phase of the postglacial retreat. The infilling prograding nature of the reflectors in the North Sound channel, suggests a rising sea-level, while the infilling nature of this unit indicates meltwater deposits created by a retreating glacier, and marine deposits, in a deepening environment.

6.1.4 Acoustic sub-unit 3b

The top of this acoustic sub-unit represents the present-day sea floor. This sub-unit is found predominantly in the inner and mid-bay areas where it is at its thickest at 8.5m (Fig. 5.27) and is not common in the outer central bay or outer North or South Sounds (Fig. 5.24). As the strongest wave and current strengths occur in these areas of the bay, it is unlikely that deposition would occur here, and if it did, it would likely be quickly eroded. Parallel reflectors in this sub-unit represent a steady rate of

deposition, while the sigmoidal prograding clinofolds visible from the inner bay towards the South Sound (Fig. 5.23) represent a transgressive deposit (Mitchum, 1977). Sea-level rise was rapid enough to preserve the clinofolds and in a quiet enough environment to minimize erosion (Catuneanu, 2006). All of the cored material falls within this sub-unit, and radiocarbon dates are Holocene in a transgressive environment. This corresponds to the cores taken by Wood (2010) which also fall within this unit. As there is no seismic data available for the very inner bay, it is unknown if the cores taken by Novak (2017), and the borehole cores taken during the harbour extension project in Galway Bay extend deeper than sub-unit 3b.

The cores from this study, taken in the South Sound, suggest a lower energy depositional environment, unaffected by strong waves, in the late post-glacial and early Holocene period (Fig. 5.25). They correspond to a quieter depositional environment, with less erosion, which would have preserved the clinofolds. The thickness of this sub-unit, which is the thinnest in the bay at only 8.5m and covers at least the past 13,100 years and likely the past 15,000 years, suggests that the average sedimentation rate was likely less than 0.65mm/yr (possibly as low as 0.57mm/yr), in the mid and outer bay. Even compared with Novak's (2017) cores in the inner bay, which show a sedimentation rate in the early Holocene of 1-2mm/yr, the mid and outer bay appears to have been sediment starved. Although erosion could also account for a thinner sub-unit, the depositional sequence in the sediment cores from this study, appears to be intact throughout the bay.

6.2 Lithostratigraphical Interpretation

6.2.1 Lithofacies 1: Mud with occasional laminations

This sedimentary unit corresponds to the upper part of acoustic sub-unit 3b, and although LF1 has not been dated, further westwards in the inner sound the overlying facies has been dated to 13.1 cal ka BP. Considering this radiocarbon date, LF1 may have been deposited during the Woodgrange interstadial, between ~15 and 11 ka cal BP.

The dominant species of foraminifera in this facies, *Quinqueloculina sp.*, *Lagena sp.*, *Spirillina vivipara* and *Miliolinella subrotunda* (Table 5.2), represent a temperate, inner

shelf environment (marine to estuarine). In particular the dominance of the foraminifera *Miliolinella subrotunda* which is a shallow water species, at its northern limit in Ireland (Murray, 2003) suggests that this facies had a warm water influence. However, due to time constraints, this interpretation is based upon only one foraminifera sample and potentially may be under-representative of the microfossil component in this facies.

While finer laminated sediments such as mud and silt are commonly found in glaciomarine environments (Merritt et al, 1995; Ó Cofaigh and Dowdeswell, 2001; Peters et al, 2015), the absence of common indicator foraminifera species such as *Nonionella labradorica*, *Elphidium excavatum forma clavata*, or *Cassidulina reniforme* (Peters et al, 2015; Weilbach, 2018), suggests this is not the case here. Furthermore, there are low Fe/Ti and magnetic susceptibility values, which is in contrast with higher peaks that are sometimes observed in glaciomarine sediments in which ice rafted debris is commonly found (Richter et al, 2001; Peck et al, 2007).

The upwardly increasing Ca/Ti suggests an increase in marine carbonate content, while the decreasing Ba/Ca and Sr/Ca, indicative of freshwater inputs, suggest a shallow water environment that is deepening upcore. Together these proxies indicate an estuarine environment with a strong marine influence that is experiencing sea-level rise.

While the finer grain size typical of this facies can be found in deltas dominated by oceanic processes (Postma, 1995; Galloway, 1975; Bhattacharya and Giosan, 2003), the lack of shell, low number of foraminifera, and overall lack of any brackish water foraminifera, albeit from a single sample, suggests that, once again, this is not the case in Galway Bay.

The increase in S/Ti upcore represents an increase in terrestrial organic matter (Rothwell and Croudace, 2006) and anoxic conditions. Combined with the lack of bivalves and other species known to oxygenate the sediment through bioturbation, these anoxic conditions in the sediment may be preventing colonisation of the area by other organisms commonly found in this type of muddy habitat and may be influencing the lower relative abundance of foraminifera in the sample in this facies.

The fine grain size and the presence of predominantly intact foraminifera are indicative of low energy environments and sediments that are not strongly influenced by high velocity currents and waves. The influx of Si/Ti and S/Ti at the facies top indicates an increase in terrestrial input (Blanchet et al, 2007). The medium shear strength and wet bulk density measurements suggest a certain degree of compaction in the cores. It is possible that an increased terrestrial runoff in riverine material has provided an increase in angular grains, lessening the sorting of the sediments and allowing for compaction. The constant Fe/Ti trend upcore represents an unchanging terrestrial input of ferromagnetic content and a relatively constant grain size. The only elemental ratios that show a noticeable change between lithofacies 1 and the overlying LF3, are Ca/Ti and Si/Ti, suggesting a jump in marine carbonate content and a drop in terrestrial detrital material input to the bay. This may be due to rising sea levels and opening of the bay causing changes in the current patterns and more oxygenated sediments allowing for colonisation by more species. The changes between this lithofacies and the overlying facies are relatively gradual with no major fluctuations, suggesting a transition that is unmarked by extreme changes. Overall this lithofacies is interpreted to have been deposited in a semi-enclosed bay with low currents, in a sheltered, marine environment with a scarcity of biological material due to high terrestrial input causing anoxic conditions. All the data suggest an increasing marine influence upcore, likely due to rising sea-levels and an opening of the bay.

6.2.2 Lithofacies 2: Gravelly sand and silt

Lithofacies with the exception of one sample, which is found in the South Sound, is confined to the North Sound area (Fig. 5.24). The dates are contemporary with dates from the silty sand/sandy silt (LF3) in the South Sound and with the coarsening upwards sandy mud (LF4) in the North Sound area. This facies appears to be a time-transgressive unit that is migrating inland over time, as the older dates are found in core 20VC, which is further offshore.

Based on the presence of larger grains sizes including sand and gravel, these sediments were likely deposited in shallow, higher energy, environments. The rounded

cobbles in a fine to medium sand matrix indicate transport and may suggest a nearby shingle beach deposit, or strong currents (McLean and Kirk, 1969), something reinforced by the abundant broken shell and foraminifera tests.

The high Ba/Ca and Si/Ti and low Br/Cl and Sr/Ba ratios, which are the highest and lowest in the cores, respectively, represent a shallow water environment with more terrestrial influence, larger grain sizes, low marine organic content and low salinity levels (Rothwell et al, 2006; Cao et al, 2016; He and Xu, 2015). The fluctuating nature of the S/Ti content in this facies, as seen by large peaks and dips throughout the facies, suggests rapidly changing organic content, likely through changing fluvial input (Kasten and Jorgensen, 2000), also indicative of a nearshore environment. This corresponds to the Sr/Ca content in this facies, which is variable, indicating variability in the freshwater input.

The dominant foraminifera in this facies include *Textularia sp.*, *Sahulia conica*, *Quinqueloculina sp.* and *Miliolinella subrotunda* (Table 5.2). These are all marine or estuarine species and common in a nearshore environment (Naeher et al, 2012). *Quinqueloculina sp.* has been found to be indicative of mid-latitude, temperate environments in other areas of the UK (Horton et al, 1999), while *Miliolinella subrotunda* is at its northern limit in Ireland (Murray, 2003), indicating a relatively temperate water marine environment. The presence of the minor species *Planorbulina mediterraneensis*, primarily found within the photic zone, generally shallower than 30m (Murray, 2006), accompanied by the minor species *Haynesina germanica*, which prefers a brackish water habitat, is also suggestive of a nearshore environment. The shells used for dating this facies included *Scrobicularia plana*, an intertidal species that burrows in softer substrata of fluctuating salinity (Murray, 2006), and *Moerella balthica*, an intertidal species known for making a habitat in sandy substrates (Luttikhuisen et al, 2003; Murray, 2006). The increasing trend of Ca/Ti content is indicative of a strengthening marine influence towards the top of the facies (Sluijs et al, 2011). This correlates with the increasing trends of Sr/Ba and Br/Cl upcore, which show increasing levels of salinity and marine organic content. The S/Ti and Si/Ti values have a decreasing trend upcore and suggest a decrease in the terrestrial input, both organic and inorganic, probably due to decreased runoff towards the top of the facies.

The decreasing trend of S/Ti also indicates a move from a more anoxic to a more oxygen-rich environment. This suggests that the water is deepening upcore and there is a lesser terrestrial influence in this area of the bay, likely due to sea-level rise. Fe/Ti values show a low, constant to increasing trend upcore, fitting with a decrease in terrestrial input as well as the slight fining of the grainsize towards the top of the facies. In general, this shows a rising sea-level, an increase in marine influence and full connection of the bay with the Atlantic Ocean.

This lithofacies is found only at the core bottom and is generally a thinner facies than any of the others. This may be due to core penetration being insufficient to obtain a higher volume of material. The high p-wave velocity, low electrical resistivity and medium shear strength values all suggest that this sediment is relatively compacted. The radiocarbon dates in this facies in core 20VC are out of sequence, with the younger shell date of 11.5 ka cal BP located deeper in the facies than the foraminifera date of 12.6 ka cal BP (Fig. 5.30), suggesting that there is reworking in this facies. Although every attempt was made to avoid picking foraminifera species that were damaged or appeared transported, it is likely, due to the high number of specimens used for dating, that this sample may have contained foraminifera that were reworked from underlying sediment. The shell dates in this facies place it between 11.7 and 8.8 ka cal BP.

Overall, the combination of mixed sediments, intertidal foraminifera and burrowing molluscs alongside reworked, compacted sediments, suggests that this facies is a shoreline deposit, with fluctuations in terrestrial input, but an overall reduction towards the facies top.

As no data from the elemental ratios are available on the actual boundary between this facies and the overlying lithofacies 4, no obvious changes are evident. The boundary between lithofacies 2 and the overlying lithofacies 5 is quite gradual in the geochemical data, indicating a transition without significant geochemical changes. However, the transition between LF2 and LF5 in the sediment composition indicates a sharp change, likely a shift to a lower energy environment, due to the significant increase in intact shell content, particularly gastropods.

6.2.3 Lithofacies 3: Silty sand / Sandy silt

Lithofacies overlies lithofacies 1 in core 03VC but forms the base of all other cores. The water depth of this facies is similar to both LF1 and LF2, and the radiocarbon dates in core 13VC of 13.1 and 9.9 ka cal BP, correspond with the timeframe from LF2 and LF4. Based on the fine grain size (silt and fine sand) and presence of both broken and intact foraminifera tests, it is likely that LF3 was deposited in higher energy conditions than the underlying LF1 but lower energy conditions than LF2. The grain size throughout the facies is uniform, supported by the relatively unchanging Fe/Ti content upcore.

The species of foraminifera found in this facies are commonly found in shallow water, marsh and subtidal areas (Table 5.2). More specifically, *Haynesina germanica* is indicative of brackish intertidal marsh and estuarine conditions in which muds and silts accumulate (Murray, 1991). *Quinqueloculina sp.* is found in intertidal environments (Horton et al, 2006) and *Ammonia beccarii* are tolerant to low salinities, such as those in brackish conditions. They are at the limit of their northern range in Ireland (Murray, 1979, 1991), suggesting that this is also an environment with temperate waters (similar to those of modern conditions). *Jadammina macrescens* is only found in marsh areas, in <10m water depth (Horton et al, 2006), while *Elphidium excavatum* is a species tolerant of brackish conditions and is abundant in areas with eutrophic conditions, such as tidal flats (Murray 1971; Nooijer et al, 2008). Overall, the species found in this facies, particularly at the bottom, are commonly found on middle to low marsh areas and are indicative of temperate temperatures and low salinity (Horton and Murray, 2007). This facies also has a very high diversity and relative abundance of foraminifera in the cores (Appendix 2), which is suggestive of a high level of productivity.

The Ba/Ca, Sr/Ca, Br/Cl and Sr/Ba content in this facies all indicate a shallow water environment, with low marine organic content and salinity. The changing species types upcore suggests an increasing marine influence and a move towards a more estuarine environment with the introduction of *Lagena sp.*, while the increase in size and abundance of the dominant species suggests higher productivity, possibly from increased nutrients carried into the bay by ocean currents. The reduction of *Nonionella turgid*, a species that tends to prefer more anoxic environments, as well as

the overall increases in size and diversity of foraminifera suggests an increase in the oxygen levels upcore (Bernhard and Sen Gupta, 1999; Naeher et al, 2012). This is supported by a decrease in S/Ti upcore, which indicates a drop in terrestrial organic content and a more oxygen-rich environment upcore. Again, this indicates an opening up of the bay and an increased marine influence.

The reduction of *Elphidium excavatum* upcore is likely related to a reduction in the sediment input, as this species prefers high loads of fresh organic material (Nooijer et al, 2008). This may be due to a reduction in terrestrial runoff, as the decreasing Si/Ti upcore suggests a decrease in detrital material. This reduction in Si/Ti is seen until near the facies top, where there is an increase in Si/Ti, coinciding with a similar decrease in Br/Cl, suggesting an influx of terrestrial detrital material. As there are no other significant changes in the chemical or biological proxies in the facies, this may indicate a wetter climate and increased hinterland runoff.

The p-wave velocity and shear strength values decrease from the bottom to the mid facies, indicating that there was compaction of this facies near the base. Compact sediments are also more likely to experience anoxic conditions as there is less bioturbation and therefore ventilation (Aller and Yingst, 1978; Kristensen and Blackburn, 1987). The trends visible in the Ba/Ca, Ca/Ti, Sr/Ba and Br/Cl content upcore shows a deepening environment with increased carbonate content, salinity and marine organic content. This suggests a continuous increasing marine influence. Overall this facies is interpreted to have been a sheltered, sub-tidal environment with an increasing marine influence caused by increasing sea-level, leading to estuarine conditions towards the facies top. The increase in oxic conditions coupled with sea-level rise, suggests a continuation of the opening, and increased circulation, in the bay. There is a seamless transition in the elemental data between lithofacies 3 and the overlying lithofacies 5, suggesting no abrupt changes and a continuation in deposition. However, the visible changes in biological material are sharp, with a distinct increase in intact shell content showing the environment favours the colonisation by gastropods, possibly due to a change in the sediment supply.

6.2.4 Lithofacies 4: Coarsening upwards sandy mud

The only radiocarbon date in LF4 was from the base of core 22VC, at 10 ka cal BP. This date is contemporary with the deposition of both the gravelly sand and silt (LF2) and silty sand/sandy silt (LF3) units. However, the sediment in LF4 was deposited in a much deeper environment.

This facies is composed of coarsening upwards, sandy mud and it is interpreted as sediment deposited in a fully marine environment. The foraminifera content in this facies shows a marked transition from the underlying lithofacies 2, with none of the dominant species remaining the same and a decrease in abundance and diversity (Table 5.2; Appendix 2) This, along with the preservation of intact bivalves and lack of fragments, suggests low current velocities and wave strength. The dominant foraminifera species in this lithofacies include: *Lagena spp.*, *Nonionella turgida*, *Stainforthia fusiformis* and *Bolivina spp.* (Table 5.2). *Lagena spp.* is a delicate species commonly found on the shelf, preferring more marine conditions with salinities >32ppm (Murray, 1979; Jingxing and Luping 2012). *Stainforthia fusiformis* is found in most types of subtidal clastic sediments from mud to sand, between 5-16°C (Collison, 1980; Murray, 1986) and salinities generally above 28ppm (Gustafsson and Nordberg, 2000) and is a known opportunist of organically enriched sediments (Gooday & Alve, 2001; Duijnsteet et al, 2005). *Nonionella turgida* is known to reflect higher chlorophyll concentrations in the water (Gustafsson and Nordberg, 2000; Murray, 2006) but is intolerant of low oxygen environments (Brattstrom et al, 2015). *Bolivina spp* are resistant to short term anoxia but cannot survive in low oxygen environments for longer periods of time (Alve, 1995). The presence of *Rosalina praegeri* and *Quinqueloculina spp* also suggest a temperate environment (Austin and Kroon, 1996). The presence of these foraminifera species together with low S/Ti levels, indicate less terrestrial organic content and a more oxic environment. These foraminifera species also suggest a rising sea-level. This may have caused an increase in circulation and oxygenation of the water in the bay. This is supported by the trends upcore in Ca/Ti, Br/Cl, and Ba/Ca (Fig. 5.10), which show an increase in the carbonate content, marine organic content, and salinity, corresponding to an increasingly open marine environment. The Sr/Ca trend is variable and suggests that it is being affected by

freshwater input to the bay. This is supported by peaks in other proxies for terrestrial input, including S/Ti and Fe/Ti.

The scarcity of shell (both bivalve and gastropod) species and low abundance of foraminifera, found in this temperate, nutrient rich, well oxygenated lithofacies suggests that another factor is causing species not to colonise an otherwise ideal habitat. This is likely an indication of a high sediment supply to the area, supported by the sedimentation rate in this facies, one of the highest in the bay (0.78mm/yr), which would also explain why many of the dominant foraminifera species that are present are opportunistic foraminifera that can survive in a higher stress environment.

This facies has the lowest p-wave velocity and lowest electrical resistivity and shear strength measurements in the bay (Fig. 5.9 & 5.10). This may be due to the relatively unchanging nature of the well oxygenated sediment causing an increase in porosity. Although the p-wave velocity is low, there are large peaks throughout the facies and correspond to changes in the shear strength measurements. It is possible that fluxes of sediment led to less well sorted material and caused some compaction at various points in this facies. The low magnetic susceptibility values correlate to the low Fe/Ti and Si/Ti content and also correspond with the relatively uniform grain size throughout the facies.

Overall, this is a low energy, oxygenated environment with a large sediment supply and an increase in sea level upcore. The boundary between this lithofacies and the overlying shell hash (LF5) is sharp with major changes in nearly all elements. This indicates a significant change in the depositional environment represented by a sharp boundary that is visible in the lithology, chemistry and biology, across the bay. The presence of this facies, only in the North Sound, in the cores in the greatest water depth, may be due to the steep gradient of the topography in this area. This may have meant that even though sea-level was rising, the deposition of these sediments was laterally confined (Swift, 1976; Kidwell, 1989).

6.2.5 Lithofacies 5: Shell hash

The shell hash (LF5) has been dated across the bay, between 7.4 to 4.1 ka cal BP, with dates of 7.4 and 4.4 ka cal BP taken near the base and top of this unit respectively, in

core 10VC. Although this facies is found at varying depths, from 33.2 to 57.2m, the dates in core 10VC indicate an environment suitable for the deposition of *Turritella* over a prolonged period of time. These dates are also contemporary with *Turritella* layers found in cores from other locations, including those found in Scotland and France (Baltzer et al, 2015) and may be indicative of wider regional climatic trends. This facies, dominated by shell, both gastropods and large intact bivalves in layers, is interpreted as a deposit not in the surf zone. The overwhelming presence of *Turritella communis*, a burrowing filter feeder that does not survive in turbid waters (Yonge, 1946) and is predominantly found on soft bottoms (Hayward and Ryland, 1995), suggests that there was a change in the level of sediment in the water column, compared to the underlying lithofacies. This species indicates a lower sediment supply in a quieter depositional environment. The presence of molluscs such as oysters, cockles and mussels show that the environment was estuarine with a significant freshwater flow, in the subtidal range (Tully and Clarke, 2012; Hayward and Ryland, 1995). This is reinforced by the foraminifera that are dominant in this facies: *Quinqueloculina spp.*, and *Haynesina germanica*. These are commonly found in subtidal and brackish/estuarine conditions (Horton et al, 1999; Murray et al, 1971). Due to the size and abundance of the molluscs in this facies, a high level of nutrients and an oxygenated environment would have been necessary, while the presence of *Quinqueloculina spp* suggests a temperate environment (Horton et al, 1999). The intact shell beds and relatively intact foraminifera species in this facies combined with the grain size, ranging from medium/fine sand to silt, suggests a lower energy environment than the underlying gravelly sand and silt (LF2) but a higher energy environment than the underlying sandy silt/silty sand (LF3) and the coarsening upwards sandy mud (LF4) units.

The chemical data in this lithofacies are highly variable with gaps throughout. This is due to the sheer volume of shell and subsequent uneven scanning surface. This means that the chemical data for this lithofacies needs to be treated with caution. However, general trends can still be recognised.

The Ca/Ti levels show an increasing trend upcore that could be attributed to an environment that is becoming deeper up facies or to the exceptionally high content of

calcium carbonate in the shell hash. Although the Ca/Ti content may be due to the composition of this facies, the trends in Ba/Ca, Sr/Ca, Br/Cl and Sr/Ba also support increasing water depths, with increasing marine organic content and salinity up facies. Fe/Ti content generally remains constant or increases slightly upcore, indicating less ferromagnetic material. This is an inverse relationship to the Si/Ti levels which show a decrease. Since grainsizes in this facies are variable, it is likely that this trend is due to terrestrial runoff, in particular from a source high in silica and lower in iron. This source appears to be more dominant in the deeper water as the North Sound cores experience peaks in iron input. In 2 of the cores, 03VC and 06VC the Fe/Ti concentration is decreasing up facies. This may be due to their geographical locations in the bay, as 06VC is close to Inishmor and 03VC is further towards the inner bay. This may indicate different sediment sources but is more likely an indication of a decrease in the fine sediment and a coarsening upwards trend (Fig. 5.12). The variable p-wave velocity and low gamma density measurements are most likely due to the sheer abundance of shell in this facies, causing a high level of disturbance in the readings and the fact that the shell is much less dense than sediment. Overall, this facies, which is saturated with shell, is interpreted as a medium energy environment with high productivity and an oxygenated water supply, during a period of sea-level rise. The changes in biological content between this facies and the overlying poorly sorted, coarsening upwards silt to coarse sand (LF8) are significant, while the chemical changes are minor, with the transition interpreted to be due to a change in sediment supply, possibly due to rising sea-levels and changing circulation in the bay, as well as, terrestrial runoff. The chemical changes between this facies and the underlying facies are also gradual, with the exception of the coarsening upwards sandy mud (LF4), in the North Sound, which shows a marked change across all chemical elements (Fig. 5.10), and represents a very different environment, with a much higher sediment supply.

6.2.6 Lithofacies 6: Interbedded sandy silt and silty sand

LF6 is interpreted to be a subtidal environment, with the laminated, interbedded nature of this facies indicative of variable currents capable of moving and depositing different sediment sizes. This is supported by the level of preservation of the

foraminifera species, with a combination of broken and intact tests. However, as only 2 microfossil samples have been examined in this facies, caution has been used with the use of foraminifera species as environmental indicators. Instead interpretations were based primarily upon the geochemical and sedimentary information and reinforced by the microfossil content in this facies, which also indicates a subtidal area, with species such as *Ammonia beccarii* and *Elphidium excavatum* composing a majority of the facies and *Haynesina germanica* present in lesser numbers (Table 5.2). *Elphidium excavatum* is a species that flourishes in environments with a large volume of fresh organic material and is commonly found in strong tidal areas (Murray, 1971; Nooijer et al, 2008). *Spirillina vivipara*, a species found in smaller amounts in this facies, is a species that attaches itself to objects, such as seaweed, and can be found in estuary mouths (Murray, 2003). *Haynesina germanica* and *Ammonia beccarii* are species commonly found in brackish conditions (Murray, 1979). These species are all commonly found in temperate environments (Murray, 1979, 2003; Holzmann and Pawlowski, 2000). The brackish water foraminifera indicate the presence of a nearby freshwater input during the deposition of this lithofacies. This is supported by high levels of S/Ti, indicating a high organic content in the environment. Although other processes such as river floods and storms could generate this type of environmental conditions, the low Ba/Ca and Sr/Ca ratios suggest no massive freshwater input events. Storms affecting areas this far into the bay would have been very powerful and would likely have caused higher breakage in the microfossil content.

Shell fragments and extensive bioturbation, indicative of tidal flat areas (Reise, 1985; Vernberg, 1993; Dittmann, 1996; NPWS, 2006), are evident throughout the facies, however, no intact shells have been found. This suggests that there is a high level of sediment that may be preventing filter feeders from colonising this area. Medium shear strength values in this facies (Fig. 5.20), in comparison with the rest of the bay, indicate a degree of compaction in the sediment. This may have been caused by the variations in grain size (from medium to fine sand and silt) leading to a lower level of sorting and higher compaction.

The overall trends of decreasing Ba/Ca and increasing Br/Cl and Sr/Ba content upcore show a deepening environment with increased marine organic content and salinity,

suggesting a rising sea-level. The Ca/Ti, Sr/Ca and Si/Ti content is constant upcore until the top 30cm of this facies where an increase in Ca/Ti and a decrease in Sr/Ca indicate a sudden deepening of the environment, while an increase in the Si/Ti indicates a sudden rise in detrital input. The deepening environment corresponds with the overall trend of rising sea levels. The rise in detrital input at this point may be due to the migration of a river system and a change in the deposition of terrestrial material. While there is no seismic data available for the inner bay area in this study, Clarke (2013) recognises migrating palaeo-channels in his seismic data in the inner bay, though he attributes this to deglacial and early Holocene changes. The evidence from this study suggests that this facies is older than 2.2 ka cal BP, as the overlying LF8 has been dated in the outer bay. As this environment is not terrestrial, sea-level was at least at -31m, something which is unlikely to have been true before 8 ka cal BP, based on GIA derived RSL predictions for the bay (Brooks et al, 2008; Bradley et al, 2011; Kucher et al, 2012). This places the deposition of this unit within the mid-Holocene, a period known for fluctuating wet and dry climatic events (Kaufmann et al, 2004; Bjune et al, 2005; McDermott et al, 2005; Caseldine, 2006; Magny et al, 2006; Roland et al, 2015; Wanner et al, 2011). The variability that is evident throughout the chemical analysis, with peaks and dips common in almost all the elemental proxies, also supports a dynamic tidal environment with fluctuating terrestrial input. Overall this facies represents a variable energy subtidal environment, in the vicinity of a river.

6.2.7 Lithofacies 7: Silty sand

Like the underlying LF6 there are no radiocarbon dates for LF7, but it is interpreted to have been deposited in the mid-Holocene, based on the water depth which it is found in, and the constraining date for the overlying facies of poorly sorted, coarsening upward silt to coarse sand (LF8) in the outer bay dated to 2.2 ka cal BP (Fig. 5.25). LF7 is interpreted to be a shallow water deposit near the mouth of a river. The broken shell fragments throughout this facies suggest a high energy environment. The presence of *Elphidium excavatum* also suggests a high energy environment with an abundant sediment supply (Murray, 1971; Nooijer et al, 2008), while the grain size shows a distinct coarsening from the underlying interbedded silty sand and sandy silt

(LF6) (Fig. 5.14), which may indicate either shallowing or an increase in energy. The chemical proxies of Si/Ti and Sr/Ba, which are high and low respectively, suggest a large influx of terrestrial material and a fresher water environment.

The drop in abundance of foraminifera in this facies, in comparison to the underlying unit, may be due to an increased sediment supply, as the foraminifera species show no indication of a decrease in nutrients, however, as there is only one foraminifera sample, this may not be representative of the entire facies. The S/Ti content is low, suggesting a relatively well oxygenated environment. The Si/Ti content supports this as it is the highest in the core, in this facies, showing a jump from the underlying facies (Fig. 5.15). Alongside the increase in grain size, this is interpreted as a large influx of detrital material. The sharp change in density evident in the x-ray (Fig. 5.15), between this facies and the underlying interbedded silty sands and sandy silt (LF6), also supports a change from tidal/subtidal to shallow water.

The dominant foraminifera in this facies include: *Haynesina germanica*, *Quinqueloculina spp.* and *Ammonia beccarii* (Table 5.2). These are all common species in intertidal/subtidal areas, in particular in brackish conditions (Murray, 1979), suggestive of an environment with a stronger freshwater influence, at least during the period of deposition near the facies top.

Ca/Ti levels show a strong increase in the carbonate content up facies alongside a decreasing trend in Ba/Ca and Sr/Ca trends upcore is representative of a deepening environment and sea-level rise. The Br/Cl content remains constant upcore (Fig. 5.15) suggesting an overall unchanging level of marine organic content throughout this facies.

The high levels of Ba/Ca, in particular at the base of the facies, which are the highest in the core and which shows a significant increase from the underlying facies, indicate a significant freshwater influx, something that correlates with the significant decrease in Sr/Ba, a salinity indicator, from the underlying facies. The Sr/Ba remains low throughout this facies and immediately returns to previous levels in the overlying facies, suggesting that this was a period of lower salinity caused by a freshwater influx rather than a sea-level fall.

Overall this facies is interpreted to represent a high energy shallow water deposit characterised by a large increase in freshwater and detrital material, likely from a riverine source during a flooding or storm event.

6.2.8 Lithofacies 8: Poorly sorted, coarsening upwards silt to coarse sand

Lithofacies 8, which represents the core top across the bay, is dated mid facies at 2.2 ka cal BP in the outer bay, in core 10VC, suggesting this facies is at least 2200 years old, though it is likely older than this.

This facies represents the modern seafloor and is interpreted as a fully marine, coarsening upwards, silt and sand unit deposited in a high energy environment. The range of grainsizes, from sandy silt to coarse sand, and abundant shell fragments in this unit supports the interpretation of a high energy environment, likely affected by both strong currents and waves. This is supported by the thickness of the facies, which is thinnest in the deeper areas of the North Sound, corresponding to the stronger currents in this area (Fig. 3 & 5.26). Many of the cores with coarser lithologies are found near the coastline around the bay and are likely to have terrestrial sediment sources. A difference in sediment sources due to the varying core locations may be the cause of the range in the p-wave velocity, magnetic susceptibility and electrical resistivity, all of which are highly variable. This is supported by the S/Ti content which is also highly variable, suggesting changing terrestrial organic content throughout this facies.

Many of the cores in the North and South Sounds show a decrease in S/Ti up facies while the cores in the mid-inner bay area show an increasing trend, likely due to their closer proximity to land. The lack of gastropods, in particular *Turritella communis*, suggests that there is an abundant sediment supply, making the environment intolerable for these filter feeders. The diverse range of foraminifera and abundance of bivalve shells suggests a high level of productivity. Many of the dominant foraminifera species found are common marine and inner shelf species, while *Quinqueloculina spp.* and *Ammonia spp.* are found in warm temperate waters (Horton et al, 1999; Murray, 1971, 1979). *Cibicides lobatulus* and *Planorbulina mediterraneensis* are epifaunal, known to cling to substrates, including seaweeds (Murray, 1979). This

suggests that the depositional environment was temperate and marine, with abundant organic material, representing optimum environmental conditions for a range of species. Although the foraminifera species are more diverse and abundant, they are also smaller in size than those found in other facies. It is possible that while there is a high level of productivity, increased competition for food has meant smaller test sizes (Lipps, 1983).

The Ca/Ti is high throughout this facies and shows a decreasing trend upcore. The high content of Ca/Ti corresponds to the abundant shell fragments and layers of intact shells throughout the facies. The decreasing carbonate content upcore may be tied to shell layers that, in all cores analysed with XRF, have larger shell content nearer the base of the facies. Ba/Ca and Br/Cl content are, respectively, the lowest and highest in all cores in the bay in this facies and are decreasing and increasing upcore. This represents a deepening environment and increase in marine organic content, also suggesting that this facies represents a rising sea-level. This is reinforced by increasing salinity levels upcore, with Sr/Ba showing an increasing trend (Fig. 5.18). Conflicting with this is the Sr/Ca trend which shows variability, but a generally increasing trend up facies. However, this may be due to an increase in freshwater to the bay, possibly through increased hinterland runoff. This corresponds to the increasing trend in Fe/Ti content and the variability in the other terrestrial proxies. Si/Ti and Fe/Ti content decreases and increases upcore, respectively, something which does not appear to be related to the grain size. This represents a change in the provenance of detrital input upcore and suggests a terrestrial source that is higher in iron. This increase in terrestrial material may be due to a wetter climate, or a change in the land use of terrestrial habitats, such as the increase in human settlements and the implementation of farming in the area, causing increased runoff into the bay (Ren et al, 2009).

Overall this facies suggests a fully marine environment, with abundant resources available for colonisation by various species. This may suggest a good level of circulation in the bay, providing oxygenated waters and a high level of productivity across the bay. The changes in grain size within this facies may also be due to the way

the currents have transported material around the bay, winnowing of the finer sediments in areas with higher currents and stronger waves or marine energy.

6.3 Sedimentation Rates

Sedimentation Rates in Galway Bay are based on the literature for known ice limits, deglaciation and ice retreat from the bay (References in Table 2.1), as well as radiocarbon dates taken in different lithofacies in the cores in this study. These sedimentation rates cover the time period from when ice began to retreat from the bay until present day.

The sedimentation rates during the deglacial period are <12.5mm/year, based on the maximum thickness of seismic unit 3a (12.5m) and a 1000-year time period from 16 - 15 ka cal BP, based on the accepted literature of when deglaciation in the bay began and when the bay was ice free. For the period from the post-glacial to present day the sedimentation rate is <0.57mm/year, based on the maximum thickness of the seismic unit 3b (8.5m) across a 15,000-year time period, from when the bay is accepted to have been ice-free. The sedimentation rate during the post-glacial to early Holocene is 0.1mm/year, based on the radiocarbon dates of 13.1 and 9.9 ka cal BP and the thickness of the facies between these 2 dates (220cm). The sedimentation rates between the early-mid Holocene in the north of the bay vary between 0.19 and 0.78mm/year. The former was calculated based on radiocarbon dates between 11.7 and 7.3 ka cal BP, taken in LF2 and LF5, respectively, While the latter was calculated based on radiocarbon dates between 10 and 6.8 ka cal BP, taken in LF4 and LF5, respectively. The difference in sedimentation rates during this period is clearly based on the lithofacies, with the deeper, western most area of the bay experiencing much higher sedimentation rates than the more easterly beach environment. In the south of the bay the mid-Holocene sedimentation rate is 0.25mm/year, based on radiocarbon dates of 7.4 and 7.4 ka cal BP in LF5 and the thickness of the facies between these dates (0.75cm). The sedimentation rate for the late Holocene is 0.47mm/year, based on a single radiocarbon date at 2.2 ka cal BP, taken in LF8 and the thickness of the facies between this date and the core top, which is taken to represent present day.

All of these sedimentation rates assume that no erosion has taken place in order to provide estimates of the sedimentation rates in the bay.

Table 6.1: A table showing the sedimentation rates in Galway Bay from deglaciation to present day. These rates all assume that there is no erosion of sediment occurring within the bay and have assumed that the core top/seabed represents present day. Rates in Blue have used the literature to obtain time ranges. Rates in Black are those where 2 radiocarbon dates are present within a sediment core. Rates in Red have a single radiocarbon date.

Location	De-glacial	Post-glacial	Early-Holocene	Mid-Holocene	Late-Holocene	Description
Seismic Unit 3a	<12.5mm/yr					Average rate based on the maximum thickness of unit 3a, between 16 and 15 ka cal BP (accepted dates from literature for when deglaciation began to when the bay was ice free).
Seismic Unit 3b		<0.57mm/yr				Minimum average rate based on the maximum thickness of unit 3b, from the post glacial period (15 ka cal BP) until present day.
Core 13VC			0.1mm/yr			Average rate based on the radiocarbon dates between 13.1 and 9.9 ka cal BP, both found within lithofacies 3 (sandy silt/ silty sand).
Core 20VC			0.19mm/yr			Average rate based on the radiocarbon dates between 11.7 and 7.3 ka cal BP, found within lithofacies 2 (gravelly sand to silt) and lithofacies 5 (shell hash).
Core 22VC			0.78mm/yr			Average rate based on the radiocarbon dates between 10 and 6.8 ka cal BP, found within lithofacies 4 (coarsening upwards sandy mud) and lithofacies 5 (shell hash).
Core 10VC				0.25mm/yr	0.47mm/yr	Average rates during the mid-Holocene based on the radiocarbon dates between 7.4 and 4.4 ka cal BP, both found within lithofacies 5 (shell hash). The late-Holocene rate is based on the radiocarbon date at 2.2 ka cal BP lithofacies 8 (poorly sorted, coarsening upwards silt to coarse sand) and present day.

6.4 Sequence stratigraphy interpretation

6.4.1 Inner bay stratigraphy

The analysis of seismic data in the inner bay is restricted to areas westward of Ballyvaughan due to unavailability of seismic lines further eastwards (Fig. 3.5), while these data had been acquired by INFOMAR, the portion from the inner bay was lost, and no other studies using this data have been published. There is almost no evidence of the bedrock unit in the inner bay, while the till unit is also sparse and confined to near the boundary of the mid-bay. Unit 3a is at its thickest (up to 12.5m) where it is visible along the mid-bay boundary. The concentration of 3a in this area suggests that as deglaciation in the bay was occurring there was high levels of glaciofluvial deposition, depositing large volumes of sediment, possibly along a paleo river system in the inner bay (Clarke, 2013). Where the sediment is thickest in unit 3a, there is less sediment deposited as unit 3b, though it is still up to 4m thick in the centre of the bay. Along the northern coastline, once again very close to the mid-bay boundary, there is an increase in the volume of sediment (~8m thick). This suggests that a palaeo river system in the inner bay may have migrated towards the north after total deglaciation in the bay. A rising sea-level may also have contributed to the lower levels of deposition in this area, as the coastline moved inland.

LF6 is the oldest facies cored in the inner bay. This layered/laminated, inter-bedded sandy silt and silty sand unit with shell fragments and an abundant mixture of broken and preserved foraminifera tests is representative of a variable energy, tidal flat. The foraminifera species and elemental data indicate a nearby riverine source and a high sediment supply. The chemical elements show a constant sea-level upcore until near the facies top, where a deepening environment is evident. This implies that sea-level was static at the base of this facies (28.5m bsl), and then started to display a deepening trend near the top. Although no dates were obtained from this facies, on the seismic lines it is seen to correspond to (the middle) of U3b (Fig. 6.1). In the core, the boundary between LF6 and the overlying LF7 is sharp.

LF7 is a silty sand facies with abundant shell fragments. The chemical data and foraminifera species suggest a shallow, high energy environment with an abundant sediment supply, near a riverine source, that has input a significant level of freshwater.

The elemental trends suggest a deepening environment upcore. However, the salinity levels remain constant throughout this facies, and there is significant terrestrial indicators in this facies, perhaps suggesting a slower sea-level rise. The boundary between LF7 and the overlying LF8 is sharp.

Overlying LF7 is LF8, a silty sand facies with abundant shell, both intact in layers and fragments. The elemental data and foraminifera species abundance and diversity suggest a fully marine, oxygenated facies with high terrestrial input and rich in nutrients, deepening upcore. There is no evidence of significant changes in lithology or biological content that would indicate the speed of sea-level rise (Fig. 6.1).

6.4.2 Mid-bay stratigraphy

The limit of penetration in the mid bay, unlike the inner bay, is generally not represented by glaciofluvial deposition. In this area, glacial till is evident as a thinner sheet (~4m) that overlies the bedrock, at ~25m bsl. Unit 3a is present across the inner bay, but thickest in the South West and North West directions of the Sounds (Fig. 5.23B & 5.23C). This pattern of deposition follows the topography with these areas deeper than other parts of the mid bay, suggesting that once again the glaciofluvial deposition was enhanced by the presence of palaeo channels, with the inner bay representing a deltaic system and the final outwash present in the mid bay.

Unit 3b is thickest in the mid-bay, once again in northwest and southwest directions, overlying the glaciofluvial unit. This indicates that rising sea-levels are depositing sediment and infilling the topographically lower South Sound area and the glaciofluvially cut palaeochannel along the northern shoreline of the mid-bay. The thickest deposition in unit 3b also corresponds to a prolonged period of stable conditions during a sea-level slowstand that corresponds to the deposition of LF3. The mid-bay area contains the highest number of different lithofacies. LF1, LF2, LF3 and LF5 are found in the South Sound area of the mid-bay, while LF8 is found across the entire mid-bay area.

LF1 is found in only 1 core, O3VC, below the oldest dated lithofacies (LF3) in the bay. However, its age cannot be confirmed in the mid bay as the dated facies was from a core lying further westwards, which is slightly deeper and does not contain LF1. LF1 is

composed of silty mud, with occasional laminations and almost no shell content. When combined with the foraminiferal and elemental data, this facies is found to represent an anoxic, low energy, estuarine/marine environment (Fig. 6.1) with a significant terrestrial input and deepening upcore. There are no drastic changes upcore in this facies, suggesting a stable environment. This may also suggest that sea-level rise was constant upcore. Overlying LF1 is LF3, composed of silty sand with shell fragments and is interpreted to be a middle-low marsh, low energy, high productivity, sheltered environment which deepens upcore. LF3 is the oldest dated facies in the bay, between 13.1 and 9.9 ka cal BP, but has not been dated directly in the mid-bay area. As the transition between the underlying facies and this facies shows a clear increase in the abundance and diversity of foraminifera species, minor elemental changes and a change in grain size, this may represent a period of faster sea-level rise (Fig. 6.1). This continues upcore in the facies, with steady changes in the geochemistry and foraminifera.

Contemporary with LF3 is LF2, which is dated at 11.5 ka cal BP, in core 12VC. LF2 is composed of gravelly sand and silt, with cobbles reaching up to 11cm in diameter, and abundant shell fragments. The lithological, foraminiferal and elemental data for this facies is suggestive of a high energy shoreline deposit, at a depth of 42.6m bsl, with a strong terrestrial input, that is deepening upcore. Overlying LF2 or LF3 is LF5, found in all mid-bay, South Sound cores. This shell hash unit, with an abundance of intact *Turritella sp.*, represents a medium energy, marine environment with a low sediment supply, which is deepening upcore. Dates from LF5 are 5.6, 4.1 and 0.9 ka cal BP, although the 0.9 ka cal BP is considered to be reworked from the overlying facies and the date of 4.1 ka cal BP is considered to represent the top of this facies.

While the other cores in the mid-bay area only contain LF8, it is possible that penetration of the vibrocorer merely did not extend far enough to capture LF1, 2, 3 & 5 in cores 11VC and 16VC as they are both under 0.7m. It is also possible that these cores represent a different depositional environment.

Overlying LF5 is LF8, a coarsening upwards sandy silt to fine sand with abundant shell fragments, found in all mid-bay cores. The facies represents a more open bay, in a high energy, high productivity, oxygen rich environment, that is deepening upcore (Fig.

6.1). Although there are no dates in this facies in the mid bay, it represents the modern-day seafloor and most recent deposit in this area.

6.4.3 Outer bay – South Sound stratigraphy

The most extensive seismic unit in this area is the bedrock, which is outcropping in the outer South Sound. Along the sides of the Sound there is a thin drape of other sedimentary units, generally glacial till and marine sediments, which are less than ~4m thick (Fig. 5.23). The lack of sediment, coinciding with the strongest current and wave velocities in the Sound (Fig. 4.3) suggests that erosion is extensive, and sediment has been removed. A drop in current and wave velocities and the presence of prograding clinoforms moving eastwards represents an increase in sediment deposition and a reduction in erosion (Fig. 6.1). This is also seen in the thickness of each lithofacies in the cores, becoming progressively thicker moving eastwards (Fig. 5.24).

Of the 3 sediment cores in the outer bay, South Sound, two cores (13VC and 14VC), contain LF3, LF5 and LF8, while one core (15VC) contains only LF8. It is highly likely that this is due to the penetration of the corer.

LF3, is the oldest facies in the outer bay, South Sound, with dates of 13.1 and 9.9 ka cal BP, taken in core 13VC. The foraminifera species abundance, diversity and preservation as well as the elemental trends for this unit suggests a shallow, anoxic, nutrient rich, middle-low marsh environment, at depths between 39m and 43m, with a high terrestrial organic input at the base of the facies. This changes upcore, with increased oxygenation and a deepening towards an estuarine environment. This facies is found only in the South Sound, in both the mid and outer bay areas. The transition between this facies and the overlying LF5 is sharp, with an increase in shell content.

LF5 is a shell layer, containing both gastropods and intact bivalve shells, which is dated in the outer bay, South Sound to 6.4 ka cal BP. As this date is taken mid-facies in core 13VC, it is likely that this facies covers the same time period, from 7.4 to 4.3 ka cal BP, found in other areas of the bay. The upper boundary of this facies with the overlying LF8 is sharp, with an obvious decrease in the shell content.

LF8 is a silt and sand unit that is coarsening upwards and contains abundant shell fragments. Bivalve layers are present within this unit, differing from the underlying

facies in their smaller size, lack of gastropods and greater abundance of shell fragments. The foraminifera species, abundance and preservation as well as the elemental data in this facies represents a high energy, well oxygenated, nutrient rich, fully marine depositional environment, which is deepening upcore (Fig. 6.1). Like the inner and mid- bay areas there are no radiocarbon dates for this facies.

6.4.4 Outer central bay stratigraphy

The seismic data show the bedrock to be the most extensive unit in this area, while the other units are missing from large portions of the central outer bay (Fig. 5.22). A combination of topographical relief and current intensity in this area (Fig. 4.3) have likely driven both the non-deposition and erosion of the sedimentary units in central outer bay (Fig. 5.22). The high bedrock outcrops (less than 20m bsl), would have made deposition more unlikely, something which is reinforced by the presence of thick sediment patches in areas where the bedrock is not outcropping (Fig. 5.23).

Furthermore, the increased strength of the currents around the bedrock likely caused the erosion of any sediments that were deposited.

In the 5 cores in the outer central bay, 3 lithofacies are present. LF3 is the oldest facies, found only in core (10VC) and, as in the South Sound, represents a very shallow, anoxic, low energy, subtidal environment with a significant terrestrial input which changes towards a more oxic, nutrient rich, estuarine environment upcore (Fig. 6.1). This facies is very thin in the outer central bay, and it is likely that it represents only the top of LF3.

Overlying LF3 in core 10VC, and forming the base of core 06VC, is LF5. It has been dated in the outer central bay between 7.4 and 4.4 ka cal BP (Fig. 5.26), covering a 3000-year period (Fig. 6.1). This suggests that the presence of *Turritella* is not time transgressive. This is a medium energy environment with a low sediment supply that was deposited in a temperate, subtidal environment that is deepening upcore and is composed of a shell unit, containing both gastropods and bivalves. This is a thick unit in the outer central bay, over a metre thick in both cores. As these latter 2 cores are only 0.62 and 0.32m long, respectively, it is likely that they merely did not penetrate deep enough to reach the other facies.

LF 8 overlies LF5 in cores 06VC and 10VC, and forms the base of cores 05VC, 08VC and 09VC. This open marine facies, dated at 2.2 ka cal BP, near its base in core 10VC, is composed of silty sand to coarse sand, suggesting strong currents and a high energy environment (Fig. 6.1). This is reinforced by cores 05VC and 08VC, where the coarsest sediment is found, and which are located very close to the Aran Islands, known as an area with the strongest tidal currents and waves in the bay (Fig. 4.3).

6.4.5 Outer bay- North Sound stratigraphy

In the South Sound, the bedrock is the most prominent seismic unit in the North Sound (Fig. 5.22), where it outcrops extensively along the sides (<20m bsl) leaving a deep channel in the middle. Overlying the bedrock in the channel is glacial till, which forms a relatively thick unit (4-16m). This suggests that the ice movement through the bay was influenced by the underlying topography and deposition was concentrated in the depressions. The lack of the glaciofluvial/marine unit 3b in the very outer North Sound indicates that erosion was occurring in this area. As these sediments are found further inland, this may indicate significant erosion during the sea-level lowstand, ~15 ka cal BP, when this area would have been coastline, and prone to the full force of the Atlantic Ocean. The modern marine sediments in this area are represented by seismic unit 3b and are extensive (Fig. 5.22). The preservation of these sediments suggests that as sea-level rose, the erosive force of currents and waves was less influential and allowed for the deposition and preservation of thick sediment patches, generally protected behind bedrock outcrops (Fig. 5.22 & 5.23). Overall, the deposition of the till, glaciofluvial and marine sediments have clearly been influenced by the topographical relief of the bedrock in this area (Fig. 6.1).

LF2 is the oldest unit in the North Sound, with dates at 12.6, 11.7 and 8.8 ka cal BP. The extensive shell fragments, broken foraminifera tests, range of grain sizes and reversed radiocarbon dates are indicative of a shoreface deposit in a high energy environment which has experienced reworking. While the chemical analysis shows a deepening environment upcore, there are only minor changes in the input of terrestrial material and no significant changes in the foraminifera species, in either

their diversity, size or level of preservation, or in the grain size or sorting. This suggests that sea-level rise was not rapid during the deposition of this facies.

Overlying LF2 in core 17VC and forming the base of cores 01GC, 18VC and 22VC, is LF4, a silty mud facies low in biogenic content that is coarsening upwards (LF4). This facies is dated at the base of core 22VC, 57.3m bsl, to 10 ka cal BP, suggesting it is contemporary with LF2. This change in facies in contemporary cores is interpreted to represent transgression, as LF4 is generally found further westwards, in deeper water (Fig. 6.1).

The foraminifera content and elemental data in this facies indicate an oxic, low energy, enriched, marine environment with a large sediment supply. The changes in the chemical data and foraminifera species between LF2, a shoreface deposit, and this facies, a fully marine environment, where LF4 overlies LF2, suggests a significant sea-level rise. This resulted in the opening of the bay and an increase in the circulation of water. This change appears to have taken place across the transition between these facies. Whilst there is a deepening trend in this facies, there are no major changes upcore that would suggest a change in the speed of sea-level rise. Both LF2 and LF4 are contemporary with LF3 and suggest very different depositional environments between the north and south of the bay. While the difference between LF4 and the other 2 is due to differing water depths, the difference between LF2 and LF3, which are located at similar water depths (~40m bsl) has been interpreted to represent a terrestrial barrier between the North and South Sounds. This barrier would have created differing hydrological regimes in the separate inlets, causing different depositional environments. However, as lithofacies boundaries are not identifiable in the seismic data, this cannot be confirmed.

Overlying LF2 and LF4 is LF5, a condensed *Turritella* layer with almost no sediment, found in all but one of the cores in the North Sound (21VC). This facies has been dated between 7.8 – 6.3 ka cal BP in the North Sound (Fig. 5.24 & 5.26). The abundance of intact filter feeding gastropods indicates deposition in a low-medium energy environment, with a low sediment supply. The foraminifera and shell species also indicate a medium energy environment, with a freshwater source while the elemental data shows a gradual change from the underlying LF2, but a drastic change from the

underlying LF4. This may be due to the position of these cores in deeper waters, further westwards, up to 57m bsl.

Overlying LF5, is LF8, the most recent facies and the modern-day seafloor. This facies is composed of silt and sand with abundant shell fragments and is coarsening upwards. The diverse foraminifera species and elemental data show that this is a fully marine, oxygenated, nutrient rich environment, with a significant terrestrial input, which is deepening upcore. The drastic change in shell content from the *Turritella* rich LF5, to a bivalve fragment dominated LF8, suggests a variation in the sediment supply, possibly an increase. This, alongside an increase in energy, as *Turritella* are filter feeders that cannot tolerate suspended sediment in the water column (Fig. 6.1).

Chapter 7: Discussion

This chapter brings together all the evidence presented previously in order to reconstruct the palaeoenvironmental evolution of Galway Bay since the last glacial maximum until present day. Together with previously published literature about the area, the seismic, sedimentological, biological and geochemical data are used to determine environmental changes in the bay. The radiocarbon results are used to constrain the timing of these changes and compare them to known environmental and climatic events on a regional and global scale.

7.1 Glacial – Deglaciation period (>24.7 – ~15.5ka calBP)

This period covers the time from when the ice reached its maximum extent during the last glacial period until the end of the deglaciation.

The data from this study show that the underlying structural geology of Galway Bay slopes gradually westward (Fig. 5.24). This profile may have facilitated the offshore flow of ice (Fig. 7.1B) which is known to have reached its maximum extent at the shelf edge after 24.7 ka cal BP (Fig. 7.1A) (Benetti et al, 2010; Dunlop et al, 2010; Clark et al, 2012; Ó Cofaigh et al, 2012; Chiverrell et al, 2013; Peters et al, 2015, 2016; Ballantyne and Ó Cofaigh, 2017).

This movement of ice would have had implications for the sedimentary environment in Galway Bay, likely removing most of the pre-LGM sediments down to the underlying bedrock. This is common in Ireland, with only a handful of pre-LGM deposits found on the island (McCabe, 1987; Coxon et al, 2017). Where they occur, these interglacial sequences are generally found under till deposits, indicating that the till is later in advance (Jensen et al, 1959; Watts, 1964, 1985; Coxon et al, 1996; Dowling et al, 1999; Dowling and Coxon, 2001; Coxon and Dowling, 2015). There is no evidence of similar sequences in Galway Bay.

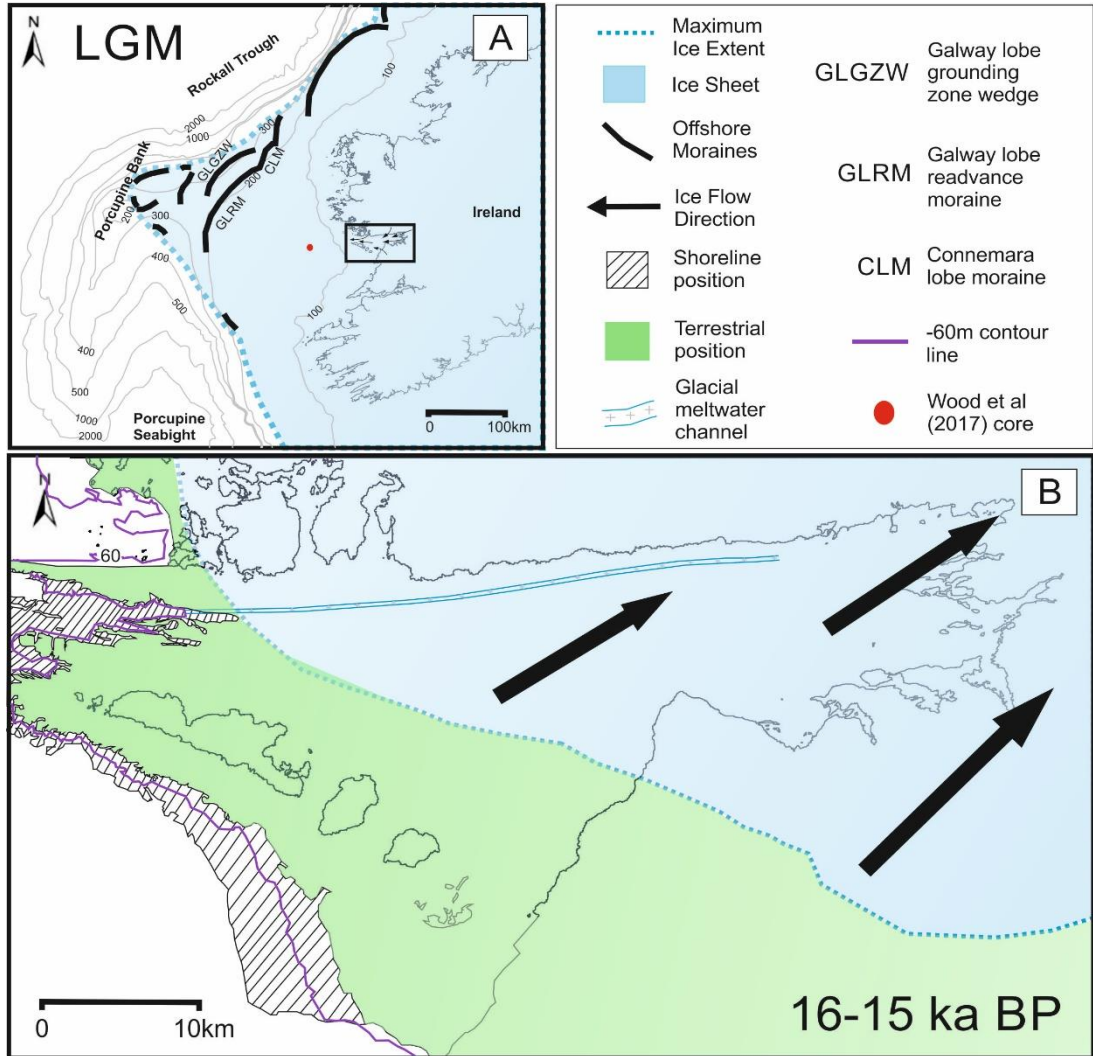


Figure 7.1: (A) BISS extension off the west coast of Ireland (based on the works of Benetti et al, 2010; Dunlop et al, 2010; Ó Cofaigh et al, 2012; Sacchetti et al, 2012; Peters et al, 2015, 2016). (B) Retreat of ice through Galway Bay during deglaciation, between 16 – 15 ka cal BP (based on the References found in Table 2.1).

Seismic data suggest that the first sedimentary acoustic unit in Galway Bay (unit 2; Fig. 5.21) is glacial till, based on the chaotic and contorted internal reflectors and diffraction hyperbolae commonly observed in diamicton deposits characteristic of glacial till (Jennings et al, 2000; Principato et al, 2005; Evans et al, 2006; Cotterill et al, 2017; Dove et al, 2017; Roberts et al, 2018). As there are no distinctive boundaries within the glacial till sheet, no inferences can be made about sequences of advance and/or retreat of the ice sheet within the bay.

Glacial till is the thickest sub-bottom unit in the seismic sequence in Galway Bay, up to 16m in the outer bay (Fig. 5.25), compared to the maximum thickness of 12.5m for the deglacial unit (3a) and 8.5m for the post-glacial/modern unit (3b). The depocentres of the glacial till appear to be in the North Sound and central areas of the outer bay, in front of the outcropping bedrock (Fig. 5.25). This suggests that the location of deposition was somehow influenced by the bedrock outcrops as the larger build-up of sediments is in the low lying areas in front of them. This position in front of the outcropping bedrock would also have protected the glacial till from erosion by subsequent marine processes as the sea-level in the bay began to rise.

From terrestrial dates, initial deglaciation is considered to have occurred in western Ireland by ~20 ka cal BP (Ballantyne et al, 2008; Bowen et al, 2002; Clark et al, 2009; McCabe et al, 1986, 2005), triggered by an increase in solar insolation (Clark et al, 2009). In the marine sector, meltwater pulse 1A0, at 19 ka BP, and the sea-level rise which accompanied it, is considered to have accelerated the rate of ice sheet break up, which was already underway (Clark et al, 2012). In Ireland, evidence from Kilkeel in the north-east in the form of marine mud found in formerly eroded channels (Clark et al, 2004), has indicated that a ~10m rise in sea-level during MWP 1A0 can be correlated to sites in Barbados and Australia (Carlson and Clark, 2012), indicating that this was a global event. However, MWP 1A0 has been subject to extensive debate, particularly in studies from the Irish Sea, where its existence has been disputed (McCarroll et al, 2001; Hiemstra et al, 2006). In other areas across the North Atlantic, meltwater events have meant the rapid emplacement of laminated, fine, marine sediments (Lekens et al, 2005; Tripsanas and Piper, 2008; Lucchi et al, 2015) through sea-level rise.

During deglaciation, readvances of the ice margin occurred across Ireland, with two of the best documented glacial readvances in Ireland during the Clogher Head Stadial (18.2 – 17.1 ka cal BP) (McCabe and Haynes, 1996; McCabe et al, 2007; Clark et al, 2012b) and the Killard Point Stadial (17.1 – 16 ka cal BP) (McCabe et al, 2005; Clark et al, 2012b). The Galway Lobe Readvance Moraine, located 130km offshore of Galway Bay, formed between 18.4 – 15.85 ka cal BP (Peters et al, 2016), also fits within these readvance periods. The Connemara lobe moraine (Fig. 7.1A), located ~25km offshore, just north of the Galway lobe moraine (Fig. 7.1A), is age constrained to 15.1 ka cal BP (Peters et al, 2016). These offshore features suggest that during these readvances ice flowed through Galway Bay.

In Galway Bay there is only evidence of 1 till sheet, with no stratification and no evidence of glaciomarine material between till deposits. While we know there are global MWP's (Fairbanks, 1990; Yokoyama et al, 2000; Deschamps et al, 2012) and local readvances (Peters et al, 2016) they do not appear to be resolved in the data from Galway Bay.

The movement of ice through the bay may have resulted in the deformation and reworking of previously deposited glacial till, therefore it is not possible to determine if the till in Galway Bay was deposited during initial glacial advance or during subsequent readvances and retreats. The drumlins along the coastline and in the inner bay (Fig. 4.1) have been interpreted to be contemporary with those in Clew Bay, which have been dated to ~17 ka cal BP (McCabe and Dardis, 1989; McCabe et al, 1986). This corresponds with the Killard Point stadial readvance and the deposition of the Galway Lobe re-advance phase (Peters et al, 2016). It is therefore possible that some of the till in the bay is of this age. However, as no seismic data were available for the inner bay area (Fig. 3.7), it has not been possible to determine if these drumlins correlate with the glacial till unit found in the mid and outer bay.

Many re-advances observed in other ice sheets at this time are believed to be linked to Heinrich event 1 (H1) (Heinrich, 1988; Hemming, 2004), which occurred ~17.5 ka BP and saw the release of large volumes of meltwater and icebergs into the North Atlantic (Bond et al, 1997), causing a cooling phase which delayed deglaciation (McCabe et al, 1998). To the south of Galway Bay, Lough Inchiquin, in the Burren region, has

sedimentation of clay and marl above till at 16.2 ka BP (Diefendorf et al, 2006), suggesting deglaciation of the area by this time. This corresponds with terrestrial dates along the west coast at Furnace Lough and the Ox Mountains by Clark et al (2009b), which returned cosmogenic nuclide dates of 16 ± 0.7 ka, and 16.6 ± 0.8 ka (recalibrated by Ballantyne and Ó Cofaigh, 2017) respectively, indicating that the region, was free of ice sourced from land by this point. Overall, the west coast of Ireland is considered by all studies (Table 2.1) to be completely ice free by 13.7 ka cal BP and total deglaciation of Galway bay in this study is confirmed by 13.1 ka cal BP with the deposition of the silty sand/sandy silt facies (LF3). It is likely that the bay was totally ice free earlier than this as there is non-glacial sediment below the sample where the radiocarbon date was taken in this facies (Fig. 5.29). It is entirely possible that Galway Bay was ice free during the Rough Island interstadial, by 15 ka cal BP (Knight et al, 2004; Ballantyne and Ó Cofaigh, 2017). If this was the case, it would constrain the deposition of glacial till from before the main extent of ice at 24.7 ka cal BP, until ~ 15 ka BP.

By 15 ka cal BP, relative sea-level in the bay is predicted to have been at its lowest, with the base of the deglacial seismic unit (3a) found up to 70m bsl in the outer bay. This corresponds with the GIA model-derived RSL predictions, which show RSL between 56 and 69m lower than present day (Brooks et al, 2008; Bradley et al, 2011; Kuchar et al, 2012) (Fig. 7.10). This lower sea-level would have meant a very different coastal landscape, where all but the deepest areas of the North and South Sounds would have been terrestrial. This correlates with the channel observed within the glacial till unit (Fig. 5.19), which lies at a maximum depth of ~ -58 m in the North Sound.

As the overlying sedimentary unit shows no evidence of channels, this indicates that whatever processes shaped this channel had ceased to influence the bay by the time the overlying strata were deposited. The straightness of the channel, which follows the Galway Bay Fault, indicates that the underlying geology of the bay likely influenced the formation of the channel. The channel was probably partially glaciofluvially cut by large inputs of meltwater from the receding glacier to the north east (Fig. 7.1C), during deglaciation of the bay, sometime between 16 and 15 ka cal BP.

7.2 Deglaciation – Early Holocene period (~15.5 – 11.7 ka cal BP)

During deglaciation, the climate in Ireland warmed continually. However, the region still experienced climatic variability and periods of climate deterioration (Watson et al, 2010; Molloy and O’Connell, 2014; Woodman, 2015; Barr et al, 2017).

In Galway Bay, there is a clear transition from a glacial to a temperate marine influenced environment during this time (Fig. 7.2C). However, the resolution of the data during the early deglacial period (pre-13.1 ka cal BP), which consists only of seismic data, means that although sediment deposition and sea-level rise are evident, smaller climatic oscillations cannot be detected.

After deglaciation, Galway Bay underwent a period of rapid sediment deposition, with the deglacial unit (3a) up to 12.5m thick (Fig. 5.26). This thick sedimentary unit between 18 - 70m bsl was formed by a mixture of glaciofluvial and marine deposition. This time-transgressive unit has lenticular reflectors at its base, indicative of deposition in a variable energy environment (Catuneau, 2006). As deposition of the deglacial acoustic unit (3a) began as soon as glacial retreat in the bay started, the impact of glaciofluvial processes, especially along the aforementioned channel cut into the glacial till, were important. This is supported by GIA derived RSL predictions, which show that the bay was primarily terrestrial between 16 and 15 ka cal BP (Brooks et al, 2008; Bradley et al, 2011; Kuchar et al, 2012). The meltwater channels to the north of Galway Bay (Fig. 2.4) suggest that the bay may have acted as a drainage area for ice present on elevated zones in the Connemara region.

The thickest areas of the deglacial unit (3a), in the inner bay (Fig. 5.26), suggest that, as the ice retreated on land in a northeast direction, there was an ample sediment supply. As studies indicate a relatively dry climate in Ireland at this time (O’Connell et al, 1999), this suggests that material was delivered into the bay glaciofluvially, possibly along the proto-Corrib system in the inner bay (Clarke, 2013). The lack of the deglacial unit (3a) in the outer bay area (Fig. 5.24) may indicate that the bay was prone to significant erosion from the Atlantic Ocean in the outer Sounds (Fig. 7.2C). As these areas were closest to the Atlantic Ocean, without the protection of the Aran Islands, they would have been most affected by the impact of currents and waves. It is

probable that these processes were actively causing erosion and transport of material offshore during the post-glacial period.

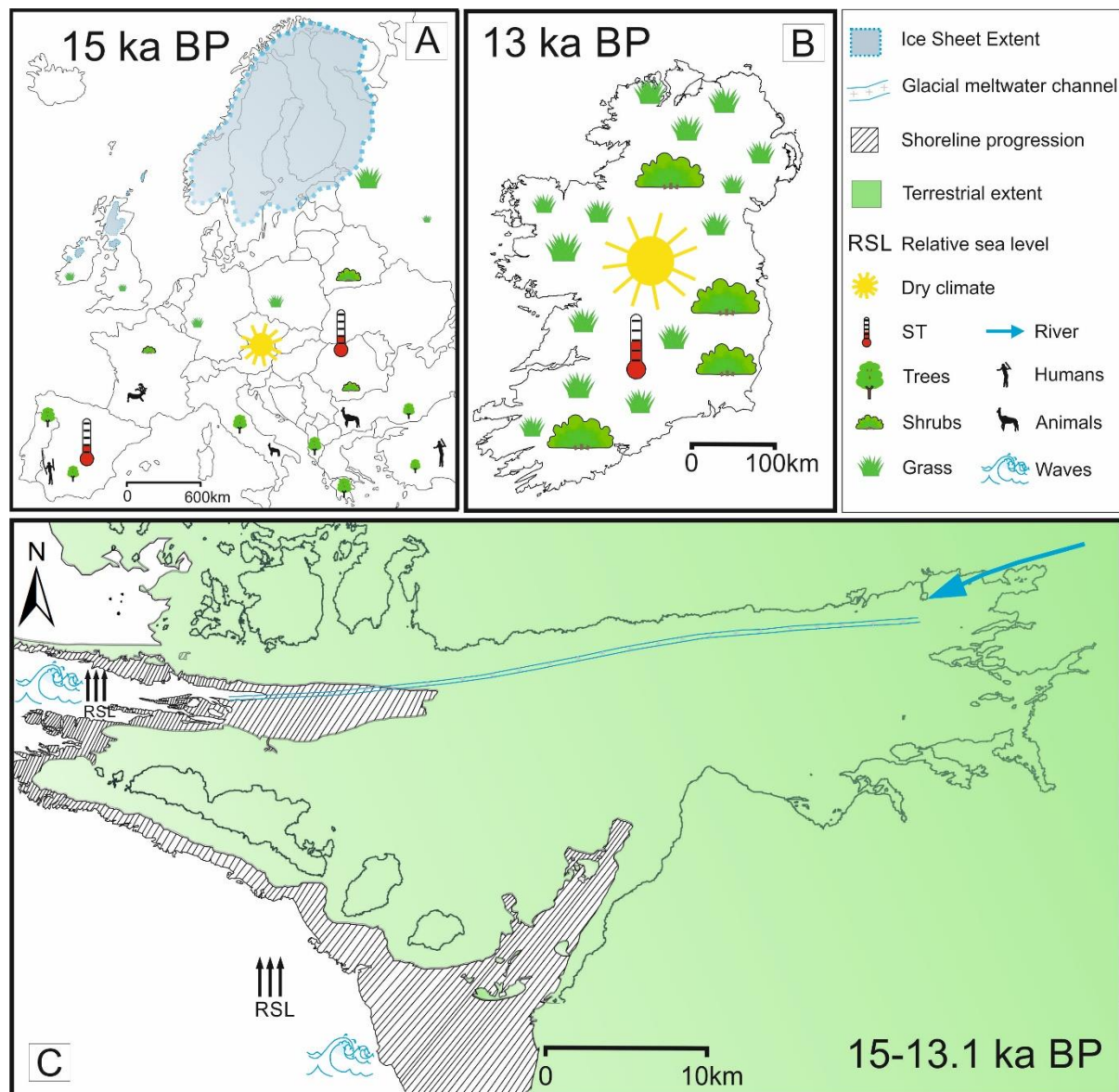


Figure 7.2: Summary of the post glacial terrestrial environmental conditions in (A) Europe (Booth et al, 2012a, 2012b; Mortensen et al, 2014; Seddon et al, 2015; Binney et al, 2017) and (B) Ireland (Harrison et al, 2010; Watson et al, 2010; Ballantyne and Ó Cofaigh, 2017). (C) Summary of the post glacial environment in Galway Bay between 15 and 13 ka cal BP, with the retreating shoreline positions based on GIA derived RSL predictions (Brooks et al, 2008; Bradley et al, 2011; Kuchar et al, 2012), data from this study (Table 5.3) and references found in Table 2.1.

Following deglaciation was the climatic warm period known as the Woodgrange interstadial, which occurred in Ireland between 14.7 – 12.9 ka cal BP (Harrison et al, 2010; Ballantyne and O’Cofaigh, 2017) (Fig. 7.2B). It is possible that the boundary between the deglacial (3a) and post-glacial (3b) seismic units represents the transition to the Woodgrange interstadial. This boundary is conformable suggesting that the change, while clear, is not abrupt. Based on the thickness of these units, up to 12.5m and 8.5m for 3a and 3b respectively, (Fig. 5.23) and the period of time they are interpreted to have been deposited in, ~1000 years (3a) and ~15,000 years (3b), this transition may represent a decrease in the sediment supply signalling the cessation of glaciofluvial processes.

The retreat of the ice meant that the much of the bay was terrestrial immediately following deglaciation. The subsequent retreat of ice sheets across the globe (Bassett et al, 2005), including the Irish ice sheet (Fig. 7.2A), led to meltwater pulse 1A. This was a global sea-level rise, from 14.65 – 14.3 ka cal BP (Fairbanks, 1990; Peltier and Fairbanks, 2006; Stanford et al, 2006; Deschamps et al, 2012), which saw an increase of between 8.6 – 14.6m in global mean sea-level (Liu et al, 2015), caused by an influx of freshwater into the ocean. Wood et al (2017) also noted a prolonged increase in $\delta^{18}\text{O}$ sometime after 16.2 ka cal BP and before 12.8 ka cal BP in their study, ~70km south of the Connemara lobe moraine (Fig. 7.1A), suggestive of a cooling phase, possibly due to MWP 1A. In Galway Bay MWP 1A appears to have led to a transition from terrestrial to marine depositional processes, in previously exposed parts of the bay.

The base of marine sediment core 13VC is >13.1 ka cal BP and the dominant foraminifera species, including *Quinqueloculina sp.*, *Ammonia beccarii*, and *Haynesina germanica* are all characteristic of an estuarine environment with no glacial influence. The base of this facies was deposited in the outer bay South Sound, at least 43.3m below current sea-level. This means relative sea-level in this area was likely above 38.3m bsl, allowing for a tidal range of 5m. The lenticular reflectors at the base of the deglacial unit (3a) are indicative of a variable energy environment, defined as shallow water. The parallel/sub-parallel reflectors at its top are suggestive of a more stable, lower energy environment. This indicates that there is a clear change in the

depositional environment from the base of this unit to the top. The prograding, infilling nature of the channel (Fig. 5.19) in the North Sound, suggests that this change is a transition to deeper water. As the deglacial unit (3a) is older than 13.1 ka cal BP, this demonstrates sea-level rise of at least 18.7m between glaciofluvial deposition at ~16-15 ka cal BP to a more estuarine environment at ~13.1 ka cal BP. This sea-level rise occurs within the same timeframe as MWP 1A suggesting that MWP 1A may have affected Galway Bay.

The Nahanagan Stadial (Younger Dryas), a cooler climatic period that occurred between 12.9 – 11.7 ka cal BP, was felt across much of Europe (Colhoun and Synge, 1980; Bowen et al, 2002; Wilson, 2004; Diefendorf et al, 2006; Ballantyne et al, 2008; Harrison et al, 2010; Ballantyne and O’Cofaigh, 2017; Wood et al, 2017). This cold period caused the development and the readvances of ice masses across Europe (Fig. 7.3A), including in the mountainous regions in the northeast of Ireland as cirque glaciers (Harrison et al, 2010; Bendle and Glasser, 2012; Boston et al, 2015; Renssen et al, 2015; Barr et al, 2017) (Fig. 7.3B).

While there is evidence of the climatic cooling of the Nahanagan Stadial across Ireland (Barr et al, 2017; Diefendorf et al, 2006; Anderson et al, 1998) (Fig. 7.3B), the extent of marine terminating ice remains less well known. Evidence of the Nahanagan Stadial has been found in deeper water, with IRD layers found well off the Irish coast (Knutz et al, 2007; Scourse et al, 2009; Tarlati et al, 2018), however, evidence of IRD is much rarer in shallower water. The exception to this is the work by Wood et al (2017), just offshore (~75km) of Galway Bay, who identified a cooling phase that coincides with the Nahanagan Stadial. In this phase they identified peaks in the foraminifera species *Elphidium sp.*, known to prefer Arctic waters (Jennings et al, 2004) and *Nonionellina labradorica*, a species commonly seen in polar waters and during deglaciation (Knudson and Austin, 1996; Cannariato et al, 1999), as well as an increasing trend in the $\delta^{18}\text{O}$ isotope and deposits of IRD. This evidence is suggestive of a significant cold-water influence and floating icebergs, all pointing toward the presence of a nearby ice margin.

Interestingly, there is no such evidence of this cold period in Galway Bay. The silty sand/sand silty unit (LF3) has been dated between 13.1 and 9.9 ka cal BP and the

gravelly sand and silt unit (LF2) between 12.6 and 11.7 ka cal BP, covering the period of the Nahanagan Stadial, in both the South and North Sounds. This study shows a constant grain size in the silty sand/sandy silt unit (LF3). There are larger grains present in the gravelly sand and silt unit (LF2), namely the gravel, but these are interpreted to have been a high energy beach deposit rather than IRD, due to their rounded nature. The foraminifera species in both these facies represent a warm temperate climate, and there is no evidence in the seismic or geochemical data that suggests a significant or abrupt shift in environmental conditions during this time (Fig 5.1 & 5.2).

While it is possible that this colder water signature is missing from this study due to the low sampling resolution of foraminifera species, it is also possible that this colder climate did not register in the shallower waters of Galway Bay because they are sheltered from the oceanic currents by the Aran Islands.

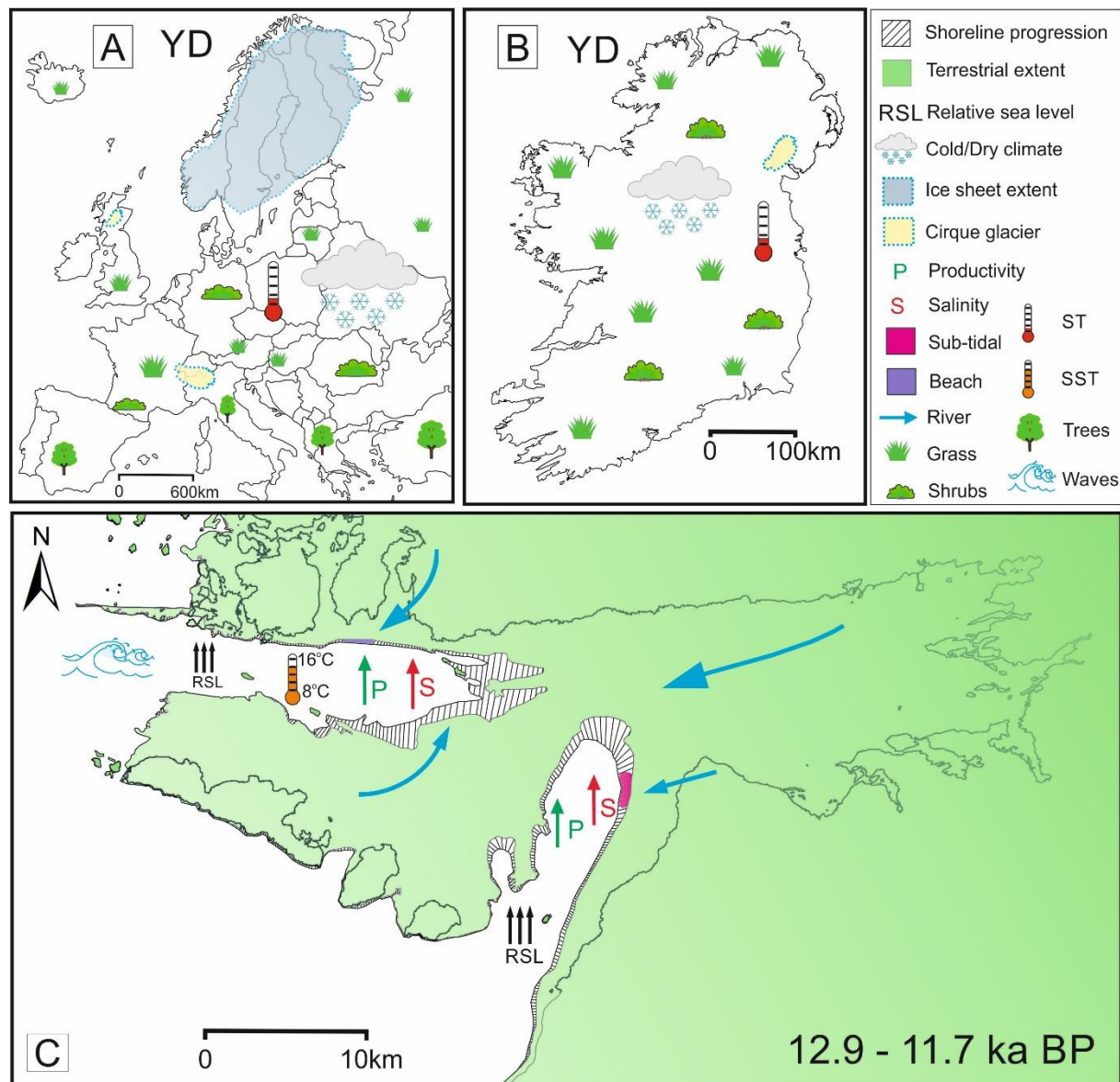


Figure 7.3: Summary of the Younger Dryas terrestrial environmental conditions in (A) Europe, (B) Ireland and (C) Galway Bay, with retreat of shoreline positions between 12.9 – 11.7 ka cal BP, based on GIA-derived RSL predictions (Brooks et al, 2008; Bradley et al, 2011; Kuchar et al, 2012), data from this study (Fig. 5.6 & Table 7.1), and references found in Table 2.1. ST: Surface Temperature. SST: sea surface temperature, based on foraminifera preferences (Appendix 3).

7.3 Early Holocene period – Greenlandian (11.7 – 8.3ka calBP)

The early Holocene is considered to have begun after the Nahanagan Stadial (Younger Dryas) ended around 11.7 ka cal BP and covers a 3,400-year period between 11.7 – 8.3 ka cal BP (Walker et al, 2018). This period is marked by a warming phase that saw an

increase in the spread of vegetation and fauna across Europe (Walker et al, 1994; Sommor and Benecke, 2005; Bos et al, 2007) (Fig 7.4A).

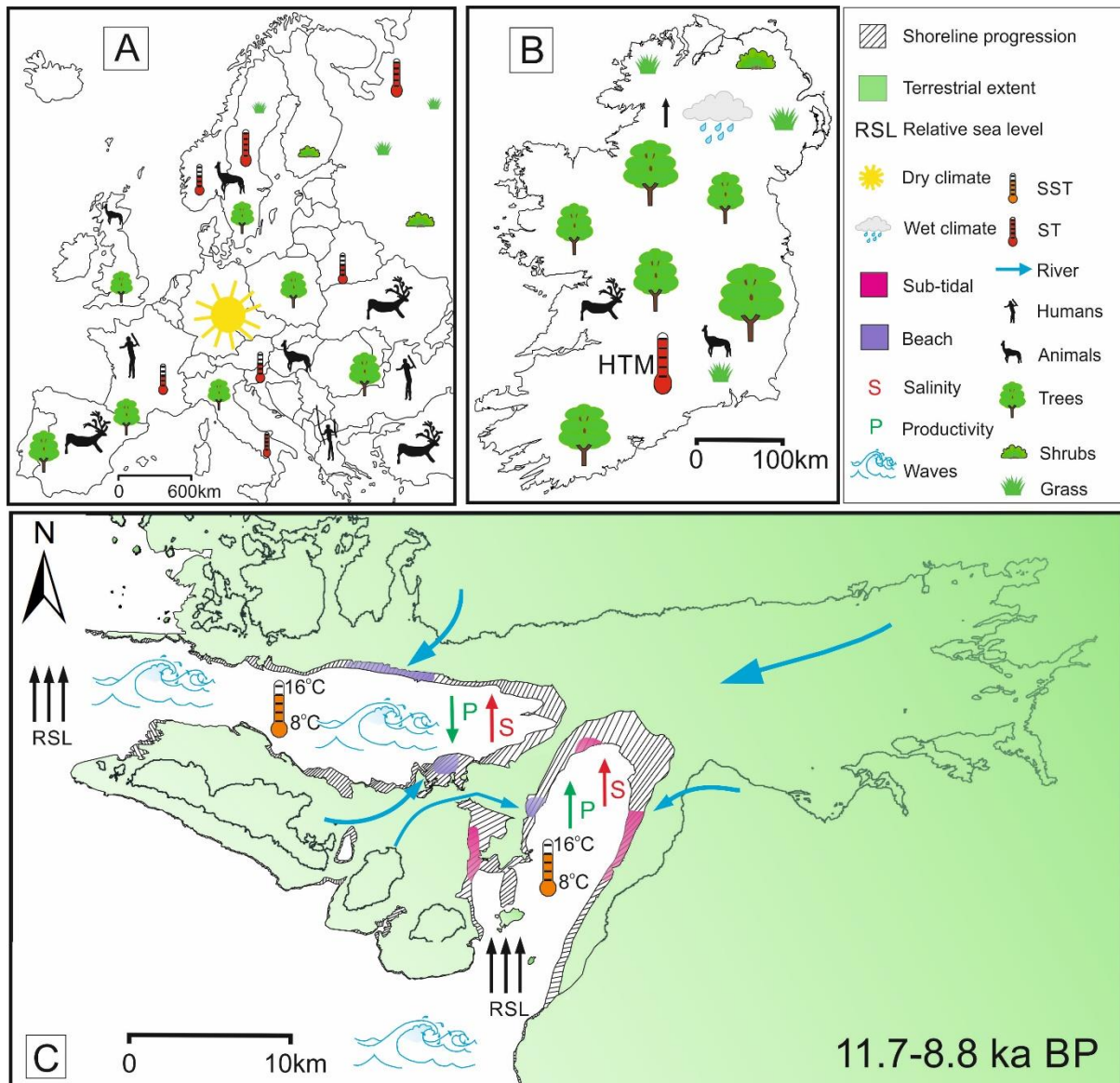


Figure 7.4: Summary of the early Holocene environmental conditions in (A) Europe, (B) Ireland and (C) Galway Bay, with the retreat of shoreline positions between 11.7 – 8.8 ka cal BP, based on GIA-derived RSL predictions (Brooks et al, 2008; Bradley et al, 2011; Kuchar et al, 2012) and data from this study (Fig. 5.6 & Table 7.1). ST: Surface Temperature. SST: sea surface temperature, based on foraminifera preferences (Appendix 3).

Although the early Holocene marks the beginning of the era we are currently in, it is not well documented in western Ireland, particularly in the marine records, as previous studies have tended to focus on either the glacial, or younger Holocene

periods. The main records of this time period in western Ireland include lake studies in counties Galway, Mayo and Clare (Schettler et al, 2006; Holmes et al, 2007; McKeown et al, 2013; Diefendorf et al, 2006), speleothem studies in county Kerry (McDermott et al, 2001) and marine studies, both in and offshore of Galway bay (Novak et al, 2017; Wood et al, 2017). Even in these records the entirety of the early Holocene is not always covered. However, in this study early Holocene sediments are present in both the North and South Sounds in the outer bay, in the gravelly sand and silt (LF2), silty sand/sandy silt (LF3) and coarsening upward sand mud (LF4) units (Fig. 5.28).

A high abundance and diversity of foraminifera species, including *Quinqueloculina sp.* and *Miliolinella subrotunda*, which are known to be temperate/warm water species (Murray, 2003; Horton et al, 1999), is seen in both the silty sandy/sand silt unit (LF3) and the gravelly sand and silt facies (LF2). These types of species are consistent with RSL rise, whilst the abundance and diversity point to a warming climate at the beginning of the Holocene (Fig. 7.4C). While the gravelly sand and silt (LF2) and silty sand/sandy silt (LF3) units both indicate sea-level rise, there are no indicators in either of the pre-boreal climatic oscillation (PBO), a short lived cooling phase that lasted between 150-250 years at 11.4 ka cal BP, causing climate deterioration across Europe (Bjorck et al, 1998; Hald and Hagen, 1998; Merkt and Müller, 1999; Litt et al., 2003; Bos et al, 2007). This is believed to have been caused by a freshwater influx into the oceans, from the drainage of Lake Agassiz (Fisher et al, 2002; Teller et al, 2002) and the Baltic Ice Lake (Bjorck et al, 1998; Hasum and Hald, 2002). This suggests that, either this climatic cooling affected the bay and the sampling resolution of foraminifera was not detailed enough to capture such a short-lived event, or this cooling event did not affect Galway Bay. As larger cooling events such as the Younger Dryas are also not evident in the bay, the PBO is interpreted to have left no signal in Galway Bay.

Another global event, of which there is no evidence in Galway Bay, is MWP 1B, a massive release of freshwater into the oceans from melting ice sheets, causing global sea-level rise of up to 14m between 11.45 – 11.1 ka cal BP (Abdul et al, 2016; Edwards et al, 1993; Liu and Milliman, 2004). In fact, the bay appears to be experiencing a drastic slowing of sea-level rise during this time (See Section 7.6, Fig. 7.8), with the

environment represented by the silty sand/sandy silt (LF3) unit, remaining a sub-tidal environment over a period of at ~3200 years. Although a deepening trend is evident in the Sr/Ba, Ba/Ca and Br/Cl ratios, and in the foraminiferal diversity (Fig. 5.7; Appendix 1), the sea-level rise is not significant enough to move this area out of the sub-tidal zone.

This indicates that although global sea-level was still continuing to rise (Smith et al, 2011), the bay must have experienced isostatic rebound that was matching sea-level rise, allowing for a relatively unchanging RSL in Galway Bay. This rebound likely maintained separation of the North and South Sounds, rather than opening up the bay, as deposition in the North and South Sounds differ, with the gravelly sand and silt (LF2) and coarsening upward sandy mud (LF4) units the main deposits in the North and silty sand/sandy silt (LF3) unit in the South. This is also supported by the work of Novak et al (2017), in water depths of 13.4m, in the inner bay, where the marine foraminifera record does not begin until after 10.2 ka cal BP, suggesting that the inner bay area likely did not experience a marine intrusion before this time.

As the foraminifera *Quinqueloculina sp.* and *Miliolinella subrotunda* remain evident in the gravelly sand and silt (LF2) and *Quinqueloculina sp.* increases upcore in the silty sand/sandy (LF3) unit, the environment in Galway Bay appears to have remained temperate throughout the early Holocene (Fig. 7.4C), though this is based on a small number of foraminifera samples in these facies. This parallels the Holocene Thermal Maximum (HTM) in Ireland, which studies place between 10.8 and 9 ka cal BP (Diefendorf et al, 2005,2006; Holmes et al, 2007; Ghilardi and O'Connell, 2013; McKeown, 2013). On land, the HTM saw an increase in the spread of vegetation, when trees, especially hazel, began to rapidly colonise former grassland areas (Hall, 1997; Smith and Goddard, 1991, Mitchell, 2006; Holmes et al, 2007) (Fig 7.4B).

Furthermore, there is a consistent freshwater input into the bay, evident in geochemical peaks and increasing trends in S/Ti, Si/Ti, Ba/Ca and Sr/Ca, as well as the presence of molluscs that need a freshwater supply, in the gravelly sand and silt (LF2) and silty sand/sandy silt (LF3) units. This provides evidence of not only a warmer, but a wetter climate with an increase in fluvial discharge. A similar trend is recorded as a rise in lake-level rise on Inis Mór, at the mouth of Galway Bay, which is related to increased

precipitation at this time (Holmes et al., 2007). While the climate is wetter than during previous time periods, the expansion of mesophilous trees such as oak and elm into Ireland (Brewer et al, 2002), indicate moderate precipitation, rather than a significantly wetter period.

The climate remained temperate in Ireland until the end of the Greenlandian period at 8.3 ka cal BP, evidenced by the spread of pine, elm and oak across the entire island (Mitchell, 2006) (Fig. 7.4B). High sedimentation rates in the Corrib estuary and inner areas of Galway Bay, between 1 – 2mm/yr from 10,235 to 8000 years BP (Novak, 2017), support the terrestrial evidence that the areas surrounding the inner bay did not have an arid climate. This indicates that, while there was an increase in vegetation cover, it was not dense enough to significantly interrupt terrestrial runoff into the bay. The lower sedimentation rates in this study, ~0.1mm/yr during the same time period of the early Holocene, compared with the inner bay, generally suggest that sediment influx to the bay is influenced more by the proximity of rivers, rather than by hinterland run off.

The temperate, moderate climate of the late Greenlandian seen in this study, is represented not only in the marine environment, with high diversity and abundances of foraminifera species, test preservation and increasing salinity and marine organic content in the geochemistry upcore, but in the terrestrial environment (Holmes et al, 2007) as well (Fig 7.4).

7.4 Mid-Holocene period – Northgrippian (8.3- 4.2ka cal BP)

The mid-Holocene period began around 8.3 ka cal BP, marked by a deteriorating climate and a cooling event, known as the 8.2 ka event, which caused a disturbance in the circulation of the Atlantic Ocean, affecting the transfer of heat in the North Atlantic region (Matero et al, 2017). The mid-Holocene period lasted 4100 years until 4.2 ka cal BP and is interpreted to be represented in Galway Bay by post-glacial acoustic unit 3b, silty sand/sandy silt (LF3), coarsening upward sandy mud (LF4) and shell hash (LF5) (Figs. 5.7 & 5.8, 5.9 & 5.10, 5.11 & 5.12 and Table 5.1 & 5.3). The seismic data throughout this period is represented by prograding clinoforms and infilling, indicating a constant transgression across the bay (Fig. 5.21). The upper

portion of the silty sand/sandy silt (LF3) and coarsening upwards sandy mud (LF4) units are considered to represent the time period between ~10 and 7.4 ka cal BP, while the shell hash (LF5) unit is dated between 7.4 – 4.1 ka cal BP. In this study changes are evident in the geochemistry and physical properties of the cores within this mid-Holocene time period.

After 9.9 ka cal BP, the silty sand/sandy silt (LF3) unit shows increased sorting and terrestrial input to the bay through low values in gamma density and variability in the Si/Ti and Sr/Ca ratios (Fig. 5.6 & 5.7). There is also an increase in foraminiferal abundance and diversity in the 3 samples taken in this facies. Around the same time, coarsening upwards sandy mud (LF4), deposited elsewhere in the bay also records an increase in terrestrial runoff as peaks in gamma density, magnetic susceptibility and Sr/Ca ratios and a decrease in Ca/Ti ratios. These fluctuations occurred sometime between 10 and 7.4 ka cal BP and may potentially represent a wetter climate with increased hinterland runoff, providing a higher nutrient supply to the bay.

The boundary between the gravelly sand and silt (LF2) and coarsening upward sandy mud (LF4) units in core 17VC, which occurred after 8.8 ka cal BP, represents an environmental change in the bay. In the coarsening upward, sandy mud (LF4) the foraminifera show a transition to much smaller, less abundant and less diverse species that are tolerant to more stressful conditions. This has been interpreted to represent an increase in fine grained sediments, with sedimentation rates the highest in the bay (0.78mm/yr) between 10 and 6.8 ka cal BP. As foraminifera tend to prefer coarser sediments, due to better aeration, easier movement and better penetration of food supplies (Inabinet and Fish, 1979), this change to a muddy habitat may have adversely affected the foraminifera populations.

The increased variability in the geochemical signature combined with the change in sedimentation may represent the transition between the early and mid-Holocene periods and increased terrestrial runoff due to a cooler, wetter climate, during the 8.2 ka event, caused by changes in the atmospheric circulation (Baldini et al, 2010; Holmes et al, 2016). While the foraminiferal evidence in these facies does not suggest a major drop in water temperatures, the transition to smaller, less abundant and less diverse foraminifera species in the coarsening upwards sandy mud (LF4), does suggest a more

hostile environment and falls within the timeframe of this event. That said, this change could also be linked to variability in local conditions.

Novak (2017) presents a possible signature of the 8.2 ka event in the inner most core in the bay. She found disturbed laminations between 8801-8393 cal BP and 8140-7825 cal BP as well as geochemical evidence indicating increased terrestrial runoff, but no clear change in the microfossil record.

Overall, we can only determine that there was increased runoff into Galway Bay between the end of the late and beginning of the mid-Holocene periods. This correlates to the open woodland, dominant in Ireland at the time, which would have allowed for higher runoff than full canopy cover woodlands.

In this study, at ~ 7.4 ka cal BP, there is a sharp change in lithofacies to a shell hash (LF5) from all underlying units (Fig. 5.29 & 5.30). Allowing for the error (± 0.1) in the radiocarbon results, this coincides with MWP 1C, a rapid sea-level rise at ~ 7.5 ka cal BP (Blanchon and Shaw, 1995; Christensen, 1995, 1997; Behre, 2007; Yu et al, 2007). The shell hash (LF5) unit, dominated by the gastropod *Turritella communis*, has been dated between 7.4 and 4.1 ka cal BP. This change at 7.4 ka cal BP, corresponded with the end of the wetter climate in Europe. However, terrestrial sources in western Ireland (Diefendorf et al, 2006) suggest that the wetter climate in Ireland persisted until ~ 7 ka cal BP. If this was the case, then the signature of this prolonged precipitation is not seen in the bay. It is possible that the increasing tree populations, particularly the spread of alder (Molloy and O'Connell, 2004), reduced the sediment erosion in the hinterland surrounding Galway Bay and lowering sediment runoff into the bay. The lower sediment influx in Galway Bay is evident, as *Turritella communis* is a filter feeder that cannot survive in environments with a high sediment concentration in the water column (Younge, 1946). The presence of this species in such large numbers through Galway Bay alone indicates that the water column is relatively clear of suspended sediment.

In Galway Bay, the GIA model-derived RSL predictions (Brooks et al, 2008; Bradley and Kuchar et al, 2012) (See Section 7.6; Fig. 7.9) all indicate a slowing of sea-level rise that coincides with the deposition of the shell hash (LF5).

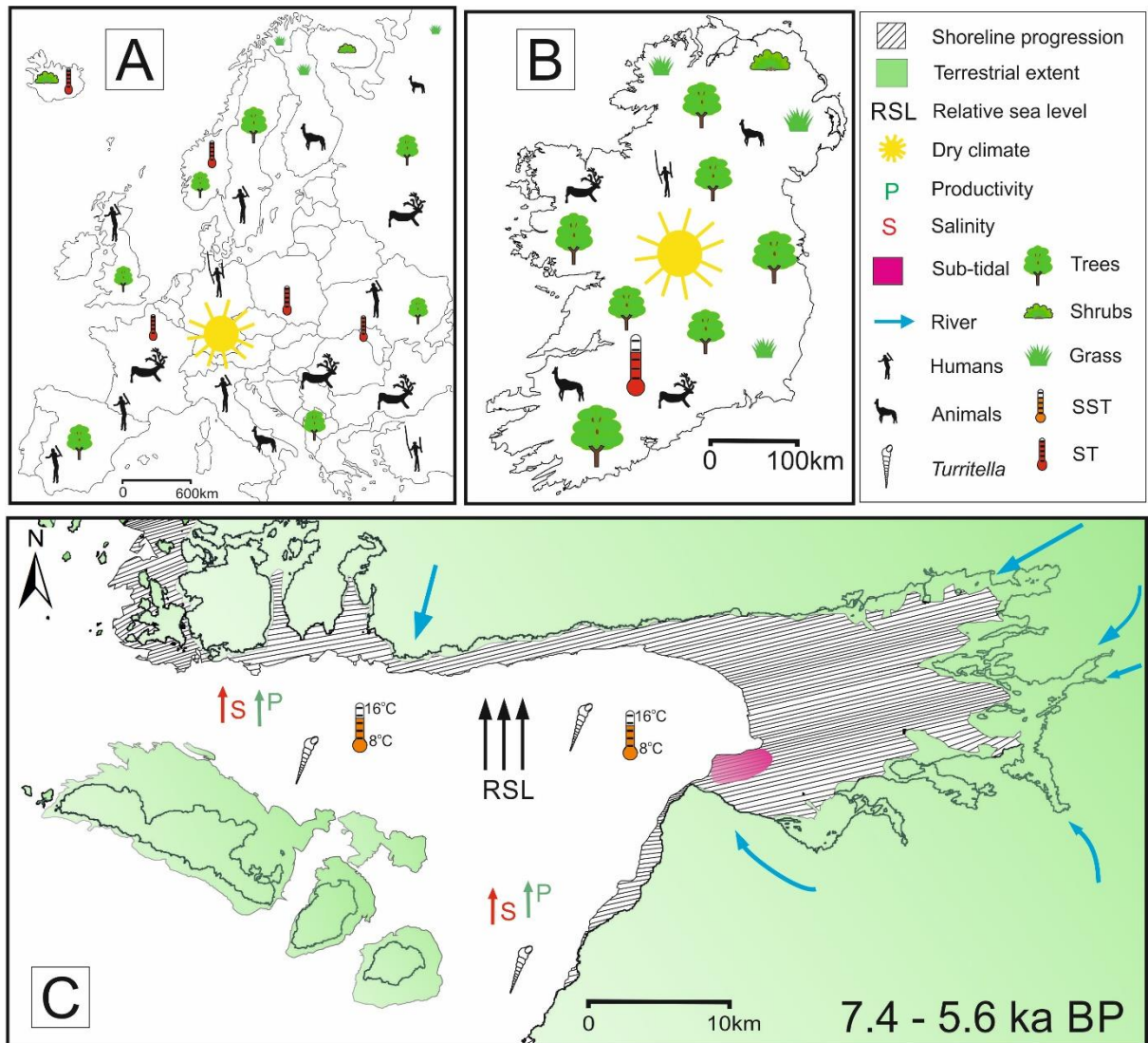


Figure 7.5: Summary of the mid Holocene environmental conditions in (A) Europe, (B) Ireland and (C) Galway Bay, with the retreat of shoreline positions between 7.4 – 5.6 ka cal BP, based on GIA derived RSL predictions (Brooks et al, 2008; Bradley et al, 2011; Kuchar et al, 2012), data from this study (Fig. 5.6 & Table 7.1) and references found in Table 2.1. ST: Surface Temperature. SST: sea surface temperature, based on foraminifera preferences (Appendix 3).

The Holocene Thermal Maximum and an enhanced number of dry events were occurring across much of central Europe between 7.2 – 5.7 ka BP (Andrews and Giraudeau, 2003; Davis et al, 2003; Bjune et al, 2005; Caseldine, 2006; Wanner et al, 2008, 2011; Stivirins et al, 2017), and while this period does not represent the thermal maximum in Ireland, it is known as a period of generally warmer climatic conditions. As the *Turritella sp.* thrived in Galway Bay for over 3000 years, during this time period,

it indicates that there was a reduction in suspended sediment and terrestrial runoff, likely due to a drier more stable climate (Fig. 7.6).

Similar shell hash facies, dominated by *Turritella communis* have been found in cores in other bays in Ireland, as well as further afield in Scotland and France. The *Turritella communis* found in Bantry Bay (Plets et al, 2015) and Belfast Lough in Ireland (Plets et al, 2019), and in Loch Sunart in Scotland (Baltzer, 2015) generally fall into the same timeframe as Galway Bay. This suggests that drier conditions were present not only in Galway Bay, but in the south west and north east of Ireland and the north west of Scotland. This once again indicates a link between the presence of *Turritella* and the surrounding terrestrial climate.

Evidence of an abrupt global decrease in solar activity (Finkel and Nishiizumi, 1997; Stuiver et al, 1998; Steinhilber et al, 2012), a transition to a colder, wetter climate in Europe and South America and to a colder and drier climate in Asia, Africa and North America (Valiranta et al, 2003; Heikkika and Seppa, 2003; Mayewski et al, 2004; Wanner et al, 2008; Brooks, 2012) are all evident between 6.4 and 5.9 ka cal BP.

Novak (2017) presents evidence of a hiatus in the inner area of Galway Bay that covers all of the mid-Holocene period, beginning at 6 ka cal BP and extending throughout most of the late-Holocene period. This hiatus has not been recognised in this study. A possible theory for this hiatus, suggested by Novak (2017), includes sediment removal due to increased river inflows, which would correspond with a wetter climate.

The sedimentology and micro and macro-fossil material in the cores from this study, show no major changes throughout the shell hash (LF5) unit in the mid and outer bay, which represents the time period from 7.4 to 4.1 ka cal BP. The shell hash (LF5) unit indicates a temperate environment, with no evidence of a temperature drop, and has a higher sedimentation rate than the underlying gravelly sand and silt (LF2) and silty sand/ sandy silt (LF3). This links with the work of Wood (2010), who presents a relatively stable climatic $\delta^{18}\text{O}$ record, with no major oscillations from 6 to 5 ka cal BP, also suggesting that the climate variations that were occurring across Europe were not evident further offshore. While the geochemical records from the shell hash (LF5) unit in this study show a variable terrestrial and freshwater input to the bay, suggesting

variability in the terrestrial hydrological conditions, there is no evidence that would indicate a significantly wetter climate over a prolonged time period.

However, the single sediment core from the inner bay (01VC), shows a significant peak in Ba/Ca between interbedded sandy silt and silty sand (LF6) and silty sand (LF7) (Fig. 5.15), suggesting a massive influx of freshwater to the inner bay. While this core has not been dated, it is interpreted to be older than 4.1 ka cal BP based on the presence of the overlying poorly sorted, coarsening upwards silt to coarse sand (LF8), and the connection to the freshwater signature to a freshwater signal noted in the diatom inferred (DI) salinity just prior to the hiatus at ~6 ka BP in Novak's (2017) work.

Also, within the mid-Holocene period is a series of short multi centennial climatic deteriorations, between 5.6 and 5 ka cal BP, that are collectively known as the 5.2 ka BP event (Magny et al, 2006). A wetter and cooler climate is seen in various Irish bogs (Roland et al, 2010), human (O'Connell and Molloy, 2001; Caseldine, 2005; Schettler et al, 2006) and speleothem records (McDermott et al, 2001) (Fig. 7.6).

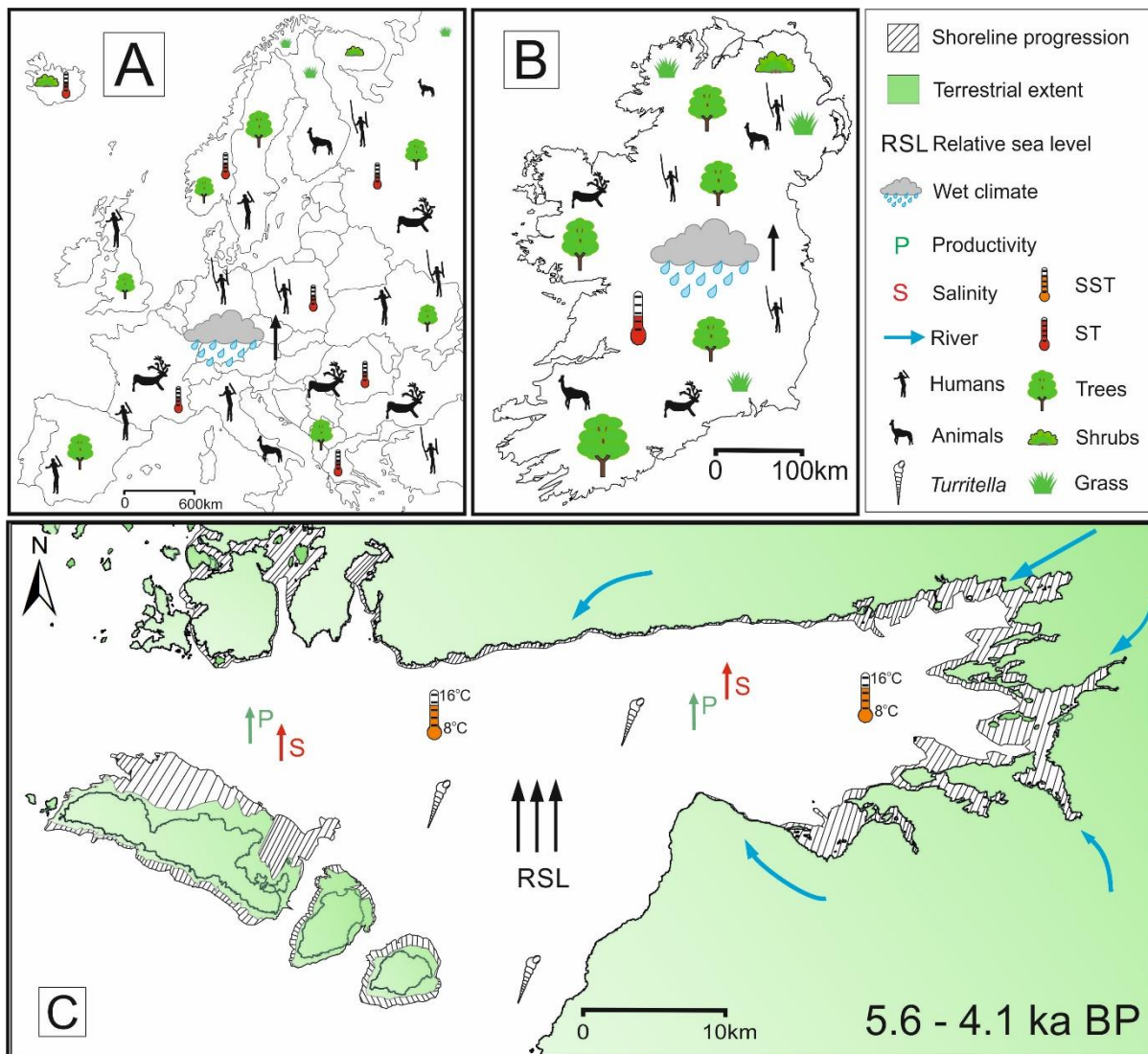


Figure 7.6: Summary of the mid Holocene environmental conditions in (A) Europe, (B) Ireland and (C) Galway Bay, with the retreat of shoreline positions, between 5.6 – 4.1 ka cal BP, based on GIA derived RSL predictions (Brooks et al, 2008; Bradley et al, 2011; Kuchar et al, 2012), data from this study (Fig. 5.6 & Table 7.1) and references found in Table 2.1. ST: Surface Temperature. SST: sea surface temperature, based on foraminifera preferences (Appendix 3).

Once again, although there is variability in the Ba/Ca and Sr/Ca ratios representing the terrestrial input to the bay, within this study this variability is not time constrained, nor does it show evidence of a significant influx of freshwater or terrestrial material to the bay. It is possible that the reduction in Neolithic farming allowed for re-afforestation (Whitehouse et al, 2014) and that this increase in vegetation cover is the

reason for a reduced signal in hinterland runoff into the bay. If there was a climatic cold phase during this time, the resolution of the records from Galway Bay, may not be high enough for it to be identified.

The boundary between the Northgrippian and Megahalyan periods is marked by a global climatic change that occurred between 4.4 and 3.8 ka cal BP, in what is known as the 4.2 ka event (Walker et al, 2012; Walker et al, 2018). This resulted in drier conditions at lower altitudes and colder/wetter conditions at higher altitudes (Booth et al, 2005; Roland et al, 2014). Studies on raised bog systems in Northern Ireland do not show this substantial trend towards wetter conditions which have been observed elsewhere (Roland et al, 2014). While a severe climatic shift is not evident, observed changes in the North Atlantic Oscillation (NAO) at ~4 ka cal BP (Olsen et al, 2012; Faust et al, 2016), may have had a knock on effect on the Atlantic Meridional Overturning Circulation (AMOC) and affected the local climatic conditions in Ireland through variability in precipitation, and evaporation during the beginning of the late Holocene.

In Galway Bay, the termination of the shell hash (LF5) unit has been dated to 4.1 ka cal BP, which falls within this period. An abrupt change is evident between the shell hash (LF5) and the overlying poorly sorted, coarsening upwards silt to coarse sand (LF8), with a sharp boundary dividing the two, and a complete disappearance of *Turritella communis* in the upper unit. While the geochemical data across all cores, particularly Si/Ti, Sr/Ca and Ba/Ca, which are indicators of runoff, do not show any abrupt or significant peaks between the shell hash (LF5) and the overlying facies of poorly sorted coarsening upwards silt to coarse sand (LF8), there is variability within these ratios. This may suggest that smaller local events are affecting changes in sediment delivery to the bay, perhaps enabling enough suspended sediment in the bay to disrupt the *Turritella* habitat. Alternatively, this depositional shift may be due to changes in sea-level rise and circulation patterns within the bay causing an increase in suspended sediment in the water column. The change in circulation in the bay is supported by the silty sand (LF7) unit in the inner bay. Although LF7 has not been dated, the transition between the underlying interbedded sandy silt and silty sand (LF6) and silty sand (LF7) is believed to be contemporary with the hiatus in Novak's (2017) cores at ~6 ka cal BP,

based on similar freshwater signals. The high geochemical signal indicative of freshwater influx (increasing Ba/Ca) at the base of the silty sand (LF7) unit, combined with the abrupt increase in salinity (decreasing Sr/Ba) at the boundary with the poorly sorted, coarsening upwards silt to coarse sand (LF8), suggests a change in the circulation and delivery of freshwater to this area. The timing of this change in geochemistry and the disappearance of the *Turritella sp.* coincides with the beginning of the Meghalayan period and changing climates across the world (Cullen et al, 2000; Bond et al, 2001; Marchant and Hooghiemstra, 2004; Drysdale et al, 2006; Liu and Feng, 2012).

7.5 Late Holocene period - Meghalayan (4.2 ka cal BP - Present)

The beginning of the late-Holocene period is marked globally by the after-effects of the 4.2 ka aridification event, which had far reaching climatic consequences and caused devastation in civilisations across the world (Weiss et al, 1993; Hassan, 1997; Cullen et al, 2000; Staubwasser et al, 2003). This (Meghalayan) period extends from after 4.2 ka cal BP until the present day.

In Galway Bay, the sediment record following 4.1 ka cal BP is suggestive of a warm, wet climate with high levels of terrestrial runoff. Biological indicators of this include the presence of foraminifera species such as *Quinqueloculina spp.* and *Ammonia spp.* which are found in temperate waters (Horton et al, 1999; Murray, 1971, 1979) and the presence of abundant and diverse mollusc species, indicating a high level of nutrient input and productivity. Geochemical environmental indicators in the uppermost lithofacies in the cores (poorly sorted, coarsening upwards silt to coarse sand; LF8) include increasing Sr/Ca and Fe/Ti content, representing increased freshwater influx to the bay. Evidence on farming activity and from pollen, microfossils and speleothem records from across Ireland suggests that the conditions at this time in Galway Bay are caused by a combination of human impact (farming and land clearance), and a wetter climate (Fig. 7.7) (Molloy and O'Connell, 1995, 2004, 2012; Baillie, 1995; McDermott et al, 1999; Schettler et al, 2006; Holmes et al, 2007; Overland and O'Connell, 2008; O'Connell et al, 2014; Chique et al, 2017).

In Galway Bay, the sedimentation rate at the transition from late Northgrippian into the early Meghalayan is quite low, with a rate of 0.1mm/yr calculated from core 10VC, between 4.4 and 2.2 ka cal BP (Fig. 5.29). While there is a clear peak in the Sr/Ca ratio in core 10VC at the boundary between the shell hash (LF5) and the poorly sorted, coarsening upwards silt to coarse sand (LF8) units, suggesting a freshwater influx, there are no other indicators of substantial terrestrial inputs during this time. This suggests that, if the bay received large inputs of terrestrial material, it was either deposited further inshore /offshore or has been eroded away.

Throughout the poorly sorted, coarsening upwards silt to coarse sand (LF8) unit, there is no evidence of any abrupt significant changes. Lithological changes such as the coarsening upwards nature of this facies are gradual, as are all biological and geochemical changes, such as the increased diversity in foraminiferal content and clear trend towards a more marine environment with increasing Br/Cl, and Ca/Ti and decreasing Ba/Ca ratios. This constant and gradual change is at odds with the literature for the late Holocene where cyclicity is clearly obvious, with climatic changes every 1000 - 1500 years (Mayewski et al, 1997). Climatic deterioration is recognised at 4.2 ka, 2.7 ka, 1.4 ka, and at 0.4 ka cal BP across almost all of the northern hemisphere and in many parts of the southern hemisphere (Magny, 2004; Parker et al, 2006; Roberts et al, 2011; Larsen et al, 2012). These changes must therefore have been influenced by global climate drivers. Many studies have recognised that changes in solar insolation and ocean circulation are interconnected (Bond et al, 1999, 2001) and changes in either of these can result in significant climatic changes (Hurrell et al, 2003; Hurrell and Deser, 2010; Franke et al, 2017). In particular, the NAO plays a major part in the climate of Ireland due to its proximity to the Atlantic Ocean. Of the major climatic 'events' however, changes in Galway Bay are only recognised during the 4.2 ka event, where there is a clear sedimentological change from shell hash to poorly sorted coarsening upwards silt to coarse sand which is interpreted to mark the boundary between the Northgrippian and Meghalayan.

Galway Bay does not show any abrupt significant jumps that would be consistent with any major environmental change for the Roman Warm Period (RWP), Dark Ages Cold Period (DACP), Medieval Warm Period (MWP) or Little Ice Age (LIA) (See Chapter 2).

The lack of any signature of these climatic changes in Galway Bay in either the sedimentary or seismic records, even though they are visible in many of the Irish climatic proxies and documented historically, may be due to several reasons: (1) the resolution of the record, (2) the sheltered nature of the bay, or (3) erosion/non-deposition of sediments in the bay.

Though the sampling resolution of the foraminifera may not be high enough to capture major climatic signals, there are no significant changes in the geochemical ratios, sedimentology or seismic data, suggesting that if a climatic signature was present it should have been captured. The second possibility for lack of a climatic signal, is that the Aran Islands acted as a barrier. This would mean that any storm events associated with these events, in particular during the latter half of the LIA (~300 BP), which is known to have experienced intense storm activity (Dezileau et al, 2011), were severely reduced in force by the time they reached the bay. This is supported by the large boulder deposits along the outside of the Aran Islands, but reduced number inside the bay (Scheffers et al, 2010; Erdmann et al, 2015). The final reason for the lack of a signal in the record may be the strong currents and circulation pattern in areas of the bay, causing the removal of material. While the cores in this study show no recognisable hiatus or evidence of extensive erosion in line with these climatic events, there is evidence of possible reworking, with a young radiocarbon date (0.9 ka cal BP) on the boundary between the shell hash (LF5) and poorly sorted, coarsening upwards silt to coarse sand (LF8) units. Cores within Galway Bay, analysed by Wood (2010), also show evidence of reworking and erosion. The clear coarsening upwards trend in the lithology of poorly sorted, coarsening upwards silt to coarse sand (LF8) is gradual, without any abrupt changes visible. This may be the result of winnowing of the finer sediments, as modern tidal patterns and circulation in the bay is very strong, especially between the Aran Islands (evident in sand dunes/waves and ripples) and in the Sounds, particularly the North (See Chapter 4). This is reinforced by the high level of shell fragmentation and the out of sequence radiocarbon date, in the poorly sorted, coarsening upwards silt to coarse sand (LF8) unit. This may all indicate reworking, typical in areas with strong currents.

The parallel reflectors in the post-glacial (3b) unit, represent uniform deposition (Mitchum et al, 1977), suggesting that there were no major changes in sediment delivery to the bay. Although it is not possible to accurately determine the sedimentation rate, as there is only 1 radiocarbon date within the poorly sorted, coarsening upwards silt to coarse sand (LF8) unit, the post-glacial (3b) unit, which covers the entire Holocene, is only 8.5m thick in its entirety. This suggests low sedimentation rates, significant erosion, or non-deposition in the bay. All of these would make capturing any of the aforementioned Meghalayan climatic events difficult due to the short timescales involved.

The work by Novak (2017) in the inner bay, indicates a hiatus over a large part of the mid and late Holocene, however they also show much higher sedimentation rates for the early Holocene and modern deposits. These extremely high sedimentation rates in the inner bay correspond with the isopach maps from this study, which also show the highest accumulation of sediments in the inner bay (Fig. 5.23). Overall, the thickness of the post-glacial (3b) unit and poorly sorted, coarsening upwards silt to coarse sand (LF8) unit indicates a relatively low sedimentation rate in the mid and outer bay and a higher accumulation of sediments in the inner bay. This also corresponds to the offshore records, as Wood et al (2017) note a very condensed sediment record for the mid-late Holocene. This may indicate changing circulation patterns over time, which allowed for the build-up of material in the inner bay during the early and very late Holocene, but reduced deposition in the mid and outer bay during the mid-late Holocene. In Galway Bay it is likely that the circulation patterns and low deposition of sediments in the mid and outer bay combined with the short timescales of major climatic events during the Meghalayan have resulted in the lack of a signature of in the late Holocene record in this study.

This research demonstrates evidence of prograding clinofolds, typical of transgression, evident in the South Sound in the post-glacial (3b) unit (Fig. 5.23), and an increase in the abundance and diversity of marine foraminifera species upcore throughout the bay. Increasing trends in the geochemical ratios of Ca/Ti, Br/Cl and decreasing trends in the Sr/Ba and Ba/Ca ratios, all of which indicate an increasingly open, productive, marine environment, throughout the poorly sorted, coarsening

upwards silt to coarse sand (LF8) unit This reinforces previous studies carried out in Galway Bay which show that sea-level rise and transgression is continuous throughout the late Holocene (Wood, 2010; Novak, 2017). This information correlates with the GIA model derived RSL predictions for the bay which also show a continuously rising sea-level throughout the late-Holocene period (Brooks et al, 2008; Bradley et al, 2011; Kuchar et al, 2012) (Fig. 7.9)

The modern-day Galway Bay is an open water marine environment, with the seafloor composed of the coarsest sediments in the cores, with the exception of gravel in the gravelly silt and sand (LF2) unit. The pattern of erosional features, which are concentrated in the outer central bay (See Chapter 4), and the lithology of the seabed surrounding them (Fig. 4.1), indicate that gyres are present in this area. The majority of depositional features, however, are found between the Aran Islands, one of the strongest areas of water movement (Fig. 4.2), indicating that the tidal currents are the main influence on sediment deposition in the bay. The combination of the modern lithology, which suggests winnowing, and the location and shape of features in the bay indicates that currents are a driving force in the topography of Galway Bay and appear to have become stronger over time.

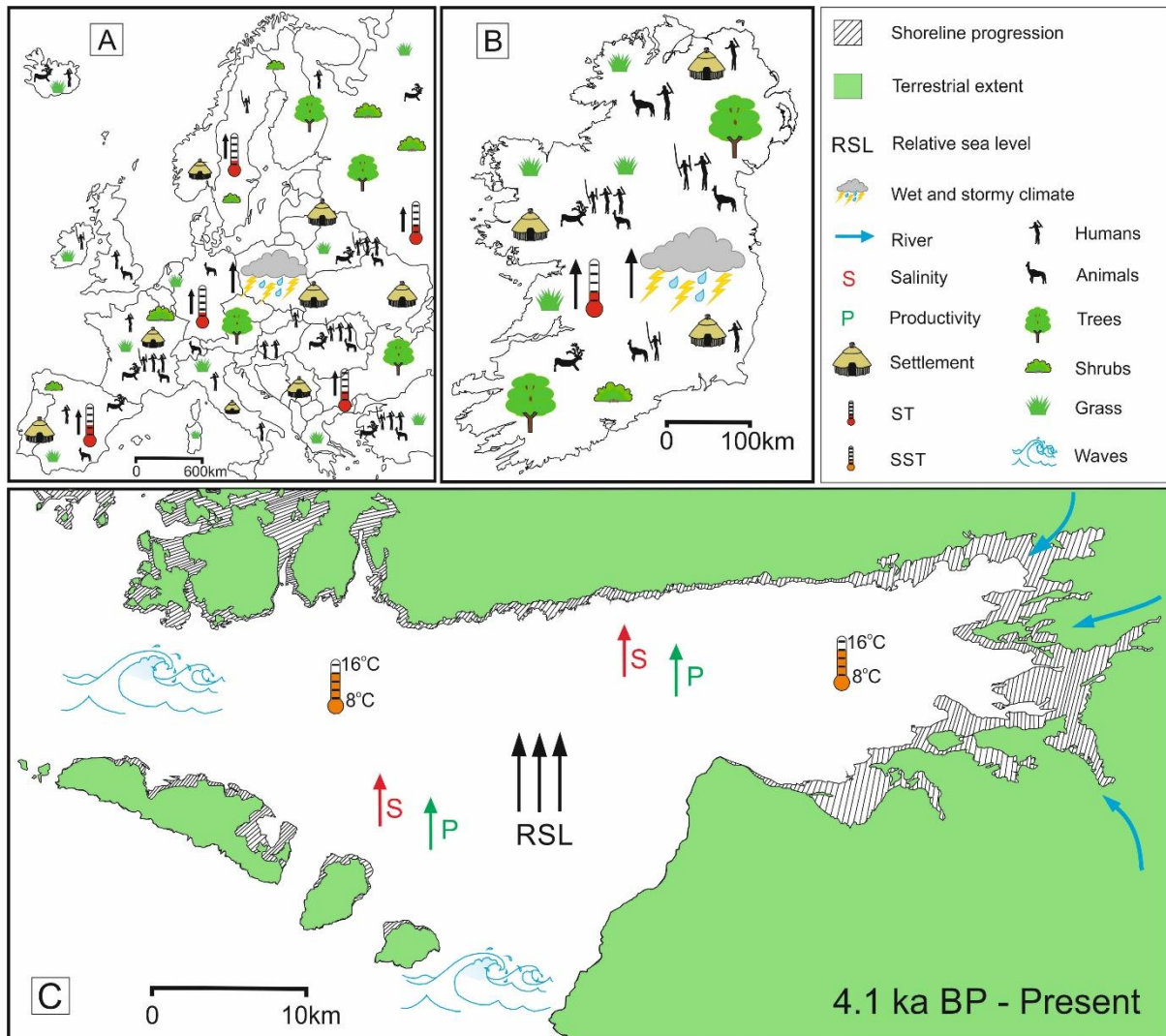


Figure 7.7: Summary of the late Holocene environmental conditions in (A) Europe, (B) Ireland and (C) Galway Bay, with shoreline positions based on GIA derived RSL predictions (Brooks et al, 2008; Bradley et al, 2011; Kuchar et al, 2012) and data from this study (Fig. 5.6 & Table 7.1). ST: Surface Temperature. SST: sea surface temperature, based on foraminifera preferences (Appendix 3).

7.6 Sea-level changes in Galway Bay since the last deglaciation

Currently there are 3 GIA derived RSL reconstructions available for the region, (Brooks, Bradley and Kuchar). These have partly been validated with groundtruth data (Brooks et al, 2008; Shennan et al, 2018). They have differing outputs, due to differing parameters decided on by the authors. The models of both Brooks and Bradley use an ice model with a larger lateral extent, with ice reaching onto the continental shelf, and use trimline evidence as a maximum thickness for the ice sheet. On the other hand,

Kuchar's model uses a much less laterally extensive ice model but uses the trimline evidence as an indication of minimum rather than maximum ice thickness.

In order to provide real world observations on the changing sea-level, SLIPs are needed. As discussed in Chapter 2, the only available data available to constrain sea-level in Galway Bay are limiting data, which means that only maximum and minimum constraints can be applied, but exact sea-level at a particular time cannot be precisely identified. Currently there are 119 sea-level data points in the Irish database, of which only 33 are index points and the rest are limiting points (Edwards et al, 2017) (Fig. 1.2). Only 22 of the sea-level data points are from Galway Bay and all of them are limiting points (Mitchell, 1976; Williams and Doyle, 2014; and O'Connell and Molloy, 2017). In Galway Bay specifically, this means that constraints for the sea-level models in the bay are based on a very small range of limiting data (Edwards and Craven, 2017). This research provides a further 16 marine limiting dates for this area, based on the radiocarbon dates and depth of the samples (Table 7.1). To provide the best sea-level curve for the bay, all reworked dates have been excluded. A further 2 points (A and B) are time constrained based on ice retreat dates from literature on the surrounding area, while another point (K) is time constrained based on its position in the sediment core between 2 radiocarbon dates taken from a core in the bay (Table 7.1).

In the following paragraphs the data collected in this study are compared to all 3 existing sea-level curves for Galway Bay (Fig. 7.7). These data provide key information on the sea-level in the bay before 8.8 ka cal BP. This can be used to expand the Irish database, as there are no sea-level data for the entire west coast of Ireland between 13 and 9 ka BP and only secondary limiting data from 19 to 13 ka cal BP. Overall the terrestrial and marine evidence in western Ireland suggests that there were readvances of the ice sheet in Galway Bay after initial deglaciation at ~20 ka cal BP and that the youngest age for glacial till (U2) is constrained to 15 ka cal BP. The channel through the North Sound in the glacial till (U2) is interpreted to have been glaciofluvially cut during the retreat of ice, as it extends seawards from the Corrib River (Fig. 5.22 & 7.1) and is likely part of a palaeo-riverine system identified by Clarke (2013). At its deepest terrestrial point, in the outer-most area of the bay, this channel

is ~58m in depth, suggesting that sea-level during or immediately after the retreat of ice from the bay was ~58m lower than present day.

Table 7.1: Table showing all of the data points used in RSL prediction based on data from this study. OB represents outer bay, while MB represents mid bay. All data points except point A are marine.

Transitional water represents water levels between 8m and 36.45m above the sample.

Point	Depth (m LAT)	Area	Unit/ Facies	Feature/ Material	Date (ka cal BP)	Environment
A	-58 - -53	OB-North Sound	U2	Base of Channel	16 – 15	Terrestrial
B	-70 - -57	OB-North Sound	U3A	Base of unit	16 – 15	Shallow
C	-43	OB-South Sound	LF3	Foraminifera	13.1	Sub-tidal
D	-40.4	OB-North Sound	LF2	Bivalve	11.7	Beach
E	-42.7	MB-South Sound	LF2	Bivalve	11.5	Beach
F	-59.8	OB-North Sound	LF4	Foraminifera	10	Transitional
G	-43.4	OB- South Sound	LF3	Bivalve	9.9	Sub-tidal
H	-44.4	OB-North Sound	LF2	Bivalve	8.8	Beach
I	-37.2	OB-Central Bay	LF5	Turritella	7.4	Transitional
J	-39.8	OB-North Sound	LF5	Turritella	7.3	Transitional
K	-41.6	OB-North Sound	LF5	Oyster	-	Transitional
L	-57.4	OB-North Sound	LF5	Turritella	6.8	Transitional
M	-42.6	OB-South Sound	LF5	Turritella	6.4	Transitional
N	-41	OB-North Sound	LF5	Turritella	6.2	Transitional
O	-34.2	Mid Bay	LF5	Bivalve	5.6	Transitional
P	-36.5	OB-Central Bay	LF5	Turritella	4.4	Transitional
Q	-39.3	OB-Central Bay	LF5	Bivalve	4.3	Transitional
R	-39.7	MB-South Sound	LF5	Turritella	4.1	Transitional
S	-36.3	OB-Central Bay	LF8	Bivalve	2.2	Deep
T	-	-		Modern SL	0	-

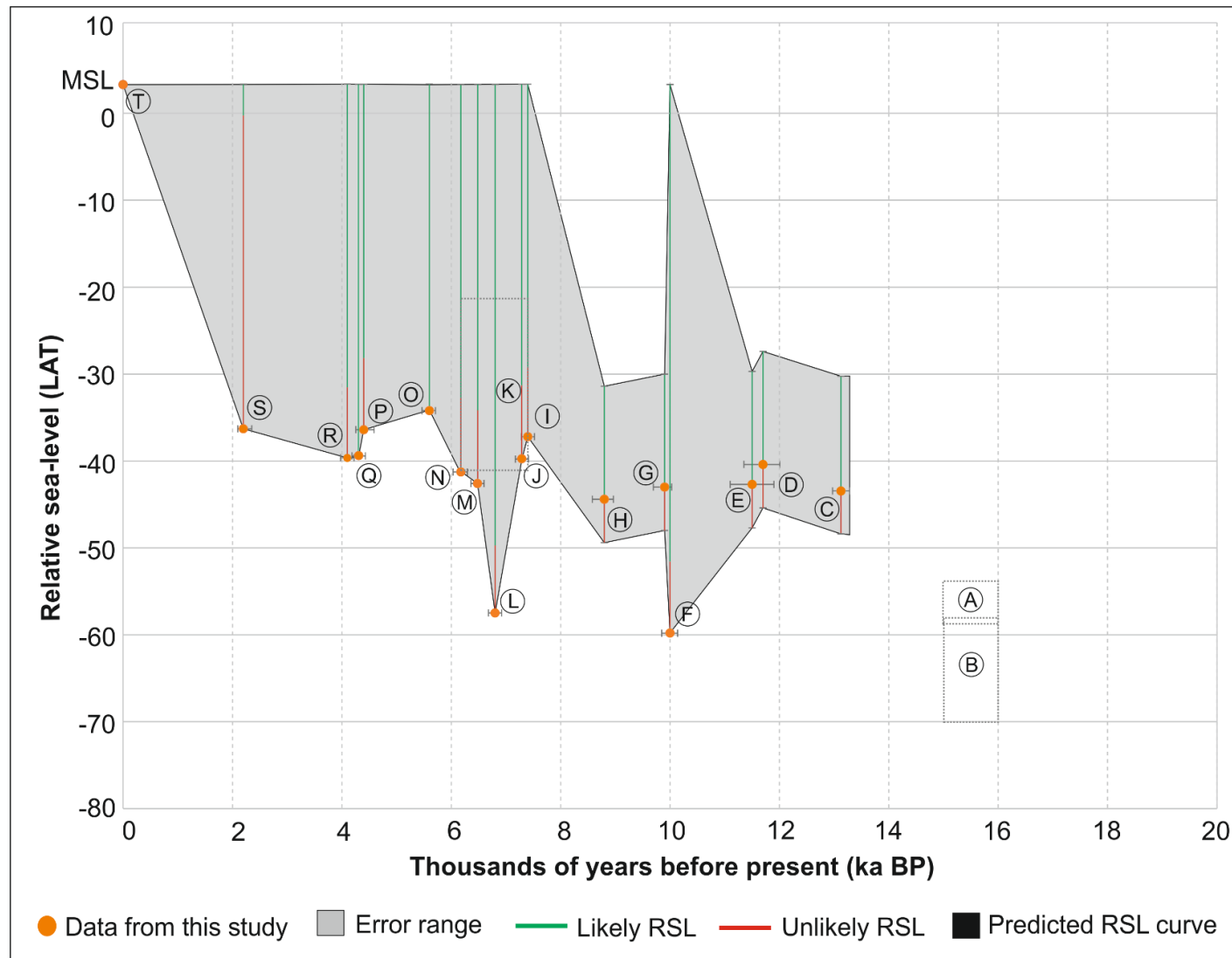


Figure 7.8: Graph based on the dates in Table 7.1 acquired from this research, showing sea-level progression in Galway Bay from deglaciation until present day.

The maximum, present day, tidal range in Galway Bay is up to ~5m and this is the tidal range assumed for all data points. This corresponds with the work of Scourse et al (2018) who defines the bay as megatidal during early and mid-deglaciation. This suggests that sea-level was between 53 and 58m below modern-day levels. This is represented as point A (dashed box) (Fig. 7.7), the only terrestrial data on the graph, between 16 and 15 ka BP, and the error bar allows for a 5m upper limit, based on the tidal range.

Deglacial sub-unit 3a, represented by point B (dashed box) on the graph, is up to 70m lower than present day at its lowest limit on the seismic data (outer North Sound) (Fig. 5.24 & 5.26). The base of unit 3a is composed of lenticular reflectors, suggesting it was deposited in a shallow, variable energy environment (Catuneanu, 2006). Shallow water for this study is defined as anything less than 8m in depth. As this unit is a shallow water deposit the RSL would have been between -57m and -70m in the western North Sound, allowing for the depth of shallow water and the tidal range. Deglacial sub-unit 3a was interpreted to have been deposited after ice began to retreat from the outer North Sound, between 16 and 15 ka BP, though likely nearer to 16 ka BP (Fig. 7.7).

The oldest date in post-glacial seismic sub-unit 3b is found in silty sand/sandy silt (LF3) in the South Sound at 13.1 ka cal BP (core 13VC) (Fig. 5.29) and was deposited in a sub-tidal, shallow water, estuarine environment at -43m (Fig. 6.1 & 7.2). This indicates that sea-level was between 31 and 48m bsl, as indicated by point C on the graph (Fig. 7.7). At the beginning of the early Holocene, with a much lower sea-level, the bay would have been 2 separate inlets. This is reinforced by the different, contemporary lithofacies in the North and South Sounds. Gravelly silt and sand (LF2), a nearshore beach deposit, is found primarily in the North Sound, as is coarsening upwards sandy mud (LF4), a fully marine, deeper water deposit. The silty sand/sandy silt (LF3), a sub-tidal deposit, is found only in the South Sound. In order to have a land barrier separating the North and South Sound areas of the bay, the sea-level would have been at least 35m lower than present day (Fig. 7.4).

LF2 has 2 dates at 11.7 and 11.5 ka cal BP, points D and E on the graph (Fig. 7.8), respectively. Points D and E are both constrained to a lower limit of -5m by the maximum tidal range and to an upper limit of 13m by the maximum tidal range and

the maximum depth of the surf zone. The surf zone is calculated as approximately the same depth as the maximum wave height in the bay, recorded as 8m (Marine Institute, 2017, 2018). Point D is located at 40.4m bsl, while point E is located 42.7m bsl and although the error bars indicate a possible lower limit, it is much more likely that sea-level was located closer to the upper limits due to the presence of marine foraminifera such as *Textularia sp* and *Quinqueloculina sp*.

The deepest lithofacies deposit within sub-unit 3b is found in the North Sound in coarsening upwards sandy mud (LF4) at 59.8m bsl (at the base of core 22VC) and is dated to 10 ka cal BP (Fig. 5.26). This lithofacies is indicative of a marine deposit in a transitional water environment and is represented on the graph as point F.

Transitional water is defined as between shallow and deep. Deep water is calculated as the wavelength/2 (The Open University, 1999), using the significant wave period average over the past 5 years (Ireland's Digital Ocean, 2018). In Galway Bay, deep water is therefore determined as more than 36.25m, while shallow water is defined as less than 8m. It is therefore likely that RSL was between -23m and -52m bsl at 10 ka cal BP (Fig. 7.8).

Points G and H show that this RSL remained below -40m in Galway bay between 9.9 and 8.8 ka cal BP (Fig. 7.8). Point G is a subtidal deposit, at 43.4m bsl, in the inner South Sound, containing the foraminifera species *Jadammina macrescens*, while point H is a nearshore beach deposit that is 44.4m deep (Fig. 7.8). The error bars for these points have an upper limit of 13m and a lower limit of 5m, accounting for the surf zone and tidal range. With evidence of both marine and estuarine foraminifera such as *Textularia sp.*, *Quinqueloculina sp.* and *Planorbulina mediterraneensis*, it is much more likely that the sea level at point H, like point G, is closer to the upper range of the error bar.

Between 8.8 and 7.4 ka cal BP, evidence from this study shows a likely sea-level rise of ~14.5m in the bay (Fig. 7.8). The presence of LF5, visible across the entire bay from 7.4 ka cal BP (Fig. 7.5), suggests a changing circulation system with ongoing transgression and deepening water, likely due to the opening up of the bay into a single area. This increase in sea level matches well with the evidence of *Turritella sp.* in core 10VC at 37.2m bsl, represented by point I on the graph (Fig. 7.7). Points J, L, M and N (Fig. 7.9)

are also *Turritella*, at 39.8m (7.3 ka cal BP), 57.4m (6.8 ka cal BP), 42.6m (6.4 ka cal BP) and 41m (6.2 ka cal BP), respectively (Table 7.1). The error bar for these points, have no upper limit, however it is likely sea-level was at least 8m above this point as *Turritella sp.* are filter feeders that would not thrive in the surf zone. The samples are all likely located in transitional water between the shoreline and deep water, based on the presence of estuarine foraminifera such as *Quinqueloculina spp.*, and *Haynesina germanica*. This would constrain RSL between 8 and 36.25m above each sample. Point J represents an oyster shell, found in core 07VC, in the North Sound, at 41.6m bsl. Although the error bar for this point ranges from 41.6 – 21.6m (Fig. 7.7), it is much more likely the sea-level was between 7 – 20m above the sample, based on the typical habitat in which oysters are found (Todorova et al, 2009). The age of this oyster sample must be between 7.4 and 6.2 ka BP based on the oldest age of the lithofacies in which it was recovered and the radiocarbon date of 6.2 ka cal BP located above the sample. This sample constrains relative sea-level between 7.4 and 6.2 ka cal BP to below -21.5m (Fig. 7.9).

The sea-level in Galway Bay continues to rise throughout the rest of the Holocene. The rate of increase is difficult to determine, due to the high error bars on the constraining data (Fig. 7.8). The samples taken at 5.6 ka cal BP, 4.4 ka cal BP, 4.3 ka cal BP and 4.1 ka cal BP, represented on the graph by points O (-34.2), P (-36.5m), Q (-39.3m) and R (-39.7m) (Fig. 7.7) respectively, are either bivalves or *Turritella sp.* As the surf zone in Galway Bay is 8m deep and since *Turritella sp.* do not occupy turbid waters, this indicates that the likely RSL was between 8 and 36.25m above the samples.

The sample at 2.2 ka cal BP is located 36.3m bsl, in core 10VC. This sample is represented on the graph as point S (Fig. 7.8). Point S is interpreted to have been deposited in a deeper inner shelf environment. As deep water is calculated as anything more than 36.25m bsl in Galway Bay, it is likely the sea-level when point S was deposited was 0.05m bsl (LAT) (Fig. 7.8). The upper constraining limit at this point, like all points after 8.8 ka cal BP, with the exception of point K, is the modern day mean sea-level. It is very unlikely that the sea level was higher than present day during this period, as there is no evidence of raised beaches, in or around the bay, suggesting

there was never a recession or sea-level drop after 15 ka cal BP. Point T represents the current day sea level at 0m (Fig. 7.8).

7.6.1 Comparison of data points with GIA derived RSL curves for the Bay

In the GIA derived RSL predictions, the dropping sea-level between 19 and 16 ka BP and the lowstand between 16 and 15 ka BP (Fig. 7.9) is contrary to the global sea-level rise caused by meltwater pulse 1A0 at 19 ka BP (Clark et al, 2004). This indicates that the regional effects of isostatic rebound from the BHS were significantly more influential in Galway Bay than the global trend of sea-level rise, with ice present in the bay until 16 - 15 ka BP. From this study it is impossible to determine sea-level position before 16 cal ka BP, as the glacial till unit is a reworked chaotic structure whose age cannot be defined (Fig. 5. 19) and earlier sediments are not preserved.

The maximum depth of the sea level models for the bay show a lowstand at 68m bsl in Kuchar's model between 17 and 15 ka cal BP, while the Brooks and Bradley models show lowstands at 60m bsl and 56m bsl at 15 ka BP, respectively (Fig. 7.9). This indicates that only Brooks and Kuchar's models have a sea-level depth that would allow for glaciofluvial erosion of the North Sound channel. However, if the maximum tidal range of 5m is accounted for, Bradleys model would also have been terrestrial at 58m bsl. Deglacial sub-unit 3a was interpreted to have been deposited after ice began to retreat from the outer North Sound, likely nearer to 16 ka BP, and the lowstand in the RSL curve from this study is 58m bsl at 16 ka cal BP, fitting best with Brooks model. After 15 ka cal BP, all models show a significant sea-level rise until ~13.5 ka cal BP, of ~19.5 - 22.5m. This correlates closely with the rapid sea-level rise attributed to meltwater pulse 1A between 14.65 and 14.3 ka BP (Fig. 7.8) (Fairbanks, 1990; Peltier and Fairbanks, 2006; Stanford et al, 2006; Deschamps et al, 2012). The rapid RSL rise has been recorded in the data as a change from the terrestrial extension of a glaciofluvially cut channel to a sub-tidal deposit (point A and point C). After 13.5 ka BP, all models for Galway Bay show a slowstand (Fig. 7.8), with a sea-level rise of less than 5m over a 2000-year period (Brooks et al, 2008; Bradley et al; 2011; Kuchar et al, 2012). However, the models show significantly differing predicted RSL for the bay, with Kuchar's model almost 3m lower than the predicted RSL from this study at 13.1 ka cal

BP (Fig. 7.8). Both Brooks (2008) and Bradley's (2011) models show sea-levels higher than our reconstructed curve for the bay. Brooks' model is only 3 m higher, and would fall within the intertidal, rather than subtidal range, suggesting it is an unlikely representation of RSL at this time. Kucher's model cannot be an accurate estimate of sea-level at this time as the upper tidal range of points C, which is a subtidal deposit, is above RSL. The best fit model for the bay at this time is that of Bradley's model. There is no evidence to suggest a sea-level rise affecting the bay between 11.45 and 11.1 ka BP, an event commonly known as MWP 1B (Bard et al, 2010). Although the sea-level rise during MWP 1B is seen in some areas, in particular at Barbados (Abdul et al, 2016), many other coral records around the world, particularly the sites in the Pacific Ocean, do not show a significant sea-level rise at this time (Edwards et al, 1993; Bard et al, 1996; Cabioch et al, 2003; Cutler et al, 2003). This suggests that this sea-level rise may not be as significant as previously believed, or that local isostatic adjustment effects are much more influential in different areas at different times. The major differences in the data from this study and the sea-level models for the bay, are after 11.5 ka cal BP (points F, G and H) (Fig. 7.9). Following 11.5 ka BP, all GIA derived RSL predictions show an abrupt increase in sea-level. Based on points G and H, which are beach deposits, this study shows that this sea-level rise was not immediately evident in Galway bay (Fig. 7.8). Instead, the slowstand appears to have continued for another ~1800 years. This differs significantly from Novak's (2017) work in the inner bay and Corrib estuary, where a possible marine intrusion is first recognised at 10.2 ka cal BP, at a depth of 18.4m, when diatoms were found in the sediment core VC003 east of Barna. In the same core Novak (2017) also identified the foraminifera species *Jadammina macrescens*, distinctive of marsh environments, at 9.8 ka cal BP in 17.9m water depth. Point G (Fig. 7.8) is a subtidal deposit, in the inner South Sound, containing the foraminifera species *Jadammina macrescens* at a depth of 43.4m and is found ~25km away from the Corrib estuary at 9.9 ka cal BP. Even allowing for deposition at the upper limit of the error bar, these deposits do not coincide, unless the tidal zone extended this far inland. This suggests that the bathymetry in the bay would have had to have been very different in order to have similar deposits so far apart.

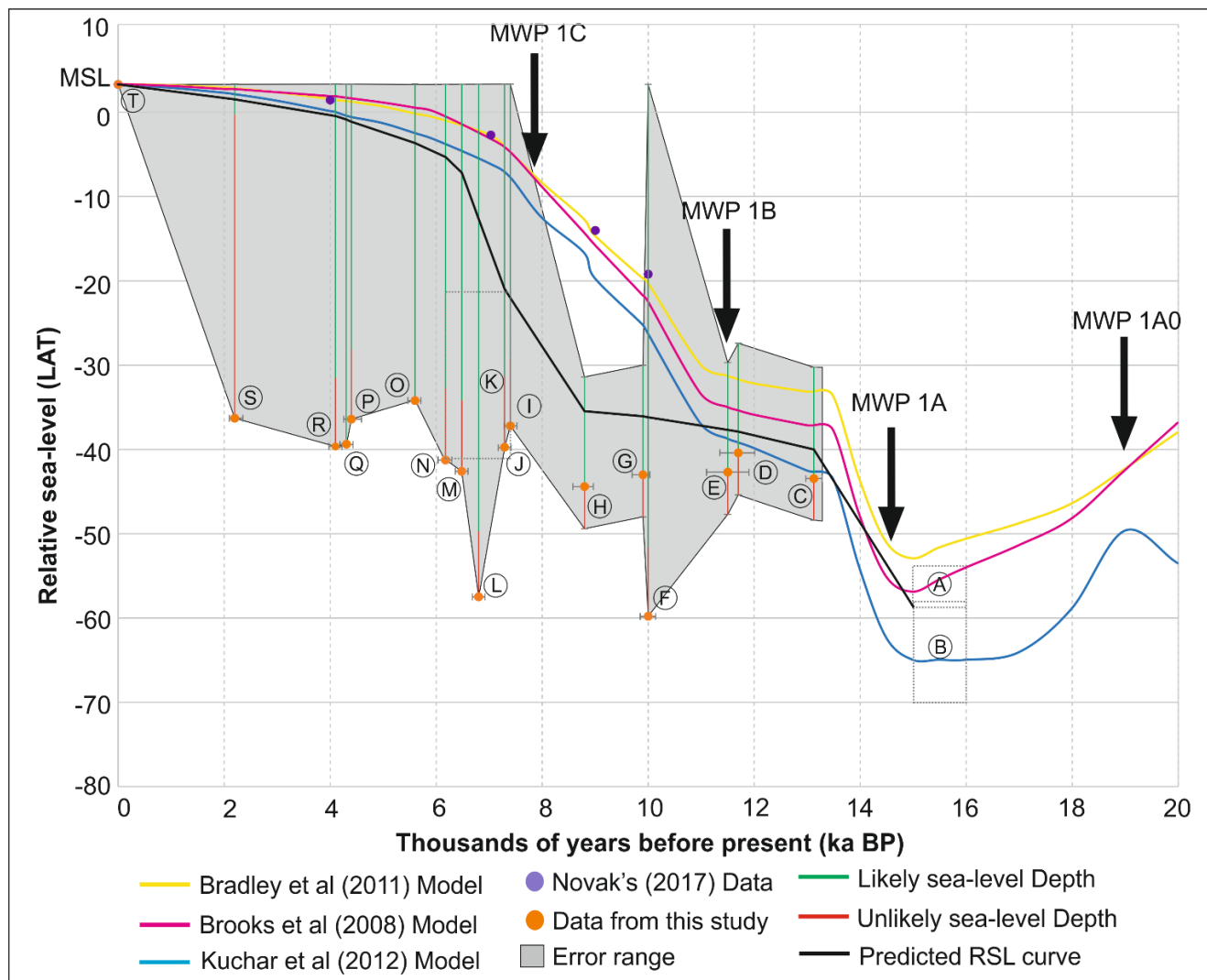


Figure 7.9: Graph showing sea-level progression in Galway Bay from this research, alongside all GIA derived RSL predictions and other sea-level work carried out in the bay. Significant global sea-level events are also included.

However, Novak (2017) also notes that due to the fragmented nature of the shell hash and diatoms, these may have come from a fluvial deposit, while she also states that both the diatom and foraminifera found in the cores were present only in small numbers, with only 10-250 foraminifera specimens per sample until after 9 ka cal BP. Wood fragments and organic deposits are also found throughout Novak's (2017) cores until 9 ka BP, suggestive of a more terrestrial environment, or deposition along a river floodplain. Combined with the location of the cores, which are positioned in a palaeo-channel/deltaic environment, it is possible that these marine microfossils were

transported inland, along this system, during severe storm events. Storms of such magnitude have affected Galway bay and the Aran Islands throughout the Holocene, with Erdmann et al (2015, 2017) presenting evidence of storms that have transported boulders weighing up to 15 tonnes during a single event in the early Holocene. As the gravelly silt and sand (LF2) unit in this study shows extensive breakage in the fossil and microfossil evidence and evidence of pebbles and cobbles transported into the nearshore areas, it is possible that significant storms events were occurring during this time.

After 9.9 ka cal BP, GIA derived RSL predictions in Galway Bay show a continued RSL rise (Fig. 7.8). In this study, the sea level position was found to be much lower than represented by in the models for the bay, and than Novak's (2017) predicted sea-level in the inner bay (-13.5m in depth at ~9 ka BP). Brooks' model shows an RSL at 16m bsl, while Kuchars model shows RSL at 19m bsl. There is at least 16.5m of difference between Novak's (2017) sea-level representation and the upper error bay on the curve from this study at ~9 ka BP (Fig. 7.8). The predicted RSL from data in this study suggests a prolonged slowstand during this period.

It is possible that the discrepancy between the extended slowstand in Galway bay seen in this study and rising GIA derived RSL predictions is due to the parameters used in the GIA models. In Kuchar's model, the ice sheet parameters used are much less laterally extensive than recent studies (Benetti et al, 2010; Clark et al, 2012; Praeg et al, 2015; Peters et al, 2015, 2016) have shown the BIIS to have been. In both Brooks' and Bradley's models, the extent of the ice sheet is much closer to current studies, with the ice extending on to the continental shelf. However, these models differ from Kuchar's in that they use trim line evidence to constrain ice thickness to a maximum, rather than to a minimum, something recent studies have shown to be incorrect (Ballantyne, 2010; Ballantyne and Stone, 2015). If all models are failing to incorporate both the ice thickness and extent, it is possible that these models are underestimating the effect of the ice sheet depressing the land, meaning that the isostatic rebound may have been more significant and continued for longer than previously realised, as the evidence found in this study suggests.

Between 8.8 and 7.4 ka cal BP, evidence from this study shows a predicted RSL rise of ~14m in the bay (Fig. 7.8), which coincides with the period of MWP 1C (Deschamps, 2012) and a global sea rise between 8.2 and 7.6 BP (Liu and Milliman, 2004). Although sea-level in Galway Bay begins to rise before the occurrence of MWP 1C, it is possible its signal is causing a more significant increase. This rise in sea-level in the bay is supported by the change in lithofacies across the bay to shell hash (LF5) (Fig. 5.28). This led to the opening of the bay into a single area (Fig. 7.5), as opposed to the 2 separate inlets (Fig. 7.4). Although this study indicates rapidly rising sea-level until 5.6 ka cal BP, it is still well below the GIA derived RSL predictions and the data presented by Novak (2017). After 5.6 ka cal BP, all RSL predictions and sea-level data in the bay begin to coincide, with very similar predictions between 5.6 ka cal BP and present-day levels (Fig. 7.8).

Throughout the post-glacial period to the present, the evidence from Galway Bay suggests continuous transgression, with the seismic, geochemical, microfossil and sedimentary data all supporting sea-level rise across the bay. The geochemical data in particular shows an increasing salinity and marine organic and carbonate content. The microfossil evidence also shows a clear move away from marsh, brackish and estuarine foraminifera towards marine foraminifera upcore throughout the bay, supporting a deepening environment. Overall, the evidence from this study fits well with the general pattern of transgression in both the GIA derived RSL predictions and previous studies in the bay (Wood, 2010; Novak, 2017). However, the evidence found in Galway Bay, in particular the absence of meltwater pulse 1B and the slowstand before and during the early Holocene suggests that, while global events had an impact on the bay, local events also had a significant influence.

Chapter 8: Conclusions

This research has provided information on the dynamic nature of the environmental and sea-level conditions in Galway Bay for the period just after the LGM until present day. It used a multi-proxy investigation that includes proven techniques, such as sedimentological and microfossil analysis. It also used ITRAX analysis, a relatively novel approach to shallow water environments, which has proven to be an extremely useful tool in environmental reconstructions. The importance of this research is evident through the creation of the first geomorphology map of the bay, the first sea-level curve constrained by actual evidence from the bay (rather than modelled data) and the first environmental reconstruction combining multiple datasets across the entire bay. Overall this research contributes significantly to the investigation of the dynamic behaviour of shallow water environments on the western Irish coast following deglaciation and highlights the interplay between sea-level rise and environmental change.

8.1 Main findings

The analysis of the bathymetric, backscatter, altimetry and hydrological data supplies new knowledge on the modern-day coastal and seafloor morphology of Galway Bay. Through the creation of a detailed map of the current seabed and connection with hydrological models, the following can be concluded:

- Maerl and *Zostera* communities are confined between Oranmore and Ballyvaughan in the inner bay and Rossaveel and Lettermullan in the outer bay. These represent areas of stronger tidal action, where fine particles have been removed and turbidity in the water column is lower.
- The pattern of sediment deposition in the bay, in particular along the northern coastline, indicates that sediment deposition is driven by tidal currents moving in and out of the bay.
- Outcropping bedrock is evident across large areas of the bay, including the northern shoreline and surrounding the Aran Islands. This bedrock is a major driver in the direction of the movement of bottom currents around the central

area of the outer bay, where an accelerated, anticlockwise water movement is observed.

- The centre of the bay is relatively free from depositional features, both glacial and modern. Evidence of erosion, such as scour marks, confined to this central bay area suggests this is linked to erosional currents.
- Strong currents and wave action have a major influence on the deposition of bedforms. This is supported by the presence of ripples and dunes between the Sounds, and near Kinvarra in the inner bay, the areas of most intense wave action and strongest current circulation.

The analysis of the seismic, sedimentological and geochemical data from sediment cores has allowed for the reconstruction of the environmental conditions in the bay and surrounding areas since the last deglaciation:

- During deglaciation and the early Holocene, there is a significant difference in the rate of sediment deposition across the bay both spatially and temporally. The sedimentation rate in the post glacial and early Holocene is greatly reduced compared to during deglaciation, evidenced by the thickness of the seismic units. During the early Holocene, lower sedimentation rates are observed in the outer bay suggesting that while terrestrial runoff may have been high in the inner bay (cf. Novak, 2017), the sediment supply to the mid and outer bay was massively reduced. This indicates that the palaeo-Corrib river system identified by Clarke (2013) in the inner bay was an important delivery mechanism for sediment into and through the bay, before rising sea-levels drowned it.
- A clear north/south divide is evident in the post glacial and early Holocene depositional environments. This is due to the separation of the bay into two separate inlets, with a land barrier likely separating the north and south, between 13.1 and 8.8 ka cal BP. Between 12.6 and 8.8 ka cal BP, there is a high-energy, shallow water, gravelly sand beach environment, with low

sedimentation rates in the North. This is followed by a time transgressive, low energy, muddy, transitional water, fully marine environment, dated to 10 ka cal BP, associated with higher sedimentation. In the south, between 13.1 and 9.9 ka cal BP, a low energy, sand and silt, shallow water, sub-tidal environment, with relatively low sedimentation rates dominates.

- There is no evidence of distinct colder intervals in Galway Bay during the globally significant Younger Dryas or 8.2 ka event. This suggests that this sheltered coastal location was not as susceptible to the effects of major climatic events, compared to terrestrial and deeper water areas in the North Atlantic.
- Opening of the bay at the beginning of the mid-Holocene period and a lowering of turbidity levels, due to an increase in vegetation and a decrease in runoff from the hinterland areas, led to the deposition of a shell hash dominated by the gastropod *Turritella sp.* across most of Galway Bay over the course of ca. 3,300 years, between 7.4 and 4.1 ka cal BP.
- The bay was a fully marine, deep water environment approaching modern day conditions, by the beginning of the late Holocene at 4.1 ka cal BP.
- The increase in sedimentation rates and trends in geochemistry in the bay during the late Holocene indicates that a combination of factors, including; changes in oceanographic conditions, a wetter climate and an increase in the anthropogenic influence in the surrounding areas, likely through deforestation, were influential in establishing the environment in Galway Bay.

Additionally, the data obtained from the analysis of the seismic, sedimentological and microfossil data also allowed a new RSL reconstruction. This research has shown that:

- There was a sea-level lowstand in the bay between 16 and 15 ka cal BP, when sea-level was up to 70m lower than present day.
- A sea-level slowstand occurred between 13.1 and 8.8 ka cal BP in the bay. This exceeds previous estimates of the length of such slowstand (Brooks et al, 2008; Bradley et al, 2011; Kuchar et al, 2012) by over 3000 years and suggests that

the regional influences affecting isostatic rebound are significantly more influential than previously believed.

- Evidence of global meltwater pulses 1A and 1C is found in Galway Bay as major environmental and coastline changes following such substantial sea-level rises.
- There is evidence of continuous transgression throughout the entire period from deglaciation of the bay to present day, with sea-level in the bay increasing by ~70m over 16,000 years and the bay changing from a primarily terrestrial to a fully marine environment.
- This information can help refine the modelled sea-level curves for the bay and improve the knowledge of the pre-Holocene sea-level in western Ireland, as no data between 13 and 9 ka BP has previously been included in such reconstructions.

This research indicates that Galway Bay is a dynamic region that has evolved from a terrestrial environment, during the deglacial lowstand, to 2 separate inlets composed of very different shallow environments during the post glacial and early Holocene, to a single inlet, estuarine/marine environment in the mid-Holocene, before finally transforming into the fully marine, deep water, modern day bay, during the late Holocene. This trend of transgression and general encroachment of sea-level into coastal areas fits with the global picture of climate and sea-level change. It emphasises the importance of palaeoenvironmental research in order to develop management strategies for the impact that future environmental change will cause.

8.2 Limitations

While this research has substantially improved our understanding of the bay following the last glacial maximum, limitations within the study are also acknowledged below.

- The lack of seismic data and sediment cores in the inner bay has left a gap in our knowledge of the nearshore processes during the mid and late Holocene and how this region has developed into the thriving (protected) benthic habitat it has become today. The quality of the available seismic data has also prevented a more detailed reconstruction of the processes which shaped the bay following deglaciation.

- The time constraints of the project have meant that a detailed, high resolution microfossil (foraminifera and ostracod) analysis was not viable. Therefore, statistical analysis and zonation was not carried out and all microfossil results were qualitative and used as additional information to reinforce the sedimentary and geochemical evidence. Although caution was used with the results of the microfossil analysis, the low resolution of microfossil sampling intervals allows for possible non-representative results which can be misleading in interpreting the environmental conditions.
- All analysis involving MSCL, XRF, grainsize and radiocarbon dating was subject to both time and financial constraints. This reduced the resolution at which these analyses could be carried out and has prohibited a higher resolution environmental reconstruction.

8.3 Future Research

The research carried out in this study has provided an excellent basis for the study of environmental reconstructions in a shallow, marine area on the west coast of Ireland. Further investigation in both the terrestrial and marine environments could provide a more complete picture of the effects of the last glaciation, subsequent deglaciation and transition to interglacial conditions throughout the Holocene. Particular areas of focus could include:

- Investigation of the glacial till unit in the bay through sediment coring (6m corer), in order to constrain the timing of retreats and advances of the BIIS, following initial deglaciation, through Galway Bay.
- A high resolution, foraminifera analysis including counts and statistical analysis, in order to better define changing coastline positions and to help identify major climatic events, such as those caused by global climatic deterioration.
- Further investigation into the timing and rate of marine intrusion through additional sediment coring and analysis from the mid to the inner bay.

- Further coring and analysis of sediment cores along the inner and mid bay areas in order to determine the reason for the prolonged hiatus in the inner bay, something which is not evident in the outer bay.
- Repeat high resolution bathymetric surveys in order to determine sediment mobility and distribution in the bay, and to track the changing geomorphology of the bay over time.
- Intergration of all data collected in the bay to date.
- Investigation of other shallow water coastal and terrestrial areas along the western Irish coastline in order to determine if the signals from Galway Bay represent regional or local climatic changes.
- Creation of a depository for information on Galway Bay. This would allow for the synthesis of valuable information on the bay and the collaboration between environmental, biological and social aspects of research.

Since this research has been completed, the author has become aware of further data collection and studies involving microfossil analysis. The combination of all datasets from Galway Bay, in particular a wider investigation into the range of sediment cores, and the subsequent synthesis of all data would be extremely beneficial to providing a continuous, detailed, high resolution picture of the entire bay. Any data that provides constraining information on sea-level change should be added to the Irish sea-level database so that GIA derived sea-level predictions can be better validated.

Furthermore, climatic information can be used to validate Irish climate models.

By combining the information from Galway Bay with similar studies from other areas we can add to our overall knowledge of the changing dynamic processes across larger regions and the effect this had on the environment.

As Galway is an important urban coastal area, any climatic or sea-level changes will have significant knock on impacts on economic, infrastructural and environmental assets. To minimise this, coastal action plans need to be developed. In order to do this, a substantial level of information on the environmental history of the region is necessary, something that this and subsequent research can provide.

References

References

- Abdul, N.A., Mortlock, R.A., Wright, J.D. and Fairbanks, R.G. (2016). Younger Dryas sea level and meltwater pulse 1B recorded in Barbados reef crest coral *Acropora palmata*. *Palaeoceanography*, 31, 330-344.
- Agnihotri, R., Altabet, M.A., Herbert, T.D. and Tierney, J.E. (2008). Subdecadally resolved palaeoceanography of the Peru margin during the last two millennia. *Geochemistry, Geophysics, Geosystems*, 9(5), 1-15.
- Albert, B. and Innes, J. (2015). Multi-profile fine-resolution palynological and micro-charcoal analyses at Esklets, North York Moors, UK, with special reference to the Mesolithic-Neolithic transition. *Vegetation History and Archaeobotany*, 24, 357-375.
- Aller, R.C. and Yingst, J.Y. (1978). Biogeochemistry of tube-dwellings: a study of the sedentary polychaete *Amphitrite ornate* (Leidy). *Journal of Marine Research*, 36, 201-254.
- Allen, J.R.L. (1980). Sand waves: A model of origin and internal structure. *Sedimentary Geology*, 26(4), 281-328.
- Alley, R.B. and Clark, P.U. (1999). The deglaciation of the northern hemisphere: A global perspective. *Annual Reviews of Earth and Planetary Sciences*, 27, 149-182.
- Alley, R. B., Mayewski, P. A., Sowers, T., Stuiver, M., Taylor, K. C. and Clark, P. U. (1997). Holocene climate instability: a prominent, widespread event 8200 years ago. *Geology*, 25, 483-486.
- Alve, E. (1995). Benthic foraminiferal distribution and recolonization of formerly anoxic environments in Drammensfjord, southern Norway. *Marine Micropalaeontology*, 25, 169-185.
- Alve, E. (2003). A common opportunistic foraminiferal species as an indicator of rapidly changing conditions in a range of environments. *Estuarine, Coastal and Shelf Science* 57, 501–514.
- Andrews, J.T. and Giraudeau, J. (2003). Multi-proxy records showing significant Holocene environmental variability: the inner N. Iceland shelf (Húnaflói). *Quaternary Science Reviews*, 22, 175-193.
- Andrews, J.T., Smith, L.M., Preston, R., Cooper, T. and Jennings, A.E. (1997). Holocene Patterns of ice-rafted setritus (IRD) in cores from the East Greenland shelf. *Journal of Quaternary Science*, 12, 1-13.

References

- Annandale, G.W. (2006). *Scour Technology. Mechanics and Engineering Practice*. New York: McGraw-Hill.
- Araneda, A., Torrejón, F., Aguayo, M., Torres, L., Cruces, F., Cisternas, M. and Urrutia, R. (2007). Historical records of San Rafael glacier advances (North Patagonian Icefield): another clue to “Little Ice Age” timing in southern Chile? *The Holocene*, 17, 987-998.
- Arz, H.W., Pätzold, J. and Wefer, G. (1999). Climatic changes during the last deglaciation recorded in sediment cores from the northeastern Brazilian continental margin. *Geo-Marine Letters*, 19, 209-218.
- Arz, H.W., Pätzold, J., Moammar, M.O. and Röhl, U. (2001b). Late Quaternary climate records from the Northern Red Sea: results on gravity cores retrieved during the R/V METEOR cruise M44/3. *Marine Science*, 12, 101-113.
- Arz, H.W., Pätzold, J., Müller, P.J. and Moammar, M.O. (2003). Influence of Northern Hemisphere climate and global sea-level rise on the restricted Red Sea marine environment during termination 1. *Palaeoceanography*, 18(2), 1-13.
- Allmon, W.D. (1988). Ecology of Recent Turritelline Gastropods (Prosobranchia, Turritellidae): Current Knowledge and Paleontological Implications. *Palaios*, 3(3), 259-284.
- Armitage, S.J., Bristow, C.S. and Drake, N.A. (2015). West African monsoon dynamics inferred from abrupt fluctuations of Lake Mega-Chad. *Proceedings of the National Academy of Sciences of the United States of America*, 112(28), 8543-8548.
- Ashley, G.M. (1990). Classification of Large-scale subaqueous bedform: A new look at an old problem. *Journal of Sedimentary Petrology*, 60, 160-172.
- Austin, W.E.N. and Kroon, D. (1996). Late glacial sedimentology, foraminifera and stable isotope stratigraphy of the Hebridean continental shelf, northwest Scotland. *Geological Society London Special Publications*, 111(1), 187-213.
- Bahr, A., Lamy, F., Arz, H., Major, C., Kwiecien, O. and Wefer, G. (2008). Abrupt changes of temperature and water chemistry in the late Pleistocene and early Holocene Black Sea. *Geochemistry, Geophysics, Geosystems*, 9(1), 1-16.
- Baillie, M.G.L. (1991). Marking in marker dates: towards an archaeology with historical precision. *World Archaeology*, 23, 233-243.
- Baillie, M.G.L. (1995). *A slice through time: dendrochronology and precision dating*. London: Routledge.

References

- Baillie, M.G.L. and Brown, D. (2002). Oak dendrochronology: some recent archaeological developments from an Irish perspective. *Antiquity*, 76, 497-505.
- Baldini, L.M. (2007). *An investigation of the controls on the stable isotope signature of meteoric precipitation, cave seepage water, and Holocene stalagmites in Europe* (Unpublished doctoral dissertation). University College Dublin, Dublin, Ireland.
- Baldini, L.M., McDermott, F., Baldini, J.U.L., Fischer, M.J. and Molhoff, M. (2010). An investigation of the controls on Irish precipitation $\delta^{18}\text{O}$ on monthly and event timescales. *Climate Dynamics*, 35(6), 977-993.
- Baldini, J.U., McDermott, F. and Fairchild, I.J. (2002). Structure of the 8200-year cold event revealed by a speleothem trace element record. *Science*, 296(5576), 2203-2206.
- Ballantyne, C.K. (2010). Extent and deglacial chronology of the last British-Irish ice sheet: implications of exposure dating using cosmogenic isotopes. *Journal of Quaternary Science*, 25, 515-534.
- Ballantyne, C.K. and Ó Cofaigh, C. (2017). The Last Irish Ice Sheet: Extent and Chronology. In P. Coxon, S. McCarron and F. Mitchell (Eds.), *Advances in Irish Quaternary Studies* (pp. 101-149). Paris: Atlantic Press.
- Ballantyne, C.K. and Stone, J.O. (2015). Trimlines, blockfields and the vertical extent of the last ice sheet in Southern Ireland. *Boreas*, 44(2), 277-287.
- Ballantyne, C.K., Stone, J.O. and McCarroll, D. (2008). Dimensions and chronology of the last ice sheet in Western Ireland. *Quaternary Science Review*, 27(3-4), 185-200.
- Ballantyne C.K., McCarroll, D. and Stone J.O. (2006). Vertical dimensions and age of the Wicklow Mountains ice dome, Eastern Ireland, and implications for the extent of the last Irish Ice Sheet. *Quaternary Science Reviews*, 25(17-18), 2048–2058.
- Ballantyne, C.K., McCarroll, D. and Stone, J.O. (2011). Periglacial trimlines and the extent of the Kerry-Cork Ice Cap, SW Ireland. *Quaternary Science Reviews*, 30(27), 3834-3845.
- Baltzer, A., Mokeddem, Z., Goubert, E., Lartaud, F., Fournier, J. and Bourillet, J-F. (2015). The “Turritella Layer”: A potential proxy of a drastic Holocene environmental change on the north-east Atlantic coast. In: M. Maanan and M. Robin (Eds.) *Sediment fluxes on coastal areas* (pp. 3-21). Dordrecht: Springer.
- Bahr, A., Lamy, F., Arz, H., Kuhlmann, H. and Wefer, G. (2005). Late glacial to Holocene climate and sedimentation history in the NW Black Sea. *Marine Geology*, 214(4), 309-322.

References

- Barber, D.C., Dyke, A., Hillaire-Marcel, C., Jennings A. E., Andrews J. T., Kerwin, M. W., Bilodeau, G., McNeely, R., Southon, J., Morehead, M.D. and Gagnon, J.M. (1999). Forcing of the cold event of 8,200 years ago by catastrophic drainage of Laurentide lakes. *Nature*, 400, 344-34.
- Barber, K.E., Chambers, F.M. and Maddy, D. (2003). Holocene palaeoclimates from peat stratigraphy: macrofossil proxy climate records from three oceanic raised bogs in England and Ireland. *Quaternary Science Reviews*, 22(5-7), 521-539.
- Barber, K.E., Chambers, F.M. and Maddy, D. (2004). Late Holocene climatic history of northern Germany and Denmark: peat macrofossil investigations at Dosenmoor, Schleswig-Holstein, and Svanemose, Jutland. *Boreas*, 33, 132-144.
- Bard, E., Hamelin, B. and Delanghe-Sabatier, D. (2010). Deglacial meltwater pulse 1B and younger dryas sea levels revisited with boreholes at tahiti. *Science*, 327, 1235-1237.
- Bard, E., Hamelin, B., Arnold, M., Montaggioni, L., Cabioch, G., Faure, G. and Rougerie, F. (1996). Deglacial sea-level record from Tahiti corals and the timing of global meltwater discharge. *Nature*, 382, 241-244.
- Barnard, P.L., Erikson, L.H., Elias, E.P.L. and Dartnell, P. (2013). Sediment transport patterns in the San Francisco Bay Coastal System from cross-validation of bedform asymmetry and modelled residual flux. *Marine Geology*, 345, 72-95.
- Barr, I.D., Robertson, S., Flood, R. and Dortch, J. (2017) Younger Dryas glaciers and climate in the Mourne Mountains, Northern Ireland. *Journal of Quaternary Science*, 32(1), 104-115.
- Barrett, C. (1998). *Benthic foraminifera and their oceanographic parameters, Dingle Bay, South West Ireland*. (Unpublished master's thesis). National University of Ireland, Galway, Ireland.
- Barth, A.M., Clark, P.U., Clark, J., McCabe, A.M. and Caffee, M. (2016). Last Glacial Maximum cirque glaciation in Ireland and implications for reconstructions of the Irish Ice Sheet. *Quaternary Science Reviews*, 141, 85-93.
- Barth, A.M., Clark, P.U., Clark, J., Roe, G.H., Marcott, S.A., McCabe, A.M., Caffee, M., Cuzzone, J.K., He, F. and Dunlop, P. (2018). Persistent millennial-scale glacier fluctuations in Ireland between 24 ka and 10 ka. *Geology*, 46(2), 151-154.
- Bartlein, P.J., Harrison, S.P., Brewer, S., Connor, S., Davis, B.A.S., Gajewski, K., Guiot, J., Harrison-Prentice, T.I., Henderson, A., Peyron, O., Prentice, I.C., Scholze, M., Seppä, H., Shuman, B., Sugita, S., Thompson, R.S., Viau, A.E., Williams, J. and Wu, H. (2011).

References

- Pollen based continental climate reconstructions at 6 and 21 ka: a global synthesis. *Climate Dynamics*, 37, 755-802.
- Bassetti, M.A., Berné, S., Sicre, M-A., Dennielou, B., Alonso, Y., Buscail, R., Jalali, B., Hebert, B. and Menniti, C. (2016). Holocene hydrological changes of the Rhone River (NW Mediterranean) as recorded in the marine mud belt. *Climate of the Past*, 12(7), 1539-1553.
- Batchelor, C.R., Branch, N.P., Allison, E.A., Austin, P.A., Bishop, B., Brown, A.D., Elias, S.A., Green, C.P. and Young, D.S. (2014). The timing and causes of the Neolithic elm decline: New evidence from the lower Thames valley (London, UK). *Environmental Archaeology: The Journal of Human Palaeocology*, 19(3), 263-290.
- Baxter, S., Graham, N.T., Feely, M., Reavy, R.J. and Dewey, J.F. (2005). A microstructural and fabric study of the Galway Granite, Connemara, western Ireland. *Geological Magazine*, 142(1), 81-95.
- Bay, G., O'Carra, B., Williams, D.M., Mercer, B. and Wood, B. (2014). Evidence of environmental change since the earliest medieval period from the inter-tidal zone of, Source: *The Irish Naturalists' Journal*, 33(2), 83-88.
- Beavington-Penney, S.J. and Racey, A. (2004). Ecology of extant nummulitids and other larger benthic foraminifera; applications in palaeoenvironmental analysis. *Earth Science Reviews*, 67, 219-265.
- Behre, K.-E. (2007). A new Holocene sea-level curve for the southern North Sea. *Boreas*, 36, 82–102.
- Benetti, S., Cronin, M., Evans, J., Fitzpatrick, F., Lyons, K., McGrath, F., Nolan, G., O'Brien, F., Sheehan, K., Cullen, S., Hardy, D., Monteys, X., O'Toole, R. and Verbruggen, K. (2007). *INFOMAR Ground Truthing and Sampling Strategy*. Report prepared for the Integrated Mapping for the Sustainable Development of Ireland's Marine Resource, at the Marine Institute of Ireland, Galway, Ireland.
- Benetti, S. (2007). *INFOMAR: Ground truthing and sampling strategy*. Integrated mapping for the sustainable development of Ireland's marine resource.
- Benetti, S., Dunlop, P. and Ó Cofaigh, C. (2010). Glacial and glacially-related features on the continental margin of northwest Ireland mapped from marine geophysical data. *Journal of Maps* 6(1), 14-29.
- Benito, X., Trobajo, R., Cearreta, A. and Ináñez, C. (2016). Benthic foraminifera as indicators of habitat in a Mediterranean delta: Implications for ecological and palaeoenvironmental studies. *Estuarine, Coastal and Shelf Science*, 180, 97-113.

References

- Bennett, K.D., Tzedakis, P.C. and Willis, K.J. (1991). Quaternary refugia of north European trees. *Journal of Biogeography*, 18(1), 103-115.
- Benumof, B.T. and Griggs, G.B. (1999). The dependence of seacliff erosion rates on cliff material properties and physical processes: San Diego County, California. *Journal of the American Shore and Beach Preservation Association*, 67(4), 29-41.
- Berger, A. and Loutre, M.F. (1991). Insolation values for the climate of the last 10 million years. *Quaternary Science Reviews*, 10(4), 297-317.
- Berglund, B.E. (2003). Human impact and climate changes—synchronous events and a causal link? *Quaternary International*, 105(1), 7-12.
- Berglund, B.E., Barnekow, L., Hammarlund, D., Sandgren, P. and Snowball, I.F. (1996). Holocene forest dynamics and climate changes in the Abisko area, northern Sweden: the Sonesson model of vegetation history reconsidered and confirmed. *Ecological Bulletins*, 45, 15-30.
- Berner, K.S., Koç, N., Divine, D., Godiliebson, F. and Moros, M. (2008). A decadal-scale Holocene sea surface temperature record from the subpolar North Atlantic constructed using diatoms and statistics and its relation to other climate parameters. *Palaeoceanography*, 23, 1-15.
- Bernhard, J.M. and Sen Gupta, B.K. (1999). Foraminifera in Oxygen-Depleted Environments. In B.K. Sen Gupta (Ed.), *Modern Foraminifera*. (pp. 201-216). Springer: Dordrecht.
- Best, A.L. and Gunn, D.E. (1999). Calibration of marine sediment core-loggers for quantitative acoustic impedance studies. *Marine Geology*, 160(1-2), 137-146.
- Bevan, A., Colledge, S., Fuller, D., Fyfe, R., Shennan, S. and Stevens, C. (2016). Holocene fluctuations in human population demonstrate repeated links to food production and climate. *Proceedings of the National Academy of Sciences of the United States of America*, 114(49), 524-531.
- Bhattacharya, J. and Giosan, L. (2003). Wave-influenced deltas: geomorphological implications for facies reconstruction. *Sedimentology*, 50(1), 187-210.
- Bianchi, G. and McCave, I. (1999). Holocene periodicity in North Atlantic climate and deep ocean flow south of Iceland. *Nature*, 397, 515-517.
- Binney, H., Edwards, M., Macias-Fauria, M., Lozhkin, A., Anderson, P., Kaplan, J.O., Andreev, A., Bezrukova, E., Blyakharchuk, T., Jankovska, V., Khazina, I., Krivonogov, S., Kremenetski, K., Nield, J., Novenko, E., Ryabogina, N., Solovieva, N., Willis, K. and

References

- Zernitskaya, V. (2017). Vegetation of Eurasia from the last glacial maximum to present: Key biogeographic patterns. *Quaternary Science Reviews*, 157(1), 80-97.
- Biolchi, S., Furlani, S., Devoto, S., Gauci, R., Castaldini, D. and Soldati, M. (2016). Geomorphological identification, classification and spatial distribution of coastal landforms of Malta (Mediterranean Sea). *Journal of Maps*, 12(1), 87-99.
- Birks, H.H. and Ammann, B. (2000). Two terrestrial records of rapid climate change during the glacial-Holocene transition (14,000-9,000 calendar years B.P.) from Europe. *Proceedings of the National Academy of Sciences of the United States of America*, 97, 1390-1394.
- Birks, H.H., Eide, W. and Birks, H.J.B. (1999). Early Holocene atmosphere CO² concentrations. *Science*, 286, 1815-1816.
- Birks, H. J. B. (1996). Contributions of Quaternary palaeoecology to nature conservation. *Journal of Vegetation Science*, 7(1) 89–98.
- Björck, S., Rundgren, M., Ingólfsson, Ó. and Funder, S. (1998). The Preboreal oscillation around the Nordic Seas: terrestrial and lacustrine responses. *Journal of Quaternary Science*, 12(6), 455-465.
- Bjune, A.E., Bakke, J., Nesje, A. and Birks, H.J.B. (2005). Holocene mean July temperature and winter precipitation in western Norway inferred from palynological and glaciological lake-sediment proxies. *The Holocene*, 15(2), 177-189.
- Blaauw, M., van Geel, B. and van der Plicht, J. (2004). Solar forcing of climatic change during the mid-Holocene: indications from raised bogs in The Netherlands. *The Holocene*, 14, 1-35.
- Blanchet, C., Thouveny, N., Vidal, L., Leduc, G., Tachikawa, K., Bard, E. and Beaufort, L. (2007). Terrigenous input response to glacial/interglacial climatic variations over southern Baja California: a rock magnetic approach. *Quaternary Science Reviews*, 26(25-28) 3118–3133.
- Blanchon, P. and Shaw, J. (1995). Reef drowning during the last deglaciation: evidence for catastrophic sea-level rise and ice-sheet collapse. *Geology*, 23, 4–8.
- Blott, S.J. and Pye, K. (2001). GRADISTAT: a grain size distribution and statistics package for the analysis of unconsolidated sediments. *Earth Surface Processes and Landforms*, 26(11), 1237-1248.

References

- Boelens, R., Minchin, D. and O'Sullivan, G. (2005). 'Climate Change: Implications for Ireland's Marine Environment and Resources'. *Marine Foresight Series, 2*, Marine Institute, Galway, Ireland.
- Bohncke, S.J.P. and Hoek, W.Z. (2007). Multiple oscillations during the Preboreal as recorded in a calcareous gyttja, Kingbeekdal, The Netherlands. *Quaternary Science Reviews, 26*, 1965-1974.
- Boltovskoy, E. and Wright, R. (1976). *Recent Foraminifera*. The Hague: Price Dutch Guilders.
- Bond, G., Showers, W., Cheseby, M., Lotti, R., Almasi, P., Priore, P., Cullen, H., Hajdas, I. and Bonani, G. (1997). A pervasive millennial-scale cycle in North Atlantic Holocene and glacial climates. *Science, 278*(5341), 1257-1266.
- Bond, G.C., Showers, W., Elliot, M., Evans, M., Lott, R., Hajdas, L., Bonani, G. and Johnson, S. (1999). The North Atlantic's 1-2 Kyr Climate Rhythm: Relation to Heinrich Events, Dansgaard/Oeschger Cycles and the Little Ice Age. In: P.U. Clark, R.S Webb and L.D. Keigwin (Eds.) *Mechanisms of Global Climate Change at Millennial Time Scales, 35-58*. AGU. *Geophysical Monograph Series, 112*.
- Bond, G., Kromer, B., Beer, J., Muscheler, R., Evans, M.N., Showers, W., Hoffmann, S., Lotti-Bond, R., Hajdas, I. and Bonani, G. (2001). Persistent solar influence on North Atlantic climate during the Holocene. *Science, 294*(5549), 2130-2136.
- Bonfils, C., deNoblet, N., Braconnot, P. and Joussaume, S. (2001). Hot desert albedo and climate change: Mid-Holocene monsoon in North Africa. *Journal of Climate, 14*(17), 3724-3737.
- Booth, D. A. (1975). The water structure and circulation of Killary Harbour and of Galway Bay. (Unpublished master's thesis), National University of Ireland, Galway, Ireland.
- Booth, R.K., Jackson, S.T., Forman, S.L., Kutzbach, J.E., Bettis III, E.E., Kreig, J. and Wright, D.K. (2005). A severe centennial-scale drought in mid-continental North America 4200 years ago and apparent global linkages. *The Holocene, 15*(3), 321-328.
- Bos, J.A.A., van Geel, B., van der Plicht, J. and Bohncke, S.J.P. (2007). Preboreal climate oscillations in Europe: Wiggle match-dating and synthesis of Dutch high-resolution multi-proxy records. *Quaternary Science Reviews, 26*, 1927-1950.
- Bowen, D.Q. (1973). The Pleistocene succession of the Irish Sea. *Proceedings of the Geologists' Association, 84*, 249-272.

References

- Bowen, D.Q., Rose, J., McCabe, A.M. and Sutherland, D.G. (1986). Correlation of Quaternary glaciations in England, Ireland, Scotland and Wales. *Quaternary Science Reviews*, 5, 299-340.
- Bowen, D.Q., Phillips, F.M., McCabe, A.M., Knutz, P.C. and Sykes, G.A. (2002). New data for the Last Glacial Maximum in Great Britain and Ireland. *Quaternary Science Reviews*, 21(1-3), 89-101.
- Braconnot, P., Jousaume, S., de Noblet, N. and Ramstein, G. (2000). Mid-Holocene and Last Glacial Maximum African monsoon changes as simulated within the Palaeoclimate Modelling Intercomparison Project. *Global and Planetary Change*, 26, 51-66.
- Bradley, R.S., Hughes, M.K. and Diaz, H.F. (2003). Climate in Medieval time. *Science*, 302, 404-405.
- Bradley, S.L., Milne, G.A., Shennan, I. and Edwards, R. (2011). An improved glacial isostatic adjustment model for the British Isles. *Journal of Quaternary Science*, 26(5), 541-552.
- Bradwell, T., Stoker, M. and Krabbendam, M. (2008). Megagrooves and streamlined bedrock in NW Scotland: The role of ice streams in landscape evolution. *Geomorphology*, 97(1-2), 135-156.
- Brattström, T., Davisson, S., Gomes, W., Grosfeld, L., Jusslin, P., Madaj, L. and Åslund, H. (2015). *The Dynekil-Intrepretations of the foraminiferal assemblages in the Dynekil on the Swedish west coast during the last 350 years* (Unpublished doctoral dissertation). University of Gothenburg, Sweden.
- Brewer, S., Cheddadi, R., de Beaulieu, J.L. and Reille, M. (2002). The spread of deciduous *Quercus* throughout Europe since the last glacial period. *Forest Ecology and management*, 156(1-3), 27-48.
- Briffa, K.R. (2000). Annual climate variability in the Holocene: interpreting the message of ancient trees. *Quaternary Science Reviews*, 19, 87-105.
- Bristow, C.S., Bailey, S.D. and Lancaster, N. (2000) The sedimentary structure of linear sand dunes. *Nature*, 406, 56-59.
- Broecker, W.S. (2000). Abrupt climate change: causal constraints provided by the palaeoclimate record. *Earth-Science Reviews*, 51(1-4), 137-154.

References

- Brooks, S.J. and Birks, H.J.B. (2001). Chironomid-inferred air temperatures from late-glacial and Holocene sites in north-west Europe: progress and problems. *Quaternary Science Reviews*, 20, 1723-1741.
- Brooks, A. and Edwards, R. (2006). The development of a sea-level database for Ireland. *Irish Journal of Earth Science*, 24, 13-27.
- Brooks, A.J., Bradley, S.L., Edwards, R.J., Milne, G.A., Horton, B. and Shennan, I. (2008). Postglacial relative sea-level observations from Ireland and their role in glacial rebound modelling. *Journal of Quaternary Science*, 23, 175-192.
- Brooks, N. (2012). Beyond collapse: climate change and causality during the Middle Holocene Climatic transition, 6400-5000 years before present. *Danish Journal of Geography*, 112, 93-104.
- Brooks, N.J. (2006). Cultural responses to aridity in the Middle Holocene and increased social complexity. *Quaternary International*, 151, 29-49.
- Browder, A.G. and McNinch, J.E. (2006). Linking framework geology and nearshore morphology: Correlation of palaeo-channels with shore-oblique sandbars and gravel outcrops. *Marine Geology*, 231(1), 141-162.
- Brown, E.T., Johnson, T.C., Scholz, C.A., Cohen, A.S. and King, J.W. (2007). Abrupt change in tropical African climate linked to the bipolar seesaw over the past 55,000 years. *Geophysical Research Letters*, 34, L20702.
- Brown, T. (2008). The Bronze Age climate and environment of Britain. *Bronze Age Review*, 1, 7-22.
- Bryant, E. (2005). *Natural Hazards*. Cambridge: Cambridge University Press.
- Cabioch, G., Banks-Cutler, K.A., Beck, W.J., Burr, G.S., Corrège, T., Edwards, R.L. and Taylor, F.W. (2003). Continuous reef growth during the last 23 cal kyr BP in a tectonically active zone (Vanuatu, SouthWest Pacific). *Quaternary Science Reviews*, 22(15-17), 1771-1786.
- Callaghan, B. (2005). Locating the Shannawona Fault: Field and geobarometric studies from the Galway Batholith, western Ireland. *Irish Journal of Earth Science*, 23(-1), 85-100.
- Callard, S.L., Cofaigh, C., Benetti, S., Chiverrell, R.C., Van Landeghem, K.J.J., Saher, M.H., Gales, J.A., Small, D., Clark, C.D., Livingstone, S.J., Fabel, D. and Moreton, S.G. (2018). Extent and retreat history of the Barra Fan Ice Stream offshore western

References

- Scotland and northern Ireland during the last glaciation. *Quaternary Science Reviews*, 201(1), 280-302.
- Callaway, A., Smyth, J., Brown, C.J., Quinn, R., Service, M. and Long, D. (2009). The impact of scour processes on a smothered reef system in the Irish Sea. *Estuarine, Coastal and Shelf Science*, 84(3), 409–418.
- Calvert, S.E. and Pederson, T.F. (2007). Elemental proxies for palaeoclimatic and palaeoceanographic variability in marine sediments: interpretation and application. *Developments in Marine Geology*, 1, 567-644.
- Cao, Z., Siebert, C., Hathorne, E.C., Dai, M. and Frank, M. (2016). Constraining the oceanic barium cycle with stable barium isotopes. *Earth and Planetary Science Letters*, 434, 1-9.
- Carlson, A.E. and Clark, P.U. (2012). Ice sheet sources of sea level rise and freshwater discharge during the last deglaciation. *Reviews of Geophysics*, 50(4).
- Carlson, A.E., Stoner, J.S., Donnelly, J.P. and Hillaire-Marcel, C. (2008). Response of the southern Greenland Ice Sheet during the last two deglaciations. *Geology*, 36, 359-362.
- Carter, R.W.G. (1982). Sea-level changes in Northern Ireland. *Proceedings of the Geologists' Association*, 93(1), 7-23.
- Carter, R.W.G., Devoy, R.J.N. and Shaw, J. (1989). Late Holocene sea-levels in Ireland. *Journal of Quaternary Science*, 4, 7-24.
- Caseldine, C. and Gearey, B. (2005). A multiproxy approach to reconstructing surface wetness changes and prehistoric bog bursts in a raised mire system at Derryville Bog, Co. Tipperary, Ireland. *The Holocene*, 15(4), 585-601.
- Caseldine, C., Thompson, G., Langdon, C. and Hendon, D. (2005). Evidence for an extreme climatic event on Achill Island, Co. Mayo, Ireland around 5200–5100 cal. yr BP. *Journal of Quaternary Science*, 20(2), 169-178.
- Caseldine, C., Langdon, P. and Holmes, N. (2006). Early Holocene climate variability and the timing and extent of the Holocene thermal maximum (HTM) in northern Iceland. *Quaternary Science Reviews*, 25(17), 2314-2331.
- Cattaneo, A. and Steel, R.J. (2003). Transgressive deposits: a review of their variability. *Earth-Science Reviews*, 62(3-4) 187-228.
- Catuneanu, O. (2006). *Principles of Sequence Stratigraphy*. Amsterdam: Elsevier.

References

- Cave, R.R. and Henry, T. (2011). Intertidal and submarine groundwater discharge on the west coast of Ireland. *Estuarine, Coastal and Shelf Science*, 92(3) 415-423.
- Chambers, F.M., Mauquoy, D., Brain, S.A., Blaauw, M. and Daniell, J.R.G. (2007). Globally synchronous climate change 2800 years ago: proxy data from peat in South America. *Earth and Planetary Science Letters*, 253, 439-444.
- Charlesworth, J.K. (1924). The glacial geology of the north-west of Ireland. *Proceedings of the Royal Irish Academy*, 36, 199-203.
- Charlesworth, J.K. (1928) The glacial retreat from central and southern Ireland. *Quarterly Journal of the Geological Society, London*, 85, 335-358.
- Charman, D.J. (2010). Centennial climate variability in the British Isles during the mid-late Holocene. *Quaternary Science Reviews*, 29, 1539-1554.
- Charman, D.J., Blundell, A., Chiverrell, R.C., Hendon, D., Langdon, P.G. (2006). Compilation of non-annually resolved Holocene proxy climate records: stacked Holocene peatland palaeo-water table reconstructions from northern Britain. *Quaternary Science Reviews*, 25, 336-350.
- Chique, C., Molloy, K. and Potito, A.P. (2017). Mid-Late Holocene vegetational history and land-use dynamics in County Monaghan, northeastern Ireland-The palynological record of Lough Muckno. *Journal of the North Atlantic*, 32(101), 1-24.
- Chiverrell, R.C. and Thomas, G.S. (2010). Extent and timing of the Last Glacial Maximum (LGM) in Britain and Ireland: a review. *Journal of Quaternary Science*, 25(4), 535-549.
- Chiverrell, R.C., Thrasher, I.M., Thomas, G.P., Lang, A., Scourse, J.D., Van Landeghem, K.J.J., McCarrill, D., Clark, C.D., Ó Cofaigh, C., Evans, D.J.A. and Ballantyne, C.K. (2013). Bayesian modelling the retreat of the Irish Sea Ice Stream. *Journal of Quaternary Science*, 28(2), 200-209.
- Christensen, C. (1995). The Littorina transgressions in Denmark. In A. Fischer (Ed.) *Man and sea in the Mesolithic: Coastal settlements above and below present sea-level* (pp. 15-22). Oxford: Oxbow Books.
- Christensen, C. (1997). The great rise in the Storebælt. In: L. Pedersen, A. Fischer, and B. Aaby (Eds.) *The Danish Storebælt since the Ice Age: Man, Sea and Forest* (pp. 45-54). Copenhagen: A/S Storebælt Fixed Link.
- Clark, C.D., Ely, J.C., Greenwood, S.L., Hughes, A.L.C., Meehan, R., Barr, I.D., Bateman, M.D., Bradwell, T., Doole, J., Evans, D.J.A., Jordan, C.J., Monteys, X., Pellicer, X.M. and

References

- Sheehy, M. (2017). BRITICE Glacial Map, version 2: a map and GIS database of glacial landforms of the last British-Irish Ice Sheet. *Boreas*, ISSN 0300-9483.
- Clark, C.D., Hughes, A.L.C., Greenwood, S.L., Jordan, C. and Sejrup, H.P. (2012). Pattern and timing of retreat of the last British-Irish Ice Sheet. *Quaternary Science Reviews*, 44, 112-146.
- Clark, J., McCabe, A., Schnabel, C., Clark, P.U., Freeman, S., Maden, C. and Xu, S. (2009). ¹⁰Be chronology of the last deglaciation of County Donegal, northwestern Ireland. *Boreas*, 38(1), 111-118.
- Clark, J., McCabe, A.M., Bowen, D.Q. and Clark, P.U. (2012). Response of the Irish Ice Sheet to abrupt climate change during the last deglaciation. *Quaternary Science Reviews*, 35, 100-115.
- Clark, P.U., Dyke, A.S., Shakun, J.D., Carlson, A.E., Clark, J., Wohlfarth, B., Mitrovica, J.X., Hostetier, S.W. and McCabe, A.M. (2009). The last glacial maximum. *Science*, 325(5941), 710-714.
- Clark, P.U., McCabe, A.M., Mix, A.C. and Weaver, A.J. (2004). Rapid Rise of Sea Level 19,000 Years Ago and Its Global Implications. *Science*, 304(5674), 1141-1144.
- Clarke, C. (2013). *An Interpretation of the single channel high frequency seismic reflection datasets of Galway Bay, Ireland* (Unpublished master's thesis). National University of Ireland, Galway, Ireland.
- Cole, C.A.G., Kilroe, J.R., Hallissy, T. and Newell Arber, E.A. (1914). *The Geology of Clare Island, County Mayo*. Geological Survey of Ireland, Dublin.
- Collier, J.S. and Brown, C.J. (2005). Correlation of sidescan backscatter with grain size distribution of surficial seabed sediments. *Marine Geology*, 214(4), 431-449.
- Collison, P. (1980). Vertical distribution of foraminifera off the coast of Northumberland, England. *Journal of Foraminiferal Research*, 10, 75-78.
- Constantin, S., Bojar, A-V., Lundberg, J. and Lauritzen, S.E. (2007). Holocene and Late Pleistocene climate in the sub-Mediterranean continental environment: A speleothem record from Poleva Cave (Southern Carpathians, Romania). *Palaeogeography, Palaeoclimatology, Palaeoecology*, 243(3-4), 322-338.
- Corliss, B.H. (1985). Microhabitats of benthic foraminifera within deep-sea sediments. *Nature*, 314, 435-438.

References

- Cotterill, C.J., Philips, E., James, L., Forsberg, C.F., Tjelta, T.I., Carter, G. and Dove, D. (2017). The evolution of the Dogger Bank, North Sea: A complex history of terrestrial, glacial and marine environmental change. *Quaternary Science Reviews*, 171, 136-153.
- Cox, R., Zentner, D.B., Kirchner, B.J. and Cook, M.S. (2012). Boulder ridges on the Aran Islands (Ireland): recent movements caused by storm waves, not tsunamis. *The Journal of geology*, 120(3), 249-272.
- Coxon, P. (1996). The Gortian temperate stage. *Quaternary Science Reviews*, 15(5-6), 425-436.
- Coxon, P. and Dowling, L. (2015) Interglacial Deposits in Cork Harbour. In G. McGlynn and B. Stefanini (Eds.) *The Quaternary of South East Ireland* (pp. 147-157). Ireland: Quaternary Research Association Irish Quaternary Association.
- Coxon, P., Mitchell, F., von Engelbrechten, S. and Vaughan, L. (2017). Interglacial Sequences. In: P. Coxon, S. McCarron and F. Mitchell (Eds.) *Advances in Irish Quaternary Studies* (pp. 43-66). Paris: Atlantis Press.
- Croudace, I.W., Rindby, A. and Rothwell, R.G. (2006). ITRAX: description and evaluation of a new multifunction X-ray core scanner. In R.G. Rothwell (Ed.), *New Techniques in Sediment Core Analysis*, (pp. 51-63). London: Special Publication 267, Geological Society.
- Croudace, I.W., Romano, E., Ausili, A., Bergamin, L. and Rothwell, R.G. (2015). X-ray core scanners as an environmental forensics tool: a case study of polluted harbour sediment (Augusta Bay, Sicily). In I.W. Croudace and R.G. Rothwell (Eds.), *Micro-XRF studies of sediment cores* (pp. 393-421). Netherlands: Springer, Dordrecht.
- Cullen, H., DeMenocal, P.B., Hemming, S., Hemming, G., Brown, F.H., Guilderson, T. and Sirocko, F. (2000). Climate change and the collapse of the Akkadian empire: Evidence from the deep sea. *Geology*, 28(4), 379-382.
- Curtis, T.G.F. and Sheehy Skeffington, M.J. (1998). The salt marshes of Ireland: An inventory and account of their geographical variation. *Biology and Environment Proceedings of the Royal Irish Academy*, 98B(2), 87-104.
- Cutler, K.B., Edwards, R.L., Taylor, F.W., Cheng, H., Adkins, J., Gallup, C.D., Cutler, P.M., Burr, G.S. and Bloom, A.L. (2003). Rapid sea-level fall and deep-ocean temperature change since the last interglacial period. *Earth and Planetary Science Letters*, 206(3-4), 253-271.
- Cvetkoska, A., Levkov, Z., Reed, J.M. and Wagner, B. (2014). Late glacial to Holocene climate change and human impact in the Mediterranean: The last ca. 17 ka diatom

References

- record of Lake Prespa (Macedonia/Albania/Greece). *Palaeogeography, Palaeoclimatology, Palaeoecology*, 406, 22-32.
- Dale, A.L., McAllen, R and Whelan, P. (2007). Management considerations for subtidal *Zostera marina* beds in Ireland. *Irish Wildlife Manuals*, No. 28. National Parks and Wildlife Service, Department of Environment, Heritage and local Government, Dublin, Ireland.
- Dalkin, M. (2008). Mid Irish Sea reefs habitat mapping project. JNCC Report No. 411.
- Damnati, B. (2000). Holocene lake records in the Northern Hemisphere of Africa. *Journal of African Earth Sciences*, 31(2), 253-262.
- Dansgaard, W., Johnsen, S.J., Clausen, H.B., Dahl-Jensen, D., Gundestrup, N.S., Hammer, C.U., Hvidberg, C.S., Steffensen, J.P., Sveinbjörnsdottir, A.E., Jouzel, J. and Bond, G. (1993). Evidence for general instability of past climate from a 250-kyr ice-core record. *Nature*, 364(6434), 218-220.
- Davis, B.A.S., Brewer, S., Stevenson, A.C., Guiot, J. and Data Contributors. (2003). The temperature of Europe during the Holocene reconstructed from pollen data. *Quaternary Science Reviews*, 22, 1701-1716.
- Davis, M.E. and Thompson, L.G. (2006). An Andean ice-core record of a middle Holocene mega-drought in North Africa and Asia. *Annals of Glaciology*, 43, 34-41.
- Dawson, S., Smith, D.E., Jordan, J. and Dawson, A.E. (2004). Late Holocene coastal sand movements in the Outer Hebrides, N.W. Scotland. *Marine Geology*, 210, 281-306.
- De Grave, S. (1999). The influence of sedimentary heterogeneity on within maerl bed differences in infaunal crustatean community. *Estuarine, Coastal and Shelf Science*, 49(1), 153-163.
- Delaney, C. and Devoy, R. (1995). Evidence from sites in Western Ireland of late Holocene changes in coastal environments. *Marine Geology*, 124(1995) 273-287.
- DeMenocal, P.B. (2001). Cultural responses to climate change during the late Holocene. *Science*, 292(5517), 667-673.
- DeMenocal, P., Ortiz, J., Guilderson, T. and Sarnthein, M. (2000a). Coherent high-and low-latitude climate variability during the Holocene warm period. *Science*, 288(5474), 2198-2202.
- DeMenocal, P., Ortiz, J., Guilderson, T., Adkins, J., Sarnthein, M., Baker, L. and Yarusinsky, M. (2000b). Abrupt onset and termination of the African humid period:

References

rapid climate responses to gradual insolation forcing. *Quaternary Science Reviews*, 19, 347-361.

Deng, H.W. and Qian, K. (1993). *Sedimentary geochemistry and environmental analysis*. Lanzhou: Gansu Technology Publishing House.

Deschamps, P., Durand, N., Bard, E., Hamelin, B., Carmoin, G., Thomas, A.L., Henderson, G.M., Okuno, J. and Yokoyama, Y. (2012). Ice-sheet collapse and sea-level rise at the Bølling warming 14,600 years ago. *Nature*, 483(7391), 559-564.

DeVernal, A. and Hillaire-Marcel, C. (2006). Provincialism in trends and high frequency changes in the northwest North Atlantic during the Holocene. *Global Planetary Change*, 54, 263-290.

Devoy, R.J.N. (1990). Sea-level changes and Ireland. *Technology Ireland*, 22, 24–30.

Devoy, R.J.N. (2000). Climate warming and the links to the coast. *Inland Coastal Estuarine Waters*, 3, 4-5.

Devoy, R. (2008). Coastal vulnerability and the implications of sea-level rise for Ireland. *Journal of Coastal Research*, 24(2), 325– 341.

Devoy, R.J.N., Duffy, M. and Delaney C. (1996). The modern evolution of soft sedimentary Atlantic coasts of western Ireland. In: T.A.M. DeGroot (Ed.) *Climate change and coastal evolution in Europe: Final Report*. Commission of the European Communities, Research Contract Publication. Haarlem, The Netherlands: Brussels and Rijks Geologische Dienst.

Dezileau, L., Sabatier, P., Blanchemanche, P., Joly, B., Swingedouw, D., Cassou, C., Castaings, J., Martinez, P. and Von Grafenstein, U. (2011). Intense storm activity during the Little Ice Age on the French Mediterranean coast, *Palaeogeography, Palaeoclimate, Palaeoecology*, 299, 289–297.

Diaz, H.F. Trigo, R., Hughes, M.K., Mann, M.E., Xoplaki, E. and Barriopedro, D. (2011). Spatial and temporal characteristics of climate in Medieval times Revisited. *Bulletin of the American Meteorological Society*, 92(11), 1487-1500.

Diefendorf, A.F. (2005). Late-Glacial to Holocene climate variability in western Ireland (Unpublished doctoral dissertation), University of Saskatchewan, Saskatoon, Canada.

Diefendorf, A.F., Patterson, W.P., Mullins, H.T., Tibert, N. and Martini, A. (2006). Evidence for high-frequency late Glacial to mid-Holocene (16,800 to 5500 cal yr B.P.) climate variability from oxygen isotope values of Lough Inchiquin, Ireland. *Quaternary Research*, 65(1), 78-86.

References

- Dittmann, S. (1996). Effects of microbenthic burrows on infaunal communities in tropical tidal flats. *Marine Ecology Progress Series*, 134, 119-130.
- Dodson, J.R. (1990). The Holocene Vegetation of a Prehistorically Inhabited Valley, Dingle Peninsula. *Proceedings of the Royal Irish Academy. Section B: Biological, Geological, and Chemical Science*, 90B, 151-174.
- Douglas, K. (2009). *The downfall of the Spanish Armada in Ireland: The Grand Armada lost on the Irish Coast in 1588*. Dublin: Gill and Macmillan Ltd.
- Dove, D., Evans, D.J.A., Lee, J.R., Roberts, D.H., Tappin, D.R., Mellett, C.L., Long, D. and Callard, S.L. (2017). Phased occupation and retreat of the last British-Irish ice sheet in the southern North Sea: geomorphic and seismostratigraphic evidence of a dynamic ice lobe. *Quaternary Science Reviews*, 163, 114-134.
- Dowdeswell, J.A., Ó Cofaigh, C. and Pudsey, C.J. (2004). Thickness and extent of the sub-glacial till layer beneath an Antarctic palaeo-ice stream. *Geology*, 32, 13-16.
- Dowdeswell, J.A., Ottesen, D., Evans, J., Ó Cofaigh, C. and Anderson, J.B. (2008). Submarine glacial landforms and rates of ice-stream collapse. *Geology*, 36, 819-822.
- Dowling, L.A., Duffy, M.J. and Devoy, R.J.N. (1999). Contemporary process controls on the evolution of sedimentary coasts under low to high energy regimes: western Ireland. *Geology and Mining*, 77, 333–349.
- Dowling, I.A. and Coxon, P. (2001). Current understanding of Pleistocene temperate stages in Ireland. *Quaternary Science Reviews*, 20(16-17), 1631-1642.
- Dowling, L.A., Sejrup, H.P., Coxon, P. and Heijnis, H. (1998). Palynology, aminostratigraphy, and U-series dating of marine Gortian Interglacial sediments in Cork Harbour, southern Ireland. *Quaternary Science Reviews*, 17, 945-962.
- Doyle, A. (1988). *Geology of the Spiddal region, County Galway* (Unpublished batcheler's thesis). University College, Galway, Ireland.
- Drysdale, R.N., Hellstrom, J.C., Zanchetta, G., Fallick, A. E., Goni, M.F.S., Couchoud, I., McDonald, J., Maas, R., Lohmann, G. and Isola, I. (2009). Evidence for Obliquity Forcing of Glacial Termination II. *Science*, 325, 1527-1531.
- Duan, F., Wang, Y., Shen, C-C., Wang, Y., Cheng, H., Wu, C-C., Hu, H-M., Kong, X., Liu, D. and Zhao, K. (2014). Evidence for solar cycles in a late Holocene speleothem record from Dongge Cave, China. *Scientific Reports*, 4(5159), 1-7.

References

- Duffy, M.J. and Devoy, R.J.N. (1999). Contemporary process controls on the evolution of sedimentary coasts under low to high energy regimes: western Ireland. *Geologie en Mijnbouw*, 77, 333-349.
- Duijnste, I., De Nooijer, L., Ernst, S. and van der Zwann, G.J. (2005). Population dynamics of benthic shallow-water foraminifera: effects of a simulated marine snow event. *Marine Ecology Progress Series*, 285, 29-42.
- Dunlop, P., Shannon, R., McCabe, M., Quinn, R. and Doyle, E. (2010). Marine geophysical evidence for ice sheet extension and recession on the Malin Shelf: New evidence for the western limits of the British Irish Ice Sheet. *Marine Geology*, 276(1-4), 86-99.
- Dykoski, C.A., Edwards, R.L., Cheng, H., Yuan, D., Cai, Y., Zhang, M., Lin, Y., Qing, J., An, Z. and Revenaugh, J. (2005). A high-resolution, absolute-dated Holocene and deglacial Asian monsoon record from Donagge Cave, China. *Earth and Planetary Science Letters*, 233, 71-86.
- Edwards, R. and Brooks, A. (2008). The island of Ireland: Drowning the myth of an Irish land-bridge? *The Irish Naturalists' Journal*, 29, 19-34.
- Edwards, R. and Craven, K. (2017). Relative sea-level change around the Irish coast. In: P. Coxon, S. McCarron and F. Mitchell (Eds.) *Advances in Irish Quaternary Studies* (pp.181-215). Paris: Atlantic Press.
- Edwards, R., Gehrels, W.R., Brooks, A., Fyfe, R., Pullen, K., Kuchar, J. and Craven, K. (2017). Resolving discrepancies between field and modelled relative sea-level data: lessons from western Ireland. *Journal of Quaternary Science*, 32(7), 957-975.
- Edwards, R.J. and Horton, B.P. (2000). Reconstructing relative sea-level change using UK salt-marsh foraminifera. *Marine Geology*, 169(1), 41-56.
- Edwards, R.L., Beck, J.W., Burr, G.S., Donahue, D.J., Chapell, J.M.A., Bloom, A.L., Druffel, E.R.M. and Taylor, F.W. (1993). A large drop in atmospheric $^{14}\text{C}/^{12}\text{C}$ and reduced melting in the Younger Dryas, documented with ^{230}Th ages in corals. *Science*, 260, 962-968.
- Ellison, C.R.W., Chapman, M.R. and Hall, I.R. (2006). Surface and deep ocean interactions during the cold climate event 8200 years ago. *Science*, 312(5782), 1929-1932.
- Emmerson, C. and Lahn, G. (2012). *Arctic opening: opportunity and risk in the high north*. London: Llyods, Chattham House.

References

- Erdmann, W., Kelletat, D., Kuckuck, M. (2017). Boulder ridges and washover features in Galway Bay, western Ireland. *Journal of Coastal Research*, 33(5), 997-1021.
- Erdmann, W., Kelletat, D., Scheffers, A.M. and Haslett, S. (2015). *Origin and Formation of Coastal Boulder Deposits at Galway Bay and the Aran Islands, Western Ireland*. Springer Briefs in Geography, Springer International Publishing.
- Evans, D.J.A., Philips, E.R., Hiemstra, J.F. and Auton, C.A. (2006). Subglacial till: Formation, sedimentary characteristics and classification. *Earth-Science Reviews*, 78(1-2), 115-176.
- Evans, W., Benetti, S., Sacchetti, F., Jackson, D.W.T., Dunlop, P. and Monteys, X. (2014) Bedforms on the northwest Irish Shelf: indication of modern active sediment transport and over printing of paleo-glacial sedimentary deposits. *Journal of Maps*, 11(4), 561-574.
- Fagan, B.M. (2000). *The Little Ice Age: How climate made history 1300-1850*. New York: Basic Books.
- Fairbanks, R.G. (1989). A 17000-year glacio-eustatic sea level record: influence of glacial melting rates on the Younger Dryas event and deep-ocean circulation. *Nature*, 342, 637-642.
- Fairbanks, R.G. (1990). The age and origin of the "Younger Dryas climate event" in Greenland ice cores. *Palaeoceanography*, 5, 937-948.
- Fairbridge, R.W. (2004). Classification of Coasts. *Journal of Coastal Research*, 20(1), 155-165.
- Faust, J.C., Fabiana, K., Milzer, G., giraudeau, J. and Knies, J. (2016). Past changes in the North Atlantic storm track driven by insolation and sea-ice forming. *Geology*, 45, 335-338.
- Fealy, R.M., Green, S., Loftus, M., Meehan, R., Radford, T., Cronin, C. and Bulfin, M. (2009). *Teagasc EPA soil and subsoils mapping project-Final Report*. Volume 1, Teagasc, Dublin.
- Feely, M., Coleman, D., Baxter, S. and Millar, B. (2003). U-Pb zircon geochronology of the Galway Granite, Connemara, Ireland: implications for the timing of the late Caledonian tectonic and magnetic events and for the correlations with Acadian plutonism in New England. *Atlantic Geology*, 39(2), 175-184.

References

- Fernandes, L. M. J. (1988). *A study of the oceanography of Galway Bay, mid-western coastal waters (Galway Bay to Tralee Bay), Shannon Estuary and the River Shannon plume* (Unpublished doctoral dissertation). University College Galway, Galway, Ireland.
- Filoc, M., Kupryjanowicz, M. and Suchora, M. (2018). Response of terrestrial and lake environments in NE Poland to Preboreal cold oscillations (PBO). *Quaternary International*, 475, 101-117.
- Finkel, R.C. and Nishiizumi, K. (1997). Beryllium 10 concentrations in the Greenland Ice Sheet Project 2 ice core from 3–40 ka. *Journal of Geophysical Research*, 102, 26,699–26,706.
- Finlayson, A., Merritt, J., Browne, M., Merritt, J., McMillan, A. and Whitbread, K. (2010). Ice sheet advance, dynamics, and decay configurations: evidence from west central Scotland. *Quaternary Science Reviews*, 29(7-8), 969-988.
- Fischer, H., Werner, M., Wagenbach, D., Schwager, M., Thorsteinsson, T., Wilhelms, F., Kipfstuhl, J. and Sommer, S. (1998). Little ice age clearly recorded in northern Greenland ice cores. *Geophysical Research Letters*, 25(10), 1749-1752.
- Fisher, T.G., Smith, D.G. and Andrews, J.T. (2002). Preboreal oscillation caused by a glacial Lake Agassiz flood. *Quaternary Science Reviews*, 21(8), 873-878.
- Fischer, H. and Mieding, B. (2005). A 1,000-year ice core record of interannual to multidecadal variations in atmospheric circulation over the North Atlantic. *Climate Dynamics*, 25(1), 65-74.
- Folland, C.K., Karl, T.R., Nicholls, N., Nyenzi, B.S., Parker, D.E. and Vinnikov, K.Y. (1992). Observed climate variability and change. In: J.T. Houghton, B.A. Callander and S.K. Varney (Eds.) *Climate change 1992: the supplementary report to the IPCC Scientific Assessment* (pp. 135-170). Cambridge: Cambridge University Press.
- Fossitt, J.A. (1994). Late-Glacial and Holocene vegetation history of western Donegal, Ireland. *Biology and Environment: Proceedings of the Royal Irish Academy*, 94B(1), 1-31.
- Franke, J.G., Werner, J.P. and Donner, R.V. (2017). Reconstructing late Holocene North Atlantic atmospheric circulation changes using functional palaeoclimate networks. *Climate of the Past*, 13(11), 1593-1608.
- Fritz, S.C., Ito, E., Yu, Z., Laird, K.R. and Engstrom, D.R. (2000). Hydrologic variation in the northern Great Plains during the last two millennia. *Quaternary Research*, 53, 175-184.

References

- Gallagher, C. and Thorp, M. (1997). The age of the Pleistocene raised beach near Fethard, County Wexford, using infra-red stimulated luminescence (IRSL). *Irish Geography*, 30, 68-89.
- Gallagher, E.L. (2003). A note on megaripples in the surf zone: evidence for their relation to steady flow dunes. *Marine Geology*, 193(3), 171-176.
- Gallagher, S.J., MacDermot, C. V., Somerville, I.D., Pracht, M. and Sleeman, A.G. (2006). Biostratigraphy, microfacies and depositional environments of Upper Viséan limestones from the Burren region, County Clare, Ireland. *Geological Journal*, 41(1), 61-91.
- Gallego-Sala, A.V., Charman, D.J., Harrison, S.P., Li, G. and Prentice, I.C. (2016). Climate driven expansion of blanket bogs in Britain during the Holocene. *Climate of the Past*, 12, 129-136.
- Galloway, W.E. (1975). Process framework for describing the morphologic and stratigraphic evolution of deltaic depositional systems. In M.L. Broussard (Ed.) *Deltas, Models for Exploration* (pp. 87-98). Houston: Houston Geological Society.
- Gasse, F. and Van Campo, E. (1994). Abrupt post-glacial climate events in West Asia and North Africa monsoon domains. *Earth and Planetary Science Letters* 126(4), 435-456.
- Gately, S., Somerville, I.D., Morris, J.H., Sleeman, A.G. and Geological Survey of Ireland. (2005). *Geology of Galway and Offaly: A geological description of Galway-Offaly, and adjacent parts of Westmeath, Tipperary, Laois, Clare and Roscommon to accompany the bedrock geology 1:100,000 Scale Map Series, sheet 15, Galway-Offaly*. Geological Survey of Ireland: Dublin.
- Gegechkori, A. (2018). Patterns of distribution and survival of European yew (*Taxus baccata* L.) in an alpine tree line ecotone in the Greater Caucasus (Georgia). *Annals of Agrarian Science*, 16(2), 170-176.
- Geological survey of Ireland, 2007. Straie observations, Quaternary and Geotechnical Section. Geological survey of Ireland, Dublin. GSI Data downloads. [Online] Available from:
<http://www.gsi.ie/Publications+and+Data/Digital+Data/Available+Digital+Data.htm>.
- Geological Survey of Ireland, 2013. *The merging of Quaternary map datasets*. Geological Survey of Ireland, Dublin. [Online] Available from:
<https://www.arcgis.com/apps/MapSeries/index.html?appid=a30af518e87a4c0ab2fbd e2aaac3c228>.

References

- Geological Survey Ireland Spatial Resources, 2016. Bedrock geology 500k and 100k. [Online] Available from: <http://dcenr.maps.arcgis.com/apps/MapSeries/index.html?appid=a30af518e87a4c0ab2fbde2aac3c228>, accessed 25th November 2016.
- Geological Survey Ireland Spatial Resources, 2017. Geological Survey Ireland Spatial Resources [Online] Available from: <http://dcenr.maps.arcgis.com/apps/MapSeries/index.html?appid=a30af518e87a4c0ab2fbde2aac3c228>.
- Geotek (2016). MSCL operating manual. [Online] Available from: <https://www.geotek.co.uk/support/downloads>.
- Ghilardi, B. and O'Connell, M. (2013). Early Holocene vegetation and climate dynamics with particular reference to the 8.2 ka event: Pollen and macrofossil evidence from a small lake in western Ireland. *Vegetation History and Archaeobotany*, 22(2), 99-114.
- Gilbert, R. (1985). Quaternary glaciomarine sedimentation interpreted from seismic surveys of fjords on Baffin Island, NWT. *Arctic*, 38, 271-280.
- Gooday, A.J. and Alve, E. (2001). Morphological and ecological parallels between sublittoral and abyssal foraminiferal species in the NE Atlantic: a comparison of *Stainforthia fusiformis* and *Stainforthia* sp. *Progress in Oceanography*, 50, 261-283.
- Google Earth, 2018. Galway Bay. 53.1441202,-9.3637131. Satellite data layer, 3D map, viewed 18 August 2018. < <https://www.google.co.uk/maps/@53.1441202,-9.3637131,28588m/data=!3m1!1e3>>
- Gornitz, V. (2012). *Rising Seas: Past, Present, Future*. New York: Columbia University Press.
- Grabowski, R.C. (2014). Measuring the shear stress of cohesive sediment in the field. In: L. Clarke (Ed.) *Geomorphological Techniques* (online edition). London: British Society for Geomorphology.
- Graham, N., Ammann, C.M., Fleitmann, D., Cobb, K.M. and Luterbacher, J. (2011). Support for global climate reorganisation during the 'medieval climate anomaly'. *Climate Dynamics*, 37, 1217-1245.
- Greenwood, S.L. (2008). *A palaeo-glaciological reconstruction of the last Irish Ice Sheet* (Unpublished doctoral dissertation). University of Sheffield, UK.

References

- Greenwood, S. L. and Clark, C.D. (2009). Reconstructing the last Irish Ice Sheet 2: a geomorphologically-driven model of ice sheet growth, retreat and dynamics. *Quaternary Science Reviews*, 28(27-28), 3101-3123.
- Grosvenor, M.J., Jones, R.T., Turney, C.S.M., Chapman, D.J., Hogg, A., Coward, D. and Wilson, R. (2017). Human activity was a major driver of the mid-Holocene vegetation change in southern Cumbria: implications for the elm decline in the British Isles. *Journal of Quaternary Science*, 32(7), 934-945.
- Grove, C.A., Nagtegaal, R., Zinke, J., Scheufen, T., Koster, B., Kasper, S., McCulloch, M.T., Van den Bergh, G. and Brummer, G.J.A. (2010). River runoff reconstructions from novel spectral luminescence scanning of massive coral skeletons. *Coral Reefs*, 29, 579-591.
- Grove, J.M. (2004). *Little Ice Ages: Ancient and Modern, volume 2*. London: Routledge.
- Gunn, D.E. and Best, A.I. (1998). A new automated non-destructive system for high-resolution multi-sensor core logging of open sediment cores. *Geo-Marine Letters*, 18(1), 70-77.
- Guo, Z., Petit-Marie, N. and Kröpelin, S. (2000). Holocene non-orbital climatic events in present-day arid areas of northern Africa and China. *Global and Planetary Change*, 26, 97-103.
- Gustafsson, M. and Nordberg, K. (2000). Living (stained) benthic foraminifera and their response to the seasonal hydrographic cycle, periodic hypoxia and to primary production in Havstens Fjord on the Swedish west coast. *Estuarine, Coastal and Shelf Science*, 51, 743-761.
- Hajdas, I., Ivy, S.D., Beer, J., Bonani, G., Imboden, D., Lotter, A.F., Sturm, M. and Suter, M. (1993). AMS radiocarbon dating and varve chronology of Lake Soppensee – 6000 to 12,000 C-14 years BP. *Climate Dynamics*, 9, 107-116.
- Hald, M. and Hagen, S. (1998). Early Preboreal cooling in the Nordic Seas region triggered by meltwater. *Geology*, 26(7), 615-618.
- Hald, M. and Steinsund, P.I. (1992). Distribution of surface sediment benthic foraminifera in the southwestern Barents Sea. *The Journal of Foraminiferal Research*, 22(4), 347-362.
- Hall, A.M., Hansom, J.D., Williams, J.D. and Jarvis, J. (2006). Distribution, geomorphology and lithofacies of cliff top storm deposits: Examples from the high energy coasts of Scotland. *Marine Geology*, 232(3-4), 131 –155.

References

- Hall, V.H. (1997). The history of Irish forests since the ice age. *Irish Forestry*, 54, 49-54.
- Hammer, C.U., Clausen, H.B. and Tauber, H. (1986). Ice-core dating of the Pleistocene/Holocene boundary applied to a calibration of the ¹⁴C time scale. *Radiocarbon*, 28, 284-291.
- Hanebuth, T., Stattegger, K. and Grootes, P.M. (2000). Rapid flooding of the Sunda Shelf: A late-glacial sea-level record. *Science*, 288(5468), 1033-1035.
- Hansen, A. and Knudsen, K.L. (1995). Recent foraminiferal distribution in Freemansundet and Early Holocene stratigraphy on Edgeøya, Svalbard. *Polar Research*, 14(2), 215-238.
- Hansom, J.D. and Moore, M.P. (1981). Size grading along a shingle beach in Wicklow, Ireland. *Journal of Earth Sciences*, 4(1), 7-15.
- Harff, J., Endler, R., Emelyanov, E., Kotov, S., Leipe, T., Moros, M., Olea, R., Tomezak, M. and Witkowski, A. (2011). Late Quaternary climate variations reflected in Baltic Sea sediments. In: J. Harff, S. Björck and P. Hoth (Eds.) *The Baltic Sea Basin*, Vol. 3 (pp. 99-132). Central and Eastern European Development Studies (CEEDFS).
- Harrison, S., Glasser, N., Anderson, E., Ivy-Ochs, S. and Kubik, P.W. (2010). Later Pleistocene mountain glacier response to North Atlantic climate change in southwest Ireland. *Quaternary Science Reviews*, 29, 3948-3955.
- Harte, A. M., Gilroy, J. P. and McNamara, J. (1982). A computer simulation of water circulation in Galway Bay. *The Engineers Journal*, 35, 6-8.
- Haslett, S.K. and Bryant, E.A. (2007). Reconnaissance of historic (post-AD 1000) high-energy deposits along the Atlantic coasts of southwest Britain, Ireland and Brittany, France. *Marine geology*, 242(1), 207-220.
- Haslett, S.K., Strawbridge, F., Martin, N.A. and Davies, C.F.C. (2001). Vertical Saltmarsh Accretion and its Relationship to Sea-level in the Severn Estuary, U.K.: An Investigation using Foraminifera as Tidal Indicators. *Estuarine, Coastal and Shelf Science*, 52(1), 143-153.
- Hass, H.C. (1997). The benthic foraminiferal response to late Holocene climate change over northern Europe. In: H.C. Hass and M.A. Kaminski (Eds.) *Contributions to the Micropaleontology and Paleoceanology of the Northern North Atlantic* (pp.199-216). Grzybowski Foundation, Special Publication, 5.
- Hassan, F.A. (1997). Holocene palaeoclimates of Africa. *The African Archaeological Review*, 14(4), 213-230.

References

- Hassol, S.J. (2004). *Impacts of a warming Arctic, Arctic Climate impact assessment*. New York: Cambridge University Press.
- Husum, K. and Hald, M. (2002). Early Holocene cooling events in Malangenfjord and the adjoining shelf, north-east Norwegian Sea. *Polar Research*, 21, 267–274.
- Haug, G.H., Hughen, K.A., Sigman, D.M., Peterson, L.C. and Rhöl, U. (2001). Southward migration of the intertropical convergence zone through the Holocene. *Science*, 293, 1304-1308.
- Haunold, T.G. (1999). Ecologically controlled distribution of recent Textulariid foraminifera in subtropical, carbonate-rich, Safaga Bay (Red Sea, Egypt). *Beiträge Paläntologie*, 24, 69-85.
- Haynes, J.R. (1973). Cardigan Bay recent foraminifera. *Bulletin of the British Museum of Natural History*, 4, 1-245.
- Haynes, J.R. (1981). *Foraminifera*. London: Palgrave Macmillan UK.
- Hayward, B.W, Sabaa, A.T., Grenfell, H.R., Neil, H. and Bostock, H.C. (2013). Ecological distribution of recent deep-water foraminifera around New Zealand. *Journal of Foraminiferal Research*, 43, 415-442.
- Hayward, P.J. and Ryland, J.S. (1995). *Handbook of the marine fauna of north-west Europe*. Oxford: Oxford University Press.
- He, S. and Zu, Y.J. (2015). Concentrations and ratios of Sr, Ba and Ca along an estuarine river to the Gulf of Mexico- implication for sea level rise effects on trace element distribution. *Biogeosciences Discussions*, 12, 18425-18461.
- Heikkilä, M. and Seppä, H. (2003). A 11,000 yr palaeotemperature reconstruction from the southern boreal zone in Finland. *Quaternary Science Reviews*, 22, 541-554.
- Heinrich, H. (1988). Origin and consequences of cyclic ice rafting in the northeast Atlantic Ocean during the past 130,000 years. *Quaternary Research*, 29, 142-152.
- Heinrich, R., Cherubini, Y. and Meggers, H. (2010). Climate and sea-level induced turbidite activity in a canyon system offshore the hyperarid Western Sahara (Mauritania): the Timiris Canyon. *Marine Geology*, 275, 178-198.
- Helama, S., Jones, P.D. and Briffa, K.R. (2017). Dark Ages Cold Period: A literature review and directions for future research. *The Holocene*, 27(10), 1600-1606.
- Hemming, S.R. (2004). Heinrich events: Massive late Pleistocene detritus layers of the North Atlantic and their global climate imprint. *Review of Geophysics*, 42(1), 1-43.

References

Henderson, G., Collins, M., Hall, I., Lockwood, M., Palike, H., Rickaby, R., Schmidt, G., Turney, C. and Wolff, E. (2009). Improving future climate prediction using palaeoclimate data (an outcome of The Leverhulme Climate Symposium 2008 – Earth's Climate: Past, Present and Future). Oxford, UK, The Leverhulme Trust, 28pp.

Hiemstra, J.F., Evans, D.J.A., Scourse, J.D., McCarroll, D., Furze, M.F.A. and Rhodes, E. (2005). New evidence for a grounded Irish Sea glaciation of the Isles of Scilly, UK. *Quaternary Science Reviews*, 25(3-4), 299-309.

Hillenbrand, C.D., Baesler, A. and Grobe, H. (2005). The sedimentary record of the last glaciation in the western Bellingshausen Sea (West Antarctica): Implications for the interpretation of diamictos in a polar-marine setting. *Marine Geology*, 216, 191-204.

Hillenbrand, C.D., Smith, J.A., Kuhn, G., Esper, O., Gersonde, R., Larter, R.D., Maher, B., Moreton, S.G., Shimmiel, T.M. and Korte, M. (2010). Age assignment of a diatomaceous ooze deposited in the western Amundsen Sea Embayment after the Last Glacial Maximum. *Journal of Quaternary Science*, 25(3), 280-295.

Hillaire-Marcel, C., de Vernal, A. and Piper, D.J.W. (2007). Lake Agassiz final drainage event in the northwest North Atlantic. *Geophysical Research Letters*, 34(15), 1-5.

Hillaire-Marcel, C., de Vernal, A., Bilodeau, G. and Weaver, A.J. (2001). Absence of deep water formation in the Labrador Sea during the last interglacial periods. *Nature*, 410, 1073-1077.

Hillier, J.K. and Smith, M. (2008). Residual relief separation: digital elevation model enhancement for geomorphological mapping. *Earth Surface Processes and Landforms*, 33(14), 2266-2276.

Hodell, D.A., Brenner, M., Curtis, J.H., Medina-González, R., Can, E.I.C., Albornaz-Pat, A. and Guilderson, T.P. (2005). Climate change on the Yucatan Peninsula during the little ice age. *Quaternary Research*, 63(2), 109-121.

Holmes, J., Arrowsmith, C., Austin, W., Boyle, J., Fisher, E., Holme, R., Marshall, J., Oldfield, F. and Van Der Post, K. (2010). Climate and atmospheric circulation changes over the past 1000 years reconstructed from oxygen isotopes in lake-sediment carbonate from Ireland. *The Holocene*, 20, 1105-1111.

Holmes, J., Jones, R., Nicolas Haas, J., McDermott, F., Molloy, K. and O'Connell, M. (2007). Multi-proxy evidence for Holocene lake-level and salinity changes at An Loch Mór, a coastal lake on the Aran Islands, Western Ireland. *Quaternary Science Reviews*, 26(19-21), 2438-2462.

References

- Holmes, J.A., Tindall, J., Roberts, N., Marshall, W., Marshall, J.D., Bingham, A., Feeser, I., O'Connell, M., Atkinson, T., Jourdan, A.L., March, A. and Fisher, E.H. (2016). Lake isotope records of the 8200-year cooling event in western Ireland: Comparison with model simulations. *Quaternary Science Reviews*, 131, 341-349.
- Holzmann, M. and Pawlowski, J. (2000). Taxonomic relationships in the genus *Ammonia* (Foraminifera) based on ribosomal DNA sequences. *Journal of Micropalaeontology*, 19, 85-95.
- Horton, B.P. and Edwards, R.J. (2006). Quantifying Holocene sea level change using intertidal foraminifera: lessons from the British Isles. (Electronic version). *Cushman Foundation for Foraminiferal Research*, Special Publication, Volume 40.
- Horton, B.P. and Murray, J.W. (2007). The roles of elevation and salinity as primary controls on living foraminiferal distributions: Cowpen Marsh, Tess Estuary, UK. *Marine Micropalaeontology*, 63(3), 169-186.
- Horton, B.P., Corbett, R., Culver, S.J., Edwards, R.J. and Hillier, C. (2006). Modern saltmarsh diatom distributions of the Outer Banks, North Carolina, and the development of a transfer function for high resolution reconstructions of sea-level. *Estuarine, Coastal and Shelf Science*, 69(3), 13-29.
- Horton, B.P., Edwards, R.J. and Lloyd, J.M. (1999). A foraminiferal-based transfer function: implications for sea-level studies. *The Journal of Foraminiferal Research*, 29(2), 117-129.
- Horton, B.P., Peltier, W.R., Culver, S.J., Drummond, R., Engelhart, S.E., Kemp, A.C., Mallinson, D., Thieler, E.R., Riggs, S.R., Ames, D.V. and Thomson, K.H. (2009). Holocene sea-level changes along the North Carolina Coastline and their implications for glacial isostatic adjustment models. *Quaternary Science Reviews*, 28(17), 1725-1736.
- Hovland, M., Heggland, R., De Vries, M.H. and Tjelta, T.I. (2010). Unit-pockmarks and their potential significance for predicting fluid flow. *Marine and Petroleum Geology*, 27(6), 1190-1199.
- Hu, F.S., Kaufman, D., Yoneji, S., Nelson, D., Shemesh, A., Huang, Y., Tian, J., Bond, G., Clegg, B. and Brown, T. (2003). Cyclic variation and solar forcing of Holocene climate in the Alaskan subarctic. *Science*, 301(5641), 1890-1893.
- Hu, F.S., Slawinski, D., Wright, H.E., Ito, E., Johnson, R.G., Kelts, K.R., McEwan, R.F. and Boedigheimer, A. (1999). Abrupt changes in the North American climate during early Holocene times. *Nature*, 400, 437-440.

References

- Huang, C.C. (2002). Holocene landscape development and human impact in the Connemara uplands, western Ireland. *Journal of Biogeography*, 29, 153-165.
- Hubbard, A., Bradwell, T., Golledge, N., Hall, A., Patton, H., Sugden, D., Cooper, R. and Stoker, M. (2009). Dynamic cycles, ice streams and their impact on the extent, chronology and deglaciation of the British-Irish ice sheet. *Quaternary Science Reviews*, 28, 758-776.
- Huggett, R.J. (2011). *Fundamentals of Geomorphology*. London: Routledge.
- Hughen, K., Overpeck, J.T., Peterson, L.C. and Anderson, R.F. (1996). The nature of varved sedimentation in the Cariaco Basin, Venezuela, and its palaeoclimatic significance. *Geological Society London Special Publications*, 116(1), 171-183.
- Hughen, K., Overpeck, J.T., Peterson, L.C. and Trumbore, S. (1996). Rapid climate changes in the tropical Atlantic region during the last deglaciation. *Nature*, 380, 51-54.
- Hughes, A.L.C., Greenwood, S.L. and Clark, C.D. (2011). Dating constraints on the last British-Irish ice sheet: A map and database. *Journal of Maps*, 7(1), 156-184.
- Hughes, M.K. and Diaz, H.F. (1994). Was there a 'Medieval Warm Period', and if so, where and when? *Climatic Change*, 26, 109-142.
- Hull, E. (1878). *The physical geology and geography of Ireland*. London: Edward Stanford.
- Hunt, A., Dvoracek, D., Glascock, M.D. and Speakman, R.J. (2014). Major, minor and trace element mass fractions determined using ED-XRF, WD-XRF and INAA for five certified clay reference minerals: NCS DC 60102-60105; NCS DC 61101 (GBW 03101A, 031102A, 03103, and 03115). *Journal of Radioanalytical and Nuclear Chemistry*, 302(1), 505-512.
- Hurrell, J.W. and Deser, C. (2010). North Atlantic climate variability: the role of the North Atlantic Oscillation. *Journal of Marine Systems*, 79(3-4), 231-244.
- Hurrell, J.W., Kushiner, Y., Ottersen, G. and Visbeck, M. (2003). An overview of the North Atlantic Oscillation In: J.W. Hurrell, Y. Kushiner, G. Ottersen and M. Visbeck (Eds.) *The North Atlantic Oscillation* (pp. 1-35). American Geophysical Union.
- Jansen, E., Anderson, C., Moros, M., Nisancioglu, K.H., Nyland, B.F. and Telford, R.J. (2008). The Early to Mid-Holocene Thermal Optimum in the North Atlantic. In: R.W. Battarbee and H.A. Binney (Eds.) *Natural climate variability and global warming: A Holocene perspective* (pp. 123-137). New Jersey: Blackwell Publishing Ltd.

References

- Jansen, J.H.F., Van der Gaast, S.J., Koster, B. and Vaars, A.J. (1998). CORTEX, a shipboard XRF scanner for element analyses in split sediment cores. *Marine Geology*, 151(1), 143-153.
- Inabinet, J.R and Fish, A.G. (1979). Distribution and ecology of the littoral foraminifera of Timbalier Bay, Louisiana. *Rice University Studies*, 65(4), 491-509.
- INFOMAR – Integrated Mapping for the Sustainable Development of Ireland's Marine Resource, (2008). Galway Bay Charts. [Online] Available from: <http://www.infomar.ie/data/Charts/Galway/GalwayBay.php>
- INFOMAR – Integrated Mapping for the Sustainable Development of Ireland's Marine Resource, (2013). Galway Story Map. [Online] Available from: <https://infomargis.maps.arcgis.com/apps/MapTour/index.html?appid=2c2b39d99ac94a73ad6a1ef8b4318955>
- INFOMAR - Integrated Mapping for the Sustainable Development of Ireland's Marine Resource, (2011). Seabed Maps. [Online] Available from: <https://www.infomar.ie/surveying/Bays/Galway.php>
- Innes, J.B., Blackford, J.J. and Chambers, F.M. (2006). *Kretzschmaria deusta* and the northwest European mid-Holocene *Ulmus* decline at Moel y Gerddi, North Wales, United Kingdom. *Palynology*, 30, 121-132.
- Insua, T.L. (2013). *Physical properties of marine sediments and their application towards climate change studies* (Unpublished doctoral dissertation). University of Rhode Island, Rhode Island, U.S.A.
- Inversen, J. (1941). Land occupation in Denmark's Stone Age. *Danmarks Geologiske Undersøgelse*, 66(66), 1-68.
- IPCC (2013). Climate Change 2013: The Physical Science Basis. Contribution of Working Group I to the Fifth Assessment Report of the Intergovernmental Panel on Climate Change [Stocker, T.F., D. Qin, G.-K. Plattner, M. Tignor, S.K. Allen, J. Boschung, A. Nauels, Y. Xia, V. Bex and P.M. Midgley (eds.)]. Cambridge University Press, Cambridge, United Kingdom and New York, NY, USA.
- Ireland's Digital Ocean, (2018). Significant wave period in Galway Bay. [Online] Available at: <https://www.digitalocean.ie/Dashboard/Galway>
- Itambi, A.C., von Dobeneck, T. and Adegbe, A.T. (2010). Millennial-scale precipitation changes over Central Africa during the late Quaternary and Holocene: evidence in sediments from the Gulf of Guinea. *Journal of Quaternary Science*, 25, 267-279.

References

Jackson, D., O'Donohoe, P., Kane, F., Kelly, S., McDermott, T., Drumm, A., Lyons, K. and Nolan, G. (2012). Result of an epidemio-logical study of sea lice infestation in South Connemara, West of Ireland. *Aquaculture*, 364-365, 118-123.

Jacobeit, J., Jönsson, P., Barring, L., Beck, C. and Ekström, M. (2001). Zonal indices for Europe 1780-1995 and running correlations with temperature. *Climatic Change*, 48, 219-241.

Jennings, A., Syvitski, J., Gerson, L., Grönvold, K., Geirsdóttir, Á., Hardardóttir, J., Andrews, J. and Hagen, S. (2000b). Chronology and paleoenvironments during the late Weichselian deglaciation of the southwest Iceland shelf. *Boreas*, 29(3), 163-183.

Jennings, A.E. and Weiner, N. (1996). Environmental change in eastern Greenland during the last 1300 years: evidence from foraminifera and lithofacies in Nansen Fjord, 68°N. *The Holocene*, 6, 179-191.

Jessen, C.A., Rundgren, M., Björck, S., Andresen, C.S. and Conley, D.J. (2008). Variability and seasonality of North Atlantic climate during the early Holocene: evidence from Faroe Island lake sediments. *The Holocene*, 18(6), 851-860.

Jessen, K., Andersen, S.T and Farrington, A. (1959). The interglacial deposit near Gort, Co. Galway, Ireland. *Proceedings of the royal Irish Academy*, 60B, 1-77.

Jia, J., Bechtel, A., Liu, Z., Strobl, S.A.I., Sun, P. and Sachsenhofer, R.F. (2013). Oil shale formation in the Upper Cretaceous Nenjiang Formation of the Songliao Basin (NE China): Implications from organic and inorganic geochemical analyses. *International Journal of Coal Geology*, 113, 11-26.

Jingxing, L. and Luping, D. (2012). Quaternary marine transgressions in eastern China. *Journal of Palaeogeography*, 1(2), 105-125.

Johnson S.J., Clausen, H.B., Dansgaard, W., Fuhrer, K., Gundestrup, N., Hammer, C.U., Iversen, P., Jouzel, J., Stauffer, B. and Steffensen, J.P. (1992). Irregular glacial interstadials recorded in a new Greenland ice core. *Nature*, 359, 311-313.

Johnson, S.J., Dahl-Jensen, D., Gundestrup, N., Steffensen, J.P., Clausen, H.B., Miller, H., Masson-Delmotte, V., Sveinbjörnsdottir, A.E. and White, J. (2001). Oxygen isotope and palaeotemperature records from six Greenland ice-core stations: Camp Century, Dye-3, GRIP, GISP2, Renland and NorthGRIP. *Journal of Quaternary Science*, 16(4), 299-307.

Jones, P.D., Osborn, T.J. and Briffa, K.R. (2001). The evolution of climate over the last millennium. *Science*, 292, 662-667.

References

- Jones, R.W. (1994). *The Challenger Foraminifera*. UK: Oxford University Press.
- Joshi, S., Duffy, G.P. and Brown, C. (2017). Mobility of maerl-siliciclastic mixtures: Impact of waves, currents and storm events. *Estuarine, Coastal and Shelf Science*, 189, 173-188.
- Joshi, S., Duffy, G., Brown, C. and Grehan A. (2011). *Coupled hydrodynamic-sediment transport modelling and habitat modelling in Galway Bay, West of Ireland*. Poster Presentation at the Irish Geological Research Meeting, Galway, Ireland.
- Kaliraj, S., Chandrasekar, N., Ramachandran, K.K., Srinivas, Y. and Saravanan, S. (2017). Coastal landuse and land cover change and transformations of Kanyakumari coast, India using remote sensing and GIS. *The Egyptian Journal of Remote Sensing and Space Science*, 20(2), 169-185.
- Kaminski, M.A. and Gradstein, F.M. (2005). *Atlas of Palaeogene Cosmopolitan deep-water agglutinated foraminifera*. Grzybowski Foundation Special Publication 10.
- Kaniewski, D., Van Campo, E., Paulissen, E., Weiss, H., Bakker, J., Rossignol, I., Van Lerberghe, K. (2011). The medieval climate anomaly and the Little Ice Age in coastal Syria inferred from pollen-derived palaeoclimatic patterns. *Global and Planetary Change*, 78, 178-187.
- Kapsner, W.R., Alley, R.B., Shuman, C.A., Anandakrishnan, S. and Grootes, P.M. (1995). Dominant influence of atmospheric circulation on snow accumulation in Greenland over the past 18,000 years. *Nature*, 373(6509), 52-54.
- Kasten, S. and Jørgensen, B.B. (2000). Sulphate reduction in marine sediments. In: H.D Schultz and M. Zabel (Eds.) *Marine Geochemistry* (pp. 263-282). Berlin: Springer.
- Kaufman, D. S., Ager, T. A., Anderson, N. J., Anderson, P. M., Andrews, J. T., Bartlein, P. J., Brubaker, L. B., Coats, L. L., Cwynar, L. C., Duvall, M. L., Dyke, A. S., Edwards, M. E., Eisner, W. R., Gajewski, K., Geirsdóttir, A., Hu, F. S., Jennings, A. E., Kaplan, M. R., Kerwin, M. W., Lozhkin, A. V., MacDonald, G. M., Miller, G. H., Mock, C. J., Oswald, W. W., Otto-Bliesner, B. L., Porinchu, D. F., Rühland, K., Smol, J. P., Steig, E. J. and Wolfe, B. B. (2004). Holocene thermal maximum in the western Arctic (0-180°C). *Quaternary Science Reviews*, 23(5), 529-560.
- Kelly, M. and Ó Gráda, C. (2013). Debating the Little Ice Age. *Journal of Interdisciplinary History*, 45(1), 57-68.
- Kemp, A.E.S., Dean, J., Pearse, R. and Pike, J. (2001). Recognition and analysis of bedding and sediment fabric features. In: W.M. Last and J.P. Smol (Eds.) *Tracking environmental change using lake sediments, Volume 1: Basin Analysis, coring and chronological techniques* (pp. 7-22). Dordrecht: Kluwer Academic Press.

References

- Khan, N.S., Ashe, E., Horton, B.P., Dutton, A., Kopp, R.E., Brocard, G., Engelhart, S.E., Hill, D.F., Peltier, W.R., Vane, C.H. and Scatena, F.N. (2017). Drivers of Holocene sea-level change in the Caribbean. *Quaternary Science Reviews*, 155, 13-36.
- Kidwell, S.M. (1989). Stratigraphic condensation of marine transgressive records: origin of major shell deposits in the Miocene of Maryland. *Journal of Geology*, 97, 1-24.
- Kinealy, C. (2006). *This great calamity, the Irish famine, 1845-52*. Dublin: Gill and Macmillan.
- Kinahan, G.H. (1869). *Explanation to accompany sheet 105 with that portion of sheet 114 that lies on the north of Galway Bay, of the Geological Survey of Ireland*. Memoir (Sheet), Geological Survey of Ireland, Dublin.
- Kinahan, G.H., Leonard, H. and Cruise, R.J. (1871). *Explanatory memoir to accompany sheets 104 and 113 with the adjoining portions of sheets 103 and 122 (Kilkieran and Aran Sheets), of the Geological Survey of Ireland, illustrating a portion of the County of Galway*. Memoir (Sheet), Geological Survey of Ireland, Dublin.
- Kissel, C., Laj, C., Kienast, M., Bolliet, T., Holbourn, A., Hill, P., Kuhnt, W. and Braconnot, P. (2010). Monsoon variability and deep oceanic circulation in the western equatorial Pacific over the last climatic cycle: insights from sedimentary magnetic properties and sortable silt. *Palaeoceanography*, 25(3), 1-12.
- Kleiven, H.F., Kissel, C., Laj, C., Ninnemann, U.S., Richter, T.O. and Cortijo, E. (2007). Reduced North Atlantic deep water coeval with the Glacial Lake Agassiz fresh water outburst. *Science*, 319, 60-64.
- Klitgaard-Kristensen, D., Sejrup, H.P., Hafliðason, H., Johnsen, S. and Spurk, M. (1998). A regional 8200 cal. yr BP cooling event in northwest Europe, induced by final stages of the Laurentide ice-sheet deglaciation? *Journal of Quaternary Science*, 13(2), 165-169.
- Knight, J. (2004). Sedimentary evidence for the formation mechanism of the Armoy moraine and late Devensian glacial events in the north of Ireland. *Geological Journal*, 39(3-4), 403-417.
- Knight, J., Coxon, P., McCabe, A.M. and McCarron, S.G. (2004). Pleistocene glaciations in Ireland. *Developments in Quaternary Sciences*, 2(1), 183-191.
- Koch, J. and Clague, J.J. (2006). Are insolation and sunspot activity the primary drivers of Holocene glacier fluctuations? *PAGES News*, 14(3), 20-21.

References

- Koinig, K.A., Shotyk, W., Lotter, A.F., Ohlendorf, C. and Sturm, M. (2003). 9000 years of geochemical evolution of lithogenic major and trace elements in the sediment of an alpine lake- the role of climate, vegetation, and land-use history. *Journal of Palaeolimnology*, 30, 307-320.
- Kotilainen, A.T. and Kaskela, A.M. (2017). Comparison of airborne LiDAR and shipboard acoustic data in complex shallow water environments: Filling in the white ribbon zone. *Marine Geology*, 385, 250-259.
- Koutsoukos, E.A.M. and Hart, M.B. (1990). Cretaceous foraminiferal morphogroup distribution patterns, palaeocommunities and trophic structures: a case study from the Sergipe Basin, Brazil. *Transactions of the Royal Society of Edinburgh: Earth Sciences*, 81, 221-246.
- Kristensen, D.K. and Sejrup, H.P. (1996). Modern benthic foraminiferal biofacies across the northern North Sea. *Sarsia*, 81, 97-106.
- Kristensen, E. and Blackburn, T.H. (1987). The fate of organic carbon and nitrogen in experimental marine sediment systems: influence of bioturbation and anoxia. *Journal of Marine Research*, 45, 231-257.
- Kuchar, J., Milne, G., Hubbard, A., Patton, H., Bradley, S., Shennan, I. and Edwards, R. (2012). Evaluation of a numerical model of the British-Irish ice sheet using relative sea-level data: Implications for the interpretation of trimline observations. *Journal of Quaternary Science*, 27(6), 597-605.
- Kuhlemann, J., Rohling, E.J., Krumrei, I., Kubik, P., Ivy-Ochs, S. and Kucera, M. (2008). Regional synthesis of Mediterranean atmospheric circulation during the last glacial maximum. *Science*, 321, 1338-1340.
- Kwiecien, O., Arz, H.W., Lamy, F., Wulf, S., Bahr, A., Röhl, U. and Haug, G.H. (2008). Estimated reservoir ages of the Black Sea since the last Glacial. *Radiocarbon*, 50, 99-118.
- Kylander, M.E., Ampel, L., Wohlfarth, B. and Veres, D. (2011). High-resolution X-ray fluorescence core scanning analysis of Les Echets (France) sedimentary sequence: new insights from chemical proxies. *Journal of Quaternary Science*, 26(1), 109-117.
- Kylander, M.E., Klaminder, J., Wohlfarth, B. and Löwemark, L. (2013b). Geochemical responses to palaeoclimatic changes in southern Sweden since the late glacial: the Hässeldala Port lake sediment record. *Journal of Palaeolimnology*, 50, 57-70.

References

- Laird, K.R., Fritz, S.C., Grimm, E.C. and Mueller, P.G. (1996a). Century-scale palaeoclimatic reconstruction from Moon Lake, a closed basin lake in the northern Great Plains. *Limnology and Oceanography*, 41, 890-902.
- LaMarche, V.C. (1974). Palaeoclimatic inferences from long tree-ring records. *Science*, 183, 1043-1048.
- Laird, K.R., Fritz, S.C., Maasch, K.A. and Cumming, B.F. (1996b). Greater drought intensity and frequency before AD 1200 in the Northern Great Plains, USA. *Nature*, 384, 552-555.
- LaMarche, G., Lurton, X., Verdier, A-L. and Augustin, J-M. (2011). Quantitative characterisation of seafloor substrate and bedforms using advanced processing of multibeam backscatter- Application to the Cook Strait, New Zealand. *Continental Shelf Research*, 31(2), S93-S109.
- Lamb, H.H. (1965). The early Medieval warm epoch and its sequel. *Palaeogeography, Palaeoclimatology, Palaeoecology*, 1, 13-37.
- Lamb, H.H. (1967). Britain's changing climate. *The Geographical Journal*, 133(4), 445-466.
- Lamb, H.H. (1977). *Climate: Present, Past and Future*, (Volume 2). London: Methuen Publishing.
- Lamb, H.H. (1982). *Climate, History and the Modern World*. Boca Raton, Florida: Routledge.
- Lamb, H.H. (1991). *Historic storms of the North Sea, British Isles and Northwest Europe*. Cambridge: Cambridge University Press.
- Lamb, H.H. (1995). *Climate History and the Modern World* (2nd Edition). Princeton, New Jersey: Princeton University Press.
- Lamb, H. and Thompson, A. (2005). Unusual mid-Holocene abundance of *Ulmus* in western Ireland-human impact in the absence of a pathogen? *The Holocene*, 15(3), 447-452.
- Lambeck, K., Rouby, H., Purcell, A., Sun, Y. and Sambridge, M. (2014). Sea level and global ice volumes from the Last Glacial Maximum to the Holocene. *Proceedings of the National Academy of Sciences*, 111(43), 15296-15303.

References

- Lambeck, K., Smither, C. and Johnston, P. (1998). Sea-level change, glacial rebound and mantle viscosity for northern Europe. *Geophysical Journal International*, 134(1), 102-144.
- Lang, B., Bedford, A., Brooks, S.J., Jones, R.T., Richardson, N., Birks, H.J.B. and Marshall, J.D. (2010). Early-Holocene temperature variability inferred from chronomid assemblages at Hawes Water, northwest England. *The Holocene*, 20(6), 943-954.
- Langdon, P.G., Barber, K.E. and Hughes, P.D.M. (2003). A 7500-year peat-based palaeoclimatic reconstruction and evidence for an 1100-year cyclicity in bog surface wetness from Temple Hill Moss, Pentland Hills, southeast Scotland. *Quaternary Science Reviews*, 22, 259-274.
- Langdon, P.G., Brown, A., Caseldine, C.J., Blockley, S.P.E. and Stuijts, I. (2012). Regional climate change from peat stratigraphy for the mid- to late Holocene in central Ireland. *Quaternary International*, 268, 145-155.
- Larsen, D.J., Miller, G.H., Geirsdóttir, A. (2012). Non-linear Holocene climate evolution in the North Atlantic: a high-resolution, multi-proxy record of glacier activity and environmental change from Hvítárvatn, central Iceland. *Quaternary Science Reviews*, 39, 231-247.
- Larsen, D.J., Vinther, B.M., Briffa, K.R., Melvin, T.M., Clausen, H.B., Jones, P.D., Siggaard-Andersen, M-L., Hammer, C.U., Eronen, M., Grudd, H., Gunnarson, B.E., Hantemirov, R.M., Naurzbaev, M.M. and Nicolussi, K. (2008). New ice core evidence for a volcanic cause of the A.D. 536 dust veil. *Geophysical Research Letters*, 35(4), 1-5.
- Last, W. (2001). Textural analysis of lake sediment. In W.N. Last and J.P. Smol (Eds.) *Tracking environmental change using lake sediments* (pp. 41-81). Volume 1: Basin analysis, coring and chronological techniques. Dordrecht: Kluwer Academic Publishers.
- Leake, B.E. (1989). The megagabbros, orthogneisses and paragneisses of the Connemara complex, western Ireland. *Journal of the Geological Society, London*, 146, 575-596.
- Leake, B.E. (2006) Mechanism of emplacement and crystallisation history of the northern margin and centre of the Galway Granite, western Ireland. *Transactions of the Royal Society of Edinburgh: Earth Sciences*, 97, 1-23.
- Ledru, M-P., Jomelli, V., Bremond, L., Ortuño, T., Cruz, P., Bentaleb, I., Sylvestre, F., Kuentz, A., Beck, S., Martin, C., Pallès, C. and Subitani, S. (2013). Evidence of moist niches in the Bolivian Andes during the mid-Holocene arid period. *The Holocene*, 23(11), 1547-1559.

References

- Lees, A. and Feely, M. (2016). The connemara eastern boundary fault: A review and assessment using new evidence. *Irish Journal of Earth Science*, 34, 1-25.
- Lei, W. (1995). *Three Dimensional Hydrodynamic Modelling in Galway Bay* (Unpublished Doctoral Dissertation) National University of Ireland, Dublin.
- Lekins, W.A.H., Sejrup, H.P., Haflidason, H., Peterson, G.Ø., Hjelstuen, B. and Knorr, G. (2005). Laminated sediments preceding Heinrich event 1 in the Northern North Sea and Southern Norwegian Sea: origin, processes and regional linkage. *Marine Geology*, 216, 27-50.
- Leorri, E. and Cearreta, A. (2009). Quantitative assessment of the salinity gradient within the estuarine systems in the southern Bay of Biscay using benthic foraminifera. *Continental Shelf Research*, 29, 1226-1239.
- Leorri, E., Gehrels, W.R., Horton, B.P., Fatela, F. and Cearreta, A. (2010). Distribution of foraminifera in salt marshes along the Atlantic coast of SW Europe: tools to reconstruct past sea-level variations. *Quaternary International*, 221, 104-115.
- Lewis, H.C. (1887). The terminal moraine of the great glaciers of England. *Nature*, 36, 573.
- Lewis H.C. (1894). *Glacial geology of Great Britain and Ireland*. London: Longman, Green and Co.
- Li, M.Z. and King, E.L. (2007). Multibeam bathymetric investigations of the morphology of sand ridges and associated bedforms and their relation to storm processes, Sable Island Bank, Scotian Shelf. *Marine Geology*, 243(1-4), 200-228.
- Libby, W. F., Anderson, E. C., and Arnold, J. R. (1949). Age determination by radiocarbon content: world-wide assay of natural radiocarbon. *Science*, 109(2827), 227-228.
- Limber, P.W. and Murray, A.B. (2011). Beach and sea-cliff dynamics as a driver of long-term rocky coastline evolution and stability. *Geology*, 39(12), 1147-1150.
- Lipps, J.H. (1983). Biotic interactions in benthic foraminifera. In: M.J.S. Tevesz and P.L. McCall (Eds.) *Biotic interactions in recent and fossil benthic communities- Tropics in geobiology, Vol. 3* (pp. 331-376). Boston: Springer.
- Litt, T., Schmincke, H-U. and Kromer, B. (2003). Environmental response to climatic and volcanic events in central Europe during Weichselian late glacial. *Quaternary Science Reviews*, 22(1), 7-32.

References

- Liu, J.P. and Milliman, J.D. (2004). Reconsidering melt-water pulses 1A and 1B: Global impacts of rapid sea-level rise. *Journal of Ocean University of China*, 3(2), 183-190.
- Lockhart, E.A., Scourse, J.D., Praeg, D., Van Landeghem, K.J.J., Mellert, C., Saher, M., Callard, L., Chiverrell, R.C., Benetti, S., Ó Cofaigh, C. and Clark, C.D. (2018). A stratigraphic investigation of the Celtic Sea megaridges based on seismic and core data from the Irish-UK sectors. *Quaternary Science Reviews*, 198, 156-170.
- Loeblich, A.R. and Tappan, H. (1988). *Foraminiferal general and their classification*. New York: Van Nostrand Reinhold Company.
- López-Belzunce, M., Blázquez, A.M. and Pretus, J.L. (2014). Recent benthic foraminiferal assemblages and their relationship to environmental variables on the shoreface and inner shelf off Valencia (Western Mediterranean). *Marine Environmental Research*, 101, 169-183.
- Lord, T.C., Thorp, J.A. and Wilson P. (2015). A wild boar dominated ungulate assemblage from an early Holocene natural pit fall trap: Cave shaft sediments in northwest England associated with the 9.3 ka BP cold event. *The Holocene*, 26(1), 147-153.
- Lowe, J.J. and Walker, M.J.C. (1997). *Reconstructing Quaternary environments*. Longman: London.
- Lucchi, R.G., Sagnotti, L., Camerlenghi, A., Macri, P., Rebescol, M., Pedrosa, M.T. and Giorgetti, G. (2015). Marine sedimentary record of Meltwater Pulse 1A along the NW Barents Sea continental margin. *Arktos*, 1(7), 1-14.
- Lurton, X. (2010). *An introduction to underwater acoustics. Principles and Applications* (2nd Edition). New York: Springer.
- Luterbacher, J., Dietrich, D., Xoplaki, E., Grosjean, M. and Wanner, H. (2004). European seasonal and annual temperature variability, trends and extremes since 1500. *Science*, 303, 1499-1503.
- Luttikhuisen, P.C., Drent, J. and Baker, A.J. (2003). Disjunct distribution of highly diverged mitochondrial lineage clade and population subdivision in a marine bivalve with pelagic larval dispersal. *Molecular Ecology*, 12, 2215-2229.
- Magny, M. (2004). Holocene climatic variability as reflected by mid-European lake-level fluctuations, and its probable impact on prehistoric human settlements. *Quaternary International*, 113, 65-79.

References

- Magny, M., Bégeot, C., Guiot, J., and Peyron, O. (2003). Contrasting patterns of hydrological changes in Europe in response to Holocene climate cooling phases. *Quaternary Science Reviews*, 22(15-17), 1589–1596.
- Magny, M. and Bégeot, C. (2004). Hydrological changes in the European mid latitudes associated with freshwater outbursts from Lake Agassiz during the Younger Dryas event and the early Holocene. *Quaternary Research*, 61(2), 181-192.
- Magny, M. and Haas, J. N. (2004). A major widespread climatic change around 5300 cal. yr BP at the time of the Alpine Iceman. *Journal Quaternary Science*, 19(5), 423–430.
- Magny, M., Combourieu-Nebout, N., de Beaulieu, J. L., BoutRoumazeilles, V., Colombaroli, D., Desprat, S., Francke, A., Joannin, S., Ortu, E., Peyron, O., Revel, M., Sadori, L., Siani, G., Sicre, M. A., Samartin, S., Simonneau, A., Tinner, W., Vannièrè, B., Wagner, B., Zanchetta, G., Anselmetti, F., Brugiapaglia, E., Chapron, E., Debret, M., Desmet, M., Didier, J., Essallami, L., Galop, D., Gilli, A., Haas, J. N., Kallel, N., Millet, L., Stock, A., Turon, J. L., and Wirth, S. (2013). North-south palaeohydrological contrasts in the central Mediterranean during the Holocene: tentative synthesis and working hypotheses. *Climates Past*, 9, 2043– 2071.
- Magny, M., de Beaulieu, J.L, Drescher-Schneider, R., Vanniere, B., Walter-Simonnet, A.J., Millet, L., Bosseut, G. and Peyron, O. (2006). Climatic oscillations in central Italy during the last glacial-Holocene transition: the record from Lake Accesa. *Journal of Quaternary Science*, 21, 311-320.
- Magri, D. and Parra, I. (2002). Late Quaternary western Mediterranean pollen records and African winds. *Earth and Planetary Science Letters*, 200, 401-408.
- Mahony, M. (2015). Climate change and the geographies of objectivity: The case of the IPCC's burning embers diagram. *Transactions of the Institute of British Geographers*, 40, 153-167.
- Maity, H. and Mazumder, B.S. (2014) Experimental investigation of the impacts of coherent flow structures upon turbulence properties in regions of crescentic scour. *Earth Surface Processes and Landforms*, 39(8), 995-1013.
- Manley, G. (1957). Climatic fluctuations and fuel requirements. *Scottish Geographical Magazine*, 73(1), 19-28.
- Mann, M.E., Zhang, Z., Rutherford, S., Bradley, R.S., Hughes, M.K., Shindell, D., Ammann, C., Faluvegi, G. and Ni, F. (2009). Global signatures and dynamical origins of the Little Ice Age and medieval climate anomaly. *Science*, 326, 1256-1269.

References

Marine Institute (MI) of Ireland, (2017). Tide gauge observations. [Online] Available from: <http://www.marine.ie/Home/site-area/data-services/real-time-observations/real-time-data-access>.

Marine Institute (MI) of Ireland, (2018). Wave buoy observations. [Online] Available from: <http://www.marine.ie/Home/site-area/data-services/real-time-observations/wave-buoy-observations?instrumentname=SmartBay%20Wave%20Buoy>.

Marsh, R., Mills, R.A., Green, D.R.H., Salter, I. and Taylor, S. (2007). Controls on sediment geochemistry in the Crozet region. *Deep Sea Research Part II*, 54, 2260-2274.

Martinez-Martos, M., Galindo-Zaldivar, J., Lobo, F.J., Pedrera, A., Ruano, P., Lopez-Chicano, M. and Ortega-Sánchez, M. (2016). Buried marine-cut terraces and submerged marine-built terraces: The Carchuna-Calahonda coastal area (southeast Iberian Peninsula). *Geomorphology*, 264, 29-40.

Marzeion, B., Jarosch, A.H. and Gregory, J.M. (2014). Feedbacks and mechanisms affecting the global sensitivity of glaciers to climate change. *The Cryosphere*, 8, 59-71.

Mastroruzzi, G., Sansò, P., Murray-Wallace, C.V. and Shennan, I. (2005). Quaternary coastal morphology and sea-level changes – An introduction. *Quaternary Science Reviews*, 24(18), 1963-1968.

Matero, I.S.O., Gregoire, L.J., Ivanovic, R.F., Tindall, J.C. and Haywood, A.M. (2017). The 8.2 ka cooling event caused by Laurentide ice saddle collapse. *Earth and Planetary Science Letters*, 473, 205-214.

Matthews, J.A., Berrisford, M.S., Dressa, P.Q., Nesje, A., Dahl, S.O., Bjune, A.E., Bakke, J.H., Birks, J.B.m Lie, Ø., Dumayne-Peaty, L. and Barnetth, E. (2005). Holocene glacier activity of Bjørnbreen and climatic reconstruction in central Jotunheimen, Norway, based on proximal glaciofluvial stream-bank mires. *Quaternary Science Reviews*, 24, 67-90.

Mauquoy, D., van Geel, B., Blaauw, M., Speranza, A. and van der Plicht, J. (2004). Changes in solar activity and Holocene climate shifts derived from ¹⁴C wiggle-match dated peat deposits. *The Holocene*, 14, 45-52.

Mauquoy, D., van Geel, B., Blaauw, M. and van der Plicht, J. (2002). Evidence from northwest European bogs shows “Little Ice Age” climatic changes driven by variations in solar activity. *The Holocene*, 12, 1-6.

References

- Mauri, A., Davis, B.A.S., Collins, P.M. and Kaplan, J.O. (2015). The climate of Europe during the Holocene: a gridded pollen-based reconstruction and its multi-proxy evaluation. *Quaternary Science Reviews*, 112, 109-127.
- Max, M.D., Ryan, P.D. and Inamdar, D.D. (1983). A magnetic deep structural geology interpretation of Ireland. *Tectonics*, 2(5), 431-451.
- May, V.J. and Hansom, J.D. (2003). *Coastal Geomorphology of Great Britain*. Geological Conservation Review Series, No. 28. Peterborough: Joint Nature Committee.
- Mayewski, P.A., Meeker, L.D., Twickler, M.S., Whitlow, S., Yang, Q., Lyons, W.B. and Prentice, M. (1997). Major features and forcing of high-latitude northern hemisphere atmospheric circulation using a 110,000-year long glaciochemical series. *Journal of Geophysical Research*, 102, 26,345-26,366.
- Mayewski, P.A., Rohling, E.E., Curt Stager, J., Karlén, W., Maasch, K.A., Meeker, L.D., Meyerson, E.A., Gasse, F., van Kreveld, S., Holmgren, K., Lee-Thorp, J., Rosqvist, G., Rack, F., Staubwasser, M., Schneider, R.R. and Steig, E.J. (2004). Holocene climate variability. *Quaternary Research*, 62(3), 243-255.
- Mazumder, R. (2003) Sediment transport, aqueous bedform stability and morphodynamics under unidirectional current: a brief overview. *Journal of African Earth Sciences*, 36(1), 1-14.
- McCabe, A.M. (1987). Quaternary deposits and glacial stratigraphy in Ireland. *Quaternary Science Reviews*, 6(3-4), 259-299.
- McCabe, A.M. (1999). Ireland. In: D.Q. Bowen (Ed.) A revised correlation of quaternary deposits in the British Isles. *Geological Society Special Report*, 23, 115-124.
- McCabe, A.M. and Clark, P.U. (1998). Ice sheet variability around the North Atlantic Ocean during the last deglaciation. *Nature*, 392, 373-377.
- McCabe, A.M. and Clark, P.U. (2003). Deglacial chronology from County Donegal, Ireland: implications for deglaciation of the British-Irish ice sheet. *Journal of the Geological Society*, 160(6), 847-855.
- McCabe, A.M. and Dardis, G.F. (1989). A geological view of drumlins in Ireland. *Quaternary Science Reviews*, 8(2), 169-177.
- McCabe, A.M. and Dardis, G.F. (1989) Sedimentology and depositional setting of late Pleistocene drumlins, Galway Bay, western Ireland. *Journal of Sedimentary Petrology*, 59(6), 944-959.

References

McCabe, A. M. and Dunlop, P. (2006). *The Last Glacial Termination in Northern Ireland*. Belfast: Geological Survey of Northern Ireland.

McCabe, A.M. and Haynes, J. (1996). A late Pleistocene intertidal boulder pavement from an isostically emergent coast, Dundalk Bay, Eastern Ireland. *Earth Surface Processes and Landforms*, 21, 555-572.

McCabe, A.M. and Ó Cofaigh, C. (1995). Late Pleistocene morainal bank at Greystones, eastern Ireland: An example of sedimentation during ice marginal re-equilibration in an isostatically depressed basin. *Sedimentology*, 42, 647-663.

McCabe, A.M. and Williams, G.D. (2012). Timing of the East Antrim Coastal Readvance: Phase relationships between lowland Irish and upland Scottish ice sheets during the Last Glacial Termination. *Quaternary Science Reviews*, 58, 18-29.

McCabe, A.M., Clark, P.U. and Clark, J. (2005). AMS C-14 dating of deglacial events in the Irish Sea Basin and other sectors of the British-Irish ice sheet. *Quaternary Science Reviews*, 24, 1673-1690.

McCabe, A.M., Clark, P.U., Clark, J. and Dunlop, P. (2007b). Radiocarbon constraints on readvances of the British-Irish ice sheet in the northern Irish Sea basin during the last deglaciation. *Quaternary Science Reviews*, 26, 1204-1211.

McCabe, A.M., Haynes, J.R. and MacMillan, N.F. (1986). Late Pleistocene tidewater glacier and glaciomarine sequences from north County Mayo, Republic of Ireland. *Journal of Quaternary Science*, 1, 73-84.

McCabe, A.M., Knight, J. and McCarron, S. (1998). Evidence for Heinrich 1 in the British Isles. *Journal of Quaternary Science*, 13, 549-568.

McCarroll, D., Knight, J. and Rijdsdijk, K. (2001). Introduction: the glaciation of the Irish Sea basin. *Journal of Quaternary Science*, 16, 391-92.

McCarron, S., Praeg, D., Ó Cofaigh, C., Monteys, X., Thébaudeau, B., Craven, K., Saqab, M. and Cova, A. (2018). A Pilo-Pleistocene sediment wedge on the continental shelf west of central Ireland: The Connemara Fan. *Marine Geology*, 399, 97-114.

McCulloch, M., Cappo, M., Aumend, J. and Müller, W. (2005). Tracing the life history of individual barramundi using laser ablation MC-ICP-MS Sr-isotopic and Sr/Ba ratios in otoliths. *Marine and Freshwater Research*, 56, 637-644.

McDermott, F., Frisia, S., Huang, Y., Longinelli, A., Spiro, B., Heaton, T.H.E., Hawkesworth, C., Borasato, A., Keppens, E., Fairchild, I.J., van der Borg, K., Verheyden, S. and Selmo, E. (1999). Holocene climate variability in Europe: Evidence from $\delta^{18}\text{O}$,

References

- textural and extension rate variations in three speleothems. *Quaternary Science Reviews*, 18, 1021-1038.
- McDermott, F., Matthey, D.P. and Hawkesworth, C. (2001). Centennial-scale holocene climate variability revealed by a high-resolution speleothem $\delta^{18}\text{O}$ record from SW Ireland. *Science*, 294(5545), 1328-1331.
- McFadden, M.A., Mullins, H.T., Patterson, W.P. and Anderson, W.T. (2004). Palaeoproductivity of eastern Lake Ontario over the past 10,000 years. *Limnology and Oceanography*, 49(5), 1570-1581.
- McGrath, R., Nishimura, E., Nolan, P., Semmler, T., Sweeney, C. and Wang, S. (2005). *Climate Change: Regional climate model predictions for Ireland*. Ireland: Environmental Protection Agency.
- McKenzie, S.M. (2010). *Late Pleistocene to Mid-Holocene climatic variability in Ireland: Evidence from ostracod geochemistry* (Unpublished Master's thesis). University of Saskatchewan, Canada.
- McKeown, M. (2013). *A Palaeolimnological Assessment of Human and Climate Influences on Chironomid Communities in Western Ireland* (Unpublished Doctoral Dissertation). National University of Ireland, Galway.
- McLaughlin, T.R., Whitehouse, N.J., Schulting, R.J., McClatchie, M., Barratt, P. and Bogaard, A. (2016). The changing face of Neolithic and Bronze Age Ireland: A big data approach to the settlement and burial records. *Journal of World Prehistory*, 29(2), 117-153.
- McLean, R. F. and Kirk, R. M. (1969) Relationships between grain size, size-sorting, and foreshore slope on mixed sand-shingle beaches. *New Zealand Journal of Geology and Geophysics*, 12(1), 138-155.
- McNamara, M.E. and Hennessy, R.W. (2010). *Stone, Water and Ice: The geology of the Burren region, Co. Clare, Ireland*. Clare: The Burren Connect Project.
- Meehan, R. (2013). *The merging of Quaternary map datasets*. Geological Survey of Ireland, Dublin.
- Merkt, J. and Müller, H. (1999). Varve chronology and palynology of the Lateglacial in Northwest Germany from lacustrine sediments of Hämelsee in Lower Saxony. *Quaternary International*, 61, 41-59.
- Merritt, J.W., Auton, C.A. and Firth, C.R. (1995). Ice-proximal glaciomarine sedimentation and sea-level change in the Inverness area, Scotland: a review of the

References

deglaciation of a major ice stream of the British Late Devensian ice sheet. *Quaternary Science Reviews*, 14(3), 289-329.

Met Éireann, 2017. Met Éireann Rainfall [Online] Available at:
<https://www.met.ie/climate-ireland/rainfall.asp>.

Meyers, S.R. and Pagani, M. (2006). Quasi periodic climate teleconnections between northern and southern Europe during the 17th-20th centuries. *Global and Planetary Change*, 54, 291-301.

Milankovitch, M. (1941). *Canon of Insolation and the Ice-Age Problem (in German)*. Special Publications of the Royal Serbian Academy, 132(33), Israel Program for Scientific Translations: Jerusalem.

Milker, Y., Schmiiedl, G. and Betzler, C. (2011). Palaeobathymetric history of the Western Mediterranean Sea shelf during the latest glacial period and the Holocene: quantitative reconstructions based on foraminiferal transfer functions. *Palaeogeography, Palaeoclimatology, Palaeoecology*, 307, 324-338.

Mitchell, F. (1976). *The Irish Landscape*. 1st Edition. London: Collins

Mitchell, F.J.G. (1995). The dynamics of Irish post-glacial forests. In: J.R. Pilcher and S.S. Mac an T-Saoir (Eds.) *Wood, trees and forests in Ireland* (pp. 13-22). Dublin: Royal Irish Academy.

Mitchell, F.J.G. (2006). Where did Ireland's trees come from? Biology and Environment: *Proceedings of the Royal Irish Academy*, 106B(3), 251-259.

Mitchell, G.F. (1960). The Pleistocene history of the Irish Sea. *Advancement Science*, 17, 313-325.

Mitchum, R. M., Vail, P. R. Jr. and Sangree, J. B. (1977a). Seismic Stratigraphy {Applications to Hydrocarbon Exploration. AAPG Special Volumes. Chapter. Seismic Stratigraphy and Global Changes of Sea Level: Part 6. Stratigraphic Interpretation of Seismic Reflection Patterns in Depositional Sequences: Section 2. Application of Seismic Reflection Configuration to Stratigraphic Interpretation, pages 117-133.

Mitchum, R. M., Vail, P. R. Jr. and Thomson, S., III. (1977b). Seismic Stratigraphy{Applications to Hydrocarbon Exploration. AAPG Special Volumes. Chap. Seismic Stratigraphy and Global Changes of Sea Level: Part 2. The Depositional Sequence as a Basic Unit for Stratigraphic Analysis: Section 2. Application of Seismic Reflection Configuration to Stratigraphic Interpretation, pages 53-62.

References

Molloy, K. and O'Connell, M. (1995). Palaeoecological investigations towards the reconstruction of environment and land-use changes during prehistory at Céide Fields, western Ireland. *Probleme der Küstenforschung im südlichen Nordseegebiet*, 23, 187-225.

Molloy, K. and O'Connell, M. (2004). Holocene vegetation and land-use dynamics in the karstic environment of Inis Oirr, Aran Islands, western Ireland: pollen analytical evidence evaluated in light of the archaeological record. *Quaternary International*, 113, 41-64.

Molloy, K. and O'Connell, M. (2012). Prehistoric farming in western Ireland: pollen analysis at Caheraphuca, Co. Clare. In S. Delaney, D. Bayley, E. Lyne, S. McNamara, J. Nunan and K. Molloy (Eds.) *Borderlands-Archaeological excavations on the route of the M18 Gort to Crusheen road scheme* (pp. 109-122). Dublin: National Roads Authority.

Molloy, K. and O'Connell, M. (2014). Post-glaciation plant colonisation of Ireland: fresh insights from An Loch Mór, Inis Oírr, western Ireland. *The Irish Naturalist's Journal*, 33, 66-88.

Monteys, X., Hardy, D., Doyle, E. and Garcia-Gil, S. (2008, August), Distribution, morphology and acoustic characterisation of a gas pockmark field on the Malin Shelf, NW Ireland, paper presented at 33rd International Geological Congress, Symposium OSP-01, International Union of Geological Sciences, Oslo.

Morrill, C., Anderson, D.M., Bauer, B.A., Buckner, R., Gille, E.P., Gross, W.S., Hartman, M. and Shah, A. (2013a). Proxy benchmarks for intercomparison of 8.2 ka simulations. *Climate of the Past*, 9, 423-432.

Murnaghan, S., Taylor, D., Jennings, E., Dalton, C., Olaya-Bosch, K. and O'Dwyer, B. (2012). Middle to late Holocene environmental changes in western Ireland inferred from fluctuations in preservation of biological variables in lake sediment. *Journal of Paleolimnology*, 48(2), 433-448.

Murray, J.W. (1971). *An atlas of British recent foraminids*. London: Heinemann Educational Books.

Murray, J.W. (1979). *British nearshore foraminiferids; key and notes for the identification of species*. Academic Press: London.

Murray, J.W. (1986). Living and dead Holocene foraminifera of Lyme Bay, southern England. *Journal of Foraminiferal Research*, 16, 347-352.

Murray, J. W. (1991). *Ecology and Palaeoecology of Benthic Foraminifera*. Taylor and Francis: London.

References

- Murray, J.W. (2000). Revised taxonomy: An atlas of British recent foraminiferids. *Journal of Micropalaentology*, 19, 44.
- Murray, J.W. (2003). An illustrated guide to the benthic foraminifera of the Hebridean Shelf, west of Scotland, with notes on their mode of life. *Palaeontologia Electronica* 5, 1-31.
- Murray, J. (2006). *Ecology and Applications of Benthic Foraminifera*. Cambridge University Press, UK: Cambridge.
- Murray, J.W. and Alve, E. (1999). Natural dissolution of shallow water benthic foraminifera: taphonomic effects on the palaeoecological record. *Palaeogeography, Palaeoclimatology, Palaeoecology*, 146, 195-209.
- Munoz-Castelblanco, J.A., Pereira, J-M., Delage, P. and Cui, Y-J. (2012). The influence of changes in water content on the electrical resistivity of a natural unsaturated loess. *ASTM Geotechnical Testing Journal*, 35(1), 11-17.
- Naeher, S., Geraga, M., Papatheodorou, G., Ferentinos, G., Kaberi, H., and Schubert, C.J. (2012). Environmental variations in a semi-enclosed embayment (Amvrakikos Gulf, Greece) – reconstructions based on benthic foraminifera abundance and lipid biomarker pattern. *Biogeosciences*, 9, 5081-5094.
- Nagy, J., Gradstein, F.M., Kaminski, M.A. and Holbourn, A.E. (1995). Foraminiferal morphogroups, palaeoenvironments and new taxa from Jurassic to Cretaceous strata of Thakkhola, Nepal. In: M.A Kaminski, S. Geroch and M.A. Gasinski (Eds.) *Proceedings of the Fourth International Workshop on Agglutinated Foraminifera* (pp. 181-209). Grzybowski Foundation Special Publication 3.
- Nagy, J., Kaminski, M.A., Johnsen, K. and Mitlehner, A.G. (1997). Foraminiferal, palynomorph, and diatom biostratigraphy and palaeoenvironments of the Torsk Formation: A reference section for the Palaeocene-Eocene transition in the western Barents Sea. In: H.C. Hass and M.A Kaminski (Eds.) *Contributions to the Micropalaentology and Palaeoceanography of the Northern North Atlantic* (pp. 15-38). Grzybowski Foundation Special Publication 5.
- Nees, S. (1997). High-resolution benthic foraminiferal records of the last glacial termination in the northern North Atlantic. In C. Hass and M. Kaminiski (Eds.), *Palaeoceanography and Micropalaentology of the Northern Atlantic*. Grzybowski Foundation, Special Publication No. 5, 167-197.
- Nesje, A., Bakke, J., Dahl, S.O., Lie, Ø. And Matthews, J.A. (2008). Norwegian mountain glacier in the past, present and future. *Global and Planetary Change*, 60, 10-27.

References

- Nooijer, L.J., Duijnste, I.A.P., Bergman, M.J.N. and van der Zwaan, G.J. (2008). The ecology of benthic foraminifera across the Frisian Front, southern North Sea. *Estuarine, Coastal and Shelf Science*, 78, 715-726.
- Novak, J.D. (2017). *Holocene paleoenvironmental reconstruction in Galway Bay, a shallow coastal embayment along Ireland's North-East Atlantic margin* (Unpublished Doctoral Dissertation) University of Limerick, Ireland.
- NPWS, 2013. National Parks and Wildlife. Galway Bay Complex SAC (site code: 0268) Conservation objectives supporting document. Dublin: Marine habitats and species Department of Arts, Heritage and the Gaeltacht.
- O'Brien, S.R., Mayewski, P.A., Meeker, L.D., Meese, D.A., Twickler, M.S. and Whitlow, S.J. (1995). Complexity of Holocene climate as reconstructed from a Greenland ice core. *Science*, 270, 1962-1964.
- O'Carra, B., Williams, D.M., Mercer, B. and Wood, B. (2014). Evidence of environmental change since the earliest medieval period from the inter-tidal zone of Galway Bay. *The Irish Naturalists' Journal*, 33(2), 83-88.
- O'Carroll, J.P.J., Kennedy, R., Ren, L., Nash, S., Hartnett, M. and Brown, C. (2017). A comparison of acoustic and observed sediment classifications as predictor variables for modelling biotope distributions in Galway Bay, Ireland. *Estuarine, Coastal and Shelf Science*, 197, 258-270.
- Ó Cofaigh, C. and Dowdeswell, J.A. (2001). Laminated sediments in glacial marine environments: diagnostic criteria for their interpretation. *Quaternary Science Reviews*, 20(13), 1411-1436.
- Ó Cofaigh, C., Dowdeswell, J.A., Allen, C.S., Hiemstra, J.F., Pudsey, C.J., Evans, J. and Evans, D.J.A. (2005). Flow dynamics and till genesis associated with a marine-based Antarctic palaeo-ice stream. *Quaternary Science Reviews*, 24(5-6), 709-740.
- Ó Cofaigh, C., Evans, J., Dowdeswell, J.A. and Larter, R.D. (2007). Till characteristics, genesis and transport beneath Antarctic palaeo-ice streams. *Journal of Geophysical Research*, 112(F3), 1-16.
- Ó Cofaigh, C., Dunlop, P. and Benetti, S. (2016) Submarine drumlins on the continental shelf offshore of NW Ireland. In: J.A. Dowdeswell, M. Canals, M. Jakobsson, B.J. Todd, E.K. Dowdeswell and K.A. Hogan (Eds.) *Atlas of Submarine Glacial Landforms: Modern, Quaternary and Ancient* (Memoirs, pp. 195-196), Geological Society Publishing House: Bath.

References

- Ó Cofaigh, C., Taylor, J., Dowdeswell, J.A., Rosell-Melé, A., Kenyon, N.H., Evans, J. and Mienert, J. (2002). Geological evidence for sediment reworking on high-latitude continental margins and its implications for palaeoceanography: insights from the Norwegian-Greenland Sea. In: J.A. Dowdeswell and C. Ó Cofaigh (Eds.) *Glacier influenced Sedimentation on High-latitude Continental Margins*, (Special Publication, 203, pp. 325-348). Geological Society: London.
- Ó Cofaigh, C., Telfer, M.W., Bailey, R.M. and Evans, D.J.A. (2012). Late Pleistocene chronostratigraphy and ice sheet limits, southern Ireland. *Quaternary Science Reviews*, 44, 160-179.
- Ó Cofaigh, C., Weilbach, K., Lloyd, J.M., Benetti, S., Callard, L., Purcell, C., Chiverrell, R.C., Dunlop, P., Saher, M., Livingstone, S.J., Van Landeghem, K.J.J., Moreton, S.G., Clark, C.D. and Fabel, D. (2019). Early deglaciation of the British-Irish Ice Sheet on the Atlantic shelf northwest of Ireland driven by glacioisostatic depression and high relative sea-level. *Quaternary Science Reviews*, 208, 76-96.
- O'Connell, M. and Molloy, K. (2001). Farming and woodland dynamics in Ireland during the Neolithic. *Biology and Environment, Proceedings of the Royal Irish Academy*, 101B(1-2), 99-128.
- O'Connell, M. and Molloy, K. (2017). Mid- and late-Holocene environmental change in western Ireland: New evidence from coastal peats and fossil timbers with particular reference to relative sea-level change. *The Holocene*, 27(12), 1825-1845.
- O'Connell, M., Ghilardi, B. and Morrison, L. (2014). A 7000-year record of environmental change, including early farming impact, based on lake-sediment geochemistry and pollen data from County Sligo, western Ireland. *Quaternary Research*, 81(1), 35-49.
- O'Connell, M., Huang, H.H. and Eicher, U. (1999). Multidisciplinary investigations, including stable isotope studies, of thick Late-glacial sediments from Tory Hill, Co. Limerick, western Ireland. *Palaeogeography, Palaeoclimatology, Palaeoecology*, 147, 169-208.
- O'Donncha, F., Hartnett, M., Nash, S., Ren, L. and Ragnoli, E. (2015) Characterizing observed circulation patterns within a bay using HF radar and numerical model simulations. *Journal of Marine Systems*, 142, 96-110.
- Olsen, J., Anderson, N.J. and Knudsen, M.F. (2012). Variability of the North Atlantic Oscillation over the past 5,200 years. *Nature Geoscience*, 5(11), 808-812.

References

- O'Rourke, F., Boyle, F. and Reynolds, A. (2010) Tidal current energy resource assessment in Ireland: Current status and future update. *Renewable and Sustainable Energy Reviews*, 14(9), 3206-3212.
- OPW (2012). Western CFRAM Units of Management 30 - Corrib and 31 - Owengowla Inception Report. Co. Meath: Office of Public Works.
- Osborn, T.J. and Briffa, K.R. (2006). The spatial extent of 20th century warmth in the context of the past 1200 years. *Science*, 311, 841-844.
- Overland, A. and O'Connell, M. (2008). Fine-spatial palaeological investigations towards reconstructing late Holocene environmental change, landscape evolution, and farming activity in Barrees, Beara Peninsula, southwestern Ireland. *Journal of the North Atlantic*, 1(1), 37-73.
- Parker, A.G., Goudie, A.S., Stokes, S. and Kennett, D. (2006). A record of Holocene climate change from lake geochemical analyses in southeastern Arabia. *Quaternary Research*, 66, 465-476.
- Parker, A.G., Goudie, A.S., Anderson, D.E., Robinson, M.A. and Bonsall, C. (2002). A review of the mid-Holocene elm decline in the British Isles. *Progress in physical Geography*, 26, 1-45.
- Peck, V.L., Hall, I.R., Zahn, R. and Scourse, J.D. (2007a). Progressive reduction in NE Atlantic intermediate water ventilation prior to Heinrich events: response to NW European ice sheet instabilities? *Geochemistry, Geophysics, Geosystems* 8(1), 1-11.
- Peck, V.L., Hall, I.R., Zahn, R., Grousset, F., Hemming, S.R. and Scourse, J.D. (2007b). The relationship of Heinrich events and their European precursors over the past 60 ka BP: a multi-proxy ice-rafted debris provenance study in the north east Atlantic. *Quaternary Science Reviews*, 26, 862-875.
- Pe'eri, S. and Philpot, W. (2007). Increasing the existence of very shallow-water LiDAR measurements using the red-channel waveforms. *IEEE Transactions on Geoscience and Remote Sensing*, 45(5), 1217-1223.
- Peltier, W.R. (2005). On the hemispheric origins of meltwater pulse 1a. *Quaternary Science Reviews*, 24(14-15), 1655-1671.
- Peltier, W.R. and Fairbanks, R.G. (2006). Global ice volume and last glacial maximum duration from an extended Barbados sea-level record. *Quaternary Science Reviews*, 25(23-24), 3322-3337.

References

- Peltier, W.R., Shennan, I., Drummond, R. and Horton, B.P. (2002). On the postglacial isostatic adjustment of the British Isles and the shallow viscoelastic structure of the Earth. *Geophysical Journal International*, 148(3), 443–475.
- Peters, J.L., Benetti, S., Dunlop, P. and Ó Cofaigh, C. (2015). Maximum extent and dynamic behaviour of the last British-Irish Ice Sheet west of Ireland. *Quaternary Science Reviews*, 128, 48-68.
- Peters, J.L., Benetti, S., Dunlop, P., Ó Cofaigh, C., Moreton, S.G., Wheeler, A.J. and Clark, C.D. (2016). Sedimentology and chronology of the advance and retreat of the last British-Irish Ice Sheet on the continental shelf west of Ireland. *Quaternary Science Reviews*, 140, 101-124.
- Philcox, M.E. and Lees, A. (2006). *The lower carboniferous rocks of GSI map sheets 11 & 14: a dossier of source materials for the Geological Survey of Ireland*. (doc version, 185 pp). Lodged with the Geological Survey of Ireland, Dublin.
- Pierre, G. and Lahousse, P. (2006). The role of groundwater in cliff instability: An example at Cape Blanc Nez; Pas-de-Calais, France. *Earth Surface Processes and Landforms*, 31, 31-45.
- Pilcher, J.R., Smith, A.G., Pearson, G.W. and Crowder, A. (1971). Land clearance in the Irish Neolithic: new evidence and interpretation. *Science*, 172, 506-562.
- Piva, A., Asioli, A., Schneider, R.R., Trincardi, F., Andersen, N., Colmenero-Hidalgo, E., Dennielou, B., Flores, J-A. and Vigliotti, L. (2008). Climatic cycles as expressed in sediments of the PROMESSI borehole PRAD1-2, central Adriatic, for the last 370 ka: 1. Intergrated Stratigraphy. *Geochemistry, Geophysics, Geosystems*, 9(1), 1-21.
- Plets, R.M., Callard, S.L., Cooper, J.A.G., Kelley, J.T., Belknap, D.F., Edwards, R.J., Long, D., Quinn, R.J. and Jackson, D.W. (2019). Late Quaternary sea-level change and evolution of Belfast Lough, Northern Ireland: new offshore evidence and implications for sea-level reconstruction. *Journal of Quaternary Science*, *In Press*.
- Plets, R.M., Callard, S.L., Cooper, J.A.G., Long, A.J., Quinn, R.J., Belknap, D.F., Edwards, R.J., Jackson, D.W., Kelley, J.T., Long, D. and Milne, G.A. (2015). Late Quaternary evolution and sealevel history of a glaciated marine embayment, Bantry Bay, SW Ireland. *Marine Geology*, 369, 251-272.
- Plunkett, G. (2009). Land-use patterns and cultural change in the middle to Late Bronze Age in Ireland: inferences from pollen records. *Vegetation History and Archaeobotany*, 18(4), 273-295.

References

Pollack, H.N., Huang, S. and Smerdeon, J.E. (2006). Five centuries of climate change in Australia: the view from underground. *Journal of Quaternary Science*, 21, 701-706.

Poppe, L.J., DiGiacomo-Cohen, M.L., Smith, S.M., Stewart, H.F. and Forfinski, N.A. (2006). Seafloor character and sedimentary processes in eastern Long Island Sound and western Block Island Sound. *Geo-Marine Letters*, 26, 59-68.

Postma, G. (1995), Sea-level-related architectural trends in coarse-grained delta complexes. *Sedimentary Geology*, 98(1-4), 3–13.

Pracht, M., Lees, A., Leake, B., Feely, M., Long, C.B., Morris, J. and McConnell, B.J. (2004). *Geology of Galway Bay: A geological description to accompany the bedrock geology, 1:100,000 scale map series, Sheet 14, Galway Bay*. Geological Survey of Ireland, Dublin.

Pracht, M., Somerville, I.D. and Wang, Y. (2015). A revised Mississippian lithostratigraphy of County Galway (western Ireland) with an analysis of carbonate lithofacies, biostratigraphy, depositional environments and palaeogeographic reconstructions utilising new borehole data. *Journal of Palaeogeography*, 4(1), 1-26.

Praeg, D., McCarron, S., Dove, D., Ó Cofaigh, C., Scott, G., Monteys, X., Facchin, L., Romeo, R. and Coxon, P. (2015). Ice sheet extension to the Celtic Sea shelf edge at the Last Glacial Maximum. *Quaternary Science Reviews*, 111, 107-112.

Preuss, H. (1979). Progress in computer evaluation of sea-level data within the IGCP Project, no. 61. In Proceedings of the 1978 International Symposium on coastal evolution in the Quaternary, pp. 104-134.

Principato, S. (2005). X-ray radiographs of sediment cores: A guide to analysing diamicton. In: P. Francus (Ed.) *Image analysis, sediments and palaeoenvironments* (pp. 165-185). Developments in palaeoenvironmental research, Vol. 7. Dordrecht: Springer.

Purcell, C. (2014). *Late Quaternary glaciation of the continental shelf offshore of Northwest Ireland* (Unpublished Masters' thesis). Durham University, England.

Rabatel, A., Francou, B., Soruco, A., Gomez, J., Cáceres, B., Ceballos, J.L., Basantes, R., Vuille, M., Sicart, J-E., Huggel, C., Scheel, M., Lejeune, Y., Arnaud, Y., Collet, M., Condom, T., Consoli, G., Favier, V., Jomelli, V., Galarraga, R., Ginot, P., Maisincho, L., Mendoza, J., Menegoz, M., Ramírez, E., Ribstein, P., Suarez, W., Villacis, M. and Wagnon, P. (2005). Current state of glaciers in the tropical Andes: a multi-century perspective on glacier evolution and climate change. *The Cryosphere*, 7, 81-102.

References

- Radić, V., Bliss, A., Beedlow, A.C., Hock, R., Miles, E. and Cogley, J.G. (2014). Regional and global projections of twenty-first century glacier mass changes in response to climate scenarios from global climate models. *Climate Dynamics*, 42(1-2), 37-58.
- Rasmussen, S.O., Andersen, K.K., Svensson, A.M., Steffensen, J.P., Vinther, B.M., Clausen, H.B., Siggaard, Andersen, M.L., Johnsen, S.J., Larsen, L.B., Dahl-Jensen, D. and Bigler, M. (2006). A new 199 Greenland ice core chronology for the last glacial termination. *Journal of Geophysical Research: Atmospheres*, 111(D6), 1-16.
- Rasmussen, S.O., Bigler, M., Blockley, S.P., Blunier, T., Buchardt, S.L., Clausen, H.B., Cvijanovic, I., Dahl-Jensen, D., Johnsen, S.J., Fischer, H., Gkinis, V., Guillevic, M., Hoek, W.Z., Lowe, J.J., Pedro, J.B., Popp, T., Seierstad, I.K., Steffensen, J.P., Svensson, A.M., Vallelonga, P., Vinther, B.M., Walker, M.J.C., Wheatley, J.J. and Winstrup, M. (2014). A stratigraphic framework for abrupt climatic changes during the last Glacial period based on three synchronized Greenland ice-core records: refining and extending the INTIMATE event stratigraphy. *Quaternary Science Reviews*, 106, 14-28.
- Rasmussen, S.O., Vinther, B.M., Clausen, H.B. and Andersen, K.K. (2007). Early Holocene climate oscillations recorded in three Greenland ice cores. *Quaternary Science Reviews*, 26, 1907-1914.
- Reimer, P J and Reimer, R W. (2001). A marine reservoir correction database and on-line interface. *Radiocarbon*, 43, 461-463. (supplemental material URL:<http://www.calib.org>).
- Reimer, P.J., Baillie, M.G., Bard, E., Bayliss, A., Beck, J.W., Blackwell, P.G., Bronk, R.C., Buck, C.E., Burr, G.S., Edwards, R.L. and Friedrich, M. (2009). IntCal09 and Marine09 radiocarbon age calibration curves, 0-50,000 years cal BP. *Radiocarbon*, 51(4), 1111-1150.
- Reimer, P. J., Bard, E., Bayliss, A., Beck, J. W., Blackwell, P. G., Bronk Ramsey, C., Grootes, P. M., Guilderson, T. P., Hafliðason, H., Hajdas, I., HattĹ, C., Heaton, T. J., Hoffmann, D. L., Hogg, A. G., Hughen, K. A., Kaiser, K. F., Kromer, B., Manning, S. W., Niu, M., Reimer, R. W., Richards, D. A., Scott, E. M., Southon, J. R., Staff, R. A., Turney, C. S. M., and van der Plicht, J. (2013). IntCal13 and Marine13 Radiocarbon Age Calibration Curves 0-50,000 Years cal BP. *Radiocarbon*, 55(4), 1869-1887.
- Reis, A.T., Maia, R.M.C., Silva, C.G., Rabineau, M., Guerra, J.V., Gorini, C., Ayres, A., Arantes-Oliveira, R., Benabdellouahed, M., Simões, I. and Tardin, R. (2013) Origin of step-like and lobate seafloor features along the continental shelf off Rio de Janeiro State, Santos basin-Brazil. *Quaternary Science Reviews*, 111, 107-112.
- Reise, K. (1985). *Tidal flat ecology*. Berlin: Springer.

References

Ren, L., Nash, S. and Hartnett, M. (2015). Observation and modelling of tide- and wind-induced surface currents in Galway Bay. *Water Science and Engineering*, 8(4), 345-352.

Renssen, H., Seppä, H., Crosta, X., Goosse, H. and Roche, D.M. (2012). Global characterisation of the Holocene Thermal Maximum. *Quaternary Science Reviews*, 48(10), 7-19.

Renssen, H., Seppä, H., Henri, O., Roche, D.M., Goosse, H. and Fichet, T. (2009). *Nature Geoscience Letters*, 2, 411-414.

Reolid, M., Rodriguez-Tovar, F.J., Nagy, J. and Olóriz, F. (2008). Benthic foraminiferal morphogroups of mid to outer shelf environments of the late Jurassic (Prebetic zone, southern Spain): Characterisation of biofacies and environmental significance. *Palaeogeography, Palaeoclimatology, Palaeoecology*, 261, 280-299.

Reyes, A.V. and Clague, J.J. (2004). Stratigraphic evidence for multiple Holocene advances of Lilloet Glacier, southern Coast Mountains, British Columbia. *Canadian Journal of Earth Sciences*, 41(8), 903-918.

Richter, T.O., Lassen, S., van Weering, T.C.E. and de Haas, H. (2001). Magnetic susceptibility patterns and provenance of ice-rafted material at Feni Drift, Rockall Trough: implications for the history of the British-Irish ice sheet. *Marine Geology*, 173(1-4), 37-54.

Richter, T.O., Van der Gaast, S., Koster, B., Vaars, A., Gieles, R., de Stigter, H.C., de Haas, H. and van Weering, T.C.E. (2006). The Avaatech XRF core scanner: technical description and application to NE Atlantic sediments. In: R.G. Rothwell (Ed.) *New techniques in sediment core analysis* (pp. 39-50) Geological Society, Special Publication 267.

Rignot, E., Velicogna, I., Van Den Broeke, M.R., Monaghan, A. and Lenaerts, J. (2011). Acceleration of the contribution of the Greenland and Antarctic ice sheets to sea level rise. *Geophysical Research Letters*, 38(5), 1-5.

Roberts, D.H., Evans, D.J.A., Callard, S.L., Clark, C.D., Bateman, M.D., Medialdea, A., Dove, D., Cotterill, C.J., Saher, M., Ó Cofaigh, C., Chiverrell, R.C., Moreton, S.G., Fabel, D. and Bradwell, T. (2018). Ice marginal dynamics of the last British-Irish ice sheet in the southern North Sea: Ice limits, timing and the influence of the Dogger Bank. *Quaternary Science Reviews*, 198, 181-207.

Roberts, N., Eastwood, W.J., Kuzucuoğlu, C., Fiorentino, G. and Caracuta, V. (2011). Climatic, vegetation and cultural change in the eastern Mediterranean during the mid-Holocene environmental transition. *The Holocene*, 21, 147-162.

References

- Roe, H.M. and Swindles, G.T. (2008). Holocene sea-level history and coastal evolution of Glenariff. In: N.J. Whitehouse, H.M. Roe, S. McCarron and J. Knight (Eds.). *North of Ireland: field guide* (pp. 106-116). London: Quaternary Research Association.
- Rogers, J.N., Kelley, J.T., Belknap, D.F., Gontz, A. and Barnhardt, W.A. (2006). Shallow-water pockmark formation in temperate estuaries: A consideration of origins in the western Gulf of Maine with special focus on Belfast Bay. *Marine Geology*, 225(1), 45-62.
- Rohling, E.J. and Pälike, H. (2005). Centennial-scale climate cooling with a sudden cold event around 8,200 years ago. *Nature*, 434, 975-979.
- Roland, T.P., Caseldine, C.J., Charman, D., Turney, C.S.M., Amesbury, M.J. (2014). Was there a “4.2 ka event” in Great Britain and Ireland? Evidence from the peatland record. *Quaternary Science Reviews*, 83, 11-27.
- Roland, T.P., Daley, T.J., Caseldine, C.J., Charman, D.J., Turney, C.S.M., Amesbury, M.J., Thompson, G.J. and Woodley, E.J. (2015). The 5.2 ka climate event: Evidence from stable isotope and multi-proxy palaeoecological peatland records in Ireland. *Quaternary Science Reviews*, 124, 209-223.
- Rollinson, H.R. (1993). *Using Geochemical Data: Evaluation, Presentation, Interpretation*. Harlow: Longman.
- Romero, O.E., Kim, J-H. and Donner, B. (2008). Submillennial- to- millennial variability of diatom production off Mauritania, NW Africa, during the last glacial cycle. *Palaeoceanography*, 23(3), 1-17.
- Rothwell, R. G. and Croudace, I.W. (2015). *Micro-XRF studies of sediment cores: A perspective on capability and application in the environmental sciences*. Springer: Dordrecht.
- Rothwell, R. G. and Rack, F.R. (2006). New techniques in sediment core analysis: an introduction. In: R.G Rothwell (Ed.) *New techniques in sediment core analysis*. Special publication, Vol. 267. (pp. 1-29). London: Geological Society.
- Rothwell, R.G., Hoogakker, B., Thomson, J., Croudace, I.W. and Frenz, M. (2006). Turbidite emplacement on the southern Balearic Abyssal Plain (western Mediterranean Sea) during Marine Isotope Stages 1–3: an application of ITRAX XRF scanning of sediment cores to lithostratigraphic analysis. *Geological Society, London, Special Publications*, 267(1), 79-98.

References

- Rousseau, D.D., Preece, R. and Limondin-Lozouet, N. (1998). British late glacial and Holocene climatic history reconstructed from land snail assemblages. *Geology*, 26, 651-654.
- Richter, T.O., Lassen, S., van Weering, T.C.E. and de Haas, H. (2001). Magnetic susceptibility patterns and provenance of ice-rafted material at Feni Drift, Rockall Trough: implications for the history of the British-Irish ice sheet. *Marine Geology*, 173, 37-54.
- Richter, T.O. Peeters, F.J.C. and van Weering, T.C.E. (2009). Late Holocene (0-2.4 ka BP) surface water temperature and salinity variability, Feni Drift, NE Atlantic Ocean. *Quaternary Science Reviews*, 28, 1941-1955.
- Rubin, D.M. and McCulloch, D.S. (1980). Single and superimposed bedforms: a synthesis of San Francisco Bay and flume observations. *Sedimentary Geology*, 26, 207–231.
- Russell, R.J. (1958). Long straight beaches. *Eclogae Geologicae Helvetiae*, 51, 591-598.
- Rusu, E., Gonçalves, M. and Guedes Soares, C. (2011). Evaluation of the wave transformation in an open bay. *Ocean Engineering*, 38(16), 1763-1781.
- Sacchetti, F., Benetti, S., Quinn, R. and Ó Cofaigh, C. (2012). Glacial and post-glacial processes in the Irish Rockall trough from an integrated acoustic analysis of near-seabed sediments. *Geo-Marine Letters*, 33(1), 49-66.
- Sandweiss, D.W., Maasch, K.A., Burger, R.L., Richardson III, J.B., Rollins, H.B. and Clement, A. (2001). Variation in Holocene El Niño frequencies: Climate records and cultural consequences in ancient Peru. *Geology*, 29(7), 603-606.
- Saraswat, R., Lea, D.W., Nigam, R., Mackensen, A. and Naik, D.K. (2013). Deglaciation in the tropical Indian Ocean driven by interplay between the regional monsoon and global teleconnections. *Earth and Planetary Science Letters*, 375(1), 166-175.
- Satriani, A., Loperte, A., Imbrenda, V. and Lapenna, V. (2012). Geoelectrical surveys for characterisation of the coastal saltwater intrusion in Metapontum Forest Reserve (Southern Italy). *International Journal of Geophysics*, 202, 1-8.
- Scheffers, A., Kelletat, D., Haslett, S., Scheffers, S. and Browne, T. (2010) Coastal boulder deposits in Galway Bay and the Aran Islands, western Ireland. *Zeitschrift für Geomorphologie, Supplementary Issue*, 54, 247–279.

References

Schettler, G., Romer, R.L., O'Connell, M. and Molloy, K. (2006). Holocene climatic variations and postglacial sea-level rise geochemically recorded in the sediments of the brackish karst lake An Loch Mór, western Ireland. *Boreas*, 35(4), 674-693.

Schiele, C.K. (2017). *Timing, forcing and onshore-offshore correlations on the western margin of the British-Irish Ice Sheet* (Unpublished Doctoral Dissertation). Ulster University. Coleraine.

Schultheiss, P.J. and McPhail, S.D. (1989). An automated p-wave logger (PWL) for recording fine scale compressional wave velocity structures in sediments. In: W. Ruddiman and M. Sarntein (Eds.) *Proceedings of the ocean drilling program, scientific results, Vol. 108* (407-413).

Schwark, L., Zink, K. and Lechterbeck, J. (2002). Reconstruction of postglacial to early Holocene vegetation history in terrestrial Central Europe via cuticular lipid biomarkers and pollen records from lake sediments. *Geology*, 30, 463-466.

Scott, D.B., Medioli, F.S. and Schafer, C.T. (2001). *Monitoring in coastal environments using foraminifera and thecamoebian indicators*. Cambridge: Cambridge University Press.

Scourse, J.D. (2013). Quaternary sea-level and palaeotidal changes: a review of impacts on, and responses of, the marine biosphere. *Oceanography and Marine Biology: An Annual Review*, 51, 1-70.

Scourse, J.D., Austin, W.E.N., Bateman, R.M., Catt, J.A., Evans, C.D.R., Robinson, J.E. and Young, J.R. (1990). Sedimentology and micropalaeontology of glacial marine sediments from the central and southwestern Celtic Sea. *Geological Society, London, Special Publications*, 53(1), 329-347.

Scourse, J.D., Haapaniemi, A.I., Colmenero-Hidalgo, E., Peck, V.L., Hall, I.R., Austin, W.E.N., Knutz, P.C. and Zahn, R. (2009). Growth, dynamics, and deglaciation of the last British-Irish Ice Sheet: the deep-sea ice-rafted detritus record. *Quaternary Science Reviews*, 28, 3066-3084.

Scourse, J.D., Ward, S.L., Wainwright, A., Bradley, S.L. and Uehara, K. (2018). The role of megatides and relative sea level in controlling the deglaciation of the British Irish and Fennoscandian ice sheets. *Journal of Quaternary Science*, 33(2), 139-149.

Sejrup, H.P., Birks, H.J.B., Klitgaard Kristensen, D. and Madsen, H. (2004). Benthonic foraminiferal distributions and quantitative transfer functions for the northwest European continental margin. *Marine Micropaleontology*, 53(1-2), 197-226.

References

- Sejrup, H., Birks, H., Klitgaard-Kristensen, D. and Madsen, H. (2004). Benthonic foraminiferal distributions and quantitative transfer functions for the northwest European continental margin. *Marine Micropalaeontology*, 53, 197-226.
- Sejrup, H.P., Hjelstuen, B.O., Dahlgren, K.T., Hafliðason, H., Kuijpers, A., Nygård, A., Praeg, D., Stoker, M.S. and Vorren, T.O. (2005). Pleistocene glacial history of the NW European continental margin. *Marine and Petroleum Geology*, 22(9), 1111-1129.
- Selby, D., Creaser, R.A. and Feely, M. (2004). Accurate and precise Re-Os molybdenite dates from the Galway Granite, Ireland. Critical comment on "Disturbance of the Re-Os chronometer of molybdenites from the late-Caledonian Galway Granite, Ireland, by hydrothermal fluid circulation" by Suzuki et al., *Geochemical Journal*, 35, 29-35, 2001. *Geochemical Journal*, 38, 291-294.
- Selley, R.C. (2000). *Applied Sedimentology*. Academic Press: London.
- Semenov, M.A. and Stratonovitch, P. (2010). Use of multi-model ensembles from global climate models for assessment of climate change impacts. *Climate Research*, 41, 1-14.
- Setiawan, R., Wirasatriya, A., Shaari, H. Eko, S. and Rachman, F. (2017). Assessing the reliability of planktonic foraminifera Ba/Ca as a proxy for salinity off the Sunda Strait. *Indonesian Journal of Marine Science*, 22(4), 201-212.
- Setoyama, E., Kaminski, M.A. and Tyszka, J. (2011). The Late Cretaceous-Early Palaeocene palaeobathymetric trends in the southwestern Barents Sea- Palaeoenvironmental implications of benthic foraminiferal assemblage analysis. *Palaeogeography, Palaeoclimatology, Palaeoecology*, 307(1-4), 44-58.
- Shala, S., Helmens, K.F. Jansson, K.N., Kylander, M.E., Risberg, J. and Löwemark, L. (2014). Palaeoenvironmental record of glacial lake evolution during the early Holocene at Sokli, NE Finland. *Boreas*, 43, 362-376.
- Shao, X., Wang, Y., Cheng, H., Kong, X., Wu, J. and Edwards, R.L. (2006). Long-term trend and abrupt events of the Holocene Asian monsoon inferred from a stalagmite $\delta^{10}\text{O}$ record from Shennongjia in Central China. *Chinese Science Bulletin*, 51(2), 221-228.
- Shepmetkin, A.F. and McWilliams, J.C. (2005). The regional oceanic modelling system (ROMS): a split-explicit, free-surface, topography-following-coordinate oceanic model. *Ocean Modelling*, 9, 347-404.
- Shennan, I. (1982). Interpretation of Flandrian sea-level data from the Fenland, England. *Proceedings of the Geological Association*, 93, 53-63.

References

- Shennan, I., Bradley, S. and Edwards, R. (2018). Relative sea-level changes and crustal movements in Britain and Ireland since the Last Glacial Maximum. *Quaternary Science Reviews*, 188, 143–159.
- Shennan, I., Bradley, S., Milne, G., Brooks, A., Bassett, S. and Hamilton, S. (2006). Relative sea-level changes, glacial isostatic modelling and ice-sheet reconstructions from the British Isles since the Last Glacial Maximum. *Journal of Quaternary Science*, 21, 585-599.
- Shennan, S., Downey, S.S., Timpson, A., Edinborough, K., Colledge, S., Kerig, T.m Manning, K. and Thomas, M.G. (2013). Regional population collapse followed initial agriculture booms in mid-Holocene Europe. *Nature Communications*, 4(2486), 1-8.
- Shennan, I., Long, A. J. and Horton, B. P. (2015) *Handbook of Sea-Level Research*. Wiley Blackwell: Hoboken.
- Shillington, D.J., Minshull, T.A., Peirce, C. and O’Sullivan, J.M. (2007). P- and S-wave velocities of consolidated sediments from a seafloor seismic survey in the North Celtic Sea Basin, offshore Ireland. *Geophysical Prospecting*, 56, 197-211.
- Simms, M.J. (2005). Glacial and karst landscapes of the Gort lowlands and Burren. In: P. Coxon (Ed.) *The Quaternary of central western Ireland: Field Guide* (pp. 39-63). Quaternary Research Association, London.
- Sirocko, F., Sarnthein, M., Erienkeuser, H., Lange, H., Arnold, M. and Duplessy, J.C. (1993). Century-scale events in monsoonal climate over the past 24,000 years. *Nature*, 364, 322-324.
- Skog, G. and Regnell, J. (1995). Precision calendar-year dating of the elm decline in sphagnum-peat bog in southern Sweden. *Radiocarbon*, 37(2), 197-202.
- Slither, W.V. (1965). Laboratory experiments on the life cycle and ecological controls on *Rosalina globularis*, d’Orbigny. *Journal of Eukaryotic Microbiology*, 12, 210-215.
- Sluijs, A., Bijl, P.K., Schouten, S., Röhl, U., Reichart, G.J., Brinkhuis, H. and Röhl, U. (2011). Southern Ocean warming, sea level and hydrological change during the Paleocene-Eocene thermal maximum. *Climate of the Past*, 7, 47-61.
- Sluijs, A., Bijl, P.K., Schouten, S., Donders, T.H., Schoon, P.L., Röhl, U., Reichart, G.J., Sangiorgi, F., Kim, J-H., Sinninghe Damsté, J.S. and Brinkhuis, H. (2009). Warm and wet conditions in the Arctic region during Eocene Thermal Maximum 2. *Nature Geoscience*, 2, 777-780.

References

Small, D., Benetti, S., Dove, D., Ballantyne, C.K., Fabel, D., Clark, C.D., Gheorghiu, D.M., Newell, J. and Xu, S. (2017). Cosmogenic exposure age constraints on deglaciation and flow behaviour of a marine-based ice stream in western Scotland, 21-16 ka. *Quaternary Science Reviews*, 167, 30-46.

Smith, A.G. (1981). The Neolithic. In I.G. Simmons and M.J. Tooley (Eds.) *The Environment in British Prehistory* (pp. 125-209). London: Duckworth.

Smith, A.G. and Goddard, J.C. (1991). A 12,500 year record of vegetational history at Sluggan Bog, Co. Antrim, N. Ireland (incorporating a pollen zone scheme for the non-specialist). *New Phytologist*, 118, 167-187.

Smith, A.M. and Cave, R.R. (2012). Influence of fresh water, nutrients and DOC in two submarine-groundwater-fed estuaries on the west of Ireland. *Science of the Total Environment*, 438, 260–270.

Smith, D., Harrison, S., Firth, C.R. and Jordan, J.T. (2011). The early Holocene sea level rise. *Quaternary Science Reviews*, 30(15), 1846-1860.

Smith, M.J., and Clark, C.D. (2005). Methods for the visualization of digital elevation models for landform mapping. *Earth Surface Processes and Landforms*, 30, 885–900.

Solomina, O.N., Bradley, R.S., Hodgson, D.A., Ivy-Ochs, S., Jomelli, V., Mackintosh, A.N., Nesje, A., Owen, L.A., Wanner, H., Wiles, G.C. and Young, N.E. (2015). Holocene glacier fluctuations. *Quaternary Science Reviews*, 111, 9-34.

Sorrel, P., Debret, M., Billeaud, I., Jaccard, S.L., McManus, J.F. and Tessier, B. (2012). Persistent non-solar forcing of Holocene storm dynamics in coastal sedimentary archives. *Nature Geoscience*, 5, 892-896.

Soulet, G., Ménot, g., Garreta, V., Rostek, F., Zaragosi, S., Lericolais, G. and Bard, E. (2011). Black Sea “lake” reservoir age evolution since the Last Glacial- Hydrologic and climatic implications. *Earth and Planetary Science Letters*, 308, 245-258.

Speranza, A., van Geel, B. and van der Plicht, J. (2002). Evidence for solar forcing of climate change at ca. 850 cal BC from a Czech peat sequence. *Global and Planetary Change*, 35, 51-65.

Sperazza, M., Moore, J.N. and Hendrix, M.C. (2004). High-resolution particle size analysis of naturally occurring very fine-grained sediment through laser diffractometry. *Journal of Sedimentary Research*, 74(5), 736-743.

References

- Spötl, C., Nicolussi, K., Patzelt, G., Boch, R. and Daphne team. (2010). Humid climate during deposition of sapropel 1 in the Mediterranean Sea: Assessing the influence of the Alps. *Global Planetary Change*, 71, 242-248.
- Spurk, M., Leuschner, H.H., Baillie, M.G.L., Briffa, K.R. and Friedrich, M. (2002). Depositional frequency of German subfossil oaks: Climatically and non-climatically induced fluctuations in the Holocene. *The Holocene*, 12, 707-715.
- Stahle, D.W. and Cleaveland, M.K. (1994). Tree-ring reconstructed rainfall over the southeastern U.S.A. during the medieval warm period and little ice age. *Climatic Change*, 26(2-3), 199-212.
- Stanford, J.D., Rohling, E.J., Hunter, S.E., Robersts, A., Rasmussen, S.O., Bard, E., McManus, J. and Fairbanks, R.G. (2006). Timing of meltwater pulse 1a and climate responses to meltwater injections. *Palaeoceanography and Palaeoclimatology*, 21(4), 1-9.
- Stanley, J.D., Krom, M.D., Cliff, R.A. and Woodward, J. (2003). Short contribution: Nile failure at the end of the Old Kingdom, Egypt: Strontium isotopic and petrologic evidence. *Geoarchaeology*, 18(3), 395-402
- Stastney, P., Young, D.S. and Branch, N.P. (2018). The identification of late-Holocene bog bursts at Littleton Bog, Ireland: Ecohydrological changes display complex climatic and non-climatic drivers. *The Holocene*, 28(4), 570-582.
- Staubwasser, M. and Weiss, H. (2006). Holocene climate and cultural evolution in late prehistoric-early historic West Asia. *Quaternary Research*, 66(3), 372-387.
- Staubwasser, M., Sirocko, F., Grootes, P.M. and Segl, M. (2003). Climate change at the 4.2 ka BP termination of the Indus valley civilisation and Holocene south Asian monsoon variability. *Geophysical Research Letters*, 30(8), 1425-1429.
- Steinilber, F., Abreu, J.A., Beer, J., Brunner, I., Christl, M., Fischer, H., Heikkilä, U., Kubik, P.W., Mann, M., McCracken, K.G., Miller, H., Miyahara, H., Oerter, H. and Wilhelms, F. (2012). 9400 years of cosmic radiation and solar activity from ice cores and tree rings, *Proceedings of the National Academy of Science, U.S.A.*, 109(16), 5967–5971.
- Steinilber, F., Beer, J. and Fröhlich, C. (2009). Total solar irradiance during the Holocene. *Geophysical Research Letters*, 36(19), 1-5.
- Stephens, N. (1957). Some observations on the “Interglacial” platform and the early post-glacial raised beach on the east coast of Ireland. *Proceedings of the Royal Irish Academy (Section B)*, 58, 129-149.

References

- Stephens, N. and Synge, F.M. (1965). Late-pleistocene shorelines and drift limits in north Donegal. *Proceedings of the Royal Irish Academy (Section B)*, 64, 131-153.
- Stivrins, N., Liiv, M., Heinsalu, A., Galka, M. and Veski, S. (2017). The final meltdown of dead-ice at the Holocene Thermal Maximum (8500-7400 cal. yr BP) in western Latvia, eastern Baltic. *The Holocene*, 27(8), 1146-1157.
- Stoker, M.S. and Bradwell, T. (2005). The Minch palaeo-ice stream, NW sector of the British-Irish ice sheet. *Journal of the Geological Society, London*, 162, 425-428.
- Stokes, C.R. and Clark, C.D. (2001). Palaeo-ice streams. *Quaternary Science Reviews*, 20, 1437-1457.
- Stolze, S., Dörfler, W., Monecke, T. and Nelle, O. (2012). Evidence for climatic variability and its impact on human development during the Neolithic from Loughmeenaghan, County Sligo, Ireland. *Journal of Quaternary Science*, 27(4), 393-403.
- Stolze, S., Muscheler, R., Dörfler, W. and Nelle, O. (2013). Solar influence on climate variability and human development during the Neolithic: evidence from a high-resolution multi-proxy record from Templevanny Lough, County Sligo, Ireland. *Quaternary Science Reviews*, 67, 138-159.
- Stow, D. A. V., Hernandez-Molina, F. J., Llave, E., Sayago-Gil, M., Diaz del Rio, V. and Branson, A. (2009). Bedform-velocity matrix: The estimation of bottom current velocity from bedform observations. *Geology*, 37, 327-330.
- Street-Perrott, R.A. and Perrott, R.A. (1990). Abrupt climate fluctuations in the tropics-The influence of the Atlantic-ocean circulation. *Nature*, 343, 607-612.
- Stuiver, M., Reimer, P.J., Bard, E., Burr, G.S., Hughen, K.A., Kromer, B., McCormac, G., van der Plicht, J. and Spurk, M. (1998) INTCAL98 radiocarbon age calibration, 24,000-0 cal BP. *Radiocarbon*, 40(3), 1041-1083.
- Stuut, J-B.W., Temmesfeld, F. and De Deckker, P. (2014). A 550 ka record of aeolian activity near North West Cape, Australia: inferences from grain-size distributions and bulk chemistry of SE Indian Ocean deep-sea sediments. *Quaternary Science Reviews*, 83, 83-94.
- Sumida, P.Y.G., Yoshinaga, M.Y., Madureira, L.A.S-P. and Hovland, M. (2004). Seabed pockmarks associated with deepwater corals off SE Brazilian continental slope, Santos Basin. *Marine Geology*, 207(1), 159-167.
- Sunamura, T. (1992). *Geomorphology of Rocky Coasts*. John Wiley & Sons: Chichester.

References

Svendsen, J.I., Alexanderson, H., Astakhov, V.I., Demidov, I., Dowdeswell, J.A., Funder, S., Gataullin, V., Henriksen, M., Hjort, C., Houmark-Nielsen, M., Hubberten, H.W., Ingólfsson, Ó., Jakobsson, M., Kjær, K.H., Larsen, E., Lokrantz, H., Lunkka, J.P., Lyså, A., Mangerud, A., Matiouchkov, A., Murray, A., Möller, P., Niessen, F., Nikolskaya, O., Polyak, L., Saarnisto, M., Siegert, C., Siegert, M.J., Spielhagen, R.F. and Stein, R. (2004). Late Quaternary ice sheet history of northern Eurasia. *Quaternary Science Reviews*, 23(11-13), 1229-1271.

Swift, D.J.P. (1976). Continental shelf sedimentation. In: D.J. Stanley and D.J.P. Swift (Eds.) *Marine sediment transport and environmental management* (pp. 311-350). New York: Wiley.

Swindles, G. T., Blundell, A., Roe, H. M. and Hall, V. A. (2010). A 4500-year proxy climate record from peatlands in the North of Ireland: the identification of widespread summer “drought phases”? *Quaternary Science Review*, 29, 1577–1589.

Swindles, G.T., Lawson, I.T., Matthews, I.P., Blaauw, M., Daley, T.J., Charman, D.J., Roland, T.P., Plunkett, G., Schettler, G., Gearey, B.R., Turner, T.E., Rea, H.A., Roe, H.M., Amesbury, M.J., Chambers, F.M., Holmes, J., Nitchell, F.J.G., Blackford, J., Blundell, A., Branch, N., Holmes, J., Langdon, P., McCarroll, J., McDermott, F., Oksanen, P.O., Pritchard, O., Stastney, P., Stefanini, B., Young, D., Wheeler, J., Becker, K. and Armit, I. (2013). Centennial-scale climate change in Ireland during the Holocene. *Earth Science Reviews*, 126, 300-320.

Swindles, G.T., Plunkett, G. and Roe, H.M. (2007). A delayed climatic response to solar forcing at 2800 cal BP: multi-proxy evidence from three Irish peatlands. *The Holocene*, 17, 177-182.

Switzer, A.D. and Pile, J. (2015). Grain size Analysis. In: I. Shennan, A.J. Long and P. Horton (Eds.) *Handbook of Sea-Level Research*. New Jersey: John Wiley & Sons Ltd.

Synge, F.M. (1977). The coasts of Leinster. In: C. Kidson and M.J. Tooley (Eds.) *The Quaternary History of the Irish Sea* (pp. 179-198). Liverpool: Seal House Press.

Synge, F.M. and Stephens, N. (1960). The quaternary period in Ireland-an assessment, 1960. *Journal of Irish Geography*, 4(2), 121-130.

Szpak, M.T., Monteys, X., O'Reilly, S.S., Lilley, M.K.S., Scott, G.A., Hart, K.M., McCarron, S.G. and Kelleher, B.P. (2015). Occurrence, characteristics and formation mechanisms of methane generated micro-pockmarks in Dunmanus Bay, Ireland. *Continental Shelf Research*, 103, 45-59.

Szpak, M.T., Monteys, X., O'Reilly, S., Simpson, A.J., Garcia, X., Evans, R.L., Allen, C.C.R., McNally, D.J., Courtier-Murias, D. and Kelleher, B.P. (2012). Geophysical and

References

- geochemical survey of a large marine pockmark on the Malin Shelf, Ireland. *Geochemistry, Geophysics, Geosystems*, 13(1), 1-18.
- Taylor, K.J., McGinley, S., Potito, A.P., Molloy, K. and Beilman, D.W. (2018). A mid to late Holocene chironomid-inferred temperature record from northwest Ireland. *Palaeogeography, Palaeoclimatology, Palaeoecology*, 505, 274-286.
- Taylor, R.E. (1987). *Radiocarbon dating- An Archaeological Perspective*. San Diego, C.A: Academic Press.
- Teller, J.T., Leverington, D.W. and Mann, J.D. (2002). Freshwater outbursts to the oceans from glacial lake Agassiz and their role in climate change during the last deglaciation.
- Terwindt, J.H.J. (1971). Sand waves in the southern bight of the North Sea. *Marine Geology*, 10(1), 51-67.
- The Open University. (1999). *Waves, Tides and Shallow Water Processes*. Oxford: Butterworth-Heinemann.
- Theuerkauf, M. and Joosten, H. (2012). Younger Dryas cold stage vegetation patterns of central Europe—climate, soil and relief controls. *Boreas*, 41, 391–407.
- Thomas, E.R., Wolff, E.W., Mulvaney, R., Steffensen, J.P., Johnsen, S.J., Arrowsmith, C., White, J.W.C., Vaughan, B. and Popp, T. (2007). The 8.2 ka event from Greenland ice cores. *Quaternary Science Reviews*, 26, 70-81.
- Thomas, G.S.P. and Chiverrell, R.C. (2006). A model of subaqueous sedimentation at the margin of the late Midlandian Irish Ice Sheet, Connemara, Ireland and its implications for regionally high isostatic sea-levels. *Quaternary Science Reviews*, 25, 2868-2893.
- Thompson, L.G., Mosley-Thompson, E., Dansgaard, W. and Gootes, P.M. (1986). The Little Ice Age as recorded in the stratigraphy of the tropical Quelccya Ice Cap. *Science*, 234, 361-364.
- Thompson, J., Croudace, I.W. and Rothwell, R.G. (2006). A geotechnical application of the ITRAX scanner to a sediment core containing eastern Mediterranean sapropel units. In: R.G. Rothwell (Ed.) *New techniques in sediment core analysis* (pp. 65-77). Geological Society Special Publication, 267.
- Thompson, L.G., Mosley-Thompson, E., Davis, M.E., Henderson, K.A., Brecher, H.H., Zagorodnov, V.S., Mashiotta, T.A., Lin, P-N., Mikhalenko, V.N., Hardy, D.R. and Beer, J.

References

- (2002). Kilimanjaro ice core records: Evidence of Holocene climate change in tropical Africa. *Science*, 298(5593), 589-593.
- Thomson, J., Croudace, I.W. and Rothwell, R.G. (2006). A geochemical application of the ITRAX scanner to a sediment core containing eastern Mediterranean sapropel units. *Geological Society, London, Special Publications*, 267(1), 65-77.
- Tibert, N.E., Patterson, W.P., Diefendorf, A.F., Martini, A. and Stanton, C. (2007). Holocene temperature variability in western Ireland: Evidence from limnic ostracode assemblages and stable isotope values. *Stratigraphy*, 4(4), 353-361.
- Tjallingii, R., Röhl, U., Kölling, M. and Bickert, T. (2007). Influence of the water content on X-ray fluorescence core-scanning measurements in soft marine sediments. *Geochemistry, Geophysics, Geosystems*, 8(2), 1-12.
- Todorova, V., Micu, D. and Klissurov, L. (2009). Unique oyster reefs discovered in the Bulgarian Black Sea. *Comptes rendus de l'Académie bulgare des sciences: sciences mathématiques et naturelles*, 62(7), 871-874.
- Tooley, M.J. (1978). *Sea-level changes, north-west England during the Flandrian stage*. Oxford: Clarendon Press.
- Törnqvist, T.E. and Hijma, M.P. (2012). Links between early Holocene ice-sheet decay, sea-level rise and abrupt climate change. *Nature Geoscience*, 5, 601-606.
- Tripanas, E.K. and Piper, D.J.W. (2008). Late Quaternary stratigraphy and sedimentology of Orphan Basin: implications for meltwater dispersal in the southern Labrador Sea. *Palaeogeography, Palaeoclimatology, Palaeoecology*, 260, 521-539.
- Tully, O. and Clarke, S. (2012) "The Status and Management of Oyster (*Ostrea edulis*) in Ireland", Irish Fisheries Investigations, No. 24, Marine Institute
- Turner, J.N., Holmes, N., Davis, S.R., Leng, M.J., Langdon, C. and Scaife, R.G. (2015). A multiproxy (micro-XRF, pollen, chironomid and stable isotope) lake sediment record for the Late Glacial to Holocene transition from Thomastown Bog, Ireland. *Journal Quaternary Science*, 30(6), 514-528.
- Turney, C.S.M., Baillie, M., Palmer, J. and Brown, D. (2006). Holocene climatic change and past Irish societal response. *Journal of Archaeological Science*, 33, 34-38.
- Udden, J.A. (1914). Mechanical composition of clastic sediments. *Geological Survey of America Bulletin*, 25, 655-744.
- Ussler, W., Paull, C.K., Boucher, J., Friederich, G.E. and Thomas, D.J. (2003). Submarine pockmarks: a case study from Belfast Bay, Maine. *Marine Geology*, 202, 3, 175-192.

References

Vail, P. R., Mitchum, R. M., & Thomson, S. III. (1977). Seismic Stratigraphy-Applications to Hydrocarbon Exploration. AAPG Special Volumes. Chap. Seismic Stratigraphy and Global Changes of Sea Level, Part 3: Relative Changes of Sea Level from Coastal Onlap: Section 2. Application of Seismic Reection Configuration to Stratigrapic Interpretation, pages 63-81.

Väliranta, M., Kaakinen, A. and Kuhry, P. (2003). Holocene climate and landscape evolution in the Ortino region, East-European Russian Arctic. *Journal of Quaternary Research*, 59, 335–344.

Van Asch, N., Lutz, A.F., Duijkers, M.C.H., Heiri, O., Brooks, S.J. and Hoek, W.Z. (2012). Rapid climate change during the Weichselian Lateglacial in Ireland: Chironomid-infered summer temperatures from Fiddaun, Co. Galway. *Palaeogeography, Palaeoclimatology, Palaeoecology*, 315-316, 1-11.

Van de Plassche, O. (1986). *Sea-level research: a manual for the collection and evaluation of data*. Norwich: Geo Books.

Van der Plicht, J., Van Geel, B., Bohncke, S.J.P., Bos, J.A.A., Blaauw, M., Speranza, A.O.M., Muscheler, R. and Björck, S. (2004). The Preboreal climate reversal and a subsequent solar-forced climate shift. *Journal of Quaternary Science*, 19(3), 263-269.

Van Geel, B. (1978). A palaeoecological study of Holocene peat bog sections in Germany and The Netherlands. *Review of Palaeobotany and Palynology*, 25, 1-120.

Van Geel, B., Buurman, J. and Waterbolk, H.T. (1996). Archaeological and palaeoecological indications of an abrupt climate change in The Netherlands, and evidence for climatological teleconnections around 2650 BP. *Journal of Quaternary Science*, 11, 451-460.

Van Geel, B., Heusser, C.J., Renssen, H. and Schuurmans, C.J.E. (2000). Climatic change in Chile at around 2700 BP and global evidence for solar forcing: a hypothesis. *The Holocene*, 10, 659-664.

Van Hengstum, P.J. and Scott, D.B. (2011). Ecology of foraminifera and habitat variability in an underwater cave: distinguishing anchialine versus submarine cave environments. *Journal of Foraminiferal Research*, 41(3), 201-229.

Van Landeghem, K. J. J., Wheeler, A. J., Mitchell, N. C., and Sutton, G. (2009). Variations in sediment wave dimensions across the tidally dominated Irish Sea, NW Europe. *Marine Geology*, 263, 108–119.

Vernberg, F.J. (1993). Salt-marsh processes: A review. *Environmental Toxicology and Chemistry*, 12(12), 2167-2195.

References

Verrill, L. and Tipping, R. (2010). Use and abandonment of a Neolithic field system at Belderrig, Co. Mayo, Ireland: evidence for economic marginality. *The Holocene*, 20, 1011-1021.

Vinther, B.M., Clausen, H.B., Johnsen, S.J., Rasmussen, S.O., Anderson, K.K., Buchardt, S.L., Dahl-Jensen, D., Seierstad, I.K., Siggaard-Andersen, M.L., Steffensen, J.P., Svensson, A., Olsen, J. and Heinemeier, J. (2006). A synchronized dating of three Greenland ice cores throughout the Holocene. *Journal of Geophysical Research*, 111(D13), 1-11.

Walker, B.K., Riegal, B. and Dodge, R.E. (2008). Mapping coral reef habitats in southeast Florida using a combined technique approach. *Journal of Coastal Research*, 24(5), 1138-1150.

Walker, M., Head, M.J., Berkelhammer, M., Björck, S., Cheng, H., Cwynar, L., Fisher, D., Gkinis, V., Long, A., Lowe, J., Newnham, R., Rasmussen, S.O. and Weiss, H. (2018). Formal ratification of the subdivision of the Holocene Series/ Epoch (Quaternary System/Period): two new Global Boundary Stratotype Sections and Points (GSSPs) and three new stages/ subseries. *Episodes*, 4 (4), 213-224.

Walker, M.J.C., Berkelhammer, M., Björck, S., Cwynar, L.C., Fisher, D.A., Long, A.J., Lowe, J.J., Newnham, R.M., Rasmussen, S.O. and Weiss, H. (2012). Formal subdivision of the Holocene Series/Epoch: a Discussion Paper by a Working Group of INTIMATE (Integration of ice-core, marine and terrestrial records) and the Subcommittee on Quaternary Stratigraphy (International Commission on Stratigraphy). *Journal of Quaternary Science*, 27, 649-659.

Wang, Y., Cheng, H., Edwards, R.L., He, Y., Kong, X., An, Z., Wu, J., Kelly, M.J., Dykoski, C.A. and Li, X. (2005). The Holocene Asian monsoon: links to solar changes and North Atlantic climate. *Science*, 308, 854-857.

Wanner, H. and Ritz, S.P. (2011). A web-based Holocene Climate Atlas (HOCLAT). World Wide Web Address: http://www.oeschger.unibe.ch/research/projects/holocene_atlas/.

Wanner, H., Beer, J., Bütikofer, J., Crowley, T.J., Cubasch, U., Flückiger, J., Goosse, H., Grosjean, M., Joos, F., Kaplan, J.O., Küttel, M., Müller, S.A., Prentice, I.C., Solomina, O., Stocker, T.F., Tarasov, P., Wagner, M. and Widmann, M. (2008). Mid- to Late Holocene climate change: an overview. *Quaternary Science Reviews*, 27(19-20), 1791-1828.

Wanner, H., Mercolli, L., Grosjean, M. and Ritz, S.P. (2015). Holocene climate variability and change; a data-based review. *Journal of the Geological Society*, 172, 254-263.

References

- Warren, W.P. (1979b). The Stratigraphic position and age of the Gortian Interglacial deposits. *Geological Survey, Bulletin* 2(4), 315-332.
- Watson, J.E., Brooks, S.J., Whitehouse, N.J., Reimer, P.J., Birks, H.J.B. and Turney, C. (2010). Chironomid-inferred late-glacial summer air temperatures from Lough Nadourcan, Co. Donegal, Ireland. *Journal Quaternary Science*, 25(8), 1200-1210.
- Watts, W.P. (1964). Interglacial deposits at Baggotstown, near Bruff, Co. Limerick. *Proceedings of the Royal Irish Academy*, 63B, 167-189.
- Watts, W.P. (1985). Quaternary Vegetation cycles. In K. J. Edwards and W.P. Warren (Eds.) *The Quaternary history of Ireland* (pp. 155-185). London: Academic Press.
- Weaver, A.J., Saenko, O.A., Clark, P.U. and Mitrovica, J.X. (2003). Meltwater pulse 1A from Antarctica as a trigger of the Bølling-Allerød warm interval. *Science*, 299, 1709-1713.
- Weilbach, K. (2018). *Extent, timing and nature of retreat of the British-Irish Ice Sheet offshore of north-western Ireland during and following the Last Glacial Maximum* (Unpublished doctoral dissertation). Durham University, UK.
- Weiss, H., Courty, M-A., Wetterstorm, W., Guichard, F., Senior, L., Meadow, R. and Curnow, A. (1993). The genesis and collapse of third millennium north Mesopotamian civilisation. *Science*, 261(5124), 995-1004.
- Welc, F. and Marks, L. (2014). Climate change at the end of the Old Kingdom in Egypt around 4200 BP: New geoarchaeological evidence. *Quaternary International*, 324, 124-133.
- Weldeab, S., Lea, D.W., Schneider, R.R. and Andersen, N. (2007). 155,000 years of west African monsoon and ocean thermal evolution. *Science*, 316, 1303-1307.
- Weltje, G.J. and Tjallingii, R. (2008). Calibration of XRF core scanners for quantitative geochemical logging of sediment cores: Theory and application. *Earth and Planetary Science Letters*, 274, 423-438.
- Wenau, S., Spieß, V., Pape, T. and Fekete, N. (2017). Controlling mechanisms of giant deep water pockmarks in the Lower Congo Basin. *Marine and Petroleum Geology*, 83, 140-157.
- Wentworth, C.K. (1922). A scale of grade and class terms for clastic sediments. *Journal of Geology*, 30, 377-392.

References

- Westerhold, T., Röhl, U., Lasker, J., Raffi, I., Bowles, J., Lourens, J. and Zachos, J. (2007). On the duration of magnetochrons C24r and C25n, and the timing of early Eocene global warming events: implications from the ODP Leg 208 Walvis Ridge depth transect. *Palaeoceanography*, 22(2), 1-19.
- Whelan, T., Coleman, J.M., Suhayda, J.N. and Roberts, H.H. (1977). Acoustical penetration and shear strength in gas-charged sediment. *Marine Geotechnology*, 2(1-4), 147-159.
- Whitehouse, N.J., Schulting, R.J., McClatchie, M., Barratt, P., McLaughlin, T.R., Bogaard, A., Colledge, S., Marchant, R., Gaffrey, J. and Bunting, M.J. (2014). Neolithic agriculture on the European western frontier: the boom and bust of early farming in Ireland. *Journal of Archaeological Science*, 51, 181-205.
- Whitehouse, R.J.S. (1998). *Scour at Marine Structures: A Manual for Practical Applications*. Thomas Telford: London.
- Whitehouse, R.J.S., Harris, J.M., Sutherland, J. and Rees, J. (2011). The nature of scour development and scour protection at offshore windfarm foundations. *Marine Pollution Bulletin*, 62(1), 73-88.
- Whittington, G., Edwards, K.J. and Cundill, P.R. (1991). Palaeoecological investigations of multiple elm declines at a site in north Fife, Scotland. *Journal of Biogeography*, 18, 71-87.
- Wiles, G.C., Barclay, D.J., Calkin, P.E. and Lowell, T.V. (2008). Century to millennial-scale temperature variations for the last two thousand years indicated from glacial geologic records of Southern Alaska. *Global and Planetary Change*, 60(1-2), 115-125.
- Willard, D.A., Cronin, T.M. and Verardo, S. (2003). Late-Holocene climate and ecosystem history from Chesapeake Bay sediment cores, USA. *The Holocene*, 13, 201-214.
- Williams, D.M. and Doyle, E. (2014). Dates from drowned mid-Holocene landscapes on the central western Irish seaboard. *Irish Journal of Earth Sciences*, 32, 23-27.
- Williams, D.M. and Hall, A.M. (2004). Cliff-top megaclast deposits of Ireland, a record of extreme waves in the North Atlantic—storms or tsunamis? *Marine Geology*, 206(1), 101-117.
- Williams, D.M., Armstrong, H.A. and Harper, D.A.T. (1988). The age of the South Connemara Group, Ireland, and its relationship to the Southern Uplands Zone of Scotland and Ireland. *Scottish Journal of Geology*, 24, 279-287.

References

- Wilson, S., Blake, C., Berges, J.A. and Maggs, C.A. (2004). Environmental tolerances of free-living coralline algae (maerl): implications for European marine conservation. *Biological Conservation*, 120, 283-293.
- Wilson, L.J., Austin, W.E.N. and Jansen, E. (2002). The last British Ice Sheet: growth, maximum extent and deglaciation. *Polar Research*, 21, 243-250.
- Wilson, P., Lord, T.C., Schnabel, C. and Vincent, P.J. (2013). Holocene erosion at the summit of Ingleborough, Yorkshire Dales, northern England, indicated by cosmogenic ¹⁰Be surface exposure dating. *Proceedings of the Yorkshire Geological Society*, 59(4), 247-253.
- Wolters, S., Zeller, M. and Bungenstock, F. (2010). Early Holocene environmental history of sunken landscapes: pollen, plant macrofossil and geochemical analysis from the Borkum Riffgrund, southern North Sea. *International Journal of Earth Science*, 99, 1707-1719.
- Wood, B. (2011). *Post-glacial environmental change in Galway Bay, Western Ireland; evidence from shallow marine sedimentary vibrocores* (Unpublished Master's Thesis). National University of Ireland, Galway.
- Wood, B., Williams, D.M. and Murray, J. (2017). Effects of the Younger Dryas climate event recorded in sediment near the western Irish seaboard. *Geological Journal*, 52(2), 647-659.
- Woodman, P.C. (1997). Ireland's native mammals: a survey of the archaeological record. *The Irish Naturalists' Journal*, 33, 28-43.
- Woodman, P. C. (2015). *Ireland's first settlers: Time and the Mesolithic*. Oxford: Oxbow.
- Woodroffe, C.D. (2002). *Coasts: form, process and evolution*. New York: Cambridge University Press.
- Woolf, D.K., Challenor, P.G. and Cotton, P.D. (2002). Variability and predictability of the North Atlantic wave climate. *Journal of Geophysical Research*, 107(C10), 1-14.
- Wright, W.B. (1914). *The Quaternary Ice Age*. London: MacMillan and Co.
- Wu, Y., Chaffey, J., Greenberg, D.A., Colbo, K. and Smith, P.C. (2011). Tidally-induced sediment transport patterns in the upper Bay of Fundy: A numerical study. *Continental Shelf Research*, 31(19-20), 2041-2053.

References

- Wynn Jones, R. (2013). *Foraminifera and their applications*. Cambridge: Cambridge University Press.
- Xiao, X., Haberle, S.G., Shen, J., Yang, X., Han, Y., Zhang, E. and Wang, S. (2014). Latest Pleistocene and Holocene vegetation and climate history inferred from an alpine lacustrine record, northwestern Yunnan Province, southwestern China. *Quaternary Science Reviews*, 86, 35-48.
- Yang, E., LaRocque, P.E., Guenther, G.C., Reid, D., Pan, W. and Francis, K. (2007). *Shallow water depth extraction- progress and challenges*. Proceedings of the 2007 U.S. Hydrographic Conference, Norfolk, V.A.
- Yokoyama, Y., Lambeck, K., De Deckker, P., Johnston, P., and Fifield, L. K. (2000). Timing of the Last Glacial Maximum from observed sea-level minima. *Nature*, 406, 713–716.
- Younge, C.M. (1946). On the habits of *Turritella Communis* Risso. *Journal of the Marine Biological Association of the UK*, 26(03), 377-380.
- Yu, S.Y., Berglund, B.E., Sandgren, P. and Lambeck, K. (2007). Evidence for a rapid sea-level rise 7600 yr ago. *Geology*, 35, 891-894.
- Yu, S.Y., Colman, S.M., Lowell, T.V., Milne, G.A., Fisher, T.G., Breckenridge, A., Boyd, M. and Teller, J.T. (2010). Freshwater outburst from Lake Superior as a trigger for the cold event 9300 years ago. *Science*, 328, 1262-1266.
- Yu, X., Weijian, Z., Franzen, L.G., Feng, X., Peng, C. and Jull, A.J.T. (2006). High resolution peat records for Holocene monsoon history in the eastern Tibetan Plateau. *Science in China Series D*, 49(6), 615-621.
- Zaragosi, S., Bourillet, J-F., Eynaud, F., Toucanne, S., Denhard, B., Van Toer, A. and Lanfumeu, V. (2006). The impact of the last European deglaciation on the deep-sea turbidite systems of the Celtic-Armorican margin (Bay of Biscay). *Geo-Marine Letters*, 26, 17-29.
- Zhou, X.J., Zhao, P., Liu, G. and Zhou, T.J. (2011). Characteristics of decadal-centennial-scale changes in East Asian summer monsoon circulation and precipitation during the Medieval Warm Period and Little Ice Age and in the present day. *Chinese Science Bulletin*, 56, 3003-3011.
- Zhou, Y-L., Lu, H-Y., Mason, J., Miao, X-D., Swinwhart, J. and Goble, R. (2008). Optically stimulated luminescence dating of aeolian sand in the Otindag dune field and Holocene climate change. *Science in China Series D, Earth Science*, 51(6), 837-847.

References

Zieglar, M., Jilbert, T., de Lange, G.J., Lourens, L.J. and Reichart, G-J. (2008). Bromine counts from XRF scanning as an estimate of the marine organic carbon content of sediment cores. *Geochemistry, Geophysics, Geosystems*, 9(5), 1525-2027.

Appendices

Appendix 1: Graphs and raw data table showing the physical and geochemical properties of all cores not included in the main text of the thesis.

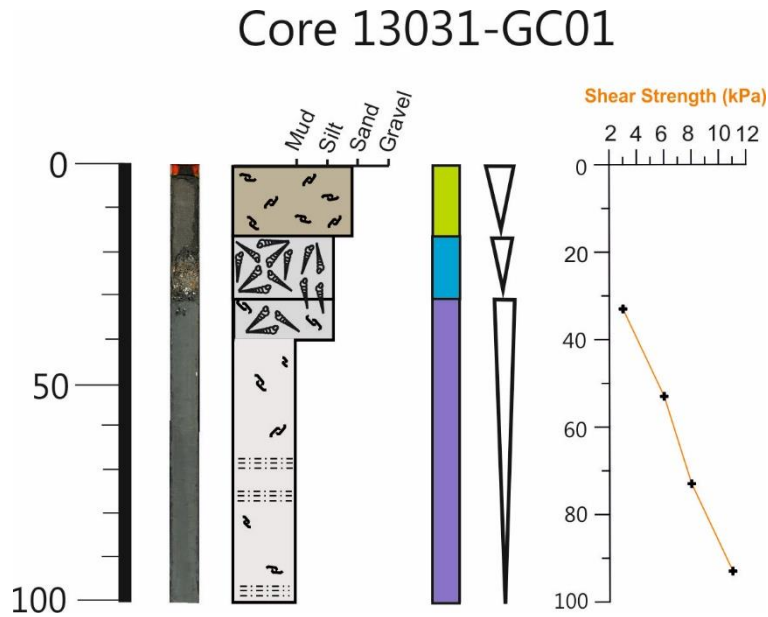


Figure A.1: A graph of core 01GC showing a core image, a core log and shear strength measurements.

Core 13031-VC04

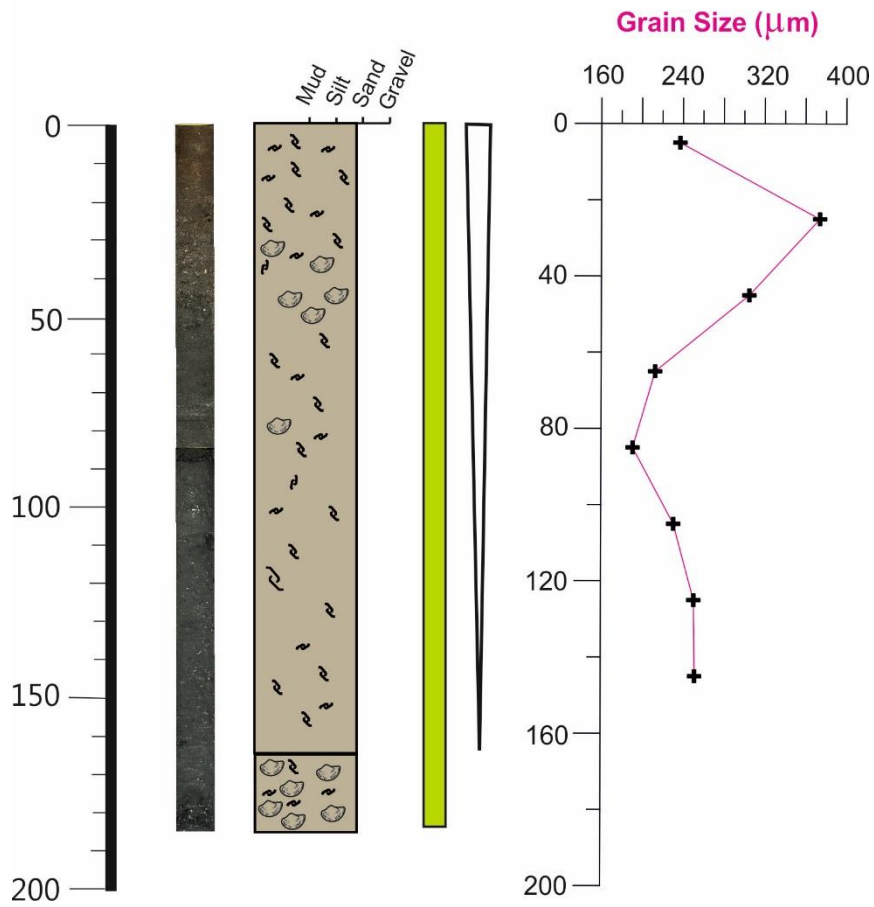


Figure A.2: A graph of core 04VC showing a core image, a core log and grainsize measurements.

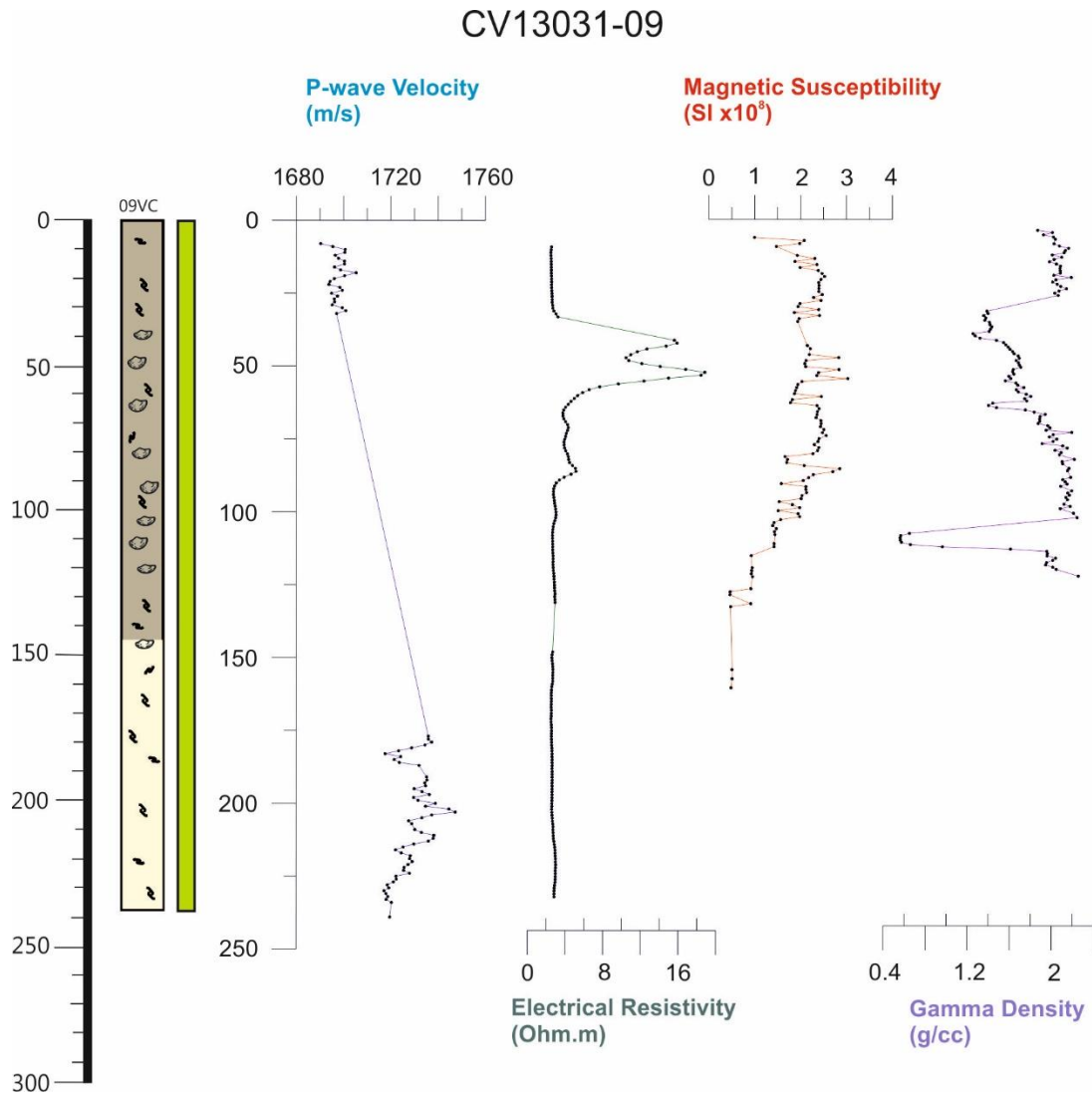


Figure A.3: A graph of core 09VC showing a core log and MSCL measurements.

Core 13031-VC10

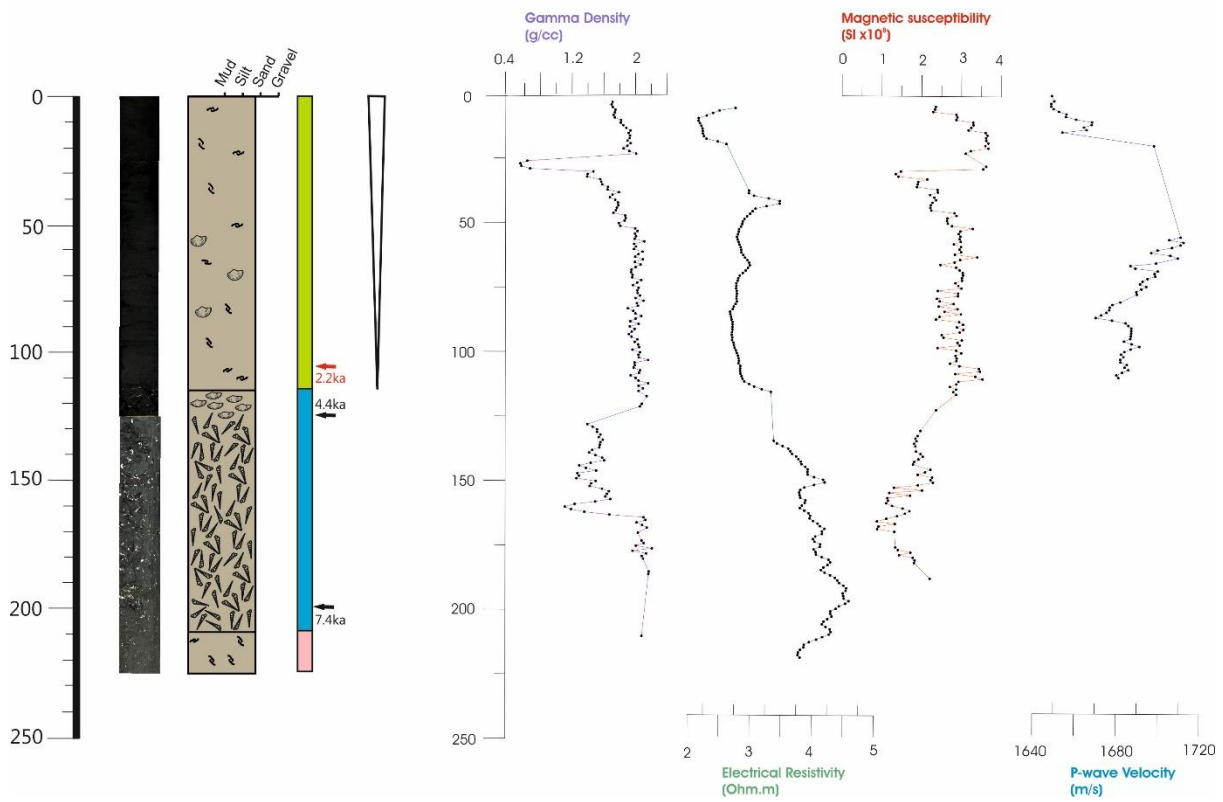


Figure A.4: A graph of core 10VC showing a core image, a core log and MSCL measurements.

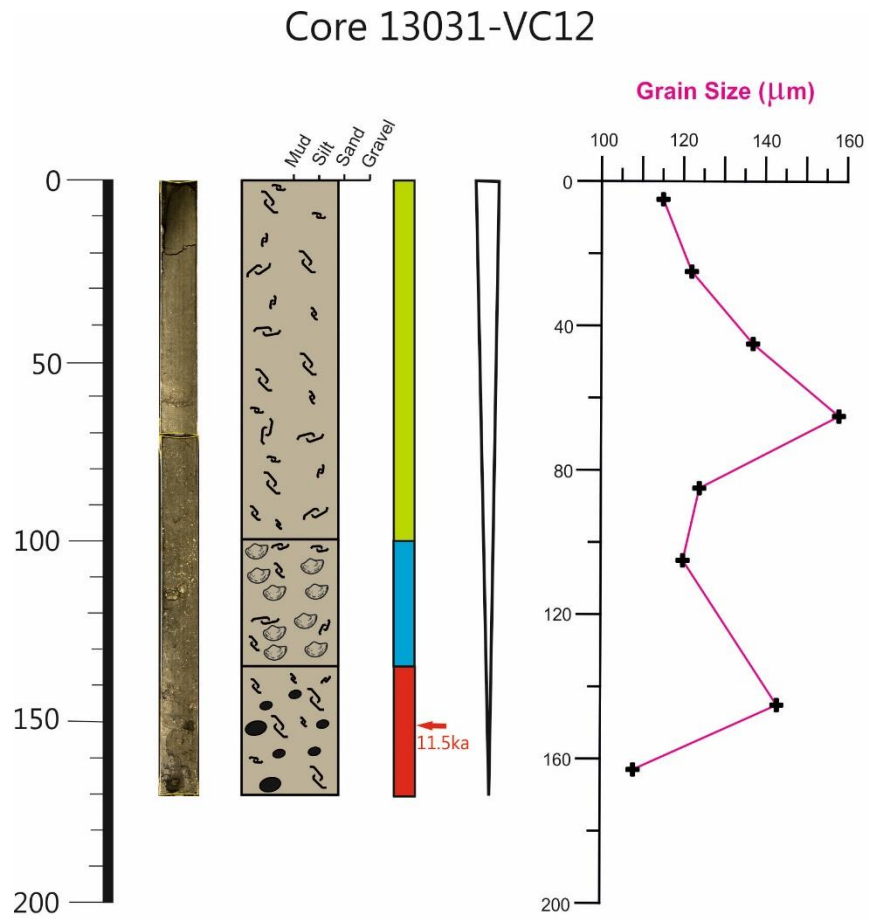


Figure A.5: A graph of core 12VC showing a core image, a core log and grainsize measurements.

Core 13031-VC14

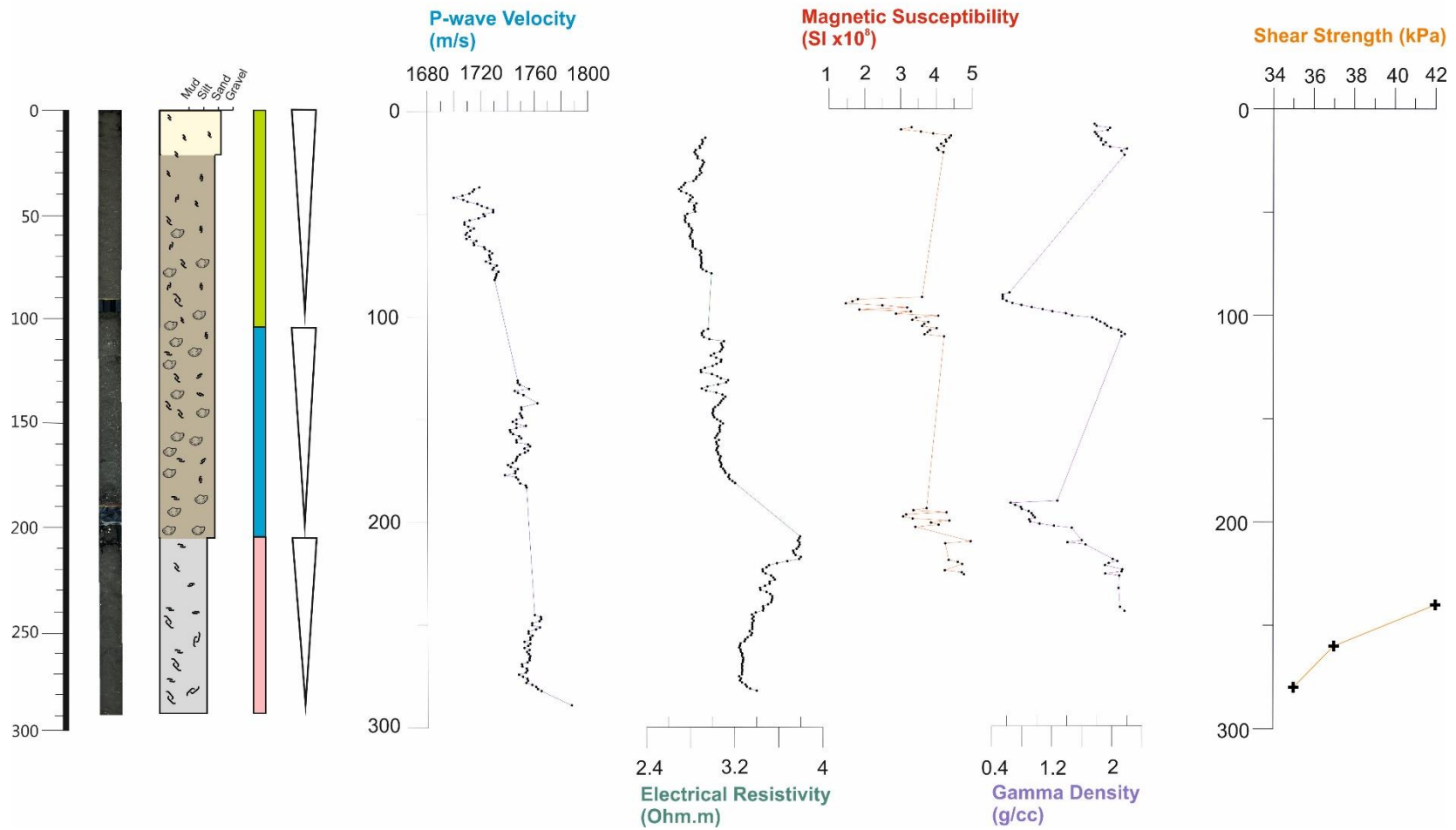


Figure A.6: A graph of core 14VC showing a core image, a core log MSCL and shear strength measurements.

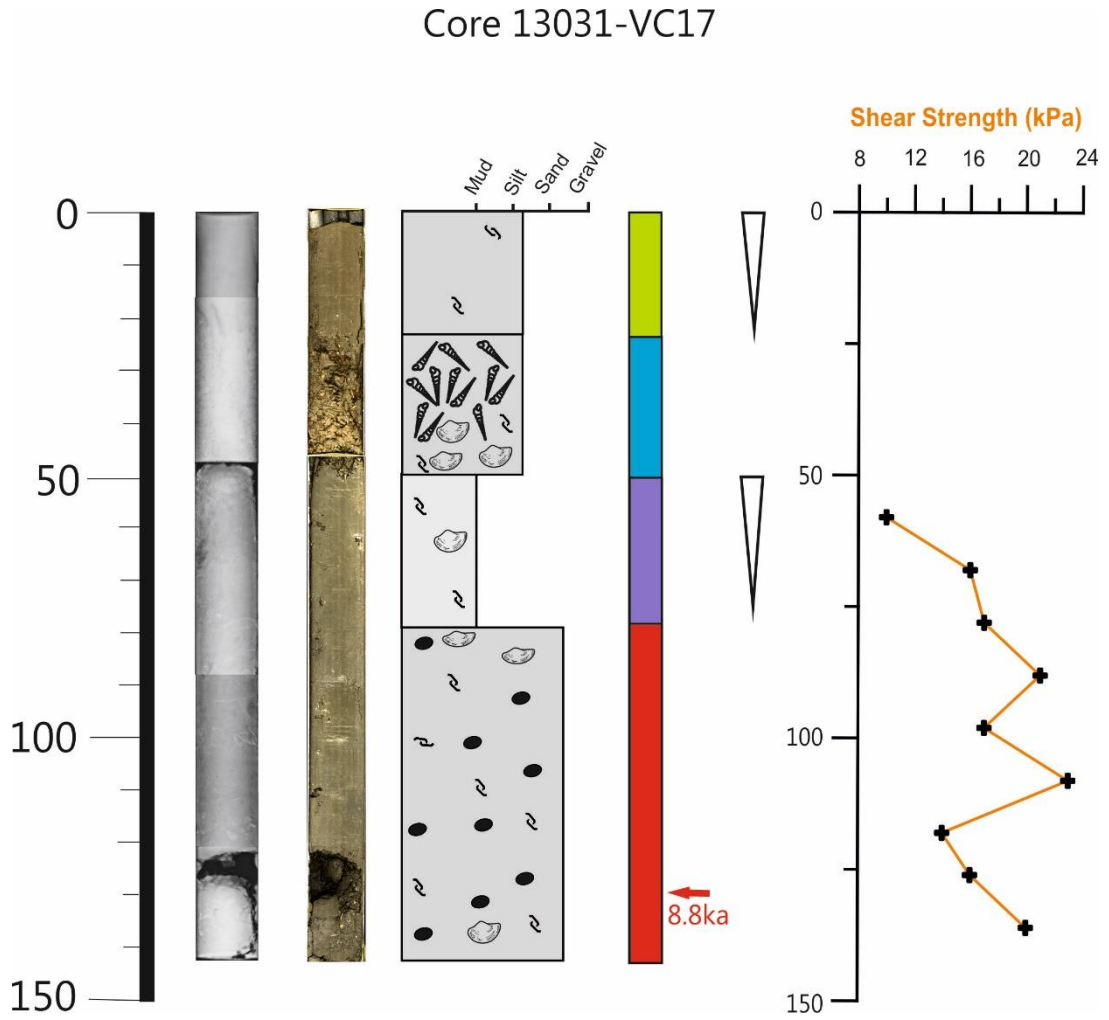


Figure A.7: A graph of core 17VC showing a core image, a core log and shear strength measurements.

Core 13031-VC18

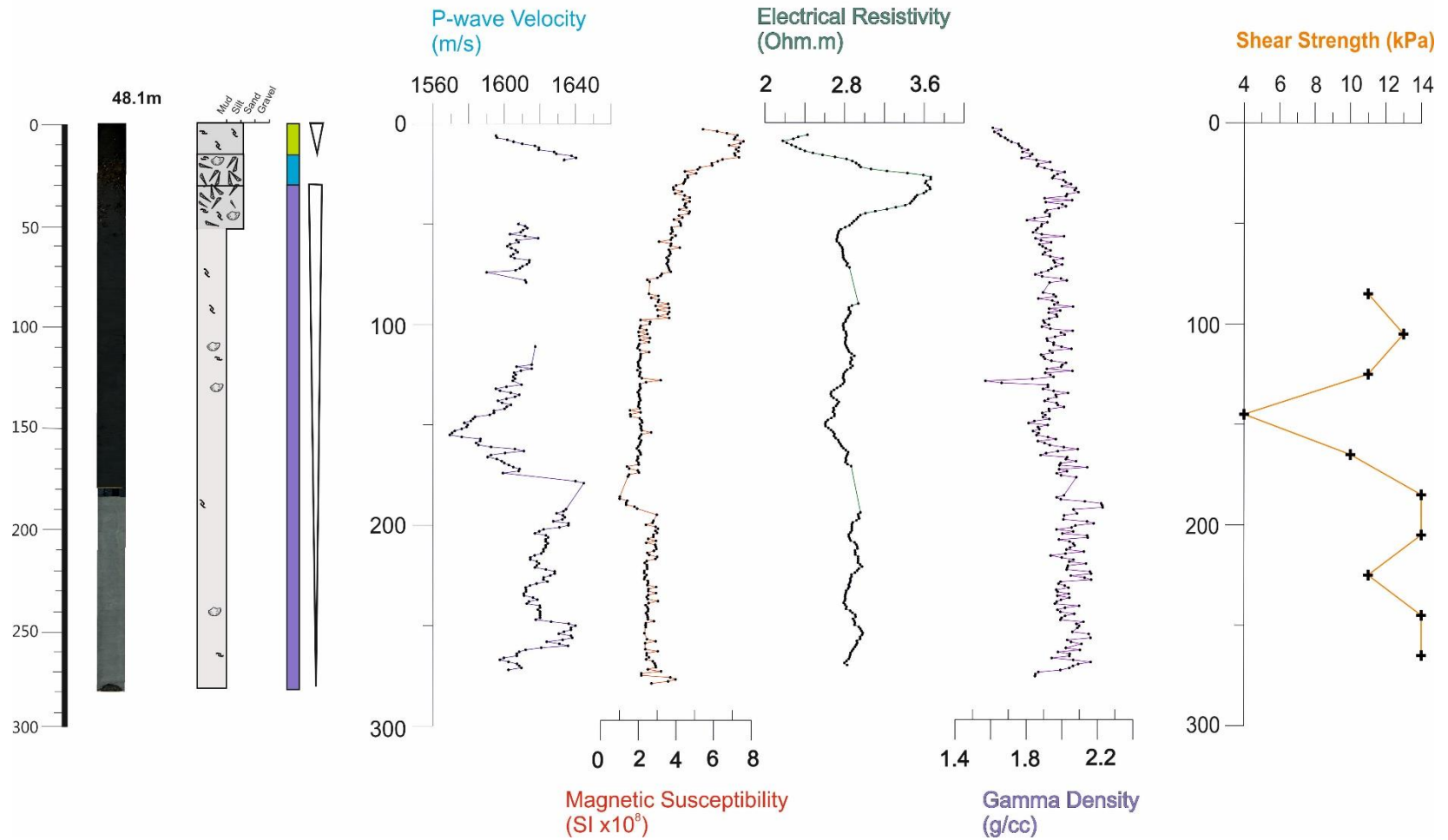


Figure A.8: A graph of core 18VC showing a core image, a core log MSCL and shear strength measurements.

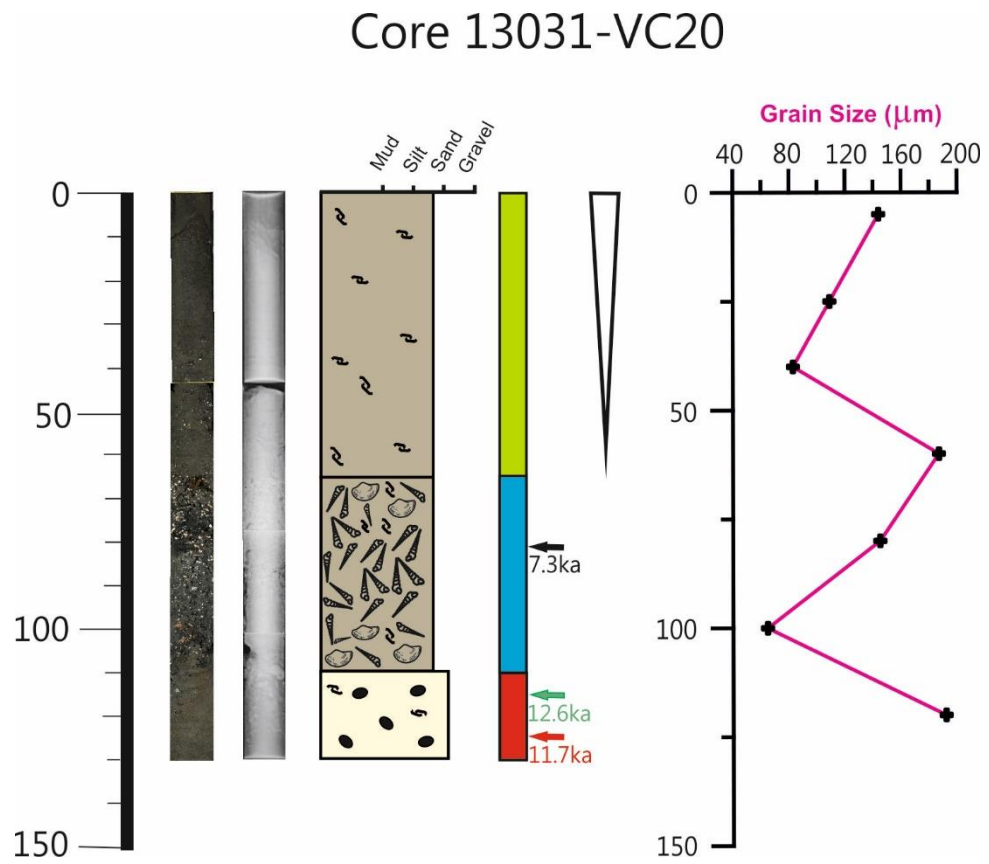


Figure A.9: A graph of core 20VC showing a core image, a core log and grain size measurements.

Appendices

Table A.1: Raw data for MSCL, Shear strength, grainsize measurements (GSA), lithology, colour, sedimentary structures, shell content and radiocarbon dates.

Facies	Core	P-Wave velocity (m/s)	Bulk Density (g/cm ³)	Magnetic Susceptibility (SI*10 ⁻⁸ m ³ /kg)	Electrical Resistivity (Ω.m)	Structures	GSA (µm)	Lithology	Radiocarbon Dates (ka cal BP)	Shear Strength (kPa)	Shell Content-estimated range (%)	Colour
1	03VC	1650 - 1730	1.9 – 2.3	3.6 – 3.7	2.7 - 3.2	Laminations	-	Mud	-	24 - 49	<5 –fragments only	Dark Grey
2	07VC	1790 - 1880	-	-	4 – 5.5	-	222 - 231	Gravel – Silty Sand	-	-	~40 -intact and fragmented	Dark Grey – Dark Greenish Grey
	12VC	-	-	-	-	-	108 - 143		11.5	-		
	17VC	-	-	-	-	-	-		8.8	14 - 23		
	20VC	-	-	-	-	-	<192		11.7 – 12.6	-		
3	03VC					-	-	Fine sand - Silt	-	42	~35 -intact and fragmented	Dark Grey
	10VC	-	-	-	-	-	-		-	-		
	13VC	1640 - 1975	0.8 – 2.25	2.6 – 3.75	2.75 – 3.7	-	-		9.9 – 13.1	23 - 42		
	14VC	1750 - 1790	1.4 – 2.2	4.2 - 5	3.22 – 3.8	-	-		-	35 - 42		
4	01GC	-	-	-	-	-	-	Fine sand - Mud	-	3 - 11	~5 -intact and fragmented	Dark Grey – Dark
	17VC	-	-	-	-	-	-		-	10 - 17		
	18VC	1568 - 1645	1.58 – 2.23	1 – 4.8	2.6 - 3	-	-		-	4 - 14		

Appendices

	22VC	1594 - 1638	1.6 - 2.2	2 - 5	2.2 - 3.7	-	40.9 - 56.2		10	10 - 25		Greenish Grey
5	01GC	-	-	-	-	-	-	Shell Hash	-	-	>75 -intact	-
	02VC	-	1.68 - 3.12	2 - 7	1.3 - 2.25	-	122 - 132		5.6	-		
	03VC	1723 - 1730	-	-	3.25 - 4.38	-	-		0.9 - 4.1	-		
	06VC	1660 - 1740	0.75 - 2.25	-1.3 - 0.5	2.55 - 3.15	-	146 - 191		4.3	-		
	07VC	1550 - 1800	0.6 - 2.3	3.5 - 5	2.5 - 5.5	-	52.8 - 60.4		6.2	-		
	10VC	-	1.1 - 2.2	0.9 - 2.9	3.7 - 4.65	-	-		4.4 - 7.4	-		
	12VC	-	-	-	-	-	120		-	-		
	13VC	-	2.2	-	3.25 - 3.75	-	-		6.4	-		
	14VC	1738 - 1763	0.68 - 2.2	3.1 - 4.4	2.9 - 3.2	-	-		-	-		
	17VC	-	-	-	-	-	-		-	-		
	18VC	1633 - 1641	1.78 - 2.05	4 - 7.4	2.58 - 3.65	-	-		-	-		
	20VC	-	-	-	-	-	64.7 - 145		7.3	-		
22VC	1595 - 1600	1.85 - 2.1	6 - 10	3.2 - 3.4	-	40.9	6.8	-				
6	01VC	-	-	-	-	Laminations	54.4 - 88.8	Sand - Silt	-	13 - 31	~10 -intact and fragmented	Dark Brown - Dark Grey

Appendices

7	01VC	-	-	-	-	-	176 - 177	Sand	-	-	~15 –fragments only	Brown
8	01GC	-	-	-	-	-	-	Coarse sand – Silt	-	-	~60 –intact and fragmented	Light Yellowish Brown - Black
	01VC	-	-	-	-	-	189 - 350		-	-		
	02VC	1708 - 1740	2.65 – 3.3	1.2 - 6	0.7 – 2.25	-	119 - 153		-	-		
	03VC	1672 - 1723	1.8 – 2.2	3.25 – 5.8	2.25 - 3	-	-		-	-		
	04VC	-	-	-	-	-	191 - 374		-	-		
	05VC	-	-	-	-	-	-		-	-		
	06VC	1725 - 1780	0.55 – 2.3	0.9 – 2.8	3 – 3.85	-	194 - 275		-	-		
	07VC	1690 - 1710	0.6 – 2.25	3.8 - 7	2.5 – 13.7	-	116 - 168		-	-		
	08VC	-	-	-	-	-	-		-	-		
	09VC	1690 - 1748	0.55 – 2.28	0.5 - 3	2.5 - 19	-	-		-	-		
	10VC	1649 - 1715	0.55 – 2.35	1.3 – 3.7	2.2 – 3.5	-	-		2.2	-		
	11VC	-	-	-	-	-	-		-	-		
	12VC	-	-	-	-	-	115 - 158		-	-		
	13VC	1625 - 1700	1.55 – 2.25	3.65 – 5.7	2.15 - 3.2	-	-		-	-		
	14VC	1700 - 1734	0.5 – 2.2	1.5 – 4.4	2.7 - 3	-	-		-	-		
15VC	-	-	-	-	-	-	-	-				

Appendices

	16VC	-	-	-	-	-	-		-	-		
	17VC	-	-	-	-	-	-		-	-		
	18VC	1595 - 1640	1.62 – 1.84	5.5 – 7.7	2.17 – 2.57	-	-		-	-		
	20VC	-	-	-	-	-	82.9 - 187		-	-		
	21VC	-	-	-	-	-	-		-	-		
	22VC	1595 - 1617	0.65 – 1.9	1.7 – 12.2	2.8 – 5.3	-	105 - 129		-	-		

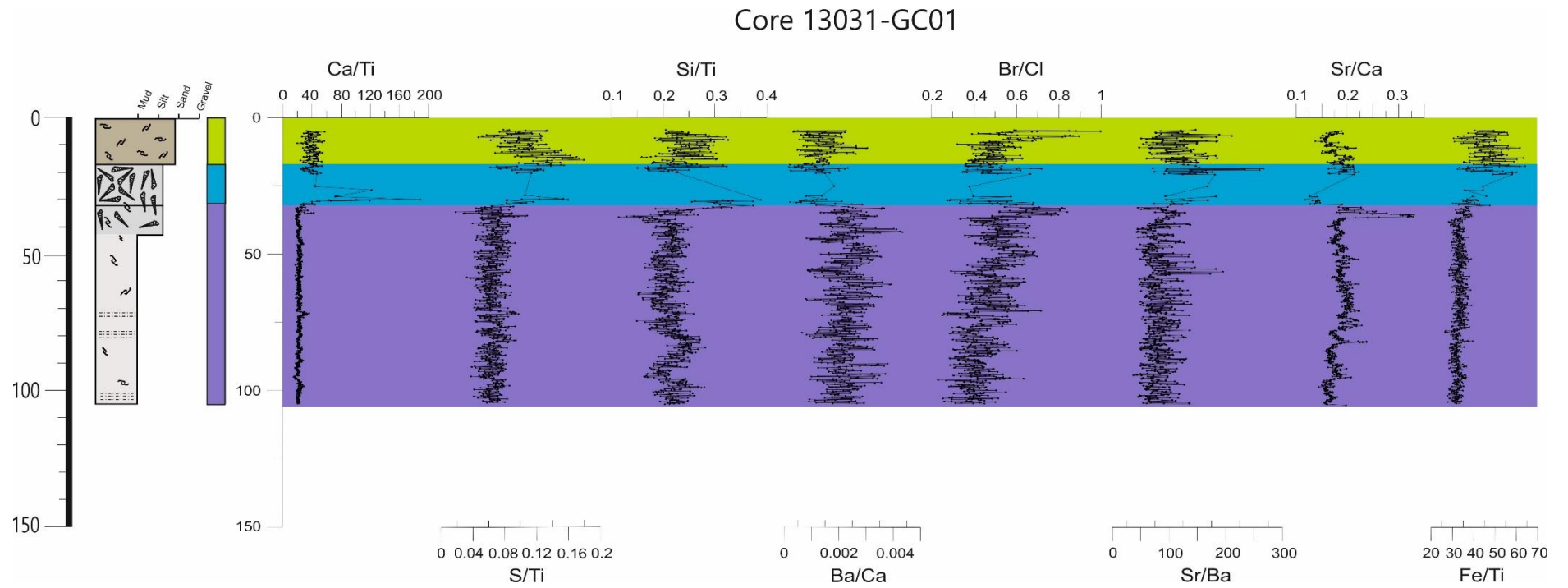


Figure A.10: A graph of core 01GC showing a core log and XRF measurements.

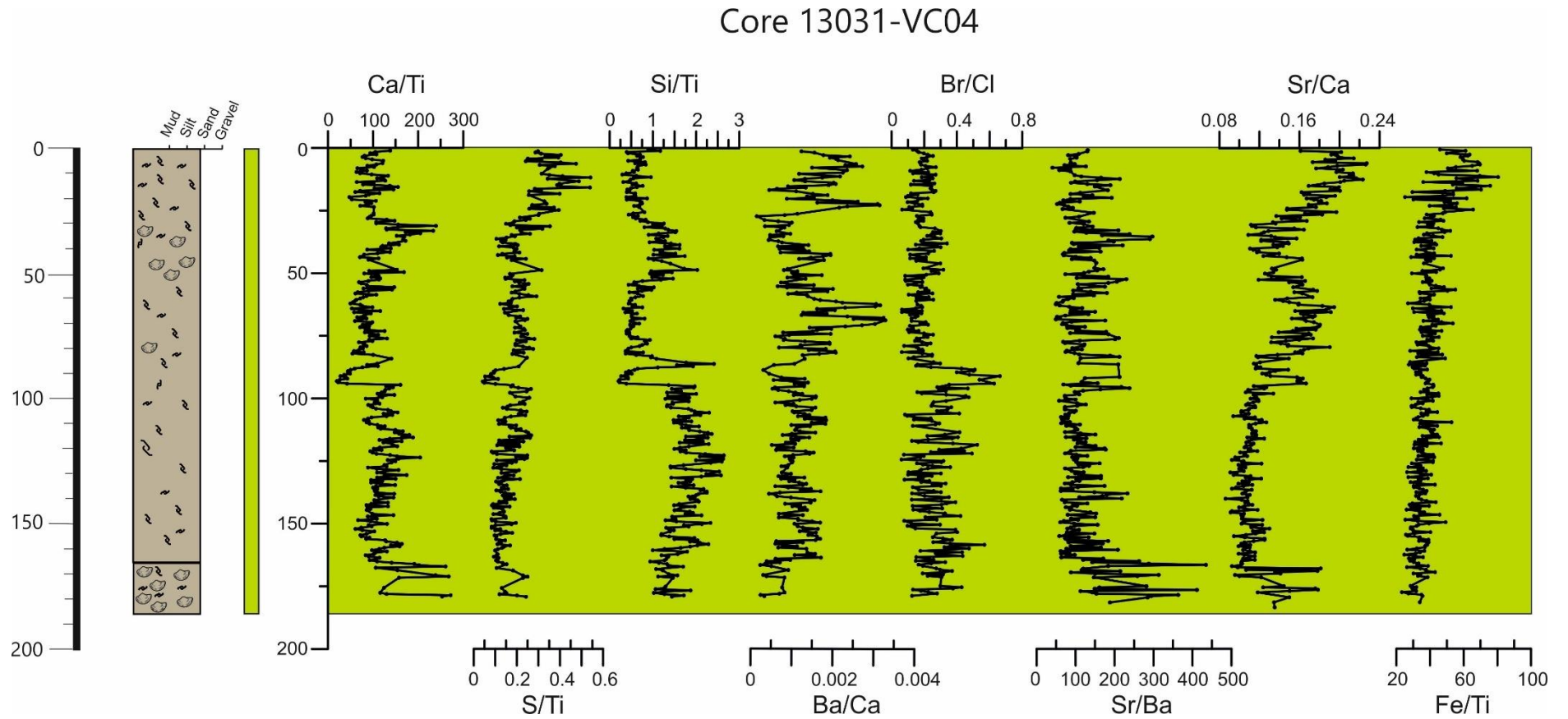


Figure A.11: A graph of core 04VC showing a core log and XRF measurements.

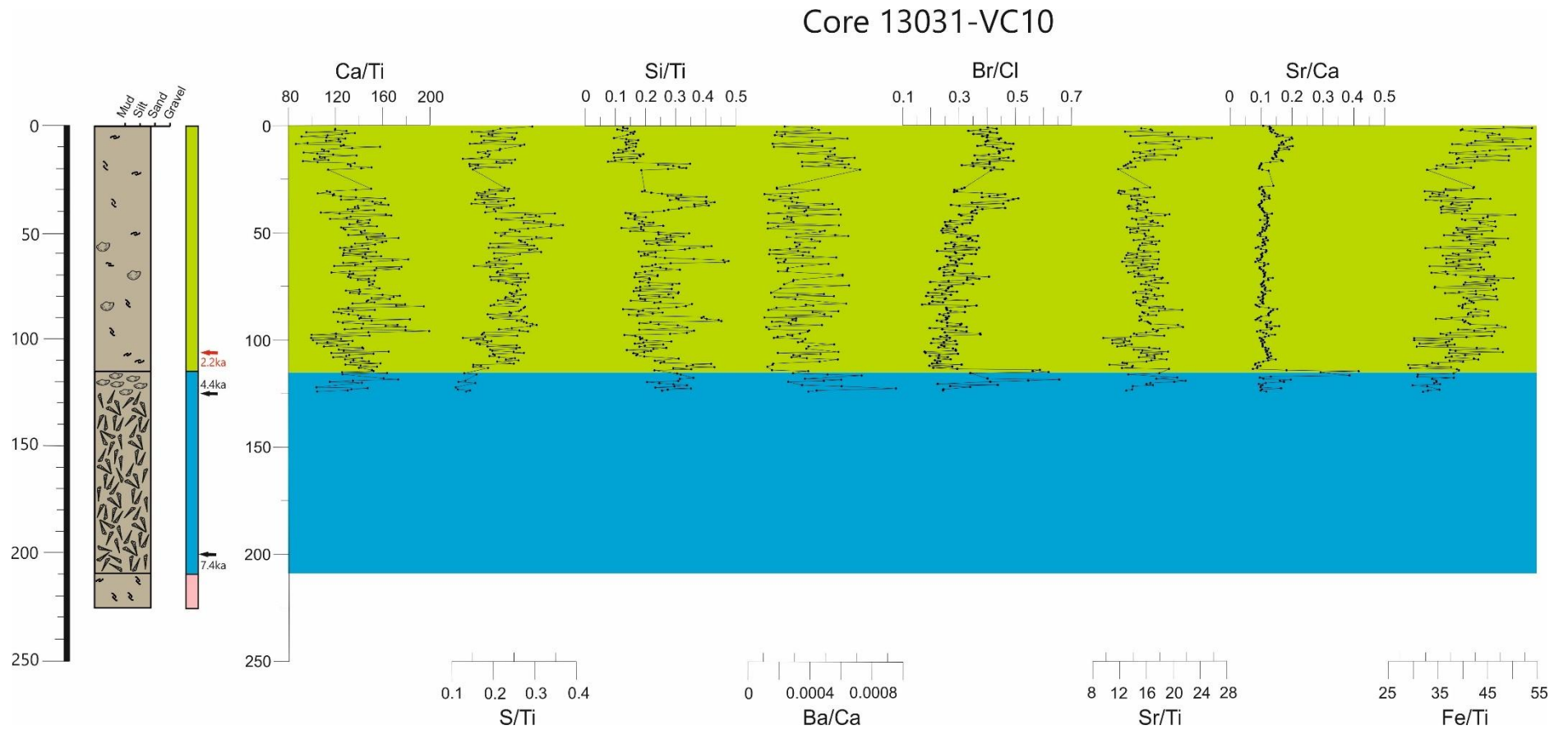


Figure A.12: A graph of core 10VC showing a core log and XRF measurements.

Appendices

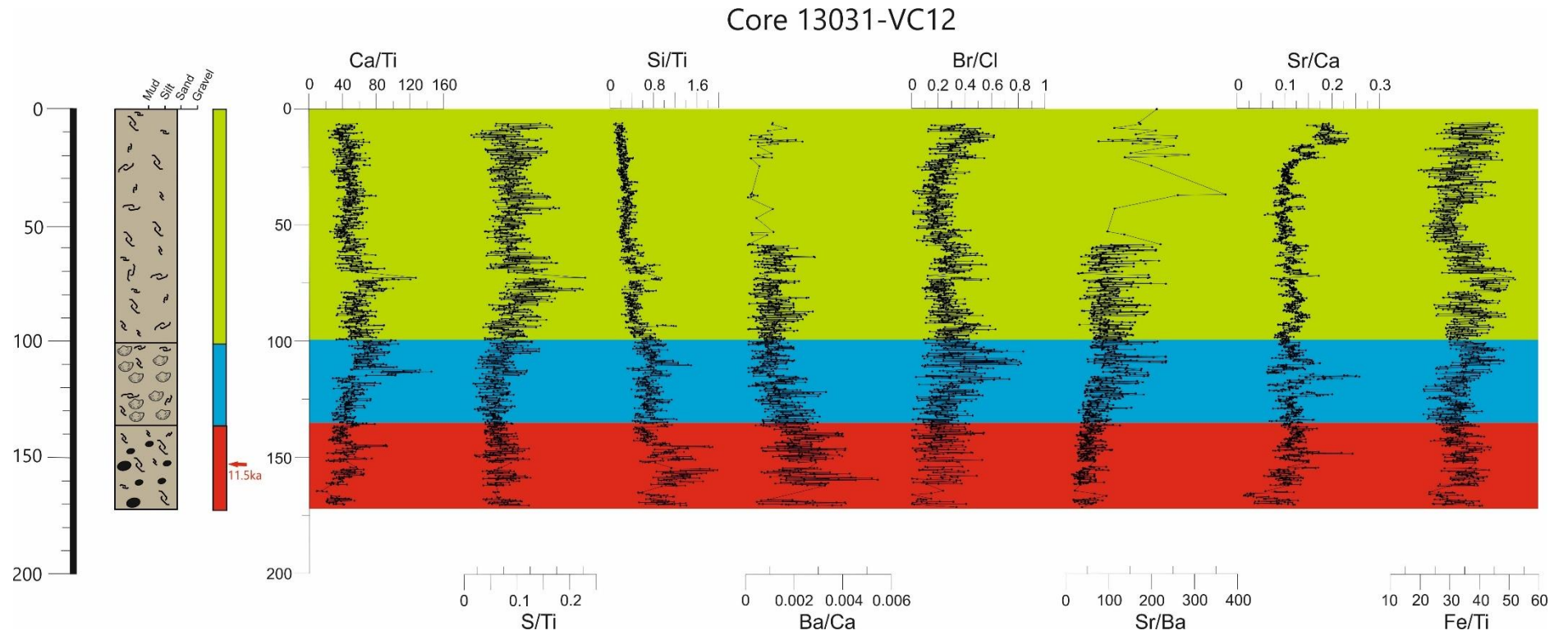


Figure A.13: A graph of core 12VC showing a core log and XRF measurements.

Core 13031-VC14

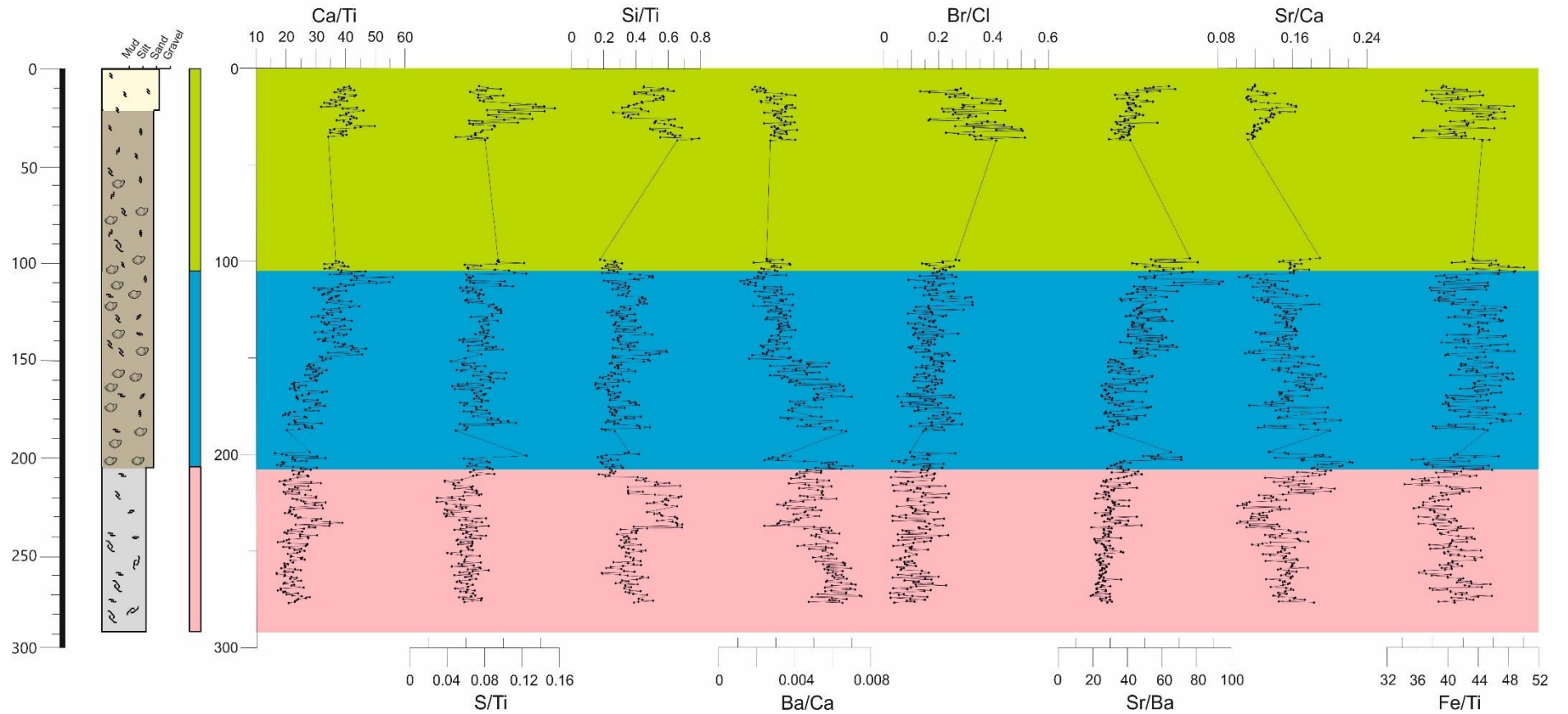


Figure A.14: A graph of core 14VC showing a core log and XRF measurements.

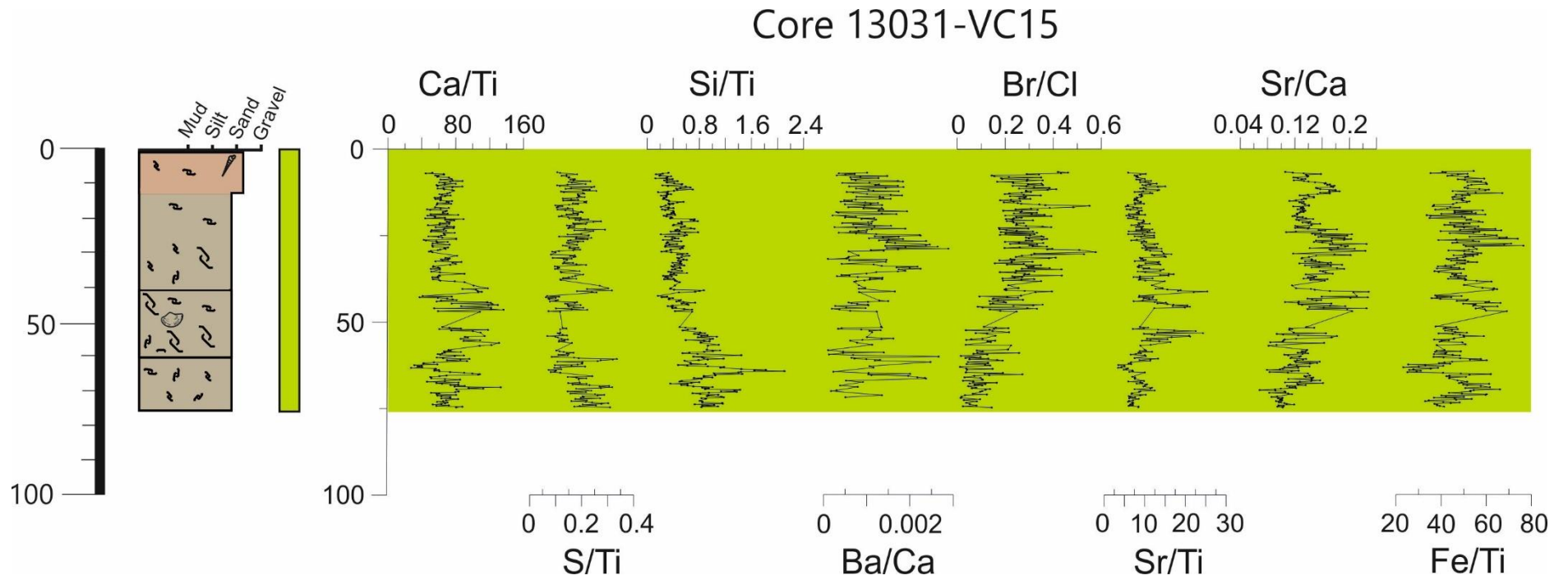


Figure A.15: A graph of core 15VC showing a core log and XRF measurements.

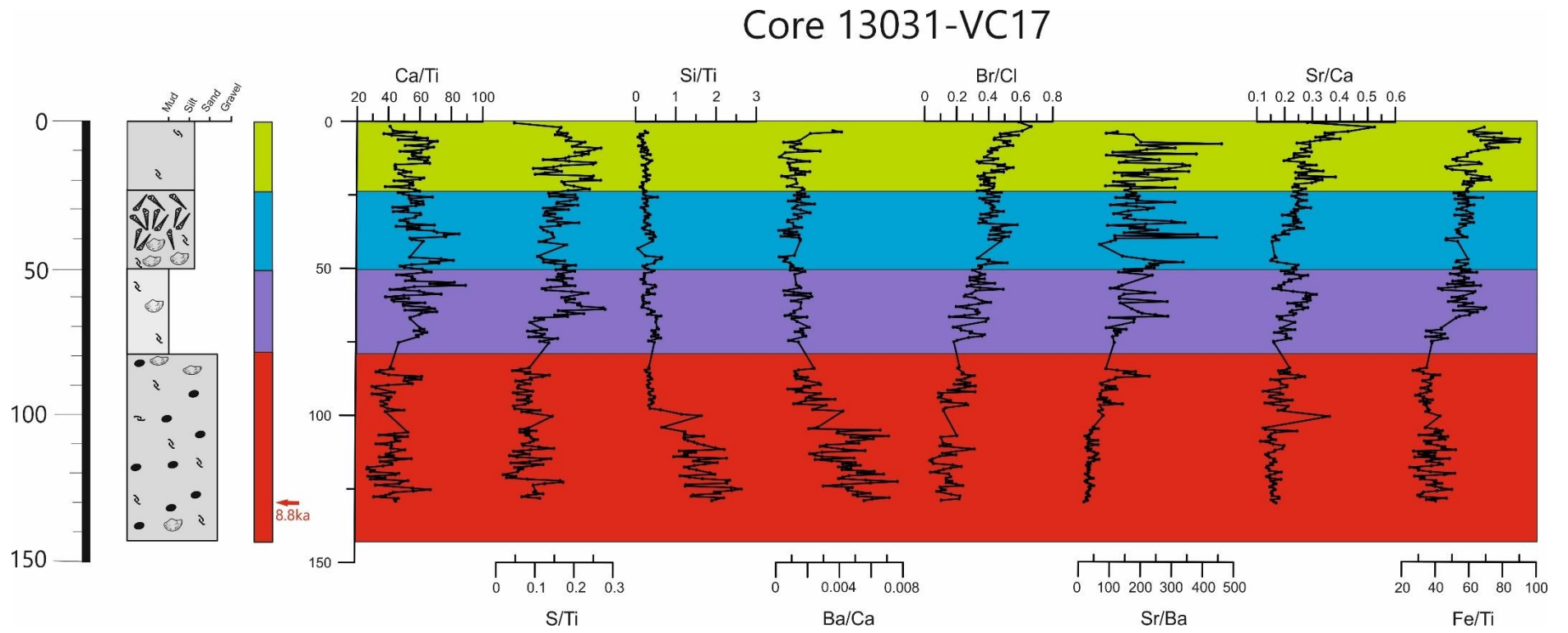


Figure A.16: A graph of core 17VC showing a core log and XRF measurements.

Appendices

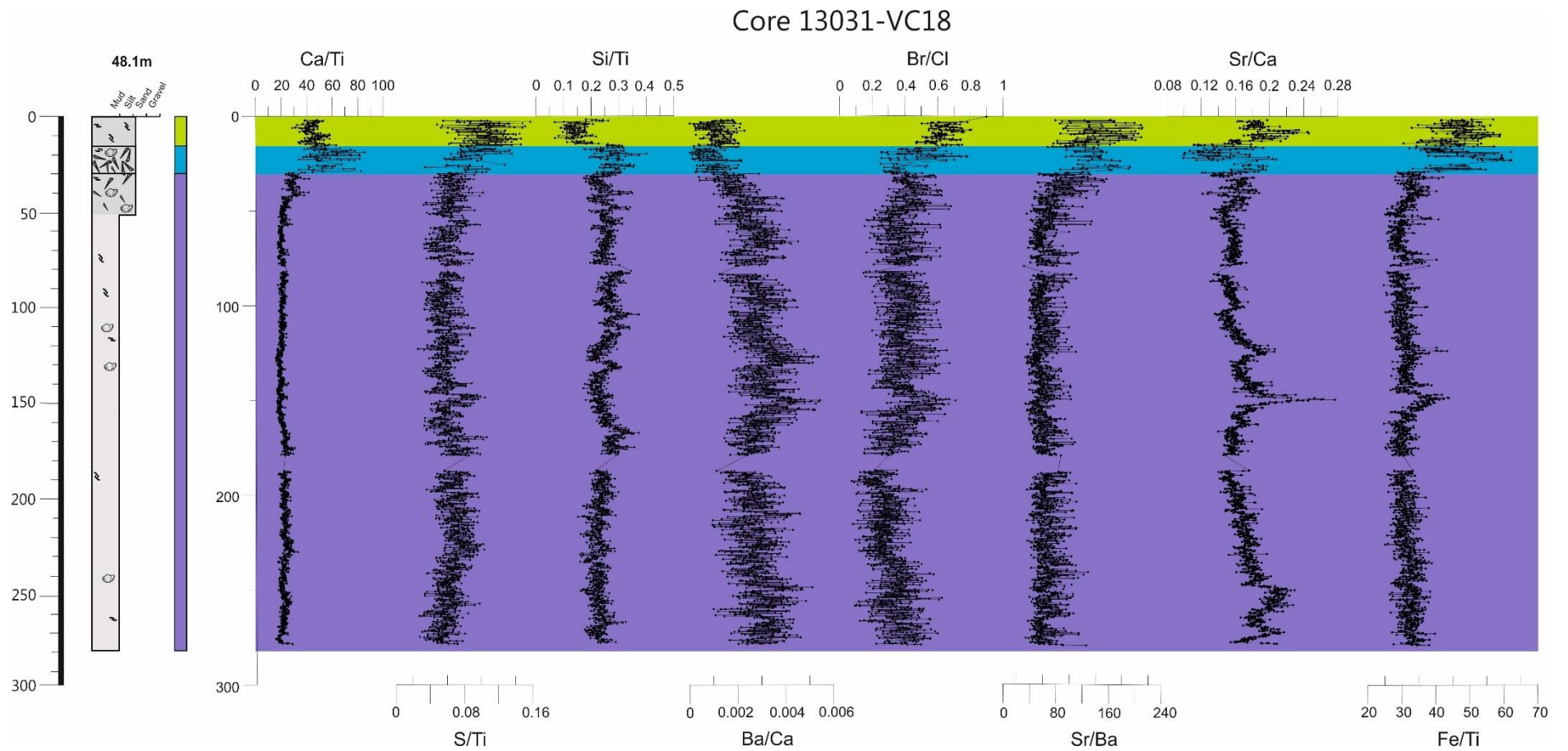


Figure A.17: A graph of core 18VC showing a core log and XRF measurements.

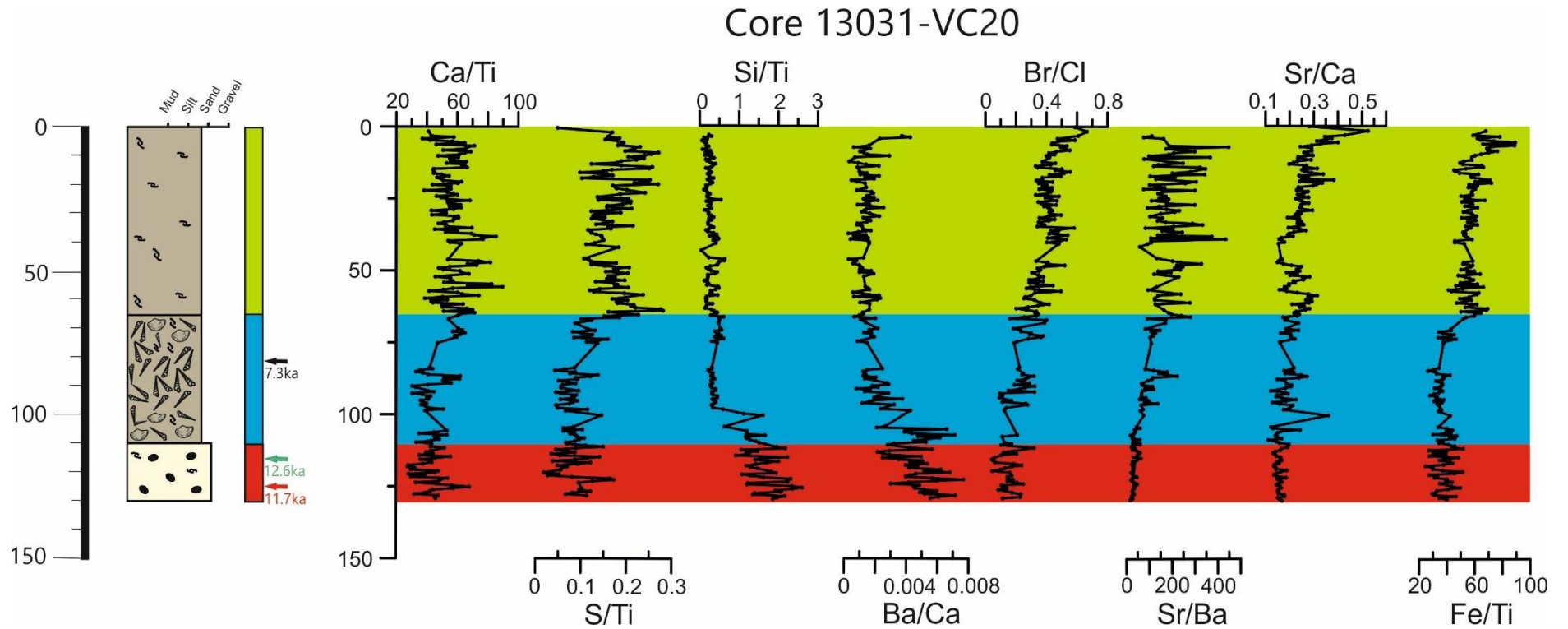


Figure A.18: A graph of core 20VC showing a core log and XRF measurements.

Appendices

Appendix 2: Total foraminifera counts including percentage of broken specimens.

Lithofacies	Broken %	Core	Depth (cm)	Total No.	<i>Lagena</i> spp	<i>Textularia</i> spp	<i>Sahulita conica</i>	<i>Bulimina marginata</i>	<i>Nonionella turgida</i>	<i>Fissurina elliptica</i>	<i>Oolina williamsoni</i>	<i>Planorbulina</i>	<i>Stainforthia fusiformis</i>	<i>Spirillina vivipara</i>	<i>Cibicides lobatulus</i>	<i>Bolivina</i> spp	<i>Quinqueloculina</i> spp	<i>Planorbulina distoma</i>	<i>Miliolinella subrotunda</i>	<i>Rosalina globularis</i>	<i>Rosalina praegeri</i>	<i>Elphidium excavatum</i>	<i>Ammonia beccarii</i>	<i>Haynesina germanica</i>	<i>Jadammina macrescens</i>
LF1	2	03VC	227-228	47	7			1					3	8			13		8					6	
LF2	17	07VC	201-202	274		47	64					13			5		73		62	3				7	
	12	17VC	82-83	134		36	27					2			6		25		31	5				2	
	24	17VC	117-118	207		41	37					6			8		55		52	5				3	
	19	17VC	139-140	252		41	49					12			6		83		52	3				6	
LF3	3	13VC	116-117	421		18		20	10		5	20			2		75			16	18	9	130	98	
	2	13VC	234-235	367		14		15	17		7	15					65				18	18	101	94	3
	3	14VC	278-279	405		18		7	16						3		78			13		19	145	108	
LF4	2	01G C	99-100	32	5				7				8			7	3				1				
	4	22VC	150-151	57	21				12				13			8	2				1				
	2	22VC	269-270	50	18				8				12			10	1				2				
LF5	6	01G C	30-31	98	3	4		2						3			34				1			51	
	3	07VC	160-161	108	3	6		5			2			1			36				3	1		52	
	9	14VC	110-111	207	6	4		6			6			1	1		79				1	3		106	
	18	14VC	197-198	134	6	5		2			4			4	3		41							59	
LF6	4	01VC	100-101	129										23			12	4			29	24	30	7	
	18	01VC	187-188	202										34			32	6			38	42	44	6	
LF7	9	01VC	60-61	98													19				3	6	37	33	
LF8	15	01G C	1-2cm	302	71	1		1	6	4	1	38			59	6	38							62	5
	23	01VC	1-2cm	378	106			1		7	3	65			66	9	58				1			61	1
	12	07VC	78-79	254	47	5		4		12		39			49	10	38				2			48	
	8	14VC	45-46	201	40					3	1	40			37	1	34				1			38	1
	21	17VC	15-16	102	19			2	1	2		19			21	2	16							20	

Appendices

Appendix 3: A reference table for the distribution and habitat preferences of the different foraminifera species found in this study in

Galway Bay.

Foraminifera	Distribution	Reference
<i>Ammonia beccarii</i>	This group is commonly found in estuaries and brackish lagoons. This group is euryhaline and tolerate large (0–35‰) diurnal salinity range. Close to its northern limit in Britain and Ireland.	Murray, 1971; Murray, 1979; Holzmann and Pawlowski, 2000; Horton et al, 2006
<i>Bolivina</i> sp.	Resistant to short term anoxia	Alve, 1995
<i>Bulimina marginata</i>	Infaunal, inner-shelf, marine species	Murray, 1979; Murray, 2003
<i>Cibicides lobatulus</i>	Marine, inner-shelf species but dead tests are transported into estuary mouths. Species is epifaunal clinging to firm substrates including seaweeds and pebbles.	Murray, 1979
<i>Elphidium excavatum</i>	An inner-shelf species that can tolerate brackish conditions. High abundance of <i>Elphidium excavatum</i> is often found in areas experiencing high physical disturbance that received high loads of fresh organic material. Often used as a proxy for eutrophic conditions. Frequently found living in areas of strong water such as tidal flats or channels.	Murray, 1979; Murray, 1971; Nooijer et al., 2008
<i>Fissurina elliptica</i>	A euryhaline species that can tolerate a large salinity range (0–35‰). Tends to be abundant in brackish environments including estuaries and lagoons.	Murray, 1979
<i>Haynesina germanica</i>	Generally found in brackish, intertidal marsh and estuarine waters, although it is Euryhaline and can survive in higher salinity environments.	Murray, 1979; Murray 1991; Holzmann and Pawlowski, 2000
<i>Jadammina macrescens</i>	Found only in marsh environments, in <10m water depth.	Horton et al, 2006
<i>Lagena</i> sp.	A marine, shelf genus commonly found in muddy substrates. This species prefers salinities >32ppm. Dead tests can be transported and deposited into estuarine muds during storm events.	Murray, 1979; Jingxing and Luping 2012
<i>Miliolinella subrotunda</i>	Epifaunal but living within the top 0.5 cm. Lives on sediment and marine plants. Tends to colonise estuarine mouths during favourable conditions. At its northern limit in Britain and Ireland.	Murray, 1971; Murray, 1979; Murray, 2003; Naeher et al, 2012
<i>Nonionella turgida</i>	An infaunal, shelf species that prefers higher chlorophyll concentrations in the water and is intolerant of low oxygen environments.	Murray, 1971; Gustafsson and Nordberg, 2000; Murray, 2003; Murray, 2006; Brattstrom et al, 2015
<i>Oollina williamsoni</i>	A marine, shelf species commonly found in muddy substrates.	Murray, 1971 Murray, 1979
<i>Planorbulina distoma</i>	A shallow marine species not tolerant of reduced depth or salinity, but which can be prone to transportation. They tend to prefer a rockier substrate.	Wynn Jones, 2013

Appendices

Planorbulina mediterraneensis	Marine, inner-shelf species but dead test can be transported into estuary mouths. Species is epifaunal clinging to firm substrates including seaweeds and pebbles. Generally found at water depth <30m, in the photic zone.	Murray, 1979; Murray, 2006
Quinqueloculina sp	Estuarine, inner-shelf to marine group, commonly found in temperate to mid-latitude environments.	Murray, 1979; Austin and Kroon, 1996; Horton et al, 1999; Horton et al, 2006; Naeher et al, 2012
Rosalina globularis	Marine, inner-shelf species. Passive grazer when food is abundant but actively forages as resources diminish.	Slither, 1965; Van Hengstum and Scott, 2011
Rosalina praegeri	Species prefer a temperate environment.	Austin and Kroon, 1996
Sahulina conica	Commonly found in marine to estuarine conditions.	Haunold, 1999; Naeher et al, 2012
Stainforthia fusiformis	Marine species, generally preferring salinities >28ppm, but commonly transported and deposited in estuarine environments. Found in most clastic sediments, in water temperatures between 5-16°C. Known opportunist of organically enriched sediments.	Murray, 1979; Collison, 1980; Murray, 1986; Gustafsson and Nordberg, 2000; Gooday and Alve, 2001; Duijnsteet et al, 2005
Spirillina vivipara	Epifaunal species, tends to cling to substrates such as pebbles and seaweeds. Marine, inner-shelf species but can also be found living in estuary mouths.	Murray, 1979; Murray, 2003
Textularia sp.	Epifaunal, shelf species and attaches to objects such as shells	Murray, 1991; Murray, 2003; Naeher et al, 2012